The good, the bad and the ugly

Developing strategies for studying the cell- and tissue-damaging effects of snake venoms

Mátyás Antal Bittenbinder

Copyright 2024 © Mátyás Antal Bittenbinder
ISBN: 978-94-6506-299-0
DOI: 10.5463/thesis.707

All rights reserved. No parts of this thesis may be reproduced, stored in a retrieval system or transmitted in any form or by any means without permission of the author.

Provided by thesis specialist Ridderprint, ridderprint.nl
Printing: Ridderprint

Illustrations: János Antal Bittenbinder
Layout: Timo Wolf Kamp, persoonlijkproefschrift.nl

VRIJE UNIVERSITEIT

The good, the bad and the ugly

Developing strategies for studying
the cell- and tissue-damaging effects of snake venoms

ACADEMISCH PROEFSCHRIFT

ter verkrijging van de graad Doctor aan
de Vrije Universiteit Amsterdam,
op gezag van de rector magnificus
prof.dr. J.J.G. Geurts,
in het openbaar te verdedigen
ten overstaan van de promotiecommissie
van de Faculteit der Bètawetenschappen
op woensdag 30 oktober 2024 om 15.45 uur
in een bijeenkomst van de universiteit,
De Boelelaan 1105

door

Mátyás Antal Bittenbinder

geboren te Nijmegen

promotoren:	prof.dr. F.J. Vonk
	dr. J. Kool
promotiecommissie:	prof.dr. A.M. Rijs
	prof.dr. M.K. Richardson
	dr. F. Cardoso
	prof.dr. A. Rucavado
	prof.dr. Y. Stienstra
	dr. M.H.A. Bos

We don't own the planet Earth, we belong to it.
And we must share it with our wildlife.

- Steve Irwin -

Table of Contents

*We only **protect** what we **love**,*
*we only **love** what we **understand**,*
*and we only **understand** what we are **taught**.*

- Jacques-Yves Cousteau -

Micruroides euryxanthus

Chapter 1

Introduction

1.1 General introduction on venomous snakes

Snakes are fascinating creatures that have played significant roles throughout human history and across various cultures. Their unique appearance, behaviour and mystique have influenced folklore and religion for centuries. Take, for example, the ancient Greek mythologies in which the Gorgons had serpents for hairs, the serpent in the Garden of Eden, or the Aztec god of wind, rain, and creation. Snakes represent or have represented a wide range of symbolic meanings, including wisdom and knowledge, danger and temptation, immortality and rebirth, and have served as a symbol of healing and medicine. The snake-entwined staff, known as the rod of Asclepius (God of Medicine), continues to serve as a symbol of medicine today. Whether it's the mesmerising movement of a snake, their role in culture or their contribution to our understanding of science, these creatures are a source of fascination to people worldwide.

To date, over 4000 snake species have been described, which are found across all continents except Antarctica [1,2]. Snakes have a unique body plan, characterised by elongation of the body and limblessness. The elongation of the body is accompanied by an increased number of vertebrae and a more extended backbone, which has evolved independently multiple times among vertebrates, including amphibians, fish, and reptiles [3–5]. Snakes are highly specialised predators, which have evolved two main ways of incapacitating prey: suffocation and envenomation. Venomous snakes belong to the superfamily Caenophidia, a taxonomic group commonly known as 'advanced snakes', which currently comprises over 3300 species [6]. Most venomous snakes possess a venom-delivery system comprised of venom-producing glands and venom-delivering teeth. Venom glands are specialised structures located behind the snake's eyes that produce and store venom. These glands consist of serous cells (i.e., capable of secreting an enzyme solution) and a venom duct leading to the base of each fang [7–9]. Depending on the snake family, some glands have a lumen that can be voluminous and capable of storing large quantities of venom. The venom glands may be enclosed by muscles, which facilitate high-pressure ejection of the venom from the glands [9–13]. Venom glands vary between the various families of venomous snakes. The glands in Colubridae are more basic in structure and considered to be different than the venom glands found in other venomous

lineages. Therefore, the Colubrid venom gland structures are often referred to as 'Duvernoy's glands' to differentiate them from the 'true' venom glands found in other lineages. The Duvernoy's glands are considered the Colubrid equivalents of the venom gland found in elapids, vipers and other front-fanged snakes. Despite being anatomically and functionally distinct, these glands share many similarities with 'true' venom glands. Because of these differences, some scientists argue that the distinction between the two gland types should be retained [14–16]. Other experts, however, consider these glands to represent an evolutionary primitive version of the venom gland [17,18].

In addition to the venom gland, venomous snakes have a pair of specialised teeth, which are modified in such a way that this makes venom delivery easier. The base of each fang is connected to the venom gland via a venom duct. Depending on the position of the fangs on the upper jaw, various groups of front- and rear-fanged snakes can be recognised. Snakes that have fangs located posteriorly in the upper jaw are considered rear-fanged snakes as opposed to front-fanged snakes, in which the fangs are located anteriorly [8,9,19]. Rear fangs are often solid or slightly grooved but never tubular, opposite to front-fanged snakes, which have teeth that are often tubular and function as hypodermic needles [7,9,19,20]. All rear-fanged snakes are found in the Colubridae family of snakes. Families of front-fanged snakes include Elapidae (cobras, mambas, kraits, and coral snakes), Viperidae (vipers and pit vipers) and Atractaspididae (e.g., stiletto snakes) (see Figure 1) [1,8,21,22].

The venom inside the gland is primarily used to immobilise and capture prey, although it may also be used defensively when threatened or provoked. In the case of snake-human interactions (which are often entirely unintended), victims may suffer from serious injury, and in severe cases, these interactions could even be fatal [21,23].

Figure 1. Striking examples of medically important snake species from Africa, the Americas and Asia. From left to right: Stiletto snake (*Atractaspis bibronii*); Boomslang (*Dispholidus typus*); Arizona Coral Snake (*Micruroides euryxanthus*) and Russell's viper (*Daboia russelii*). Photos by: Tyrone Ping (photos of *A. bibronii* and *D. typus*); David Jahn (photos of *M. euryxanthus*) and Frank Deschandol (photos of *D. russelii*).

1.2 The problem of snakebite and the antivenom crisis

Snakebite envenoming is an important public health problem that is responsible for over 1.8 million victims, with annual mortality rates estimated to range between 81,000 – 138,000 [21]. Snake venoms are capable of causing a variety of local and systemic effects in bite victims, some of which are life-threatening, while others may lead to permanent disability and disfigurement [21,23–25]. The regions of the world that are most heavily affected by snakebites include Southeast Asia, sub-Saharan Africa and Latin America (see Figure 2) [21,29]. Of these regions, Southeast Asia has the highest number of victims, followed by Africa, the Middle East and Latin America (see Figure 2). Some reasons why the burden of snakebite is typically high in these regions include the fact that 1) snake encounters are common due to rural and agricultural settings (see Figure 3); 2) lack of awareness and education on snakes, their behaviour and first aid in case of a bite; 3) there is limited access to proper healthcare in the case of a bite incident [24,27–32]. Snakebites typically affect young male agricultural workers, imposing a substantial socio-economic burden on families and local economies [24,33]. Without early and effective antivenom treatment, if victims do survive, the morbidity following snakebite can cause permanent disability and disfigurement and can severely inhibit one's ability to work [21,24,28,33].

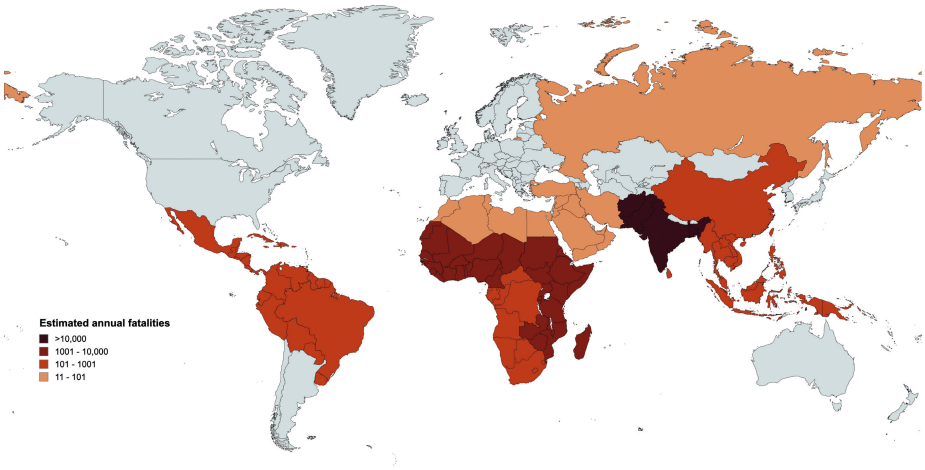

Figure 2. Geographical distribution of the estimated number of snakebite deaths and morbidities. The data provides a rough approximation of the estimated numbers of envenomings and morbidities. The highest incidence of snakebite occurs in Latin America, sub-Saharan Africa, and Asia. Data based on estimates from [21,24,34]. Map created using www.mapchart.com.

Currently, the only effective treatment for snakebite is the use of antivenom. An antivenom consists of concentrated antibodies of animal origin (i.e., horse, sheep, or other domesticated animals) that have been immunised with a single or multiple venoms over an extended period (months to years). Two main types of antivenom exist: i) monovalent (monospecific) antivenoms, which are raised against the venom of a single species and ii) polyvalent (polyspecific), which are effective against the venoms of most medically important snake species in a specific geographical area [21,31,35–37]. Most antivenom manufacturers refine the extracted antibodies by purification prior to medical use in order to reduce the risk of adverse reactions [21,31,37–39]. The process of manufacturing and the number of purification steps will significantly influence the cost of an effective treatment dose. This immediately raises the issue that the most effective antivenoms become unaffordable for those who need them the most [31,40]. As a result, several antivenom manufacturers have ceased production, primarily for commercial reasons. This has resulted in significant shortages of antivenom in the regions that they previously supplied, particularly in the African countries [21,41]. In addition to the high production costs and scarcity of antivenom products, their poor distribution and the requirement for cold storage create an additional challenge for the societies in those regions that are already experiencing the

highest burden of snakebite. Lastly, current antibody-based antivenoms offer limited protection against local tissue damage. The reason for this is the fact that the tissue-damaging effects progress quickly, and the antibodies neutralising the venom components are relatively large molecules and may, therefore, not penetrate deep into the affected tissues. Hence, only prompt antivenom treatment is effective against the local venom effects. Especially victims in rural areas who need to travel great distances before they can receive treatment can suffer significantly from the tissue-damaging effects following snakebite [21,27,31,40]. In addition to the high number of victims and the antivenom crisis, the longstanding lack of attention and funding from governments, healthcare authorities, and pharmaceutical companies has led to a problem with global proportions. As a result of this enduring challenge and international neglect, the World Health Organization (WHO) has recently designated snakebite as one of the globally neglected tropical diseases, and it has initiated efforts to raise global awareness [21,28]. The majority of (severe) snakebites cases are caused by genera within the elapid and viperid families, with mole vipers (*Atractaspis*) and rear-fanged snakes being of less medical importance. The genera responsible for the highest number of bites and fatalities include *Echis* (saw-scaled vipers), *Bothrops* (lance-headed pit vipers), and the genera *Bungarus* (kraits) and *Naja* (true cobras) [36,42,43].

Figure 3. Striking images showing venomous snakes and people living in close proximity in rural areas. The burden of snakebite is typically high in rural and agricultural settings in (sub)tropical regions of the world, as snake encounters are common. The image on the left shows an Indian cobra (*Naja naja*) and farmers in a paddy field, and the image on the right shows a Russell's viper (*Daboia russelii*) in West Bengal, India. Photos by: Wolfgang Wüster.

1.3 Snake venom composition and the pathological effects of snake venoms

Venom is a highly complex mixture consisting of various bioactive compounds, including proteins and peptides (commonly referred to as toxins) and other organic molecules and salts [44–46]. The composition of snake venoms may vary greatly at the interspecific level (between species) or the intraspecific level (within the same species) [47–51]. Intraspecific variation is found between sex (male vs female), age (i.e., ontogenetic shifts) or within a population (i.e., geographical variation). [47,48,57–59,49–56].

Snake venoms are comprised of a variety of protein families, which are generally classified as major or minor toxins classes. The major toxin families include three-finger toxins (3FTxs), phospholipases A_2 (PLA_2), snake venom metalloproteinases (SVMPs) and snake venom serine proteinases (SVSPs). In

contrast, the minor toxin families include hyaluronidases, β-defensin-like toxins, kunitz-type peptides, disintegrins, C-type lectins and C-type lectin-related proteins (CTLs/CLPs) and cysteine-rich secretory proteins (CRiSPs), plus a diversity of other toxin families [21,37,60].

The clinical effects following envenomation can be categorised into three main pathologies, including neurotoxicity, haemotoxicity, and tissue-damaging effects, with some venoms causing a combination of these effects (see Figure 4) [21]. The neurotoxic effects result from toxins affecting neurotransmission at the neuromuscular junction. Neurotoxins act on the pre- or post-synaptic junction or in the synaptic cleft and may affect nervous transfer in various ways. The actions of these toxins include blocking ion channels, acting as receptor antagonists or preventing the removal of acetylcholine by inhibiting acetylcholine esterase in the synaptic cleft [21,44,61,62]. The toxins predominantly responsible for these neurotoxic effects are generally listed as either α-neurotoxins or β-neurotoxins, based on their post- or pre-synaptic actions. A third group of toxins consists of dendrotoxins, which belong to the Kunitz-type proteinase inhibitor family [9,37,44,62–64]. The effect of neurotoxins may lead to various clinical manifestations, including muscle overstimulation, spasms and even respiratory paralysis [21,44]. The haemotoxic effects of snake venoms are an umbrella term and include various haemostatic effects and cardiovascular disruptions caused by snake venoms. Haemotoxins may cause alterations in blood coagulation, with clotting either being accelerated (procoagulation) or slowed down (anticoagulation). Toxins that enhance coagulation typically affect blood clotting by i) activating factor X, prothrombin, and other clotting factors, ii) stimulating platelet aggregation, or iii) exerting a thrombin-like (fibrinogenolytic) effect [65,66]. Anticoagulant toxins may directly inhibit haemostasis by i) inhibiting platelet aggregation, ii) modulating platelets, iii) degrading coagulation factors or iv) by hydrolysing or binding to phospholipids, which are essential co-factors involved in coagulation [9,37,63]. Toxins affecting normal coagulation include PLA_2s, SVSPs, CTLs, SVMPs, disintegrins, kunitz-type peptides and toxic forms of Factor X and Factor V [9,34,37,63]. Besides affecting haemostasis, haemotoxic compounds may affect the cardiovascular system by causing local or systemic bleeding. This is caused by SVMPs, which are capable of proteolytically degrading components in the extracellular matrix of the microvasculature, thereby affecting the integrity of endothelial cells by

weakening the capillary wall. Haemorrhage may be further potentiated by coagulopathic effects [67–71]. Additionally, some snake venom components induce increased vascular permeability, leading to plasma extravasation, which may cause hypovolemia and haemodynamic disturbances [34,72].

The tissue-damaging effects induced by specific snake venom components are the leading cause of snakebite morbidities. An estimated 450,000 bite victims each year suffer from severe morbidities, which include permanent muscle tissue loss, renal damage, blindness and other debilitating pathologies [21]. Toxins responsible for tissue damage can be broadly categorised into two groups based on their mechanisms of action on cells and tissues. The first group consists of "true" cytotoxins, which directly affect cells by disrupting the cell membrane integrity, including 3FTxs, PLA_2s and β-defensin-like toxins [21,73–78]. The second group consists of extracellular matrix (ECM)-degrading enzymes that cause cell death as a secondary effect, not by directly damaging cells. As the ECM plays an essential role in providing structural support to cells, it is considered an important target for tissue-damaging venom components. These toxins could, therefore, be considered indirectly cytotoxic and consist of SVMPs and hyaluronidases [68,70,79–81]. Other toxins capable of causing cell- or tissue damage include L-amino acid oxidases (LAAOs), disintegrins and possibly C-type lectins [21,82–84]. Tissue-damaging toxins are capable of causing various pathologies, including local and systemic haemorrhage, muscle necrosis, blistering, skin necrosis and acute kidney injury [21,63,70,73,74]. Despite the severe pathophysiological effects and high morbidity rates, research efforts have been focusing primarily on the haemotoxic and neurotoxic effects and less on venom-induced tissue damage [21,85].

In order to fully understand the venom composition, the pathological effects and the responsible mechanisms of action, numerous *in vivo* and *in vitro* assays have been developed to study venom effects in more detail. *In vivo* studies mainly involve injecting crude venom or isolated toxins into animals (e.g., mice), after which the effects on various tissues are monitored [86–90]. These include behavioural assays and electrophysiological recordings for neurotoxicity, histopathological assays and haematological parameters (e.g., clotting times, blood cell counts) for haemotoxicity and serum biomarker analysis and histological examination of organs and tissues for tissue-damaging effects [72,86–88,91]. *In vitro* assays consist

of electrophysiological assays (i.e., patch-clamp recordings of neurons or muscle cells), coagulation assays and various cell-based assays [92–96].

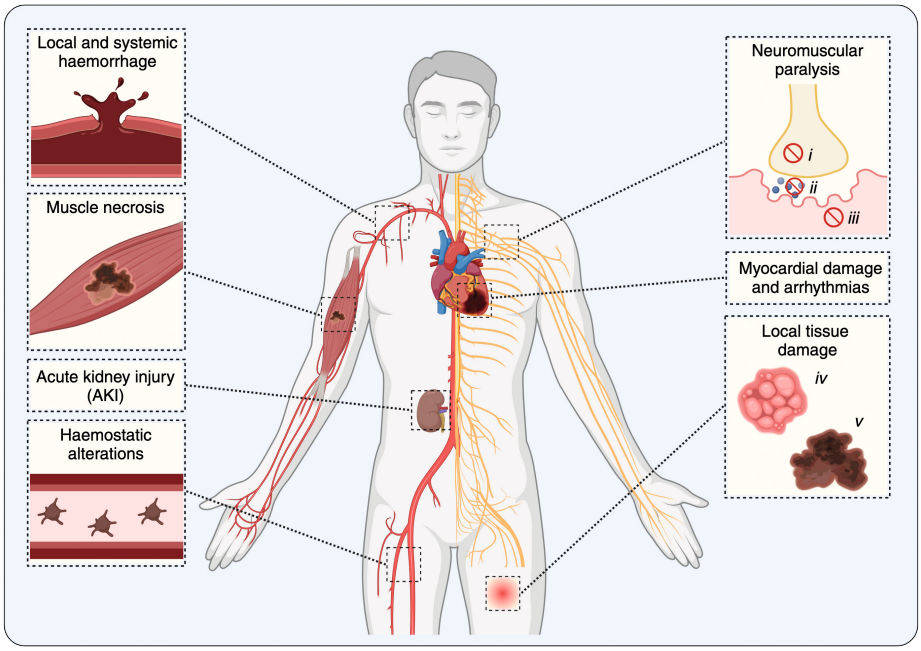

Figure 4. Overview of the effects of snake venom toxins on various pathological systems. Snake venoms may exert a wide variety of toxic activities on various parts of the body, both local and systemic. The activity of certain toxins may induce local and systemic haemorrhage and is further potentiated by coagulopathic effects. Systemic haemorrhage could ultimately lead to cardiovascular shock. Muscle necrosis (i.e., rhabdomyolysis) may result in the release of myoglobins. Acute kidney injury can be induced by ischaemia (i.e., decreased blood flow to the kidneys), deposition of microthrombi in the kidney microvasculature, accumulation of myoglobins in kidney tubules, and direct effect of nephrotoxins. Haemostatic alterations are mainly caused by consumption coagulopathy and platelet disturbances. Neuromuscular paralysis is a result of neurotoxins acting on the pre- or post-synaptic junction (*i* and *iii*) or in the synaptic cleft (*ii*). Myocardial damage is often a consequence of toxins directly affecting the heart tissue, and arrhythmias are induced by haemodynamic instability. Lastly, local tissue damage includes blistering and oedema (*iv*) and necrosis of soft tissues (*v*). This figure was based on a figure in Gutierrez et al., 2017 [21] and created via www.biorender.com (with permission).

1.4 Assays for studying cell- and tissue-damaging activities of snake venoms

The study of venom-induced tissue damage has traditionally been investigated using *in vivo* and *in vitro* models. *In vivo* assays include the histological examination

of organs and tissues of venom-injected animals and biomarker analysis, in which circulating markers of cellular damage or inflammation in blood samples are monitored [72,86–88]. However, these methods need a large number of animals, may yield variable results and provide little to no information about the molecular targets and mechanisms underlying the observed effects [97–99].

There is a variety of cell-based assays available that utilise specific markers that can be used to quantify the number of live (or dead) cells in culture. Metabolism and enzymatic activity are often used as a marker for live cells. Some of these assays are based on the fact that viable cells are capable of converting a substrate into a coloured or fluorescent product that can be measured using a plate reader [100,101]. Dead cells are unable to convert the substrate to product, which leads to a reduced signal (proportional to a lower number of viable cells compared to control). Example assays include the tetrazolium reduction and resazurin reduction assays [100–104]. The ATP assay is based on quantification of the ATP levels in cell lysates. Given the fact that ATP is involved in many enzymatic reactions and ATP declines rapidly when cells undergo apoptosis or necrosis, this assay is suitable for measuring cell viability [100,102,105–107]. Cell viability can also be measured by its membrane integrity. This can be visualised by using cell-impermeant dyes that will only give a readout whenever the dyes penetrate dead cells. Some dyes, such as Trypan blue, enter the cells without interacting with interior molecules, whereas others, such as propidium iodide and DRAQ7, selectively bind nucleic acid (i.e., DNA) [102,108–110]. This binding goes paired with an increase in fluorescence, which can be measured and used to determine cell viability.

Cell membrane degradation can also be detected by measuring the leakage of certain markers from the cytoplasm into the culturing medium [100,101]. The most commonly used marker for this type of assay is L-lactate dehydrogenase (LDH). This enzyme is released into the cell culture medium when the cell membrane is damaged. Extracellular LDH can then be quantified by making use of its enzymatic properties and the formation of a water-soluble product that can be detected on a plate reader [100,101,111,112]. Another option is loading the cells with a cell-permeable dye, after which the leakage from the cell can be measured. Calcein AM is such a dye. This is a non-fluorescent dye that passively crosses the cell membranes and which is retained in live cells. Esterases

in the cytosol subsequently convert the dye into fluorescent calcein, which can be measured. Loss of membrane integrity leads to the release of fluorescent calcein into the culture medium, which can be monitored relative to the background [101,113]. Besides the assays mentioned above, other cell viability assays exist. These include proteinase viability marker assays, mitochondrial function assays and cell proliferation assays, which will not be discussed further.

In addition to cell-based assays, other *in vitro* assays exist that focus more specifically on molecular mechanisms underlying cell damage, such as proteolytic activity and PLA_2 activity.

The activity of SVMPs has been studied chiefly via ELISA or zymography, using gelatin (or another ECM mimic) as the substrate [114–116]. Substrate zymography is an electrophoretic technique in which a substrate (i.e., a particular ECM component) is co-polymerised with SDS-PAGE gels. The venoms are subsequently separated under non-reducing conditions, which is crucial to preserve the native conformation and activity of the toxins. This method can be used to monitor substrate degradation of the proteins based on molecular weight separation [114,116–119]. Proteolytic activity has also been measured using fluorometric assays, which use a fluorescent ECM-substrate that is self-quenching. This means that the fluorescent signal is suppressed (i.e., quenched) when the substrate is intact. Upon cleavage of the substrate (i.e., due to the proteolytic activity of certain toxins), the fluorescent signal increases [99,114,116,118].

Over the years, several assays have been developed in an attempt to measure the membrane degradation activity of PLA_2s in snake venoms. Some of these assays have relied on the hydrolysis of a substrate into a product, which could then be measured using absorbance [120,121], fluorescence [122,123] or radioactively [124,125]. Another possibility is to use the change of pH as an indicator for PLA_2 activity, as hydrolysis of phospholipids results in a decrease in pH, which can be monitored [126–128]. Lastly, assays that use phospholipid vesicles (from egg yolk) as a substrate have been developed, in which a decrease of turbidity of the egg yolk emulsion is recorded and used as a measure for PLA_2 activity [57,129–132]. Hyaluronidase (HA) activity can also be determined using various assays. The classical methods include those that monitor the loss of turbidity or viscosity of a reaction mixture and assays that detect degradation products of the enzymatic reaction (i.e., specific residues from a hyaluronate substrate) [132–137]. In-gel zymography is also

used, in which hyaluronic acid is co-polymerised with SDS-PAGE gels, which is then used to monitor substrate degradation of the proteins with hyaluronidase activity in a particular venom [80,117,137,138]. Lastly, ELISA-like assays can be used to measure hyaluronidase activity by tracking the amount of HA that is hydrolysed [80,139–141]. Although some of these assays have been used to study purified venom toxins, most have been used to study the effects of crude venom samples.

In order to elucidate venom composition and to better understand the pathological effects and the molecular mechanisms behind them, it is essential to separate the venom into its individual components (i.e., its toxins) in order to study these toxins further biochemically and biologically. Separation of venoms for purification of their toxins allows researchers to better understand the specific actions and interactions of these different venom constituents within the body and mechanistically by studying these toxins using *in vitro* assays. Some venom components might have opposing effects or interact differently when combined [48,142–146]. By isolating individual components from venoms, scientists can gain insight into their individual effects and potential synergies or antagonisms between them. Additionally, studying individual venom components is essential for a comprehensive understanding of their bioactivity, enabling targeted research and the development of effective snake venom treatments.

1.5 Analytical separation and detection platforms for studying snake venom toxins

For more than 40 years, analytical techniques have been successfully used to separate and characterise bioactive components from (snake) venoms [147]. These include SDS-PAGE and various high-performance liquid chromatographic (HPLC) techniques.

Since its development in the early 1970s, SDS-PAGE has been used for separating proteins based on their electrophoretic mobility (i.e., how proteins migrate through a polyacrylamide gel matrix in the presence of an electrical current) [148,149]. Two major types of gel electrophoresis have been developed. One-dimensional (1D) SDS-PAGE separates proteins based on their molecular weight, whereas two-dimensional (2D) SDS-PAGE separation is based on isoelectric

focusing (first dimension) and molecular weight separation (second dimension). Toxin size can be roughly estimated based on protein ladders, and since the toxins remain intact, identification of the toxins can only be made after tryptic digestion [150–152].

Various HPLC methods have been used for venom separation for many decades. With ion exchange chromatography (IEX), the separation is based on the net charge of the molecules to be separated. IEX utilises the interactions between charged molecules in a sample (i.e., a snake venom) and charged sites on a solid support matrix (i.e., stationary phase) within a chromatography column. The elution of the bound analytes (e.g., protein) can be achieved by changing the pH of the liquid solution (i.e., mobile phase). When the pH of the solution is below the isoelectric point of a particular analyte, this will disrupt its interactions with the stationary phase, causing the analytes to be released from the column [151,153,154]. However, most often, salt gradients are used with IEX, in which competition of the analyte between the stationary phase and the salt ions in the mobile phase facilitates protein elution from the column. Affinity chromatography is used to isolate a specific protein or group of proteins from a mixture using a particularly small or large molecule immobilised to column material, thereby functioning as the stationary phase. This affinity stationary phase molecule has an affinity to one or more of the proteins of interest to purify from a mixture of proteins. As the stationary phase molecule has an affinity to its target protein(s) (e.g., certain toxins of interest in a venom), they specifically bind to the stationary phase molecule [151,155,156]. The stationary phase typically contains ligands that have a high affinity for the target molecule(s). When the sample containing the target molecule is applied to the column, it selectively binds to the immobilised ligands, while non-binding molecules are washed away. The bound target molecule is subsequently eluted under conditions that disrupt the binding affinity interaction. Hydrophobic interaction chromatography (HIC) separates molecules based on their hydrophobicity along a salt gradient. During separation, molecules with higher hydrophobicity interact more strongly with the stationary phase and are retained longer, leading to their slower elution from the column. With size-exclusion chromatography (SEC), venom components are separated based on size, with no physical or chemical interaction between the molecules and the stationary phase of the column. The principle relies on porous beads in the

stationary phase, with smaller molecules entering the pores and taking longer to elute. In comparison, larger molecules pass through the column more quickly as they cannot enter the pores [150,151,157,158]. Lastly, reversed-phase chromatography (RP-LC) is a separation technique that is similarly based on the hydrophobicity (or polarity) of the molecules in the venom, although the principle of separation differs. With RP-LC, the concentration of an organic solvent in the mobile phase is gradually increased during the chromatographic run, typically by applying an increasing organic solvent concentration gradient, resulting in the elution of analytes mainly in order of their polarity. In this chromatographic separation, the order of elution roughly results in polar molecules eluting first and the more non-polar analytes eluting later on in the gradient. Typically, the more non-polar an analyte is on RP-LC, the stronger its interaction with the stationary phase will be [150,151,159,160].

Depending on the scale and purpose of the separation, multiple HPLC preparation methods can be used. For separation and purification of larger quantities of the target molecules(s) from a complex mixture, (semi)preparative chromatography can be used. The goal of this approach is to isolate as much of the target component(s) as possible. For the purification of relatively large amounts of venoms into their respective purified toxins, (semi)preparative methods are preferred [161–164]. For smaller sample volumes, analytical separation methods can also be used. These analytical separations (often having a much higher resolution than semi-preparative separations) are most often employed for analytical purposes such as quantification, characterisation, and identification of analytes (e.g., venom toxins) in a biological mixture (e.g., venom). Although analytical HPLC is not suitable for purifying large quantities of toxins, it offers the advantages of higher separation resolution, faster separations and its applicability to automation.

After separation and fractionation of a venom, either performed in (semi) preparative or in an analytical fashion, the purified toxins can be studied biologically (e.g., *in vivo*) and/or biochemically (i.e., *in vitro*) [95,151,165–168]. These post-column bioassays can also be combined with parallel mass identification of the bioactive components. When performed in high-resolution format, this kind of analysis is referred to as nanofractionation analytics (see Figure 5) [165,169–171]. The nanofractionation analytics methodology involves LC separation

with UV detection followed by MS analysis in parallel with the collection of high-resolution fractions (2–10 seconds per fraction) in high-density microwell plates (i.e., 96, 384, or 1536 wells). The content of each well is then subjected to high-throughput bioactivity profiling using a suitable bioassay. The bioassay data is subsequently converted to bioactivity chromatograms by plotting the retention time of fractionation on the x-axis against the bioactivity readout on the y-axis. By directly combining bioassays and MS detection (i.e., in parallel), the bioactive toxins can be directly identified from the MS data that was acquired in parallel (i.e., LC-MS and/or toxin proteomics data) [172–174]. The nanofractionation approach enables high-throughput and high-resolution bioactivity profiling of venom in parallel with toxin identification and can, therefore, be considered complementary to venom profiling using venomics [150,151,173,175].

Venomics is an analytical strategy that was coined about two decades ago and that is used to characterise snake venom proteomes [173,176]. Given the complexity of the venoms, the evolution of the venomics field significantly advanced the way in which snake venom proteomes could be studied [150,151,173,177]. With venomics, various disciplines, including genomics, transcriptomics, and proteomics, are combined to study the protein composition of these complex biological mixtures.

In venomics, two main proteomics approaches are used. With bottom-up proteomics, proteins are first enzymatically digested into smaller peptides using enzymes such as trypsin, resulting in a mixture of peptides. Identification of the proteins can either be made from crude venom samples (i.e., shotgun analysis) or after separation by electrophoretic and/or chromatographic techniques [150,151,173]. The resulting peptides are then analysed using tandem mass spectrometry (MS/MS) to determine their masses and sequences. The obtained peptide sequences are then used to identify the toxins present in the sample, either by determining the amino acid sequence directly from the mass spectra (i.e., *de novo* sequencing) or by matching these against a protein sequence database [150,173]. More recently, partly enabled by technological advances in mass spectrometer equipment, venomics approaches are appearing in literature that incorporate analysis of intact (i.e., non-digested) venom toxins in the mass spectrometer, including measurement of their fragmentation in MS/MS. This is called the top-down approach [150,173]. With top-down proteomics, intact proteins are analysed directly (i.e., MS/MS fragmentation) instead of digesting enzymatically prior to MS/MS

analysis. Top-down proteomics can be used as a complementary to bottom-up proteomics as it may provide information on accurate intact toxin masses and post-translational modifications [173,178]. The versatility of this approach, however, is still limited, as it relies on the MS fragmentation methods and requires highly sophisticated MS equipment. Most venomics studies have been using bottom-up proteomics, although, in recent years, top-down methods have been adopted more frequently [151,173].

The original venomics approach, as developed by the Calvete group, has dramatically advanced over the years, which allowed for more accurate and more in-depth identification of venom toxin proteins [173]. To date, multiple 'generations' of venomics have been developed, which differ in their throughput, ranging from a complete proteome analysis in 4-6 weeks (1st generation) to less than one week (2nd generation) [176,179,180]. Recent advances also include 'absolute venomics' (i.e., 3rd generation venomics), which allows the absolute quantification of venom toxins [181,182]. The latest development is known as 'high-throughput (HT) venomics', which is capable of performing a complete proteomic analysis within three days and requires only several hours of manual labour [172].

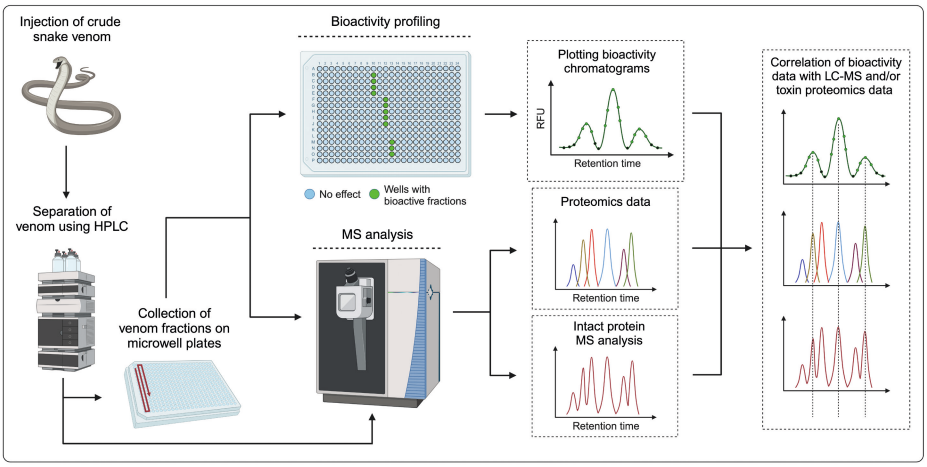

Figure 5. Graphical overview of the nanofractionation approach. Crude venom is injected and separated by HPLC (e.g., RP-LC). The post-column effluent flow with eluting toxins can be split into two parts. The majority (90%) is directed to a high-resolution fraction collector for collecting the fractions in high resolution (2-10 seconds per fraction) in high-density microwell plates, while the smaller part (10%) is directed to UV detection followed by MS analysis. Following fractionation, the microwell plates are vacuum-centrifuged to dryness, after which bioassays can be performed. So-called bioactivity chromatograms can be generated by plotting the bioassay signal per well (y-axis) against the retention time of each well (x-axis). By performing a second nanofractionation separation on another microwell plate, this workflow can also be used for subsequent proteomics/venomics analysis. By combining bioactivity profiling and MS detection, the bioactive toxins can be directly identified from the MS data that was acquired in parallel (i.e., LC-MS and/or toxin proteomics data). Abbreviations: MS, mass spectrometry; RFU, relative fluorescence units. Image created using www.biorender.com.

1.6 Aims and thesis outline

As discussed before, tissue-damaging toxins in snake venoms are capable of causing severe pathologies such as systemic bleeding and tissue necrosis and high morbidity rates in snakebite victims. Despite the relevance of studying the mechanisms of venom-induced tissue damage, research efforts have been limited compared to studies on the haemotoxic and neurotoxic effects. In order to better understand the mechanical aspects of cell- and tissue-damaging toxins, there is a need for a high-throughput screening platform that can be used to study and characterise these bioactive components specifically. It also requires the development and improvement of bioassays specific for studying toxins with direct cytotoxic effects (i.e., those directly affect cells by disrupting the cell membrane integrity) and those with indirect cytotoxic effects (i.e., ECM-degrading-enzymes). These bioassays are also used for high-throughput

bioactivity profiling of venom fractions after LC separation in combination with mass identification of LC-MS and/or toxin proteomics data that was acquired in parallel using HT venomics.

Chapter 2 will discuss the molecular mechanisms underlying venom-induced tissue damage, including 'true' cytotoxicity and extracellular matrix degradation. The chapter will first focus on the confusion that exists in the terminology describing cytotoxic venom components. Traditionally, toxin (sub)classes have been categorised according to their primary tissue targets, resulting in names such as cardiotoxins or myotoxins [75,183,184]. This classification has its limitations as it oversimplifies the complexity of these toxins and does not take into account the mechanical aspects of these components [9,21,63,75,183,184]. This chapter proposes an alternative classification for tissue-damaging toxins, which focuses on the mechanical aspects, including membrane disruption and ECM degradation. The review further provides an overview of the pathophysiological aspects associated with tissue damage and discusses potential treatment strategies.

Chapter 3 describes the development of a workflow that allows the study of the mechanisms underlying venom-induced cell- and tissue damage. For this, a selection of (established) cellular bioassays was used in combination with fluorescence microscopy to study cell-damaging activities of both crude and fractionated snake venoms. A panel of 10 medically relevant snake species was used, covering a significant part of the geographical regions most severely affected by snakebite. Based on the results from this study, two distinct mechanisms by which viper and elapid venom toxins exert their effects on cells could be identified, either by disruption of the cellular membrane or by degradation of the cell monolayer. In an effort to characterise the bioactive venom components responsible for the observed activities, the study then describes a combination of LC methods followed by bioassaying and protein identification using HT venomics. The outcomes of this study formed the basis for Chapters 4-8.

Chapter 4 will dive deeper into the venom toxins capable of affecting the ECM, which are thought to be responsible for cell monolayer degradation observed *in vitro* when exposed to viper venoms (see Chapter 3). Currently, only limited

research has been done on the development of proteolytic degradation assays that combine activity profiling with toxin identification. This study focuses on the development of such an assay. The assay principle is based on in-gel zymography, in which a specific substrate such as gelatin is co-polymerised with SDS-PAGE gels to identify the proteolytically active components within the venom [117,185]. In order to study the proteolytic activities of a panel of snake venoms, a variety of fluorescently labelled ECM-substrates (i.e., collagen, gelatin, elastin, laminin, fibronectin and hyaluronic acid) were used. The venoms were separated under non-reducing conditions, which is vital to retain the native conformation and activity of the toxins. After electrophoresis, the SDS was removed from the gel to renature the proteins. This step is crucial for zymography, as renaturation allows the proteins to regain their native conformation and enzymatic activity.

The subsequent identification of bioactive toxins was done using in-gel tryptic digestion followed by nano-LC-MS/MS analysis for bottom-up proteomics. Although this method was successful in identifying proteolytically active venom components, the process is not suitable for high-throughput screening of bioactive components.

Chapter 5 describes the development of a high-throughput plate reader assay to study proteolytic degradation by snake venom toxins using a number of fluorescently labelled ECM-substrates. With this fluorometric assay, two dye-quenched ECM-substrates were used, in which the increase in fluorescence is used to quantify the proteolytic activity of venom (components). In order to identify the bioactive toxins, the venoms were nanofractionated using size-exclusion chromatography followed by post-column plate reader-based bioassaying, measuring proteolytic activity. The reason why SEC was used instead of the for analytical post-column bioassaying of venom toxins often used 'conventional' reversed-phase separation is because reversed-phase mobile phases used for separation have a detrimental effect on the proteolytic activity of many proteolytic venom toxins. In addition, for each venom investigated this way, a second SEC separation was followed for subsequent toxin identification by HT venomics. The approach presented in Chapter 5 allowed to explore

the proteinase activity of crude and fractionated venoms in a high-throughput manner without losing the proteinase activity of venom toxins.

Chapter 6 describes the development of a bioassay that can be used to study venom-induced membrane-disrupting activity and that is suitable for high-throughput screening of crude and fractionated venoms. This assay involved chicken egg yolk to create phospholipid vesicles that were fluorescently dyed, allowing the study of the degradation of these vesicles on a fluorescence plate reader. The first part of this study focused on the development and optimisation of the assay, followed by assay validation using a panel of medically relevant snake species. Subsequent neutralisation studies with a dedicated PLA_2 inhibitor (i.e., varespladib) confirmed that the responsible toxins were likely to be part of the PLA_2 family. To further ensure the involvement of PLA_2s, two venoms were separated using RP-LC followed by high-resolution fractionation. The venom fractions were then subjected to this assay, and the responsible toxins were characterised using HT venomics. These findings highlight the potential for screening of PLA_2 activity in both crude and fractionated venoms, as well as for conducting PLA_2 activity neutralisation studies.

Of the diverse clinical manifestations that may occur after snakebite, local and systemic haemorrhage are of particular relevance, as this may result in ischemia, organ failure and cardiovascular shock. **Chapter 7** describes the development of a three-dimensional blood vessel model that allows us to study the effects of tissue-damaging snake venoms on a system that mimics *in vivo* conditions. In an attempt to take the study of tissue-damaging toxins a step further, we used organ-on-a-chip technology to investigate the effect of snake venoms on microvasculature. This technology involves creating 3D models that mimic the structure and function of human organs on small chips or platforms. Therefore, this system is an advancement of 'traditional' cell-culturing studies, such as the cell assays described in Chapter 3. The advantage of using a 3D-blood vessel model over 'traditional' cell-culturing assays is that the former includes several important physiological parameters such as 3D-tubular morphology, interaction with an ECM and exposure to flow. The use of this model allowed the study of tissue-damaging venom effects on a system that mimics *in vivo* conditions.

The model was validated using a selection of medically relevant snake species. Because this was the first time that this blood vessel model was used for studying venom toxicity, only crude venoms (and not yet purified toxins) were investigated. The use of this model may shed light on the key mechanisms by which tissue-damaging venoms exert their effects on the capillary vessels.

Chapter 8 will conclude this thesis, discuss remaining challenges and describe venom-induced cell and tissue damage from a broader perspective.

Finally, **Chapter 9** will summarise the work described in this thesis in both English and Dutch.

References

1. Pyron, R. A., Burbrink, F. T. & Wiens, J. J. A phylogeny and revised classification of Squamata, including 4161 species of lizards and snakes. *BMC Evol. Biol.* **13**, (2013).
2. The Reptile Database (search: Serpentes). https://reptile-database.reptarium.cz/search?search=serpentes&submit=Search.
3. Caldwell, M. W. 'Without a leg to stand on': on the evolution and development of axial elongation and limblessness in tetrapods. *Can. J. Earth Sci.* **40**, (2003).
4. Woltering, J. M. *et al.* Axial patterning in snakes and caecilians: Evidence for an alternative interpretation of the Hox code. *Dev. Biol.* **332**, 82–89 (2009).
5. Carroll, R. L. *Vertebrate paleontology and evolution. Vertebrate paleontology and evolution.* (1988). doi:10.2307/3514548.
6. The Reptile Database (search: Caenophidia).
7. Kerkkamp, H. M. I., Casewell, N. R., Vonk, F. J., Reid, A. & Group, E. Evolution of Venomous Animals and Their Toxins. *Evol. Venom. Anim. Their Toxins* 1–11 (2015) doi:10.1007/978-94-007-6727-0.
8. Vonk, F. J. *et al.* Evolutionary origin and development of snake fangs. *Nature* **454**, 630–633 (2008).
9. Mackessy, S. P. *Handbook of Venoms and Toxins of Reptiles*. *Handbook of Venoms and Toxins of Reptiles* (CRC Press, 2021). doi:10.1201/9780429054204.
10. Kochva, E. The origin of snakes and evolution of the venom apparatus. *Toxicon* **25**, 65–106 (1987).
11. Mackessy, S. P. Morphology and ultrastructure of the venom glands of the northern pacific rattlesnake Crotalus viridis oreganus. *J. Morphol.* **208**, 109–128 (1991).
12. Mackessy, S. P. & Baxter, L. M. Bioweapons synthesis and storage: The venom gland of front-fanged snakes. *Zool. Anz.* **245**, 147–159 (2006).
13. Rosenberg, H. I. Histology, histochemistry, and emptying mechanism of the venom glands of some elapid snakes. *J. Morphol.* **123**, 133–155 (1967).
14. Weinstein, S. A., Smith, T. L. & Kardong, K. V. Reptile venom glands : form, function, and future. *Handb. Venoms Toxins Reptil.* 65–92 (2009).
15. Kardong, K. V. Colubrid snakes and Duvernoy's 'venom' glands. *J. Toxicol. - Toxin Rev.* **21**, 1–19 (2002).
16. Kardong, K. V. Snake toxins and Venoms: an evolutionary perspective. *Herpetologica* **52**, 36–46 (1996).
17. Fry, B. G. *et al.* Analysis of Colubroidea snake venoms by liquid chromatography with mass spectrometry: Evolutionary and toxinological implications. *Rapid Commun. Mass Spectrom.* **17**, 2047–2062 (2003).
18. Mackessy, S. P. & Saviola, A. J. Understanding Biological Roles of Venoms Among the Caenophidia: The Importance of Rear-Fanged Snakes. *Integr. Comp. Biol.* **56**, 1004–1021 (2016).
19. Jackson, K. The evolution of venom-conducting fangs: Insights from developmental biology. *Toxicon* **49**, 975–981 (2007).
20. Young, B.A., Kardong, K. V. Dentitional surface features in snakes (Reptilia: Serpentes). *Amphibia-Reptilia* **17**, 261–276 (1996).
21. Gutiérrez, J. M. *et al.* Snakebite envenoming. *Nat. Rev. Dis. Prim.* **3**, (2017).
22. The Reptile Database (search: Atractaspididae).

23. Warrell, D. A. Guidelines of Management of Snake bite. *Lancet* **375**, 77–88 (2010).

24. Kasturiratne, A. *et al.* The global burden of snakebite: A literature analysis and modelling based on regional estimates of envenoming and deaths. *PLoS Med.* **5**, 1591–1604 (2008).

25. Habib, A. G. *et al.* Snakebite is Under Appreciated: Appraisal of Burden from West Africa. *PLoS Negl. Trop. Dis.* **9**, 4–11 (2015).

26. Gutiérrez, J. M., Theakston, R. D. G. & Warrell, D. A. Confronting the neglected problem of snake bite envenoming: The need for a global partnership. *PLoS Med.* **3**, 0727–0731 (2006).

27. Williams, D. J. *et al.* Ending the drought: New strategies for improving the flow of affordable, effective antivenoms in Asia and Africa. *J. Proteomics* **74**, 1735–1767 (2011).

28. Chippaux, J. P. Snakebite envenomation turns again into a neglected tropical disease! *J. Venom. Anim. Toxins Incl. Trop. Dis.* **23**, 1–2 (2017).

29. Longbottom, J. *et al.* Vulnerability to snakebite envenoming : a global mapping of hotspots. *Lancet* **392**, 673–684 (2018).

30. Williams, D. *et al.* The Global Snake Bite Initiative: an antidote for snake bite. *Lancet* **375**, 89–91 (2010).

31. Harrison, R. A. *et al.* Research strategies to improve snakebite treatment: Challenges and progress. *J. Proteomics* **74**, 1768–1780 (2011).

32. Warrell, D. A. Snake bite. *Lancet* **375**, 77–88 (2010).

33. Chippaux, J.-P., Massougbodji, A., Diouf, A., Baldé, C. M. & Boyer, L. V. Snake bites and antivenom shortage in Africa. *Lancet* **386**, 2252–2253 (2015).

34. Slagboom, J., Kool, J., Harrison, R. A. & Casewell, N. R. Haemotoxic snake venoms: their functional activity, impact on snakebite victims and pharmaceutical promise. *Br. J. Haematol.* **177**, 947–959 (2017).

35. Kini, R. M., Sidhu, S. S. & Laustsen, A. H. Biosynthetic oligoclonal antivenom (BOA) for snakebite and next-generation treatments for snakebite victims †. *Toxins (Basel).* **10**, (2018).

36. WHO Regional Office for Asia. Guidelines for the management of snakebites (2nd edition). *World Heal. Organ.* (2016).

37. Fry, B. G. *Venomous reptiles and their toxins: evolution, pathophysiology and biodiscovery. Oxford University Press, Oxford University Press.* (2015). doi:10.1016/0041-0101(71)90017-1.

38. Gutiérrez, J. M., León, G., Lomonte, B. & Angulo, Y. Antivenoms for snakebite envenomings. *Inflamm. Allergy - Drug Targets* **10**, 369–380 (2011).

39. Bermúdez-Méndez, E. *et al.* Innovative immunization strategies for antivenom development. *Toxins (Basel).* **10**, 1–37 (2018).

40. Williams, D. J., Habib, A. G. & Warrell, D. A. Clinical studies of the effectiveness and safety of antivenoms. *Toxicon* **150**, 1–10 (2018).

41. Theakston, R. D. G. & Warrell, D. A. Crisis in snake antivenom supply for Africa [14]. *Lancet* **356**, 2104 (2000).

42. WHO Regional Office for Africa. Guidelines for the prevention and clinical management of snakebite in Africa. *WHO Reg. Off. Africa* 1–145 (2010).

43. Julian White, J. M. *Handbook of Clinical Toxicology of Animal Venoms and Poisons*. (CRC Press, 1995). doi:doi.org/10.1201/9780203719442.

44. Casewell, N. R., Wüster, W., Vonk, F. J., Harrison, R. A. & Fry, B. G. Complex cocktails: The evolutionary novelty of venoms. *Trends Ecol. Evol.* **28**, 219–229 (2013).

45. Fox, J. W. & Serrano, S. M. T. Exploring snake venom proteomes: Multifaceted analyses for complex toxin mixtures. *Proteomics* **8**, 909–920 (2008).

46. Fry, B. G. *et al.* The Toxicogenomic Multiverse : Convergent Recruitment of Proteins Into Animal Venoms. *Annu. Rev. genomcs Hum. Genet.* **10**, 483–511 (2009).

47. Jackson, T. N. W. *et al.* Rapid radiations and the race to redundancy: An investigation of the evolution of Australian elapid snake venoms. *Toxins (Basel).* **8**, 1–24 (2016).

48. Kazandjian, T. D. *et al.* Convergent evolution of pain-inducing defensive venom components in spitting cobras. *Science (80-.).* **371**, 386–390 (2021).

49. Casewell, N. R., Jackson, T. N. W., Laustsen, A. H. & Sunagar, K. Causes and Consequences of Snake Venom Variation. *Trends Pharmacol. Sci.* **41**, 570–581 (2020).

50. Alape-Girón, A. *et al.* Snake venomics of the lancehead pitviper bothrops asper. Geographic, individual, and ontogenetic variations. *J. Proteome Res.* **7**, 3556–3571 (2008).

51. Sunagar, K. *et al.* Intraspecific venom variation in the medically significant Southern Pacific Rattlesnake (Crotalus oreganus helleri): biodiscovery, clinical and evolutionary implications. *J. Proteomics* **99**, 68–83 (2014).

52. van Thiel, J. *et al.* Highly Evolvable: Investigating Interspecific and Intraspecific Venom Variation in Taipans (Oxyuranus spp.) and Brown Snakes (Pseudonaja spp.). *Toxins (Basel).* **15**, (2023).

53. Rashmi, U. *et al.* Remarkable intrapopulation venom variability in the monocellate cobra (Naja kaouthia) unveils neglected aspects of India's snakebite problem. *J. Proteomics* **242**, 104256 (2021).

54. Smiley-Walters, S. A., Farrell, T. M. & Lisle Gibbs, H. High levels of functional divergence in toxicity towards prey among the venoms of individual pigmy rattlesnakes. *Biol. Lett.* **15**, (2019).

55. Durban, J. *et al.* Integrated 'omics' profiling indicates that miRNAs are modulators of the ontogenetic venom composition shift in the Central American rattlesnake, Crotalus simus simus. *BMC Genomics* **14**, 1–17 (2013).

56. Mackessy, S. P. Venom Ontogeny in the Pacific Rattlesnakes Crotalus viridis helleri and C. v. oreganus. *Copeia* **1988**, 92 (1988).

57. Senji Laxme, R. R. *et al.* Biogeographic venom variation in Russell's viper (Daboia russelii) and the preclinical inefficacy of antivenom therapy in snakebite hotspots. *PLoS Negl. Trop. Dis.* **15**, 1–26 (2021).

58. Richards, D. P., Barlow, A. & Wüster, W. Venom lethality and diet: Differential responses of natural prey and model organisms to the venom of the saw-scaled vipers (Echis). *Toxicon* **59**, 110–116 (2012).

59. Amazonas, D. R. *et al.* Molecular mechanisms underlying intraspecific variation in snake venom. *J. Proteomics* **181**, 60–72 (2018).

60. Tasoulis, T. & Isbister, G. K. A review and database of snake venom proteomes. *Toxins (Basel).* **9**, (2017).

61. Utkin, Y. N. Three-finger toxins, a deadly weapon of elapid venom - Milestones of discovery. *Toxicon* **62**, 50–55 (2013).

62. Fry, B. G. *et al.* Molecular evolution and phylogeny of elapid snake venom three-finger toxins. *J. Mol. Evol.* **57**, 110–129 (2003).

63. Gopalakrishnakone, P., Inagaki, H., Vogel, C., Mukherjee, A. K. & Rahmy, T. R. *Snake Venoms*. (Springer Berlin, Germany., 2017).

64. Harris, J. B. & Scott-Davey, T. Secreted Phospholipases A 2 of Snake Venoms: Effects on the Peripheral Neuromuscular System with Comments on the Role of Phospholipases A 2 in Disorders of the CNS and Their Uses in Industry. *Toxins (Basel).* **5**, 2533–2571 (2013).

65. Isbister, G. K. *et al.* Factor deficiencies in venom-induced consumption coagulopathy resulting from Australian elapid envenomation: Australian Snakebite Project (ASP-10). *J. Thromb. Haemost.* **8**, 2504–2513 (2010).

66. Maduwage, K. & Isbister, G. K. Current Treatment for Venom-Induced Consumption Coagulopathy Resulting from Snakebite. doi:10.1371/journal.pntd.0003220.

67. Gutiérrez, J. M., Rucavado, A., Escalante, T. & Díaz, C. Hemorrhage induced by snake venom metalloproteinases: Biochemical and biophysical mechanisms involved in microvessel damage. *Toxicon* **45**, 997–1011 (2005).

68. Escalante, T. *et al.* Role of collagens and perlecan in microvascular stability: Exploring the mechanism of capillary vessel damage by snake venom metalloproteinases. *PLoS One* **6**, (2011).

69. Gutiérrez, J. M., Escalante, T., Rucavado, A. & Herrera, C. Hemorrhage caused by snake venom metalloproteinases: A journey of discovery and understanding. *Toxins (Basel).* **8**, (2016).

70. Gutiérrez, J. M., Escalante, T., Rucavado, A., Herrera, C. & Fox, J. W. A comprehensive view of the structural and functional alterations of extracellular matrix by snake venom metalloproteinases (SVMPs): Novel perspectives on the pathophysiology of envenoming. *Toxins (Basel).* **8**, (2016).

71. Gutiérrez, J. M. & Rucavado, A. Snake venom metalloproteinases: Their role in the pathogenesis of local tissue damage. *Biochimie* **82**, 841–850 (2000).

72. Jiménez, N., Escalante, T., Gutiérrez, J. M. & Rucavado, A. Skin pathology induced by snake venom metalloproteinase: Acute damage, revascularization, and re-epithelization in a mouse ear model. *J. Invest. Dermatol.* **128**, 2421–2428 (2008).

73. Montecucco, C., Gutiérrez, J. M. & Lomonte, B. Cellular pathology induced by snake venom phospholipase A2 myotoxins and neurotoxins: Common aspects of their mechanisms of action. *Cell. Mol. Life Sci.* **65**, 2897–2912 (2008).

74. Gasanov, S. E., Dagda, R. K. & Rael, E. D. Snake Venom Cytotoxins, Phospholipase A2 s, and Zn2+ -dependent Metalloproteinases: Mechanisms of Action and Pharmacological Relevance. *J. Clin. Toxicol.* **4**, (2014).

75. Hayashi, M. A. F. *et al.* Cytotoxic effects of crotamine are mediated through lysosomal membrane permeabilization. *Toxicon* **52**, 508–517 (2008).

76. Gutiérrez, J. M. & Ownby, C. L. Skeletal muscle degeneration induced by venom phospholipases A2: insights into the mechanisms of local and systemic myotoxicity. *Toxicon* **42**, 915–931 (2003).

77. Kini, R. M. & Doley, R. Structure, function and evolution of three-finger toxins: Mini proteins with multiple targets. *Toxicon* **56**, 855–867 (2010).

78. Sunagar, K. *et al.* Three-fingered RAVERs: Rapid Accumulation of Variations in Exposed Residues of snake venom toxins. *Toxins (Basel).* **5**, 2172–2208 (2013).

79. Markland, F. S. & Swenson, S. Snake venom metalloproteinases. *Toxicon* **62**, 3–18 (2013).

80. Girish, K. S., Jagadeesha, D. K., Rajeev, K. B. & Kemparaju, K. Snake venom hyaluronidase: An evidence for isoforms and extracellular matrix degradation. *Mol. Cell. Biochem.* **240**, 105–110 (2002).

81. Bittenbinder, M. A. *et al.* Development of a high-throughput in vitro screening method for the assessment of cell-damaging activities of snake venoms. *PLoS Negl. Trop. Dis.* **17**, e0011564 (2023).

82. Du, X. Y. & Clemetson, K. J. Snake venom L-amino acid oxidases. *Toxicon* **40**, 659–665 (2002).

83. Cesar, P. H. S., Braga, M. A., Trento, M. V. C., Menaldo, D. L. & Marcussi, S. Snake Venom Disintegrins: An Overview of their Interaction with Integrins. *Curr. Drug Targets* **20**, 465–477 (2018).

84. Eble, J. A. Structurally robust and functionally highly versatile—C-type lectin (-related) proteins in snake venoms. *Toxins (Basel).* **11**, (2019).

85. Bénard-Valle, M. *et al.* Antivenom research and development. in *Venomous Reptiles and Their Toxins: Evolution, Pathophysiology and Biodiscovery; Fry, B.G., Ed.; Oxford University Press: New York, NY, USA* 61–72 (2015).

86. Escalante, T. *et al.* Wound exudate as a proteomic window to reveal different mechanisms of tissue damage by snake venom toxins. *J. Proteome Res.* **8**, 5120–5131 (2009).

87. Escalante, T., Rucavado, A., Fox, J. W. & Gutiérrez, J. M. Key events in microvascular damage induced by snake venom hemorrhagic metalloproteinases. *J. Proteomics* **74**, 1781–1794 (2011).

88. Herrera, C. *et al.* Tissue Localization and Extracellular Matrix Degradation by PI, PII and PIII Snake Venom Metalloproteinases: Clues on the Mechanisms of Venom-Induced Hemorrhage. *PLoS Negl. Trop. Dis.* **9**, 1–20 (2015).

89. Gutiérrez, J. M., Núñez, J., Escalante, T. & Rucavado, A. Blood flow is required for rapid endothelial cell damage induced by a snake venom hemorrhagic metalloproteinase. *Microvasc. Res.* **71**, 55–63 (2006).

90. Menaldo, D. L. *et al.* Effects of two serine proteases from Bothrops pirajai snake venom on the complement system and the inflammatory response. *Int. Immunopharmacol.* **15**, 764–771 (2013).

91. Oliveira, J. S. *et al.* Local and hematological alterations induced by Philodryas olfersii snake venom in mice. (2017) doi:10.1016/j.toxicon.2017.03.013.

92. Hodgson, Wayne C., Wickramaratna, J. C. Animal Toxins of Asia and Australia: In vitro neuromuscular activity of snake venoms. *Clin. Exp. Pharmacol. Physiol.* 807–814 (2002).

93. Stransky, S. *et al.* In vitro assessment of cytotoxic activities of Lachesis muta muta snake venom. *PLoS Negl. Trop. Dis.* **12**, 1–17 (2018).

94. Patel, R. N. *et al.* An in vitro assay to investigate venom neurotoxin activity on muscle-type nicotinic acetylcholine receptor activation and for the discovery of toxin-inhibitory molecules. *Biochem. Pharmacol.* **216**, 115758 (2023).

95. Slagboom, J. *et al.* High throughput screening and identification of coagulopathic snake venom proteins and peptides using nanofractionation and proteomics approaches. *PLoS Negl. Trop. Dis.* **14**, 1–26 (2020).

96. Gutiérrez, J. M. *et al.* In Vitro Tests for Assessing the Neutralizing Ability of Snake Antivenoms: Toward the 3Rs Principles. *Front. Immunol.* **11**, (2021).

97. Theakston, R. D. G. & Reid, H. A. Development of simple standard assay procedures for the characterization of snake venoms. *Bull. World Health Organ.* **61**, 949–956 (1983).

98. Kondo, H., Kondo, S., Ikezawa, H. & Ohsaka, A. Studies on the quantitative method for determination of hemorrhagic activity of habu snake venom. *Japanese J. Med. Sci. Biol.* **13**, 43–51 (1960).

99. Biardi, J. E., Nguyen, K. T., Lander, S., Whitley, M. & Nambiar, K. P. A rapid and sensitive fluorometric method for the quantitative analysis of snake venom metalloproteases and their inhibitors. *Toxicon* **57**, 342–347 (2011).

100. Riss, T. L. *et al.* Cell Viability Assays. *Assay Guid. Man.* 1–25 (2004).

101. Terry Riss, Andrew Niles, Rich Moravec, Natashia Karassina & Jolanta Vidugiriene. Cytotoxicity Assays: In Vitro Methods to Measure Dead Cells. *Assay Guid. Man. [Internet]* 1–15 (2019).

102. Riss, T. L. & Moravec, R. A. Use of multiple assay endpoints to investigate the effects of incubation time, dose of toxin, and plating density in cell-based cytotoxicity assays. *Assay Drug Dev. Technol.* **2**, 51–62 (2004).

103. O'Brien, J., Wilson, I., Orton, T. & Pognan, F. Investigation of the Alamar Blue (resazurin) fluorescent dye for the assessment of mammalian cell cytotoxicity. *Eur. J. Biochem.* **267**, 5421–5426 (2000).

104. Hamid, R., Rotshteyn, Y., Rabadi, L., Parikh, R. & Bullock, P. Comparison of alamar blue and MTT assays for high through-put screening. *Toxicol. Vitr.* **18**, 703–710 (2004).

105. Castaño, A. & Tarazona, J. V. ATP assay on cell monolayers as an index of cytotoxicity. *Bull. Environ. Contam. Toxicol.* **53**, 309–316 (1994).

106. Lundin, A., Hasenson, M., Persson, J. & Pousette, Å. Estimation of Biomass in Growing Cell Lines by Adenosine Triphosphate Assay. *Methods Enzymol.* **133**, 27–42 (1986).

107. Squatrito, R. C., Connor, J. P. & Buller, R. E. Comparison of a Novel Redox Dye Cell Growth Assay to the ATP Bioluminescence Assay. *Gynecol. Oncol.* **58**, 101–105 (1995).

108. Wlodkowic, D. *et al.* Kinetic Viability Assays Using DRAQ7 Probe. *Curr. Protoc. Cytom.* **65**, 9.41.1-9.41.8 (2013).

109. Akagi, J. *et al.* Real-time cell viability assays using a new anthracycline derivative DRAQ7®. *Cytom. Part A* **83A**, 227–234 (2013).

110. Chiaraviglio, L. & Kirby, J. E. Evaluation of Impermeant, DNA-Binding Dye Fluorescence as a Real-Time Readout of Eukaryotic Cell Toxicity in a High Throughput Screening Format. *https://home.liebertpub.com/adt* **12**, 219–228 (2014).

111. Decker, T. & Lohmann-Matthes, M. L. A quick and simple method for the quantitation of lactate dehydrogenase release in measurements of cellular cytotoxicity and tumor necrosis factor (TNF) activity. *J. Immunol. Methods* **115**, 61–69 (1988).

112. Korzeniewski, C. & Callewaert, D. M. An enzyme-release assay for natural cytotoxicity. *J. Immunol. Methods* **64**, 313–320 (1983).

113. Huang, M. Z., Wang, Q. C. & Liu, G. F. Effects of an acidic phospholipase A2 purified from Ophiophagus hannah (king cobra) venom on rat heart. *Toxicon* **31**, 627–635 (1993).

114. Kupai, K. *et al.* Matrix metalloproteinase activity assays: Importance of zymography. *J. Pharmacol. Toxicol. Methods* **61**, 205–209 (2010).

115. Bee, A., Theakston, R. D. G., Harrison, R. A. & Carter, S. D. Novel in vitro assays for assessing the haemorrhagic activity of snake venoms and for demonstration of venom metalloproteinase inhibitors. *Toxicon* **39**, 1429–1434 (2001).

116. Lombard, C., Saulnier, J. & Wallach, J. Assays of matrix metalloproteinases (MMPs) activities: A review. *Biochimie* **87**, 265–272 (2005).

117. Roldán-Padrón, O. *et al.* Snake venom hemotoxic enzymes: Biochemical comparison between Crotalus species from central Mexico. *Molecules* **24**, 1–16 (2019).

118. Quesada, A. R. *et al.* Evaluation of fluorometric and zymographic methods as activity assays for stromelysins and gelatinases. *Clin. Exp. Metastasis* **15**, 26–32 (1997).

119. Leonard, A. K. *et al. Methods for the visualization and analysis of extracellular matrix protein structure and degradation*. *Methods in Cell Biology* vol. 143 (Elsevier Inc., 2018).

120. Petrovic, N., Grove, C., Langton, P. E., Misso, N. L. A. & Thompson, P. J. A simple assay for a human serum phospholipase A2 that is associated with high-density lipoproteins. *J. Lipid Res.* **42**, 1706–1713 (2001).

121. Sharko, O. & Kisel, M. 1-Acyl-2-[N-(2,4-dinitrophenyl)aminopropionyl]-sn-glycero-3-phosphocholine as a chromogenic substrate for phospholipase A2 assay. *Anal. Biochem.* **413**, 69–71 (2011).

122. Darrow, A. L. *et al.* A novel fluorogenic substrate for the measurement of endothelial lipase activity. *J. Lipid Res.* **52**, 374–382 (2011).

123. Mitnaul, L. J. *et al.* Fluorogenic substrates for high-throughput measurements of endothelial lipase activity. *J. Lipid Res.* **48**, 472–482 (2007).

124. Aufenanger, J., Zimmer, W. & Kattermann, R. Characteristics and clinical application of a radiometric Escherichia coli-based phospholipase A2 assay modified for serum analysis. *Clin. Chem.* **39**, 605–613 (1993).

125. Katsumata, M., Gupta, C. & Goldman, A. S. A rapid assay for activity of phospholipase A2 using radioactive substrate. *Anal. Biochem.* **154**, 676–681 (1986).

126. Condrea, E., De Vries, A., Mager, J. Action of snake-venom phospholipase a on free and lipoprotein-bound phospholipids. *Biochim. Biophys. Acta* **58**, 389–397 (1962).

127. Still, K. B. M. *et al.* Development of high-throughput screening assays for profiling snake venom phospholipase A2 activity after chromatographic fractionation. *Toxicon* **184**, 28–38 (2020).

128. Price, J. A. A colorimetric assay for measuring phospholipase A2 degradation of phosphatidylcholine at physiological pH. *J. Biochem. Biophys. Methods* **70**, 441–444 (2007).

129. Marinetti, G. V. The action of phospholipase A on lipoproteins. *Biochim. Biophys. Acta (BBA)/Lipids Lipid Metab.* **98**, 554–565 (1965).

130. Joubert, F. J. & Taljaard, N. Purification, Some Properties and Amino-Acid Sequences of Two Phospholipases A (CM-II and CM-III) from Naja naja kaouthia Venom. *Eur. J. Biochem.* **112**, 493–499 (1980).

131. Senji Laxme, R. R. *et al.* Beyond the 'Big four': Venom profiling of the medically important yet neglected Indian snakes reveals disturbing antivenom deficiencies. *PLoS Negl. Trop. Dis.* **13**, e0007899 (2019).

132. Senji Laxme, R. R. *et al.* Biogeographical venom variation in the indian spectacled cobra (Naja naja) underscores the pressing need for pan-india efficacious snakebite therapy. *PLoS Negl. Trop. Dis.* **15**, 1–28 (2021).

133. Menzel, E. J. & Farr, C. Hyaluronidase and its substrate hyaluronan: Biochemistry, biological activities and therapeutic uses. *Cancer Lett.* **131**, 3–11 (1998).

134. Girish, K. S. & Kemparaju, K. The magic glue hyaluronan and its eraser hyaluronidase: A biological overview. *Life Sci.* **80**, 1921–1943 (2007).

135. Meyer, K. Chapter 11 - Hyaluronidases. in *The Enzymes* vol. 5 307–320 (1971).

136. Reissig, J. L., Storminger, J. L. & Leloir, l. F. A modified colorimetric method for the estimation of n-acetylamino sugars. *J. Biol. Chem.* **217**, 959–966 (1955).

137. Csóka, T. B., Frost, G. I., Wong, T. & Stern, R. Purification and microsequencing of hyaluronidase isozymes from human urine. *FEBS Lett.* **417**, 307–310 (1997).

138. Guntenhöner, M. W., Pogrel, M. A. & Stern, R. A substrate-gel assay for hyaluronidase activity. *Matrix* **12**, 388–396 (1992).

139. Stern, M. & Stern, R. An ELISA-like assay for hyaluronidase and hyaluronidase inhibitors. *Matrix* **12**, 397–403 (1992).

140. Frost, G. I. & Stern, R. A Microtiter-Based Assay for Hyaluronidase Activity Not Requiring Specialized Reagents. *Anal. Biochem.* **251**, 263–269 (1997).

141. Afify, A.M., Stern, M., Guntenhöner, M., Stern, R. Purification and characterization of human serum hyaluronidase. *Arch. Biochem. Biophys.* **305**, 434–441 (1993).

142. Klibansky, C., London, Y., Frenkel, A. & De Vries, A. Enhancing action of synthetic and natural basic polypeptides on erythrocyte-ghost phospholipid hydrolysis by phospholipase A. *Biochim. Biophys. Acta - Biomembr.* **150**, 15–23 (1968).

143. Louw, A. I. & Visser, L. The synergism of cardiotoxin and phospholipase A2 in hemolysis. *BBA - Biomembr.* **512**, 163–171 (1978).

144. Bougis, P. E., Marchot, P. & Rochat, H. In vivo synergy of cardiotoxin and phospholipase A2 from the elapid snake Naja mossambica mossambica. *Toxicon* **25**, 427–431 (1987).

145. Chaim-matyas, A. & Ovadia, M. Cytotoxic activity of various snake venoms on melanoma, B16F10 and Chondrosarcoma. *Life Sci.* **40**, 1601–1607 (1987).

146. Pucca, M. B. *et al.* Unity Makes Strength: Exploring Intraspecies and Interspecies Toxin Synergism between Phospholipases A2 and Cytotoxins. *Front. Pharmacol.* **11**, 1–10 (2020).

147. El-Aziz, T. M. A. *et al.* Efficient functional neutralization of lethal peptide toxins in vivo by oligonucleotides. *Sci. Reports 2017 71* **7**, 1–9 (2017).

148. Laemmli, U. K. Cleavage of Structural Proteins during the Assembly of the Head of Bacteriophage T4. *Nature* **227**, 680–685 (1970).

149. Kurien, B.T., Scofield, R. H. *Protein Electrophoresis - Methods and Protocols*. (2012). doi:https://doi.org/10.1007/978-1-61779-821-4.

150. Abd El-Aziz, T. M., Soares, A. G. & Stockand, J. D. Advances in venomics: Modern separation techniques and mass spectrometry. *J. Chromatogr. B Anal. Technol. Biomed. Life Sci.* **1160**, 122352 (2020).

151. Sahyoun, C. *et al.* Separation and Analytical Techniques Used in Snake Venomics: A Review Article. *Processes* vol. 10 1380 at https://doi.org/10.3390/pr10071380 (2022).

152. Franco-Servín, C. *et al.* Biological and biochemical characterization of coronado island rattlesnake (Crotalus helleri caliginis) venom and antivenom neutralization. *Toxins (Basel).* **13**, 582 (2021).

153. Tan, C. H. *et al.* Enzymatic and toxinological activities of Hypnale hypnale (hump-nosed pit viper) venom and its fractionation by ion exchange high performance liquid chromatography. *J. Venom. Anim. Toxins Incl. Trop. Dis.* **17**, 473–485 (2011).

154. Fekete, S., Beck, A., Veuthey, J. L. & Guillarme, D. Ion-exchange chromatography for the characterization of biopharmaceuticals. *J. Pharm. Biomed. Anal.* **113**, 43–55 (2015).

155. Hage, D. S. & Matsuda, R. Affinity chromatography: A historical perspective. *Methods Mol. Biol.* **1286**, 1–19 (2015).

156. Gomes, P. C. *et al.* The co-purification of a lectin (BJcuL) with phospholipases A2 from Bothrops jararacussu snake venom by immunoaffinity chromatography with antibodies to crotoxin. *Toxicon* **49**, 1099–1108 (2007).

157. Hagel, L. Gel Filtration: Size Exclusion Chromatography. *Protein Purif. Princ. High Resolut. Methods, Appl. Third Ed.* 51–91 (2011) doi:10.1002/9780470939932.CH3.

158. Cutler, P. Size-exclusion chromatography. *Methods Mol. Biol.* **244**, 239–252 (2004).

159. Mant, C. T. & Hodges, R. S. [1] Analysis of peptides by high-performance liquid chromatography. *Methods Enzymol.* **271**, 3–50 (1996).

160. Aguilar, M. I. & Hearn, M. T. W. [1] High-resolution reversed-phase high-performance liquid chromatography of peptides and proteins. *Methods Enzymol.* **270**, 3–26 (1996).

161. McCleary, R. J. R. & Kini, R. M. Non-enzymatic proteins from snake venoms: A gold mine of pharmacological tools and drug leads. *Toxicon* **62**, 56–74 (2013).

162. Hühmer, A.F.R., Aced, G.I., Perkins, M.D., Gürsoy, R.N., Jois, D.S.S., Larive, C., Siahaan, T.J., Schöneich, C. Separation and analysis of peptides and proteins. *Anal. Chem.* **69**, (1997).

163. Hodges', S. J., Agbaji', A. S., Harvey', A. L., Hider', R. C. & Hider, R. C. *Cobra cardiotoxins Purification, effects on skeletal muscle and structure/activity relationships. Eur. J. Biochem* vol. 165 (1987).

164. Mukherjee, A. K., Kalita, B. & Thakur, R. Two acidic, anticoagulant PLA2 isoenzymes purified from the venom of monocled cobra Naja kaouthia exhibit different potency to inhibit thrombin and factor Xa via phospholipids independent, non-enzymatic mechanism. *PLoS One* **9**, (2014).

165. Mladic, M. *et al.* At-line nanofractionation with parallel mass spectrometry and bioactivity assessment for the rapid screening of thrombin and factor Xa inhibitors in snake venoms. *Toxicon* **110**, 79–89 (2016).

166. Otvos, R. A., Still, K. B. M., Somsen, G. W., Smit, A. B. & Kool, J. Drug Discovery on Natural Products: From Ion Channels to nAChRs, from Nature to Libraries, from Analytics to Assays. *SLAS Discov.* **24**, 362–385 (2019).

167. Dauplais, M., Neumann, J. M., Pinkasfeld, S., Ménez, A. & Roumestand, C. An NMR Study of the Interaction of Cardiotoxin γ from Naja nigricollis with Perdeuterated Dodecylphosphocholine Micelles. *Eur. J. Biochem.* **230**, 213–220 (1995).

168. Neumann, C. *et al.* Development of a generic high-throughput screening assay for profiling snake venom protease activity after high-resolution chromatographic fractionation. *Toxicon* **178**, 61–68 (2020).

169. Mladic, M. *et al.* Rapid screening and identification of ACE inhibitors in snake venoms using at-line nanofractionation LC-MS. *Anal. Bioanal. Chem.* **409**, 5987–5997 (2017).

170. Zietek, B. M. *et al.* Nanofractionation Platform with Parallel Mass Spectrometry for Identification of CYP1A2 Inhibitors in Metabolic Mixtures. *SLAS Discov.* **23**, 283–293 (2018).

171. Zietek, B. M. *et al.* Liquid chromatographic nanofractionation with parallel mass spectrometric detection for the screening of plasmin inhibitors and (metallo)proteinases in snake venoms. *Anal. Bioanal. Chem.* **410**, 5751–5763 (2018).

172. Slagboom, J. *et al.* High-Throughput Venomics. *J. Proteome Res.* **22**, 1734–1746 (2023).

173. Slagboom, J. *et al.* Analytical strategies in venomics. *Microchem. J.* **175**, 107187 (2022).

174. Palermo, G. *et al.* Acetylcholine-Binding Protein Affinity Profiling of Neurotoxins in Snake Venoms with Parallel Toxin Identification. *Int. J. Mol. Sci.* **24**, 16769 (2023).

175. Calvete, J. J. Proteomic tools against the neglected pathology of snake bite envenoming. *Expert Rev. Proteomics* **8**, 739–758 (2011).

176. Juárez, P., Sanz, L. & Calvete, J. J. Snake venomics: Characterization of protein families in Sistrurus barbouri venom by cysteine mapping, N-terminal sequencing, and tandem mass spectrometry analysis. in *Proteomics* vol. 4 327–338 (John Wiley & Sons, Ltd, 2004).

177. Wilson, D. & Daly, N. L. Venomics: A Mini-Review. *High-Throughput* **7**, (2018).

178. Petras, D., Heiss, P., Süssmuth, R. D. & Calvete, J. J. Venom proteomics of indonesian king cobra, ophiophagus hannah: Integrating top-down and bottom-up approaches. *J. Proteome Res.* **14**, 2539–2556 (2015).

179. Calvete, J. J., Sanz, L., Angulo, Y., Lomonte, B. & Gutiérrez, J. M. Venoms, venomics, antivenomics. *FEBS Lett.* **583**, 1736–1743 (2009).

180. Calvete, J. J. Next-generation snake venomics: Protein-locus resolution through venom proteome decomplexation. *Expert Review of Proteomics* vol. 11 315–329 at https://doi.org/10.1586/14789450.2014.900447 (2014).

181. Calvete, J. J. Snake venomics – from low-resolution toxin-pattern recognition to toxin-resolved venom proteomes with absolute quantification. *Expert Rev. Proteomics* **15**, 555–568 (2018).

182. Calderón-Celis, F., Cid-Barrio, L., Encinar, J. R., Sanz-Medel, A. & Calvete, J. J. Absolute venomics: Absolute quantification of intact venom proteins through elemental mass spectrometry. *J. Proteomics* **164**, 33–42 (2017).

183. Feofanov, A. V. *et al.* Cancer cell injury by cytotoxins from cobra venom is mediated through lysosomal damage. *Biochem. J.* **390**, 11–18 (2005).

184. Kini, R. M. Excitement ahead: Structure, function and mechanism of snake venom phospholipase A2 enzymes. *Toxicon* **42**, 827–840 (2003).

185. Meléndez-Martínez, D. *et al.* Functional Mining of the Crotalus Spp. Venom Protease Repertoire Reveals Potential for Chronic Wound Therapeutics. *Mol. 2020, Vol. 25, Page 3401* **25**, 3401 (2020).

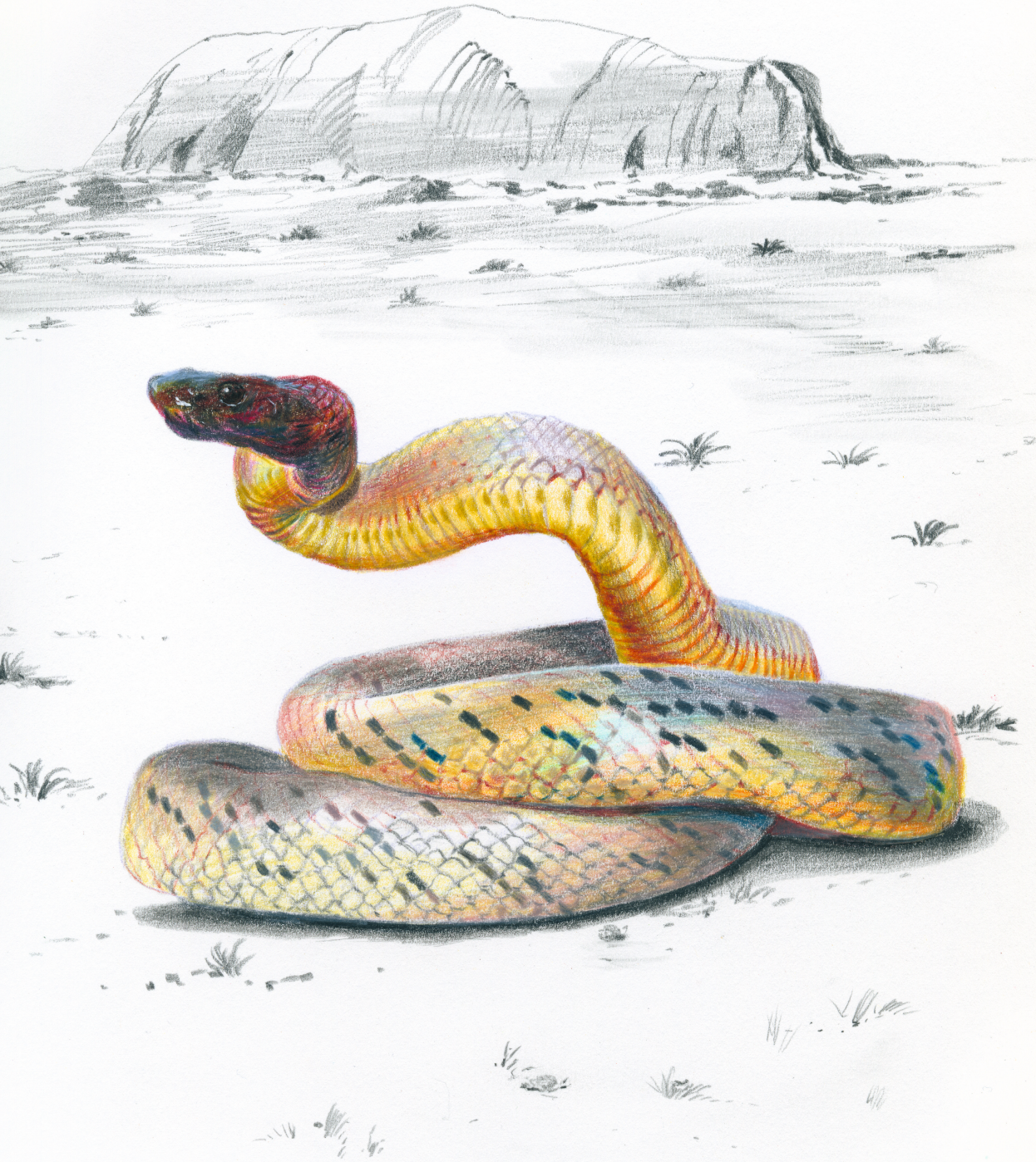

Oxyuranus microlepidotus

Chapter 2

Tissue-damaging toxins in snake venoms: mechanisms of action, pathophysiology and treatment strategies

Mátyás A. Bittenbinder, Jory van Thiel, Fernanda C. Cardoso, Nicholas R. Casewell, José-María Gutiérrez, Jeroen Kool, Freek J. Vonk

Communications Biology, 7 (358), 2024

Abstract

Snakebite envenoming is an important public health issue responsible for mortality and severe morbidity. Where mortality is mainly caused by venom toxins that induce cardiovascular disturbances, neurotoxicity, and acute kidney injury, morbidity is caused by toxins that directly or indirectly destroy cells and degrade the extracellular matrix. These are referred to as 'tissue-damaging toxins' and have previously been classified in various ways, most of which are based on the tissues being affected (e.g., cardiotoxins, myotoxins). This categorisation, however, is primarily phenomenological and not mechanistic. In this review, we propose an alternative way of classifying cytotoxins based on their mechanical effects rather than using an organ- or tissue-based description. The mechanisms of toxin-induced tissue damage and their clinical implications are discussed. This review contributes to our understanding of fundamental biological processes associated with snakebite envenoming, which may pave the way for a knowledge-based search for novel therapeutic options.

2.1 Introduction

Snakebite envenoming is a global health challenge and a neglected tropical disease. It accounts for 2.5 million victims each year, and annual mortality estimates range between 81.000 – 138.000 [1]. Snake venoms cause many local and systemic effects in humans, with some being life-threatening while others being permanently debilitating [1–3]. Without early and effective antivenom treatment, morbidity following snakebite can cause permanent disability and disfigurement [4,5]. Snakebite hotspots are found in sub-Saharan Africa, South and Southeast Asia, and Latin America [1,6]. Human snakebite victims are often young male agricultural workers, severely affecting their working abilities and daily activities. Snakebites often leave people with permanent physical and psychological disabilities, significantly affecting their lives in many ways [5]. This causes a substantial socio-economic impact on families and local economies [7].

Snake venom is a mixture of peptides and proteins that evolved to disrupt physiological pathways in a prey item but also severely affects humans during defensive snakebites. The two major families of medically important venomous snakes are the elapids (Elapidae, e.g., cobras, mambas, kraits, and coral snakes) and viperids (Viperidae, e.g., vipers and pit vipers). Other families of venomous snakes include Colubridae (i.e., non-front-fanged snakes) and Atractaspididae (e.g., stiletto snakes) [1,8]. However, these are rarely responsible for causing life-threatening human envenomings. Clinical effects of envenoming can be broadly divided into three main pathologies and pathophysiologies: neurotoxicity, haemotoxicity and tissue-damaging effects (which include cytotoxicity, e.g., myotoxicity, and degradation of the extracellular matrix), with some venoms inducing a combination of these.

Neurotoxic effects are caused by toxins affecting synaptic transmission, for example, by hydrolysing phospholipids at the presynapse, acting as antagonists of the cholinergic receptors, or blocking specific ion channels [9–11]. These effects may ultimately result in the impairment of neuromuscular transmission, resulting, among other effects, in respiratory paralysis [3]. Other toxins act in the synaptic cleft by inhibiting acetylcholine esterase, thereby reducing the removal of acetylcholine, causing overstimulation of the muscles, resulting in spasm or fasciculation [11,12]. Toxins responsible for neurotoxic effects are generally divided

into two main classes: α-neurotoxins and β-neurotoxins, depending on whether they act post- or pre-synaptically, respectively [10]. The dendrotoxins form a third group of neurotoxins, which belong to the family of Kunitz-type proteinase inhibitors [13,14].

Haemotoxicity can be considered an umbrella term for many cardiovascular disturbances and haemostatic effects caused by snake venoms. Blood clotting can be affected in such a way that coagulation is either accelerated (i.e., procoagulation) or impaired (i.e., anticoagulation). Toxins that promote coagulation generally affect blood clotting factors by i) activating factor X, prothrombin and other clotting factors, ii) inducing platelet aggregation, or iii) having a thrombin-like (fibrinogenolytic) effect [15,16]. Clinically, procoagulant venom components are responsible for venom-induced consumption coagulopathy associated with incoagulability [15]. Anticoagulant compounds include those that directly inhibit haemostasis by i) modulating platelets, ii) inhibiting platelet aggregation, iii) hydrolysing or binding to phospholipids, which are co-factors for the coagulation cascade, or iv) degrading coagulation factors [15]. In addition to influencing haemostasis, venoms may affect the cardiovascular system by causing either local or systemic haemorrhage or by inducing plasma extravasation. Haemorrhage is caused by proteolytic degradation of key components in the basement membrane of the microvasculature, thereby affecting the integrity of the capillary blood vessels. This results in the mechanical weakening of the capillary wall and subsequent extravasation [17–19]. In addition to haemorrhagic toxins, several components in snake venoms induce increments in vascular permeability, thus generating plasma extravasation, which might contribute to hypovolemia and haemodynamic disturbances [20].

Tissue-damaging effects are the leading cause of snakebite morbidity, including life-long disabilities such as permanent muscle tissue loss, contractures, hypertrophic scars, chronic ulceration, chronic renal disease, ocular damage and other debilitating pathologies (see Figure 1) [1]. Severe morbidity is conservatively estimated to occur in 450,000 bite victims each year [1]. Despite these morbidity rates, considerably less research has been performed on the tissue-damaging effects than on the neurotoxic and haemotoxic effects of venoms. Toxins with tissue-damaging capabilities can be broadly divided into two main groups based on the way they affect cells (and thus tissues). These include (a) cytotoxins,

defined as toxins that are 'truly' cytotoxic by directly affecting the viability of cells and (b) extracellular matrix (ECM)-degrading enzymes, which, in addition to this action, may be indirectly cytotoxic, meaning that cell death occurs as a secondary effect and not by directly damaging the cells. These cytotoxic components cause a range of pathologies, the most relevant of which are i) local and systemic myonecrosis, ii) dermonecrosis, and iii) acute kidney injury [21–25]. In turn, ECM-degrading enzymes are involved in i) local and systemic haemorrhage, ii) blistering and iii) dermonecrosis [26,27].

Traditionally, some toxin (sub)classes have been categorised based on the tissues they predominantly affect, e.g., cardiotoxins or myotoxins [21,28]. This classification has limitations as it oversimplifies the complexity of these compounds, as many of them affect several tissues. In addition, owing to its phenomenological nature, this categorisation does not involve the mechanical aspects of these toxins. Here, we review the molecular mechanisms of venom-induced tissue damage, revealing that snake venoms exert their cytotoxic effects via a number of distinct mechanisms, both direct and indirect. This provides the basis to reclassify the cytotoxin nomenclature based on mechanisms of action rather than on the affected tissue type. By incorporating the fundamental knowledge of the mechanistic pathways of tissue damage, we discuss their clinical impact, along with potential therapeutic options to reduce the severe morbidity of snakebite envenoming. Understanding the mechanisms of action of snake venom toxins that inflict tissue damage may shed light on other diseases involving similar cytotoxic effects.

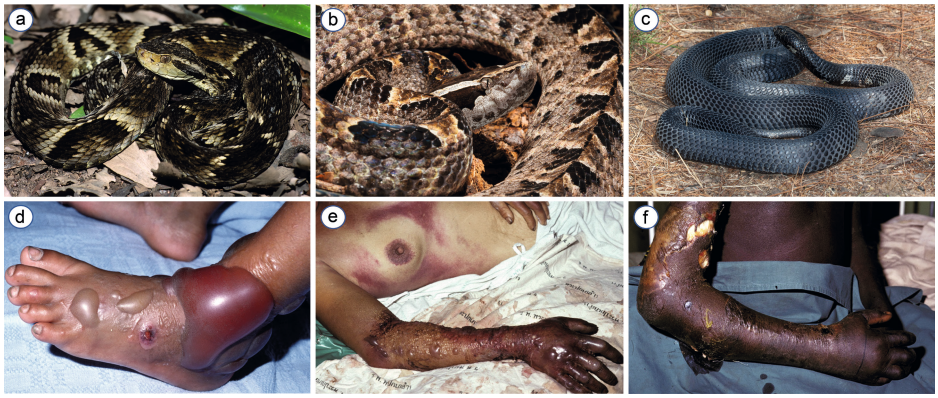

Figure 1: **Representative venomous snakes and tissue-damaging effects associated with their envenomings.**
(a-c) Medically important snake species with tissue-damaging properties in their venoms; (a) jararaca (*Bothrops jararaca*); (b) Malayan pitviper (*Calloselasma rhodostoma*); (c) black-necked spitting cobra (*Naja nigricollis*). (d-f) Pathologies caused by cytotoxic snake venoms; (d) swelling and blistering following a bite of *B. jararaca*; (e) swelling, blistering and necrosis as a result of a bite from *C. rhodostoma*; (f) extensive skin- and subcutaneous necrosis following a bite of *N. nigricollis*. Photographs of *B. jararaca* and *C. rhodostoma* courtesy of Wolfgang Wüster; the picture of *N. nigricollis* was taken by Johan Marais (African Snakebite Institute). Photographs of clinical cases by David A. Warrell, published in Gutiérrez et al. (2017) Nat. Rev. Dis. Primers 3: 17079.

2.2 A shift in the nomenclature of cytotoxic venom components

A thorough understanding of the pathological and pathophysiological effects caused by tissue-damaging toxins is crucial to grasp the complexity of snakebite envenoming and to develop effective therapies for treating venom-induced morbidity. Historically, toxin classes were categorised based on the effects they cause, with a primary division of neurotoxicity, haemotoxicity and tissue-damaging toxicity (see Figure 2). Some toxin classes are further subdivided based on the tissue type that is affected, such as myotoxins (toxins that target skeletal muscle cells) or cardiotoxins (toxins that target cardiomyocytes). However, this categorisation is inadequate as multiple toxin classes may cause similar pathologies but exert their effects via entirely different molecular mechanisms. Thus, a mechanical classification instead of a phenomenological one is needed.

The classification based on affected tissue type likely originates from the cell type on which the effect was initially tested. The most striking example can be found in the earliest records of "cardiotoxins", which were described in the 1940s.

Sakar and colleagues described a toxin from cobra venom that is '…responsible for cardiac failure' and therefore described it as "cardiotoxin" [29,30]. However, studies later showed that the primary effect of these toxins was at the membrane level, leading to a range of effects, including haemolysis, cytolysis of various cell types and muscle fibre depolarisation [31,32]. This led to many alternative names to describe these toxins, such as "cytotoxin", "direct lytic factor", "membrane toxin", and others (see Supplementary Table 1). Although the term "cytotoxin" has now been widely adopted in the literature for this group of toxins, many studies remain using alternative names. Therefore, we propose to use the term "cytotoxic three-finger toxin (3FTx)" as this describes both the basal activity as well as the venom gene family and thus prevents confusion. Interestingly, molecular analysis of so-called cytotoxic 3FTxs and cardiotoxins revealed that both 'groups' are similar in terms of their primary structure, which suggests that these are not two distinct subclasses, but rather a single group of toxins [33].

Another example of nomenclature confusion can be found within the cytotoxic phospholipases A_2 (PLA_2s), which are often named myotoxins, as they are known to disrupt the plasma membrane of muscle fibres [21]. However, studies on purified myotoxic PLA_2s on other cell types have proven that the activity spectrum of these toxins is actually much broader than previously thought [34,35]. This underpins the fact that listing these toxins as "myotoxic" is inadequate or at least not mutually exclusive, as these PLA_2s could be confused with other toxins with myotoxic effects (e.g., small basic myotoxins, metalloproteinases) that belong to a different toxin class and may exert their effects via different mechanisms [26,36–39]. We therefore suggest using the term "cytotoxic PLA_2s" to describe this specific group of toxins, regardless of which is the primary cellular target.

Although multiple studies have mentioned the limitations of the classification of cytotoxic compounds based on their effects, no decisive term has been suggested to denote this group of toxins. Our suggestion would, therefore, be to start using the term "cytotoxin" for all toxins with direct cytotoxic properties and use clear, distinctive names for categorising the specific toxin classes. Meaning that terms such as "cardiotoxins" would be regarded as "cytotoxic 3FTxs" and "myotoxins" would be considered either "cytotoxic PLA_2s" or "β-defensin-like toxins", depending on the toxin class (see Supplementary Table 1).

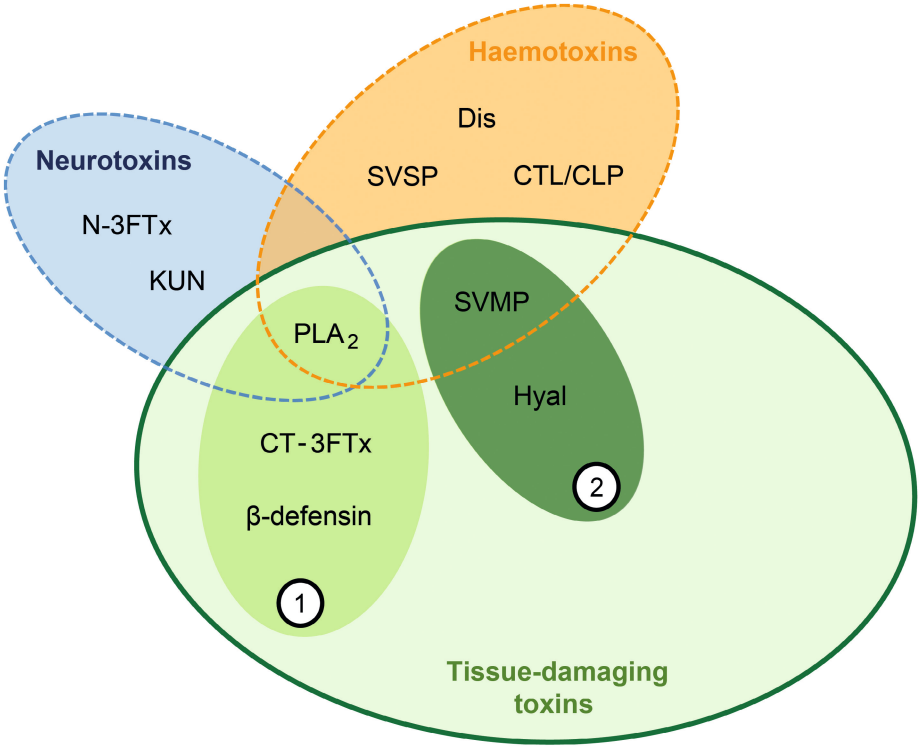

Figure 2. Main types of snake venom toxins and their mechanisms of action. Some toxins have more than one biological effect, thereby creating a multi-layered image. Numbers correspond to two categories of venom-induced tissue damage: (1) direct cytotoxic effects by 'true' cytotoxins and (2) degradation of extracellular matrix, which may result in indirect cytotoxic effect. Toxin classes: N-3FTx: neurotoxic three-finger toxins; KUN: Kunitz-type peptides; PLA_2: phospholipases A_2; CT-3FTx: cytotoxic three-finger toxins; SVMP: snake venom metalloproteinases; Hyal: hyaluronidases; CTL: C-type lectins; CLP: C-type lectin-related proteins; Dis: disintegrins; SVSP: Snake venom serine proteinases. This figure was based on Ray Morgan's 'The Venom Interviews', Part VII, It's Complicated, 2016.

2.3 A structural-mechanistic classification of venom cytotoxins

A wide variety of proteins that may cause tissue damage have been characterised in snake venoms. One way to classify these toxins is based on their primary mechanism of action, in which we differentiate between 'true' cytotoxins (i.e., toxins that have a direct cytotoxic effect on cells) and toxins that degrade the ECM and may have an indirect cytotoxic effect (e.g., by affecting the ECM which could eventually lead to cell injury) (see Figure 3).

2.3.1 Direct cytotoxic effects of 'true' cytotoxins

Cell membranes are crucial in maintaining normal cellular functioning. Membranes form an integral part of the cell by separating cellular environments from the plasma membrane to the compartment membranes of the mitochondria, lysosomes, Golgi complex, nuclei, and the endoplasmic reticulum [40]. This could explain why many snake venom toxins deploy their cytotoxic effect by altering membrane integrity, especially the plasma membrane.

2.3.2 Damage to cell membranes by cytotoxic 3FTxs

The 3FTx superfamily includes small (6-9 kDa), non-enzymatic toxins that have a wide array of biological functions, both as neurotoxins (i.e., small- and long-chain neurotoxins) and cytotoxins (i.e., cytotoxic 3FTxs) [41]. The latter are found exclusively in four related elapid genera, including *Naja*, *Hemachatus, Ophiophagus* and *Aspidelaps* [33]. The exact mechanisms by which cytotoxic 3FTxs exert their effects are not yet fully elucidated, and competing hypotheses exist. These hypotheses include cytotoxicity caused by interactions with plasma membrane components resulting in pore formation and cell damage secondary to lysosome lysis. Cytotoxic 3FTxs differ from non-cytotoxic 3FTxs by their hydrophobic character, with the hydrophobic patch being absent in the neurotoxic members of this family [32,42,43]. The highly conserved hydrophobic core in cytotoxic 3FTxs is thought to interact non-specifically with the hydrophobic structure of the lipid bilayer of cell membranes. Although the exact mechanism still needs to be elucidated, it is believed that the cytotoxic 3FTxs exert their effect by forming pores in the cell membrane [42,44,45]. These pores could be formed by cytotoxic 3FTxs alone or by an (oligomeric) association of cytotoxic 3FTxs [45]

Feofanov et al. proposed another mechanism, which included binding to the plasma membrane, followed by internalisation and subsequent transportation to lysosomes. In this event, plasma membrane permeabilisation is suggested to be a secondary effect following the lysosome rupture [46]. Additionally, it has been proposed that cytotoxic 3FTxs may be involved in the activation of intracellular signalling cascades, activating several cell death pathways [47]. However, further evidence is required to support these mechanisms.

Cytotoxic 3FTxs are known for their synergy with PLA_2s, which potentiate their cytotoxic effects. This phenomenon was first reported by Condrea *et al.*,

who showed a significant increase in erythrocyte lysis with cytotoxic 3FTx and PLA_2 fractions tested together, compared to separately [48]. This toxin synergy has then been described in numerous studies over the years [33,49–52] . Interestingly, the cytotoxic effects of cytotoxic 3FTxs from cobras can be enhanced by PLA_2s of distinct species of snakes (as shown for PLA_2s of several elapids and vipers) – suggesting that this synergy is not only restricted to venom PLA_2s of the same species [51].

In addition to the cytotoxic effects, this toxin synergy is associated with increased pain levels due to the enhanced effects on sensory neurons. It underlies the evolution of defensive venom spitting in spitting cobras [33]. Evidence suggests that some cytotoxic 3FTxs and PLA_2s form protein complexes together by homo- or hetero-oligomerisation [45,51]. However, the exact molecular mechanisms that cause cell death, as well as the actual complex formation, remain unknown. Pucca et al. proposed two mechanistic models that may explain the synergically potentiated cytotoxic effects of the cytotoxic 3FTx-PLA_2s complex [51]. First, given that PLA_2s bind more easily to outer plasma membranes compared to cytotoxic 3FTx, the cytotoxic 3FTx-PLA_2s complex would have an advantage in binding and thus could synergistically enhance the cytotoxic effects. Another explanation could be that plasma membrane integrity would be affected by PLA_2s-induced phospholipid hydrolysis, and this would render the membrane more susceptible to the lytic action of cytotoxic 3FTxs. However, more research is needed to elucidate the exact molecular mechanisms of the cytotoxic enhancing effects of this toxin synergy.

2.3.3 Destabilisation of cell membranes by cytotoxic PLA_2s through enzymatic- and non-enzymatic mechanisms

PLA_2s are one of the major toxin classes in snake venoms. This toxin superfamily has been extensively studied as they are among the most abundant toxins in viper and elapid snakes [1,53,54]. These small (~13-15 kDa) proteins have a wide toxicological profile that includes neurotoxic, haemotoxic and cytotoxic effects [53,55]. Snake venom PLA_2s can be divided into two groups based on their structural characteristics. Group I PLA_2s are found in elapid venoms, whereas PLA_2s in the viperid family are classified as Group II PLA_2s [55]. While these PLA_2s share a similar catalytic mechanism, they present distinct molecular structures.

Some group I PLA_2s are non-toxic, while some are presynaptic neurotoxins and cytotoxic and coagulopathic isoforms have also been described [55,56]. Interestingly, the neurotoxic, cytotoxic and some coagulopathic effects caused by these PLA_2s are based upon the hydrolysis of phospholipids, either present in cellular membranes or as free phospholipids in plasma [22,57]. In contrast, the mechanism of action of a few anticoagulant elapid PLA_2s is related to the binding and inhibition of coagulation factors [57]. Group II PLA_2s can be either enzymatically active or inactive depending on whether key residues at the catalytic site and the calcium-binding loop necessary for catalysis are mutated or not [55]. The enzymatically active PLA_2s disrupt the membrane by hydrolysis of membrane phospholipids. In contrast, the enzymatically inactive toxins, known as PLA_2 homologs, exert their effects via perturbation of the plasma membrane in the absence of phospholipid hydrolysis [22,55,58,59]. A mechanism of membrane disruption by catalytically-inactive Lys49 PLA_2 homologs has been proposed in which two distinct molecular regions are involved, initially in the binding to the membrane and then in the penetration and disruption of membrane integrity [60,61] (see Supplementary Figure 1).

A synergistic effect of catalytically active and inactive PLA_2s for inducing myotoxicity has been described [62]. Group II PLA_2s include neurotoxic and cytotoxic PLA_2s, the latter of which can affect skeletal muscle cells by binding to specific protein receptors or low-affinity lipid domains in the plasma membrane [22,58]. In addition, cytotoxic PLA_2s and PLA_2 homologs are cytotoxic to a variety of cell types in culture [35,63].

The destabilisation of the lipid bilayer makes the membrane more permeable to ions, thereby losing its membrane potential (becoming depolarised) and allowing a large influx of Ca^{2+} from the extracellular medium [21,22,64,65]. The uncontrolled influx of calcium causes calcium overload in affected cell types (i.e., myocytes, nerve terminals) and induces more stress on the weakened cellular membrane and mitochondrial dysfunction, resulting in decreases in ATP production, which in turn may result in necrosis [21,22]. In addition, such an increase in cytosolic calcium concentration affects the cytoskeleton, inducing hypercontraction in muscle cells [66]. The effect of cytotoxic PLA_2s on cells varies depending on toxin concentration thresholds. For example, at different concentrations, a Lys49 PLA_2 homolog devoid of enzymatic activity induces necrosis, apoptosis or cell proliferation in

a lymphoblastoid cell line, and these effects are related to variable degrees of alterations in calcium homeostasis [67,68].

2.3.4 Endocytosis followed by lysosomal degradation by β-defensin-like toxins

β-defensin-like toxins form another group of cytotoxins. These toxins are small (4-5 kDa) non-enzymatic homologs of endogenous cell-penetrating β-defensins and are only found in the venoms of certain pitvipers (subfamily Crotalinae) [69,70]. β-Defensin-like toxins penetrate plasma membranes through endocytosis via their high net-positive charge, which facilitates interactions with negatively charged cell surfaces. Upon binding their targets (i.e., ion channels and proteoglycans), β-defensin-like toxins are internalised and accumulate in lysosomal vesicles. This accumulation results in disruption of the lysosome membrane and subsequent lysosome lysis, which in turn promotes caspase activity, triggering apoptosis [71,72]. In addition to their cell-penetrating properties, these toxins interact with voltage-gated ion channels, altering their osmotic balance and inducing alterations in membrane potential [37,72,73]. The most extensively studied snake β-defensin-like toxins are crotamine (found in *Crotalus durissus*) and myotoxin-α (isolated from *Crotalus viridis viridis*) [69].

These toxins are generally named "myotoxins" because they induce muscle contracture and morphological alterations in myofibres [74]. However, other studies have shown that the cytoplasmic accumulation of these toxins occurs across various cell types [75]. Depending upon whether this internalisation in different cell types results in cytotoxicity, the word 'myotoxin' might be inaccurate, but this issue remains to be investigated. In the meantime, we suggest naming this class of cytotoxins 'β-defensin-like toxins'.

2.4 Indirect cytotoxic effects by toxins that degrade the extracellular matrix

The ECM is a macromolecular structure made up of the interstitial matrix and the basement membrane. The interstitial matrix consists of several types of collagens, as well as fibronectin, various proteoglycans, and hyaluronic

acid, and plays critical roles in the homeostasis of tissues [40,76]. The basement membrane consists of laminin, collagen type IV and VI, perlecan and nidogen, in addition to other minor components. It surrounds a variety of cell types, forming a connection between these cells and the interstitial matrix [77]. The basement membrane has multiple functions, such as providing structural support to capillary endothelial cells and many other cell types, acting as a filtration barrier, storing growth factors, preventing cells and larger molecules from passing through, and organising the tissue architecture. This barrier function is also observed in the capillaries, where the basement membrane prevents the extravasation of white blood cells until these are activated in inflammation by signalling molecules such as cytokines [78]. The basement membrane in the microvasculature also provides mechanical support to withstand the biophysical forces that generally operate in the circulation [17]. Because of its crucial role, the ECM is a primary target for various tissue-damaging components in snake venoms [79,80].

2.4.1 Degradation of key components of the ECM by snake venom metalloproteinases

Snake venom metalloproteinases (SVMPs) are found in all venomous snake families, being more abundant in species of the family Viperidae [70,81]. SVMPs are divided into three major classes (named P-I to P-III) based on their domain structure. Toxins of the class P-I (~20-30 kDa) only contain the metalloproteinase domain, while the second class, P-II (~20-60 kDa), carries an additional disintegrin domain which may remain intact or be proteolytically liberated. Finally, the P-IIIs (~60-100 kDa) have a disintegrin-like domain and a cysteine-rich domain in addition to the catalytic domain and can also be post-translationally modified in various ways [82]. The metalloproteinase domain is capable of enzymatic degradation of key components of the ECM, thereby destabilising the interactions between cells and the basement membranes and disrupting the overall structural arrangement of the ECM [80]. The degradation of the basement membrane by SVMPs affects a variety of cell types, including endothelial cells, skeletal muscle cells, keratinocytes and kidney cells [23,27,80]. The hydrolysis of the basement membrane that surrounds endothelial cells in capillaries results in the weakening of the capillary wall, followed by the

enlargement and eventual disruption of endothelial cells, leading to extravasation [17,79]. Thus, SVMPs are cytotoxic to endothelial cells *in vivo* through this indirect mechanism in which cell death occurs by the action of mechanical forces operating in the circulation secondarily to the weakening of the basement membrane as a consequence of SVMP-induced hydrolysis [17]. The hydrolysis and subsequent disruption of the ECM organisation further facilitate the diffusion of toxins into the circulation, giving SVMPs a spreading factor-like effect [80,83]. The additional domains present in P-II and P-III SVMPs are likely to bind to targets in the vasculature and in the tissue, thus directing these enzymes to specific sites and contributing to their toxicity. It has been proposed that such targeting enables these enzymes to have a more potent haemorrhagic activity as compared to P-I SVMPs [79,84,85].

By causing microvessel disruption and haemorrhage, SVMPs exert an indirect cytotoxic activity. Haemorrhage affects blood perfusion to tissues, thus generating ischemia, which affects the viability of cells. It has been shown that haemorrhagic SVMPs induce skeletal muscle necrosis through this indirect mechanism of cytotoxicity [36,86]. Moreover, hydrolysis of BM in glomeruli contributes to the renal pathology characteristic of envenomings by viperid snakes [87]. Furthermore, beyond the action of haemorrhagic SVMPs on the basement membrane, both haemorrhagic and non-haemorrhagic SVMPs degrade components of the interstitial matrix, thus contributing to the overall disorganisation of the ECM [88]. In addition to the general tissue disorganisation, the hydrolysis of ECM components by SVMPs may result in the release of growth factors stored in the matrix and in the generation of biologically active ECM fragments, which participate in inflammatory reactions and may further contribute to tissue damage [80].

2.4.2 Degradation of hyaluronic acid by hyaluronidases

Hyaluronidases are low-abundant enzymes (~52-55 kDa) found in elapid, viperid and some colubrid venoms [54,70,89]. Their main activity is the hydrolysis of hyaluronic acid, one of the key components of the ECM, and therefore contributes to ECM degradation [90,91]. The loss of the ECM structure integrity promotes the diffusion of (other) toxins, giving hyaluronidase its name as a 'spreading factor'. Therefore, hyaluronidases play a dual role in envenoming: they

degrade hyaluronic acid, thus contributing to ECM disorganisation, and they likely contribute to the local and systemic spreading of venom toxins, potentiating the tissue-damaging effect of cytotoxins and SVMPs [92–94]. Table 1 summarises the main types of tissue-damaging toxins in snake venoms, their targets and their main pathological and pathophysiological impact.

2.5 Venom components induce an inflammatory response that may contribute to tissue damage

Injection of tissue-damaging venom components in tissues, especially PLA_2s and SVMPs, promotes a complex inflammatory response associated with the synthesis and secretion of a plethora of mediators and a prominent inflammatory infiltrate of neutrophils and macrophages [20]. These processes contribute to reparative and regenerative tissue processes but may also have harmful consequences in the tissues. One outcome of this process is the generation of reactive oxygen species, resulting in oxidative stress and consequent tissue alterations [95,96]. Moreover, the toxic effects of PLA_2s and SVMPs in tissues result in the generation of 'damage-associated molecular patterns', which stimulate innate immunity and expand the inflammatory response [97,98]. ATP released from damaged cells may also amplify the cell-damaging effect by acting on purinergic receptors in neighbouring cells [99]. Thus, venom-induced tissue damage is likely to be mediated by the direct action of venom components discussed above, as well as by endogenous processes whose role in the overall venom-induced pathology remains to be determined.

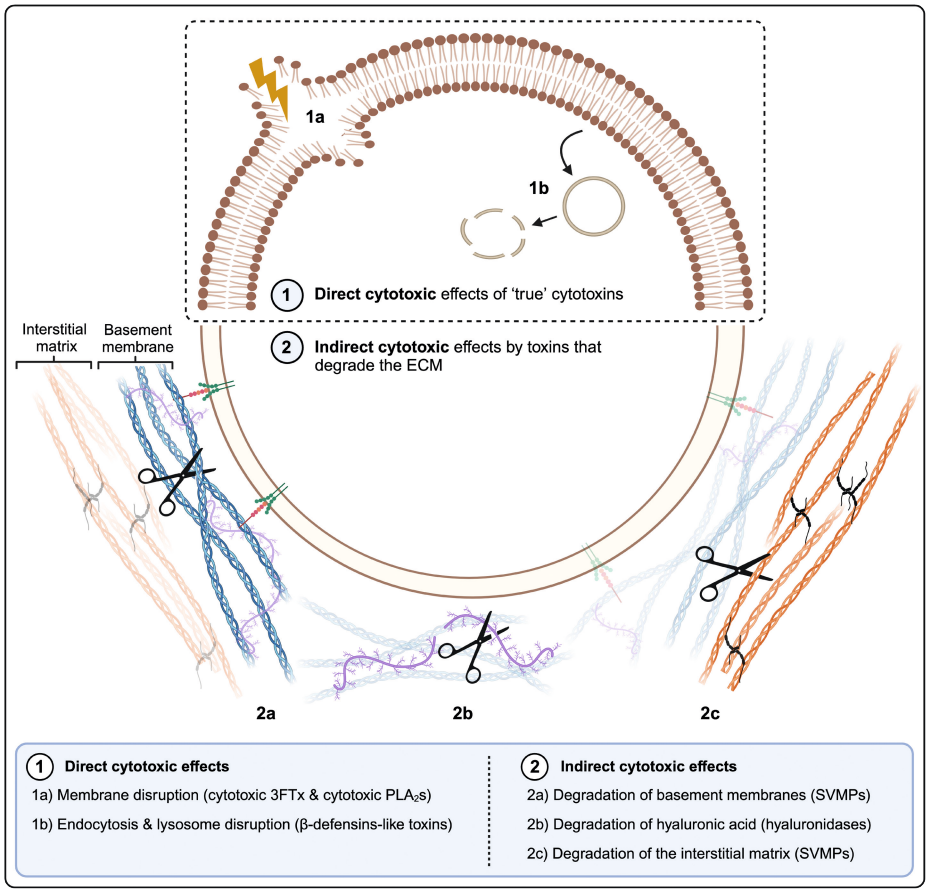

Figure 3. Schematic overview representing the various mechanisms of action of tissue-damaging toxins. (1) Direct cytotoxic effects caused by cytotoxic 3FTxs, cytotoxic PLA2s and β-defensin-like toxins. (2) Degradation of the ECM by SVMPs and hyaluronidases. Degradation of ECM contributes to the diffusion of venom components and can contribute to cellular damage indirectly by affecting the stability of endothelial cells in capillaries and by reducing blood supply as a consequence of haemorrhage, thus generating ischemia. Image created using www.biorender.com

2.6 The clinical consequences of tissue-damaging activities of venoms

The mechanisms of tissue damage induced by venom toxins discussed above have direct implications in the pathology and pathophysiology of snakebite envenoming. These clinical manifestations can be roughly divided into local and systemic effects.

2.6.1 Local tissue-damaging effects

Snake venoms are generally delivered at the bite site by the subcutaneous or intramuscular injection routes. Once in the tissue, various types of toxins exert tissue damage of rapid onset, especially in venoms of viperid species and some elapid species, such as the spitting cobras [1,3]. In the case of viperid venoms, cytotoxic PLA_2s induce acute skeletal muscle necrosis as a consequence of the direct effect of these toxins on the integrity of the plasma membrane of muscle cells, with the consequent influx of calcium ions, causing a series of intracellular degenerative events [21,22]. Cytotoxic PLA_2s also affect lymphatic vessels [100], thus contributing to the accumulation of fluid in the tissue (oedema). Cytotoxic venoms of spitting cobras (*Naja* spp.) likely cause muscle damage by the combined action of cytotoxic PLA_2s and cytotoxic 3FTx and induce cutaneous necrosis associated with drastic alterations in the various layers of the skin [25,101]. A unique clinical manifestation caused by venom spitting of certain cobras is observed as painful ophthalmic lesions, which are the result of the direct action of cytotoxic 3FTxs and PLA_2s in victims that have been spat in the eyes [33,102]. Cytotoxic cobra venoms and viperid venoms also induce the formation of skin blisters, which, in the case of the latter, is a consequence of the action of SVMPs on the dermal-epidermal interface, resulting in the separation of dermis and epidermis [27,103]. In addition to damage to muscle and skin, tissue-damaging toxins also affect nerves and arteries [104,105]. As a result of the extravasation of blood and plasma, viperid envenomings are often associated with an increase in intracompartmental pressure in some muscle compartments, which affects arterial perfusion and might end up in ischemic necrosis associated with compartmental syndrome [1].

Envenomings by viperid species are generally accompanied by widespread degradation of ECM, mediated by SVMPs and hyaluronidases. The hydrolysis of basement membrane components results in microvessel disruption and haemorrhage [1,79]. As a consequence, blood perfusion is impaired, and ischemia ensues. This effect contributes to skeletal muscle necrosis [86] and precludes the regeneration of muscle tissue [106]. ECM degradation also results in the disorganisation of the matrix [80], thus affecting a variety of processes that depend on matrix integrity. Such degradation also contributes to the diffusion of venom components locally and systemically.

2.6.2 Systemic tissue-damaging effects

Snake venoms are distributed systemically through lymphatic and blood vessels, thus reaching diverse organs where they cause harmful effects. In the case of venoms of some rattlesnakes, Australian elapids and sea snakes, cytotoxic PLA_2s induce systemic muscle necrosis, i.e., rhabdomyolysis [3,107,108]. As a consequence, there is a massive release of cytosolic muscle components, such as creatine kinase and myoglobin, into the circulation. Myoglobin, in turn, contributes to the acute kidney injury characteristic of these envenomings [1,109]. Moreover, an increase in potassium concentration in the blood (hyperkalaemia), as a result of rhabdomyolysis, may affect cardiac function [108]. In some venoms, cytotoxic components cause intravascular haemolysis by disrupting the integrity of the plasma membrane of erythrocytes [110,111]. By damaging the integrity of blood vessels in various organs, haemorrhagic SVMPs cause systemic bleeding, which is potentiated by the action of haemotoxic components that affect haemostasis [15]. This impairs blood perfusion to organs, which might lead to cardiovascular shock and multiple organ failure.

Cytotoxins and ECM-degrading enzymes may have a direct impact on the kidneys, causing acute kidney injury through a variety of mechanisms that include degradation of basement membrane in glomeruli, natural cytotoxicity on renal tubular cells, hypoperfusion associated with systemic bleeding, and the toxic effect of myoglobin and haemoglobin, released as a consequence of rhabdomyolysis and haemolysis, respectively, on renal tubular cells [112]. Likewise, venom cytotoxic components are likely to affect other tissues and cells, thus contributing to the overall pathophysiology of envenomings, including myocardial damage [113,114]. Figure 4 summarises the most important local and systemic effects induced by snake venoms.

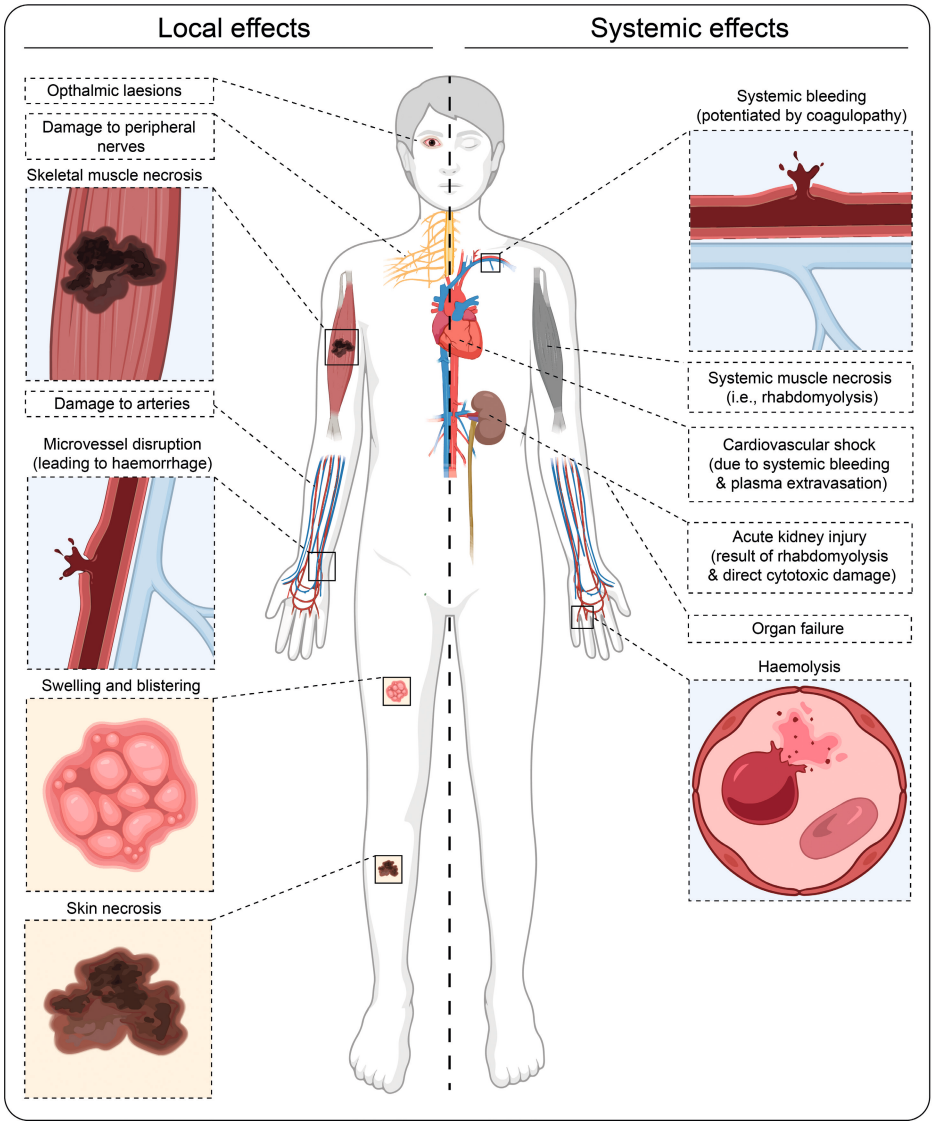

Figure 4. Overview of the tissue-damaging activities of snake venom toxins on various body systems. Snake venoms may cause a wide range of effects in the human body depending on the composition of the venom. The observed effects can be local and systemic. Image created using www.biorender.com

Table 1. Overview of effects of tissue-damaging toxins in snake venoms, which exert their actions *in vivo*, including directly cytotoxic toxins and enzymes that degrade the ECM.

Directly cytotoxic toxins		
Toxin class	**Main targets**	**Pathological and pathophysiological consequences**
3FTxs	Skeletal muscle	Myonecrosis (local and systemic)
	Skin	Dermonecrosis
	Cardiac muscle	Cardiotoxicity
	Erythrocytes	Intravascular haemolysis
	Other cell types	Cytotoxicity
PLA_2s	Skeletal muscle	Myonecrosis (local and systemic)
		Acute kidney injury (through the toxic action of myoglobin)
	Skin	Dermonecrosis
	Kidney	Acute kidney injury (secondary to cytotoxic action on renal cells)
	Erythrocytes	Intravascular haemolysis
	Other cell types	Cytotoxicity
β-defensin-like toxins	Skeletal muscle	Contracture
		Myonecrosis
Enzymes that degrade ECM		
Toxin class	**Main targets**	**Pathological and pathophysiological consequences**
SVMPs	Basement membrane in capillary vessels	Disruption of the integrity of microvessels with extravasation (haemorrhage)
		Ischemia secondary to haemorrhage and reduction of blood flow in various tissues (i.e., skeletal muscle, kidney)
	Skin	Blister formation secondary to cleavage of proteins in the dermal-epidermal junction
		Dermonecrosis
	Proteins in ECM	Widespread degradation of proteins in ECM, with loss of tissue organisation and spreading of venom components
Hyaluronidases	Hyaluronic acid in ECM	Disorganisation of the ECM
		Spreading of venom components

2.7 Mechanisms of cytotoxicity observed *in vitro* but with unknown impact on *in vivo* envenoming

Studies on the action of venoms and toxins on cells *in vitro* have revealed mechanisms of cytotoxic effects that provide valuable information on the action of these toxins and may shed light on more general aspects of cellular pathology which could be applied to the understanding of other diseases. However, the actual *in vivo* and clinical implications in snakebite envenomings of several of these *in vitro* experimental observations remain unknown. These mechanisms will be described as they illustrate possible ways through which snake toxins affect the viability of cells and might illuminate the design of future revealing *in vivo* studies.

2.7.1 Apoptosis induced by anoikis

A variety of venom components have been shown to induce apoptosis of several cell lines in culture. One of the main mechanisms of apoptosis *in vitro* occurs via anoikis, resulting from the detachment of cells from their substrate [115,116]. Upon loss of cell-cell and cell-ECM adhesions, the inhibitory effects on the cell death pathways are lifted, which causes the cell to undergo apoptosis [117,118]. Although the mechanisms of anoikis are poorly understood, it is thought that the disruption of focal contacts is the primary signal for activation of the extrinsic apoptotic pathway [117,119,120]. Cell detachment has been described as a consequence of the action of SVMPs on endothelial cells in culture [116,121]. SVMPs degrade the matrix upon which cells are adhered or might be able to cleave integrins in these cells, which interact with matrix components, thus inducing the detachment of cells. However, SVMPs also induce apoptosis through mechanisms other than anoikis, probably related to interaction with integrins and related molecules [122]. Further, some SVMPs induce apoptosis in non-adherent cell lines, suggesting that mechanisms other than anoikis might be at play [123].

Disintegrins are venom components predominately derived from the cleavage of P-II SVMPs [82,124]. They bind to integrins and induce a variety of effects on cells *in vitro* [125]. The binding of disintegrins leads to a loss of cell-cell and cell-ECM adhesions, which may trigger the anoikis pathway [125]. Another class of proteins that are thought to affect cells *in vitro* are C-type lectin family members, which are found in viperid, elapid and colubrid venoms [70,81]. A diverse range of effects

is described for these toxins, including cytotoxicity on various cancer cell lines, although the exact mechanisms have not yet been elucidated [126–128].

2.7.2 ATP release secondary to toxin-induced cytotoxicity leads to activation of cell death pathways

The direct cytotoxic action of PLA_2s results in the release of cytosolic molecules, including ATP, to the extracellular environment [99,129]. It has been shown that this nucleotide interacts with purinergic receptors in myogenic cells, acting as a 'danger signal' and spreading cell damage and inflammation, evidenced by the increase in cytosolic calcium [99,130,131]. This effect was reduced by apyrase, an enzyme that degrades ATP, thus underscoring the role of this nucleotide in the effect [99]. Moreover, a cytotoxic Lys49 PLA_2 homolog induces cell death in macrophages in culture by a mechanism related to ATP release and action on purinergic receptors [132].

2.7.3 Apoptosis induced through ROS generation by L-amino acid oxidases (LAAOs)

Reactive oxygen species (ROS) are produced as by-products during aerobic metabolism in cells. Although low ROS levels are intrinsically associated with normal cellular functioning, the accumulation of ROS (e.g., hydrogen peroxide) is suggested to be the primary inducer of oxidative stress [133]. This may affect cellular processes by denaturing enzymes, disturbing the cell membrane, and inducing DNA damage, which could ultimately result in cell death [134]. Hydrogen peroxide is generated by the action of L-amino acid oxidase (LAAO) present in snake venoms [135]. LAAOs are enzymatic flavoproteins with a molecular weight of 50–70 kDa, which are found in most snake species [70,136]. LAAOs catalyse the oxidative deamination of L-amino acids and produce hydrogen peroxide. LAAOs may induce apoptosis and necrosis depending on their concentration [137–139].

Several isoforms of LAAO, isolated from viperid and elapid snake venoms, have been shown to induce apoptosis of several cell types in culture, including cancer cell lines. In general, cytotoxicity is due to the generation of H_2O_2 as a consequence of the enzymatic activity of LAAOs [137,140–143]. Such oxidative stress induces apoptosis by the extrinsic and intrinsic pathways, with increases

in caspases and other proapoptotic enzymes, degradation of DNA and loss of mitochondrial membrane potential [141,144]. Interestingly, an LAAO can induce various forms of cell death, as shown in an enzyme from the venom of *Bothrops atrox*, which induces apoptosis, autophagy and necrosis in a keratinocyte cell line [138].

2.7.4 Activation of various cell death pathways by toxins that induce direct cytotoxicity *in vivo*

Cytotoxic 3FTxs and PLA_2s induce necrosis *in vivo* as well as in cells in culture, as described above. It has been observed that these cytotoxic components also induce apoptosis in various cell lines, including cancer cells, *in vitro*. A variety of cytotoxic 3FTxs trigger apoptotic pathways [145–147], as well as autophagy [148]. A cytotoxic Lys49 PLA_2 homolog was shown to induce necrosis, apoptosis, and proliferation in a lymphoblastoid cell line, the outcome of which is dependent on toxin concentration [67]. Therefore, it is likely that these toxins induce varying cellular responses depending on their concentration. *In vivo*, this might translate into different cell death thresholds in tissues, whereby necrosis may predominate in regions of high toxin concentration. In contrast, apoptosis and autophagy may occur in areas of lower toxin concentration, and even proliferative or stimulatory effects may be seen in areas of even lower concentrations, in a complex gradient that might vary over time [149]. Figure 5 summarises the various mechanisms of cytotoxicity induced by venom components which have been described *in vitro*.

The cytotoxic mechanisms described in this section highlight the complexity of the actions of venom components in cells. Even though these phenomena have been studied *in vitro*, they may shed light on possible pathogenic mechanisms that operate *in vivo*. It is necessary to explore the occurrence of these cell death mechanisms *in vivo* and to assess their relevance in the clinical manifestations of envenomings. Thus, it would be relevant to determine whether the various types of cell death described in cell culture conditions also occur in tissues affected by snake venom toxins *in vivo*. Moreover, the study of the mechanisms involved in cytotoxicity may shed light on potential new therapeutic options for snakebite patients.

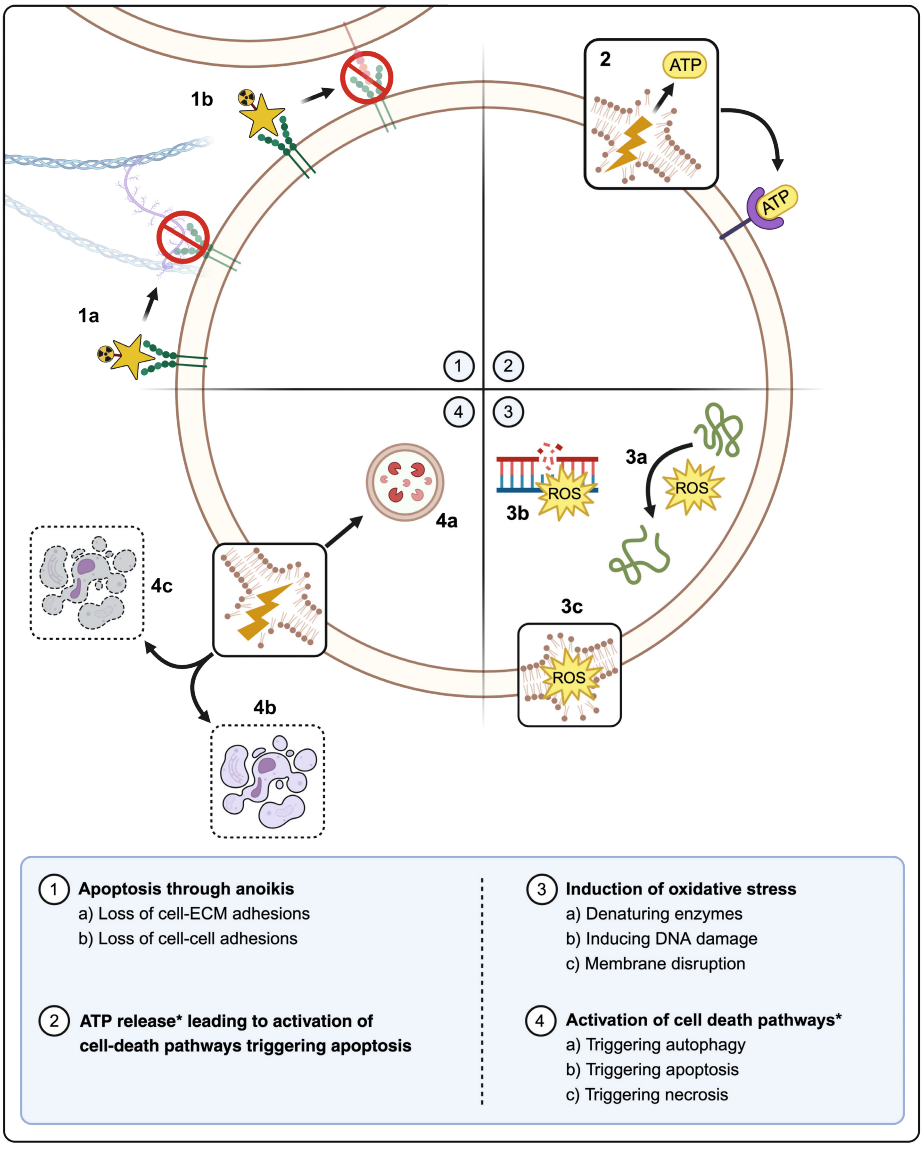

Figure 5. Schematic overview representing the various mechanisms of cytotoxicity observed *in vitro*. (1) Apoptosis through anoikis by SVMPs, disintegrins (and possibly C-type lectins). (2) ATP release leads to the activation of cell-death pathways and, thereby, triggering apoptosis by cytotoxic PLA_2s. (3) Apoptosis triggered by ROS production by LAAOs. (4) Activation of various cell death pathways by cytotoxic 3FTxs and cytotoxic PLA_2s. Asterisk depicts those mechanisms which are secondary to direct cytotoxicity. Image created using www.biorender.com.

2.8 The challenge of developing effective therapies for venom-induced tissue damage

Current snakebite treatments consist of the administration of antibodies derived from serum or plasma that are produced by hyper-immunisation of large animals (primarily equines or ovines) with snake venoms [150,151]. Animal-derived antivenoms are generally effective in the abrogation of systemic, life-threatening effects of snake venoms [1,3]. However, their efficacy in neutralising venom-induced local tissue damage is somewhat limited [25,152,153]. This is due to a number of factors, especially the rapid onset of these pathological effects, associated with the frequent delay in antivenom administration. Since antivenoms induce adverse reactions in a percentage of patients, they should be administered by health staff in hospitals and clinics, which, quite often, are located far from the location where the snakebite occurred. In addition, there are countries and regions within countries where the availability and accessibility of antivenoms is limited [1,154,155]. Moreover, some toxins responsible for tissue damage, such as cytotoxic 3FTXs and PLA_2s, are poorly immunogenic and consequently, the antibody titres against these toxins in antivenoms tend to be low [156,157]. Therefore, there is an urgent need to develop novel therapeutic strategies to confront this aspect of snakebite envenoming. To address these problems, recent studies have been focusing on the development of alternative snakebite treatments. Combining the growing body of scientific knowledge of the (tissue-damaging) snake venoms with modern bioanalytical chemistry techniques and biotechnological approaches allows for the exploration of novel inhibitory compounds.

A highly promising approach is based on the repurposing of enzyme inhibitors that have been developed for a variety of diseases in which endogenous PLA_2s and SVMPs play a crucial role. Owing to the structural similarities of these endogenous enzymes and venom enzymes, some of these inhibitors, which have already gone through clinical trials for other diseases, are particularly effective in the inhibition of venom PLA_2s and SVMPs. The most promising group of synthetic PLA_2 inhibitors are the indoles (i.e., LY315920 varespladib and LY333013 methyl varespladib). These inhibitors were proven to be effective at protecting against various PLA_2-mediated pathophysiological alterations, including inflammatory diseases [158–160]. They have also been tested in animal

models of snake envenoming, and they inhibit venom toxicity, including lethality-inducing neurotoxic effects and coagulopathy, as well as tissue-damaging effects, i.e., inhibition of myonecrosis and dermonecrosis [161–167]. Interestingly, LY333013 is administered by the oral route, therefore representing a convenient option for therapy in the field, owing to the good safety profile of this compound. A clinical trial is underway to test this oral inhibitor in snakebite envenoming [168]. It is necessary to demonstrate whether an orally administered drug would be able to reach the tissue affected by the venom in a timely manner so as to prevent or reduce tissue damage.

As with PLA_2s, there is a wide array of endogenous metalloproteinases that have a variety of physiological roles and have been implicated in human disease, which have, therefore, been intensively targeted to find inhibitory candidates [162,169,170]. As the effects of SVMPs are predominantly zinc-dependent, inhibitors that interact with the Zn^{2+} in such a way that the catalytic effect of the toxins is abrogated have been explored. Currently, two classes of SVMP inhibitors have been studied as candidates for SVMPs, both with a distinct mode of action. Peptidometic inhibitors (e.g., the matrix metalloproteinase inhibitors batimastat, marimastat, prinomastat) directly bind the zinc ion in the binding pocket of the protein while having an affinity for the catalytic site [167,171–174], whereas the metal chelators (e.g., Dimercaprol, DMPS, EDTA) work by chelating the zinc moiety required for catalysis [167,172,174,175]. Similar to varespladib, some of these drugs show exciting potential for snakebite by preventing pathology in animal models of envenoming and because the oral route can administer some of them [162,167,176]. Combination therapies of PLA_2s and SVMP inhibitors are currently being investigated and have already shown promising potential in inhibiting tissue-damaging activities [167,177].

The search for inhibitors against other groups of toxins responsible for tissue damage, such as hyaluronidases, LAAOs and other tissue-damaging toxins, has been more limited [162,169]. Although hyaluronidase inhibitors have been described, these compounds showed inhibitory concentrations (IC_{50}) in the micro- and millimolar range, raising the question of whether these can be considered promising candidates for clinical studies [93,94,178]. One advantage of enzyme inhibitors as compared to antibodies is that their spectrum of inhibition is broader since they are generally directed against the active sites of enzymes,

which are similar for each group of enzymes, in contrast to the antigenic variability of toxic enzymes from different venoms [162,169,179].

Other promising therapies include recombinant- and monoclonal antibodies or antibody fragments [169]. Recombinant antibodies can be developed against poorly immunogenic toxins responsible for tissue damage [180]. In addition, antibodies can be designed in formats that facilitate the neutralisation of these toxins in the tissues [181]. For example, low molecular mass recombinant antibodies, such as nanobodies and similar formats, have a higher volume of distribution than whole IgG molecules, having the capacity to reach tissue compartments and neutralise toxins in the tissues.

Synthetic toxin inhibitors include aptamers (i.e., single-stranded DNA- or RNA-oligonucleotides), synthetic peptides and synthetic nanoparticles, all of which have been selected for their capacity to bind and neutralise toxins [182–185]. Another promising strategy comprises a decoy-receptor approach using mimotopes (i.e., peptides mimicking the structure of the subunits of acetylcholine binding protein), thereby preventing the binding of 3FTx to native (acetylcholine) receptors [186]. The binding of the mimotopes to these toxins would prevent their interaction with native receptors, thereby neutralising their effect. Although this approach has been solely explored on neurotoxic 3FTxs, other studies have shown the affinity of cytotoxic 3FTxs for the acetylcholine-binding protein (i.e., a structural homologue of the binding domain on the acetylcholine receptor) [187,188]. Therefore, the possibility of neutralising the cytotoxic effects should not be ruled out. Identification of the sequences of receptors that bind these toxins may eventually lead to the synthesis of a wide array of these decoy receptors that may block the activity of cytotoxic 3FTxs [162]. In turn, nanoparticles of various chemical compositions can be designed with the ability to inhibit cytotoxic 3FTxs, PLA_2s and SVMPs and have been shown to be effective against the venoms of cytotoxic *Naja* spp. [185,189].

In addition to antibodies of variable formats, there is a large body of research focusing on the development of venom inhibitors from a variety of natural sources [162]. Natural inhibitors have been described in plants and animals [190–192]. For example, endogenous PLA_2 inhibitors present in the plasma of some animals (e.g., snakes and opossums) have been proposed as candidates [191,193–196]. These protein inhibitors are part of the innate immune system of these animals that

are used to counteract the effect of snake venoms and form complexes with the PLA_2 toxins [193]. Likewise, inhibitors of SVMPs have been characterised from the blood of mammals and snakes [192,196]. The inhibitory mechanism of these endogenous inhibitors remains largely unknown, but in some cases, they form macromolecular complexes with toxins [162,191,196].

Abundant literature exists on plant-derived extracts capable of inhibiting the effects of PLA_2s and SVMPs. However, less is known about the structural detail of their inhibitory effects, primarily because less research has focused on the isolation and characterisation of isolated plant-derived compounds [162,169,197–200]. Table 2 presents an overview of several novel inhibitor candidates against tissue-damaging toxins of snake venoms.

The neutralisation and inhibition of tissue-damaging toxins by antivenoms and novel therapeutic alternatives constitute a considerable challenge, mainly because these effects develop rapidly after venom injection, and some of their consequences are irreversible. Thus, delays in the administration of antivenoms and novel therapeutics preclude an effective inhibition. Therefore, ideally, these novel therapies would have to be administered in the field rapidly after a snakebite to counteract the action of tissue-damaging toxins before they exert their effects. In addition, these therapeutics should have a pharmacokinetic profile that ensures adequate access to the tissues where venom is injected. These tasks demand not only the generation of effective therapeutics but also of effective injection devices and public health interventions aimed to guarantee their availability and accessibility in regions of high incidence of snakebites. Moreover, the search for therapeutic options aimed at improving the processes of tissue repair and regeneration once tissue damage has developed constitutes another avenue to reduce the sequelae inflicted by this severe aspect of snakebite envenoming.

Table 2. Overview of novel therapeutic candidates for inhibition of tissue-damaging compounds in snake venoms.

Toxin class	Therapeutic candidate	Examples	References
Major toxin classes			
Cytotoxic 3FTxs	Aptamers	Aptamers developed against α-bungarotoxin	[182,183]
	Synthetic peptides	Peptide inhibitors against α-cobratoxin	[184]
	Nanoparticles	Nontoxic hydrogel copolymer nanoparticles	[185]
	Mimotopes (i.e., decoy receptors)	Recombinant nAChR mimics	[186,187,201,202]
Cytotoxic PLA_2s	Nanoparticles	Nontoxic hydrogel copolymer nanoparticles	[185,203]
	Polyanions	Suramin; heparin	[204–208]
	Animal-derived compounds	PLA_2 inhibitors from mammals and snakes	[191,193,195,209]
	Plant-derived compounds	Alkaloids (e.g., aristolochic acid); rosmarinic acid	[197–200,210–214]
	Small molecule inhibitors	LY315920 varespladib; LY333013 methyl varespladib	[161,164–167]
SVMPs	Nanoparticles	Synthetic polymer nanoparticles	[189,215]
	Animal-derived compounds	SVMP inhibitors isolated from mammals and snakes	[192,216,217]
	Plant-derived compounds	Flavonoids	[198,218,219]
	Small molecule inhibitors	Marimastat, batimastat, prinomastat	[167,171,172,174]
		Dimercaprol; DMPS; EDTA	[167,172,174]
Minor toxin classes			
Hyaluronidases	Plant-derived compounds	Alkaloids (e.g., aristolochic acid); flavonoids (e.g., quercetin);	[91,93,178,190,220]
	Polyanions	Heparin	[91,93,221]
β-defensin-like toxins	Currently none	-	-

2.9 Concluding remarks and forward-looking perspective

Snakebite envenoming is a severe public health issue which is responsible for causing mortality and long-term morbidity. The clinical syndromes can be broadly categorised into neurotoxicity, haemotoxicity and tissue-damaging effects, of which the latter is the leading cause of snakebite morbidity. Traditionally, some toxin subclasses were classified based on the tissues that they predominantly affect (e.g., cardiotoxins, myotoxins). Although the origin and reasoning of the latter classification method are apparent, this classification oversimplifies the complexity of these compounds and does not consider the mechanical aspects of these toxins. This review provides an alternative classification for tissue-damaging toxins based on molecular mechanisms of action, including cytotoxicity and ECM degradation. In addition, it discusses the pathological and pathophysiological effects of tissue-damaging toxins and provides an overview of potential treatment strategies.

Many challenges remain in identifying the main toxins responsible for tissue damage in a variety of snake venoms, their mechanisms of action, and their clinical impact. Likewise, the *in vivo* manifestations of toxic mechanisms described *in vitro*, as well as the role of inflammatory and other endogenous processes in the pathogenesis of venom-induced tissue damage, remain to be investigated. An area in need of strengthening is the search for novel inhibitors of tissue-damaging toxins that would complement antivenoms in the therapy of these envenomings. Understanding the harmful actions of venoms in tissues should be integrated with the study of other pathologies that involve various forms of tissue damage (e.g., infectious diseases or cancer), thus highlighting general patterns of disease that pave the way for novel therapeutic alternatives.

References

1. Gutiérrez, J. M. *et al.* Snakebite envenoming. *Nat. Rev. Dis. Prim.* **3**, (2017).
2. Alirol, E., Sharma, S. K., Bawaskar, H. S., Kuch, U. & Chappuis, F. Snake bite in south asia: A review. *PLoS Negl. Trop. Dis.* **4**, (2010).
3. Warrell, D. A. Guidelines of Management of Snake bite. *Lancet* **375**, 77–88 (2010).
4. Gutiérrez, J. M., Theakston, R. D. G. & Warrell, D. A. Confronting the neglected problem of snake bite envenoming: The need for a global partnership. *PLoS Med.* **3**, 0727–0731 (2006).
5. Waiddyanatha, S., Silva, A., Siribaddana, S. & Isbister, G. K. Long-term effects of snake envenoming. *Toxins (Basel).* **11**, (2019).
6. Longbottom, J. *et al.* Vulnerability to snakebite envenoming : a global mapping of hotspots. *Lancet* **392**, 673–684 (2018).
7. Vaiyapuri, S. *et al.* Snakebite and its socio-economic impact on the rural population of Tamil Nadu, India. *PLoS One* **8**, (2013).
8. Pyron, R. A., Burbrink, F. T. & Wiens, J. J. A phylogeny and revised classification of Squamata, including 4161 species of lizards and snakes. *BMC Evol. Biol.* **13**, (2013).
9. Fry, B. G. *et al.* Molecular evolution and phylogeny of elapid snake venom three-finger toxins. *J. Mol. Evol.* **57**, 110–129 (2003).
10. Harris, J. B. & Scott-Davey, T. Secreted Phospholipases A 2 of Snake Venoms: Effects on the Peripheral Neuromuscular System with Comments on the Role of Phospholipases A 2 in Disorders of the CNS and Their Uses in Industry. *Toxins (Basel).* **5**, 2533–2571 (2013).
11. Utkin, Y., Sunagar, K., Jackson, T.N.W., Reeks, T., Fry, B. Three finger toxins (3FTXs). in *Venomous Reptiles and Their Toxins: Evolution, Pathophysiology and Biodiscovery* (ed. Fry, B.) 215–227 (2015).
12. Karlsson, E., Mbugua, P.M., Rodriguez-Ithurralde, D. Fasciculins, anticholinesterase toxins from the venom of the green mamba Dendroaspis angusticeps. *J. Physiol* **79**, 232–240 (1984).
13. Harvey, A. L. Twenty years of dendrotoxins. *Toxicon* **39**, 15–26 (2001).
14. Harvey, A. L. & Robertson, B. Dendrotoxins: structure-activity relationships and effects on potassium ion channels. *Curr. Med. Chem.* **11**, 3065–3072 (2004).
15. White, J. Snake venoms and coagulopathy. *Toxicon* **45**, 951–967 (2005).
16. Berling, I. & Isbister, G. K. Hematologic Effects and Complications of Snake Envenoming. *Transfus. Med. Rev.* **29**, 82–89 (2015).
17. Gutiérrez, J. M., Rucavado, A., Escalante, T. & Díaz, C. Hemorrhage induced by snake venom metalloproteinases: Biochemical and biophysical mechanisms involved in microvessel damage. *Toxicon* **45**, 997–1011 (2005).
18. Gutiérrez, J. M., Escalante, T., Rucavado, A. & Herrera, C. Hemorrhage caused by snake venom metalloproteinases: A journey of discovery and understanding. *Toxins (Basel).* **8**, (2016).
19. Escalante, T. *et al.* Role of collagens and perlecan in microvascular stability: Exploring the mechanism of capillary vessel damage by snake venom metalloproteinases. *PLoS One* **6**, (2011).

20. Teixeira, C., Moreira, C., Gutierrez, J. M. Venoms. in *Inflammation: From Molecular and Cellular Mechanisms to the Clinic* (ed. Cavaillon, J.M., Singer, M.) 99–128 (Wiley, 2018).

21. Gutiérrez, J. M. & Ownby, C. L. Skeletal muscle degeneration induced by venom phospholipases A2: insights into the mechanisms of local and systemic myotoxicity. *Toxicon* **42**, 915–931 (2003).

22. Montecucco, C., Gutiérrez, J. M. & Lomonte, B. Cellular pathology induced by snake venom phospholipase A2 myotoxins and neurotoxins: Common aspects of their mechanisms of action. *Cell. Mol. Life Sci.* **65**, 2897–2912 (2008).

23. Sitprija, V. Animal toxins and the kidney. *Nat. Clin. Pract. Nephrol.* **4**, 616–627 (2008).

24. Gasanov, S. E., Dagda, R. K. & Rael, E. D. Snake Venom Cytotoxins, Phospholipase A2 s, and Zn2+ -dependent Metalloproteinases: Mechanisms of Action and Pharmacological Relevance. *J. Clin. Toxicol.* **4**, (2014).

25. Rivel, M. *et al.* Pathogenesis of dermonecrosis induced by venom of the spitting cobra, Naja nigricollis: An experimental study in mice. *Toxicon* **119**, 171–179 (2016).

26. Gutiérrez, J. M. & Rucavado, A. Snake venom metalloproteinases: Their role in the pathogenesis of local tissue damage. *Biochimie* **82**, 841–850 (2000).

27. Jiménez, N., Escalante, T., Gutiérrez, J. M. & Rucavado, A. Skin pathology induced by snake venom metalloproteinase: Acute damage, revascularization, and re-epithelization in a mouse ear model. *J. Invest. Dermatol.* **128**, 2421–2428 (2008).

28. Dubovskii, P., Konshina, A. & Efremov, R. Cobra Cardiotoxins: Membrane Interactions and Pharmacological Potential. *Curr. Med. Chem.* **21**, 270–287 (2013).

29. Sarkar, B., Maitra, S. & Ghosh, B. The Effect of Neurotoxin, Haemolysin and Choline Esterase Isolated from Cobra Venom on Heart, Blood Pressure and Respiration. *J. Ind. chem. Soc.* **30**, 453–460 (1942).

30. Sarkar, N. K. Isolation of cardiotoxin from cobra venom (Naja tripudians), monocellate variety). *J. Ind. chem. Soc.* **24**, 227–232 (1947).

31. Harvey, A. L. Cardiotoxins from cobra venoms: Possible mechanisms of action. *Toxin Rev.* **4**, 41–69 (1985).

32. Dufton, M.J., Hider, R. C. Structure and pharmacology of elapid cytotoxins. *Pharmacol Ther* **36**, 1–40 (1988).

33. Kazandjian, T. D. *et al.* Convergent evolution of pain-inducing defensive venom components in spitting cobras. *Science (80-.).* **371**, 386–390 (2021).

34. Lomonte, B., Tarkowski, A. & Hanson, L. Å. Broad cytolytic specificity of myotoxin II, a lysine-49 phospholipase A2 of Bothrops asper snake venom. *Toxicon* **32**, 1359–1369 (1994).

35. Bultrón, E., Thelestam, M. & Gutiérrez, J. Effects on cultured mammalian cells of myotoxin III, a phospholipase A2 isolated from Bothrops asper (terciopelo) venom. *Biochim. Biophys. Acta - Mol. Cell Res.* **1179**, 253–259 (1993).

36. Queiroz, L. S., Santo Neto, H., Assakura, M. T., Reichl, A. P. & Mandelbaum, F. R. Pathological changes in muscle caused by haemorrhagic and proteolytic factors from Bothrops jararaca snake venom. *Toxicon* **23**, 341–345 (1985).

37. Ownby, C. L. Structure, function and biophysical aspects of the myotoxins from snake venoms. *J. Toxicol. - Toxin Rev.* **17**, 213–238 (1998).

38. Rucavado, A., Lomonte, B., Ovadia, M. & Gutiérrez, J. M. Local tissue damage induced by BaP1, a metalloproteinase isolated from Bothrops asper (Terciopelo) snake venom. *Exp. Mol. Pathol.* **63**, 186–199 (1995).

39. Williams, H. F. *et al.* Mechanisms underpinning the permanent muscle damage induced by snake venom metalloprotease. *PLoS Negl. Trop. Dis.* **13**, 1–20 (2019).

40. Alberts, B. *et al. Essential cell biology: Fifth international student edition*. (WW Norton & Company., 2018).

41. Brahma, R.K., Modahl, C.M., Kini, R. M. Three-Finger Toxins. in *Handbook of Venoms and Toxins of Reptiles* (ed. Mackessy, S. P.) (CRC Press, 2021).

42. Bilwes, A., Rees, B., Moras, D., Ménez, R. & Ménez, A. X-ray structure at 1.55 Å of toxin γ, a cardiotoxin from Naja nigricollis venom: Crystal packing reveals a model for insertion into membranes. *Journal of Molecular Biology* vol. 239 122–136 at https://doi.org/10.1006/jmbi.1994.1357 (1994).

43. Dufton, M. J. & Hider, R. C. Conformational properties of the neurotoxins and cytotoxins isolated from Elapid snake venoms. *CRC Crit. Rev. Biochem.* **14**, 113–171 (1983).

44. Dauplais, M., Neumann, J. M., Pinkasfeld, S., Ménez, A. & Roumestand, C. An NMR Study of the Interaction of Cardiotoxin γ from Naja nigricollis with Perdeuterated Dodecylphosphocholine Micelles. *Eur. J. Biochem.* **230**, 213–220 (1995).

45. Forouhar, F. *et al.* Structural basis of membrane-induced cardiotoxin A3 oligomerization. *J. Biol. Chem.* **278**, 21980–21988 (2003).

46. Feofanov, A. V. *et al.* Cancer cell injury by cytotoxins from cobra venom is mediated through lysosomal damage. *Biochem. J.* **390**, 11–18 (2005).

47. Hiu, J. J. & Yap, M. K. K. The myth of cobra venom cytotoxin: More than just direct cytolytic actions. *Toxicon X* **14**, 100123 (2022).

48. Condrea, E., De Vries, A. & Mager, J. Hemolysis and splitting of human erythrocyte phospholipids by snake venoms. *BBA - Spec. Sect. Lipids Relat. Subj.* **84**, 60–73 (1964).

49. Klibansky, C., London, Y., Frenkel, A. & De Vries, A. Enhancing action of synthetic and natural basic polypeptides on erythrocyte-ghost phospholipid hydrolysis by phospholipase A. *Biochim. Biophys. Acta - Biomembr.* **150**, 15–23 (1968).

50. Louw, A. I. & Visser, L. The synergism of cardiotoxin and phospholipase A2 in hemolysis. *BBA - Biomembr.* **512**, 163–171 (1978).

51. Pucca, M. B. *et al.* Unity Makes Strength: Exploring Intraspecies and Interspecies Toxin Synergism between Phospholipases A2 and Cytotoxins. *Front. Pharmacol.* **11**, 1–10 (2020).

52. Bougis, P. E., Marchot, P. & Rochat, H. In vivo synergy of cardiotoxin and phospholipase A2 from the elapid snake Naja mossambica mossambica. *Toxicon* **25**, 427–431 (1987).

53. Kini, R. M. Excitement ahead: Structure, function and mechanism of snake venom phospholipase A2 enzymes. *Toxicon* **42**, 827–840 (2003).

54. Tasoulis, T. & Isbister, G. K. A current perspective on snake venom composition and constituent protein families. *Arch. Toxicol. 2022 971* **97**, 133–153 (2022).

55. Lomonte, B., Krizaj, I. Snake venom phospholipase A2 toxins. in *Handbook of Venoms and Toxins of Reptiles* (ed. Mackessy, S. P.) 389–411 (CRC Press, 2021).

56. Lynch, V. J. Inventing an arsenal: adaptive evolution and neofunctionalization of snake venom phospholipase A 2 genes. (2007) doi:10.1186/1471-2148-7-2.

57. Kini, R. M. Structure – function relationships and mechanism of anticoagulant phospholipase A 2 enzymes from snake venoms. *Toxicon* **45**, 1147–1161 (2005).

58. Lomonte, B. Lys49 myotoxins, secreted phospholipase A2-like proteins of viperid venoms: A comprehensive review. *Toxicon* **224**, 107024 (2023).

59. Fernández, J. *et al.* Muscle phospholipid hydrolysis by Bothrops asper Asp49 and Lys49 phospholipase A2 myotoxins – distinct mechanisms of action. *FEBS J.* **280**, 3878–3886 (2013).

60. Fernandes, C. A. H., Borges, R. J., Lomonte, B. & Fontes, M. R. M. A structure-based proposal for a comprehensive myotoxic mechanism of phospholipase A2-like proteins from viperid snake venoms. *Biochim. Biophys. Acta - Proteins Proteomics* **1844**, 2265–2276 (2014).

61. Fernandes, C. A. H. *et al.* Comparison between apo and complexed structures of bothropstoxin-I reveals the role of Lys122 and Ca2+-binding loop region for the catalytically inactive Lys49-PLA2s. *J. Struct. Biol.* **171**, 31–43 (2010).

62. Mora-Obando, D., Fernández, J., Montecucco, C., Gutiérrez, J. M. & Lomonte, B. Synergism between basic Asp49 and Lys49 phospholipase A2 myotoxins of viperid snake venom in vitro and in vivo. *PLoS One* **9**, (2014).

63. Lomonte, B. *et al.* Comparative study of the cytolytic activity of myotoxic phospholipases A2 on mouse endothelial (tEnd) and skeletal muscle (C2C12) cells in vitro. *Toxicon* **37**, 145–158 (1999).

64. Villalobos, J. C., Mora, R., Lomonte, B., Gutiérrez, J. M. & Angulo, Y. Cytotoxicity induced in myotubes by a Lys49 phospholipase A2 homologue from the venom of the snake Bothrops asper: Evidence of rapid plasma membrane damage and a dual role for extracellular calcium. *Toxicol. Vitr.* **21**, 1382–1389 (2007).

65. Cintra-Francischinelli, M. *et al.* Calcium imaging of muscle cells treated with snake myotoxins reveals toxin synergism and presence of acceptors. *Cell. Mol. Life Sci.* **66**, 1718–1728 (2009).

66. López-Dávila, A. J., Lomonte, B. & Gutiérrez, J. M. Alterations of the skeletal muscle contractile apparatus in necrosis induced by myotoxic snake venom phospholipases A2: a mini-review. *J. Muscle Res. Cell Motil.* (2023) doi:10.1007/s10974-023-09662-4.

67. Mora, R., Valverde, B., Díaz, C., Lomonte, B. & Gutiérrez, J. M. A Lys49 phospholipase A2 homologue from Bothrops asper snake venom induces proliferation, apoptosis and necrosis in a lymphoblastoid cell line. *Toxicon* **45**, 651–660 (2005).

68. Mora, R., Maldonado, A., Valverde, B. & Gutiérrez, J. M. Calcium plays a key role in the effects induced by a snake venom Lys49 phospholipase A 2 homologue on a lymphoblastoid cell line. *Toxicon* **47**, 75–86 (2006).

69. Mebs, D. & Ownby, C. L. Myotoxic components of snake venoms: Their biochemical and biological activities. *Pharmacol. Ther.* **48**, 223–236 (1990).

70. Tasoulis, T. & Isbister, G. K. A review and database of snake venom proteomes. *Toxins (Basel).* **9**, (2017).

71. Hayashi, M. A. F. *et al.* Cytotoxic effects of crotamine are mediated through lysosomal membrane permeabilization. *Toxicon* **52**, 508–517 (2008).

72. Kerkis, I., Silva, F. D. S., Pereira, A., Kerkis, A. & Rádis-Baptista, G. Biological versatility of crotamine a cationic peptide from the venom of a South American rattlesnake. *Expert Opin. Investig. Drugs* **19**, 1515–1525 (2010).

73. Chang, C. C. & Tseng, K. H. Effect of crotamine, a toxin of south american rattlesnake venom, on the sodium channel of murine skeletal muscle. *Br. J. Pharmacol.* **63**, 551–559 (1978).

74. Ownby, C. L., Cameron, D. & Tu, A. T. Isolation of myotoxic component from rattlesnake (Crotalus viridis viridis) venom. Electron microscopic analysis of muscle damage. *Am. J. Pathol.* **85**, 149 (1976).

75. Joshi, R. *et al.* Evaluation of crotamine based probes as intracellular targeted contrast agents for magnetic resonance imaging. *Bioorg. Med. Chem.* **69**, 116863 (2022).

76. Frantz, C., Stewart, K. M. & Weaver, V. M. The extracellular matrix at a glance. *J. Cell Sci.* **123**, 4195–4200 (2010).

77. Jayadev, R. & Sherwood, D. R. Basement membranes. *Curr. Biol.* **27**, R207–R211 (2017).

78. Grönloh, M. L. B., Arts, J. J. G. & van Buul, J. D. Neutrophil transendothelial migration hotspots – Mechanisms and implications. *J. Cell Sci.* **134**, (2021).

79. Escalante, T., Rucavado, A., Fox, J. W. & Gutiérrez, J. M. Key events in microvascular damage induced by snake venom hemorrhagic metalloproteinases. *J. Proteomics* **74**, 1781–1794 (2011).

80. Gutiérrez, J. M., Escalante, T., Rucavado, A., Herrera, C. & Fox, J. W. A comprehensive view of the structural and functional alterations of extracellular matrix by snake venom metalloproteinases (SVMPs): Novel perspectives on the pathophysiology of envenoming. *Toxins (Basel).* **8**, (2016).

81. Tasoulis, T., Pukala, T. L. & Isbister, G. K. Investigating Toxin Diversity and Abundance in Snake Venom Proteomes. *Front. Pharmacol.* **12**, (2022).

82. Fox, J. W. & Serrano, S. M. T. Structural considerations of the snake venom metalloproteinases, key members of the M12 reprolysin family of metalloproteinases. *Toxicon* **45**, 969–985 (2005).

83. Anai, K., Sugiki, M., Yoshida, E. & Maruyama, M. Neutralization of a snake venom hemorrhagic metalloproteinase prevents coagulopathy after subcutaneous injection of Bothrops jararaca venom in rats. *Toxicon* **40**, 63–68 (2002).

84. Herrera, C. *et al.* Tissue Localization and Extracellular Matrix Degradation by PI, PII and PIII Snake Venom Metalloproteinases: Clues on the Mechanisms of Venom-Induced Hemorrhage. *PLoS Negl. Trop. Dis.* **9**, 1–20 (2015).

85. Baldo, C., Jamora, C., Yamanouye, N., Zorn, T. M. & Moura-da-Silva, A. M. Mechanisms of vascular damage by hemorrhagic snake venom metalloproteinases: Tissue distribution and in Situ hydrolysis. *PLoS Negl. Trop. Dis.* **4**, (2010).

86. Gutiérrez, J. M. *et al.* Skeletal muscle necrosis and regeneration after injection of BaH1, a hemorrhagic metalloproteinase isolated from the venom of the snake Bothrops asper (terciopelo). *Exp. Mol. Pathol.* **62**, 28–41 (1995).

87. Boer-Lima, P. A., Rocha Gontijo, J. A. & Da Cruz-Höfling, M. A. Bothrops moojeni snake venom-induced renal glomeruli changes in rat. *Am. J. Trop. Med. Hyg.* **67**, 217–222 (2002).

88. Herrera, C., Escalante, T., Rucavado, A., Fox, J. W. & Gutiérrez, J. M. Metalloproteinases in disease: identification of biomarkers of tissue damage through proteomics. *Expert Rev. Proteomics* **15**, 967–982 (2018).

89. Junqueira-de-Azevedo, I. L. M., Campos, P. F., Ching, A. T. C. & Mackessy, S. P. Colubrid Venom Composition: An -Omics Perspective. *Toxins (Basel).* **8**, 1–24 (2016).

90. Kemparaju, K. & Girish, K. S. Snake venom hyaluronidase: A therapeutic target. *Cell Biochem. Funct.* **24**, 7–12 (2006).

91. Girish, K. S. & Kemparaju, K. The magic glue hyaluronan and its eraser hyaluronidase: A biological overview. *Life Sci.* **80**, 1921–1943 (2007).

92. Tu, A. T. & Hendon, R. R. Characterization of lizard venom hyaluronidase and evidence for its action as a spreading factor. *Comp. Biochem. Physiol. Part B Comp. Biochem.* **76**, 377–383 (1983).

93. Girish, K., Kemparaju, K., Nagaraju, S. & Vishwanath, B. Hyaluronidase Inhibitors: A Biological and Therapeutic Perspective. *Curr. Med. Chem.* **16**, 2261–2288 (2009).

94. Yingprasertchai, S., Bunyasrisawat, S. & Ratanabanangkoon, K. Hyaluronidase inhibitors (sodium cromoglycate and sodium auro-thiomalate) reduce the local tissue damage and prolong the survival time of mice injected with Naja kaouthia and Calloselasma rhodostoma venoms. *Toxicon* **42**, 635–646 (2003).

95. Sunitha, K. *et al.* Inflammation and oxidative stress in viper bite: An insight within and beyond. *Toxicon* **98**, 89–97 (2015).

96. Resiere, D., Mehdaoui, H. & Neviere, R. Inflammation and Oxidative Stress in Snakebite Envenomation: A Brief Descriptive Review and Clinical Implications. *Toxins (Basel).* **14**, (2022).

97. Rucavado, A. *et al.* Viperid Envenomation Wound Exudate Contributes to Increased Vascular Permeability via a DAMPs/TLR-4 Mediated Pathway. *Toxins 2016, Vol. 8, Page 349* **8**, 349 (2016).

98. Zuliani, J. P. Alarmins and inflammatory aspects related to snakebite envenomation. *Toxicon* **226**, (2023).

99. Cintra-Francischinelli, M. *et al.* Bothrops snake myotoxins induce a large efflux of ATP and potassium with spreading of cell damage and pain. *Proc. Natl. Acad. Sci. U. S. A.* **107**, 14140–14145 (2010).

100. Mora, J., Mora, R., Lomonte, B. & Gutiérrez, J. M. Effects of bothrops asper snake venom on lymphatic vessels: Insights into a hidden aspect of envenomation. *PLoS Negl. Trop. Dis.* **2**, (2008).

101. Warrell, D. A., Greenwood, B. M., Davidson, N. M., Ormerod, L. D. & Prentice, C. R. Necrosis, haemorrhage and complement depletion following bites by the spitting cobra (Naja nigricollis). *Q. J. Med* **45**, 1–22 (1976).

102. Warrell, D. A. & Ormerod, L. D. Snake Venom Ophthalmia and Blindness Caused by the Spitting Cobra (Naja Nigricollis) in Nigeria. *Am. J. Trop. Med. Hyg.* **25**, 525–529 (1976).

103. Gimenes, S. N. C. *et al.* Observation of bothrops atrox snake envenoming blister formation from five patients: Pathophysiological insights. *Toxins (Basel).* **13**, 800 (2021).

104. De Souza Queiróz, L., Marques, M. J. & Santo Neto, H. Acute local nerve lesions induced by Bothrops jararacussu snake venom. *Toxicon* **40**, 1483–1486 (2002).

105. Hernández, R. *et al.* Poor regenerative outcome after skeletal muscle necrosis induced by bothrops asper venom: Alterations in microvasculature and nerves. *PLoS One* **6**, e19834 (2011).

106. Gutiérrez, J. M. *et al.* Why is Skeletal Muscle Regeneration Impaired after Myonecrosis Induced by Viperid Snake Venoms? *Toxins 2018, Vol. 10, Page 182* **10**, 182 (2018).

107. Azevedo-Marques, M. M. *et al.* Myonecrosis, myoglobinuria and acute renal failure induced by south american rattlesnake (Crotalus durissus terrificus) envenomation in brazil. *Toxicon* **23**, 631–636 (1985).

108. White, J. Clinical toxicology of snakebite in Australia and New Guinea. in *Handbook of Clinical Toxicology of Animal Venoms and Poisons* (eds. Meier, J. & White, J.) 595–617 (CRC Press, 1995).

109. Pinho, F. M. O., Zanetta, D. M. T. & Burdmann, E. A. Acute renal failure after Crotalus durissus snakebite: A prospective survey on 100 patients. *Kidney Int.* **67**, 659–667 (2005).

110. Arce-Bejarano, R., Lomonte, B. & Gutiérrez, J. M. Intravascular hemolysis induced by the venom of the Eastern coral snake, Micrurus fulvius, in a mouse model: Identification of directly hemolytic phospholipases A2. *Toxicon* **90**, 26–35 (2014).

111. Xie, C. *et al.* Erythrocyte haemotoxicity profiling of snake venom toxins after nanofractionation. *J. Chromatogr. B Anal. Technol. Biomed. Life Sci.* **1176**, 122586 (2021).

112. Sitprija, V. & Sitprija, S. Renal effects and injury induced by animal toxins. *Toxicon* **60**, 943–953 (2012).

113. de Paola, F. & Rossi, M. A. Myocardial damage induced by tropical rattlesnake (Crotalus durissus terrificus) venom in rats. *Cardiovasc. Pathol.* **2**, 77–81 (1993).

114. Hoffman, A., Levi, O., Orgad, U. & Nyska, A. Myocarditis following envenoming with Vipera palaestinae in two horses. *Toxicon* **31**, 1623–1628 (1993).

115. Tanjoni, I. *et al.* Jararhagin, a snake venom metalloproteinase, induces a specialized form of apoptosis (anoikis) selective to endothelial cells. *Apoptosis* **10**, 851–861 (2005).

116. Díaz, C., Valverde, L., Brenes, O., Rucavado, A. & Gutiérrez, J. M. Characterization of events associated with apoptosis/anoikis induced by snake venom metalloproteinase BaP1 on human endothelial cells. *J. Cell. Biochem.* **94**, 520–528 (2005).

117. Grossmann, J. Molecular mechanisms of 'detachment-induced apoptosis - Anoikis'. *Apoptosis* **7**, 247–260 (2002).

118. Paoli, P., Giannoni, E. & Chiarugi, P. Anoikis molecular pathways and its role in cancer progression. *Biochim. Biophys. Acta - Mol. Cell Res.* **1833**, 3481–3498 (2013).

119. Meredith, J. E., Fazeli, B. & Schwartz, M. A. The extracellular matrix as a cell survival factor. *Mol. Biol. Cell* **4**, 953 (1993).

120. Aoudjit, F. & Vuori, K. Matrix Attachment Regulates FAS-Induced Apoptosis in Endothelial CellsA Role for C-Flip and Implications for Anoikis. *J. Cell Biol.* **152**, 633–644 (2001).

121. Borkow, G., Gutiérrez, J. & Ovadia, M. In vitro activity of BaH1, the main hemorrhagic toxin of Bothrops asper snake venom on bovine endothelial cells. *Toxicon* **33**, 1387–1391 (1995).

122. Araki, S., Masuda, S., Maeda, H., Ying, M. J. & Hayashi, H. Involvement of specific integrins in apoptosis induced by vascular apoptosis-inducing protein 1. *Toxicon* **40**, 535–542 (2002).

123. Brenes, O., Muñóz, E., Roldán-Rodríguez, R. & Díaz, C. Cell death induced by Bothrops asper snake venom metalloproteinase on endothelial and other cell lines. *Exp. Mol. Pathol.* **88**, 424–432 (2010).

124. Calvete, J. J. *et al.* Snake venom disintegrins: Evolution of structure and function. *Toxicon* **45**, 1063–1074 (2005).

125. Cesar, P. H. S., Braga, M. A., Trento, M. V. C., Menaldo, D. L. & Marcussi, S. Snake Venom Disintegrins: An Overview of their Interaction with Integrins. *Curr. Drug Targets* **20**, 465–477 (2018).

126. Sartim, M. A. & Sampaio, S. V. Snake venom galactoside-binding lectins: A structural and functional overview. *J. Venom. Anim. Toxins Incl. Trop. Dis.* **21**, 1–11 (2015).

127. Nunes, E. S. *et al.* Cytotoxic effect and apoptosis induction by Bothrops leucurus venom lectin on tumor cell lines. *Toxicon* **59**, 667–671 (2012).

128. Pathan, J., Mondal, S., Sarkar, A. & Chakrabarty, D. Daboialectin, a C-type lectin from Russell's viper venom induces cytoskeletal damage and apoptosis in human lung cancer cells in vitro. *Toxicon* **127**, 11–21 (2017).

129. Zhang, C., Medzihradszky, K. F., Sánchez, E. E., Basbaum, A. I. & Julius, D. Lys49 myotoxin from the Brazilian lancehead pit viper elicits pain through regulated ATP release. *Proc. Natl. Acad. Sci. U. S. A.* **114**, E2524–E2532 (2017).

130. Bours, M. J. L., Swennen, E. L. R., Di Virgilio, F., Cronstein, B. N. & Dagnelie, P. C. Adenosine 5′-triphosphate and adenosine as endogenous signaling molecules in immunity and inflammation. *Pharmacol. Ther.* **112**, 358–404 (2006).

131. Di Virgilio, F. Liaisons dangereuses: P2X7 and the inflammasome. *Trends Pharmacol. Sci.* **28**, 465–472 (2007).

132. Tonello, F. *et al.* A Lys49-PLA2 myotoxin of Bothrops asper triggers a rapid death of macrophages that involves autocrine purinergic receptor signaling. *Cell Death Dis. 2012 37* **3**, e343–e343 (2012).

133. Schieber, M. & Chandel, N. S. ROS function in redox signaling and oxidative stress. *Curr. Biol.* **24**, R453–R462 (2014).

134. Fujii, J., Homma, T. & Osaki, T. Superoxide Radicals in the Execution of Cell Death. *Antioxidants 2022, Vol. 11, Page 501* **11**, 501 (2022).

135. Du, X. Y. & Clemetson, K. J. Snake venom L-amino acid oxidases. *Toxicon* **40**, 659–665 (2002).

136. Guo, C., Liu, S., Yao, Y., Zhang, Q. & Sun, M. Z. Past decade study of snake venom l-amino acid oxidase. *Toxicon* **60**, 302–311 (2012).

137. Ande, S. R. *et al.* Mechanisms of cell death induction by L-amino acid oxidase, a major component of ophidian venom. *Apoptosis* **11**, 1439–1451 (2006).

138. Costal-Oliveira, F. *et al.* L-amino acid oxidase from Bothrops atrox snake venom triggers autophagy, apoptosis and necrosis in normal human keratinocytes. *Sci. Rep.* **9**, (2019).

139. Naumann, G. B. *et al.* Cytotoxicity and inhibition of platelet aggregation caused by an l-amino acid oxidase from Bothrops leucurus venom. *Biochim. Biophys. Acta - Gen. Subj.* **1810**, 683–694 (2011).

140. Torii, S., Naito, M. & Tsuruo, T. Apoxin I, a Novel Apoptosis-inducing Factor with L-Amino Acid Oxidase Activity Purified from Western Diamondback Rattlesnake Venom. *J. Biol. Chem.* **272**, 9539–9542 (1997).

141. Abidin, S. A. Z., Rajadurai, P., Chowdhury, E. H., Othman, I. & Naidu, R. Cytotoxic, Anti-Proliferative and Apoptosis Activity of l-Amino Acid Oxidase from Malaysian Cryptelytrops purpureomaculatus (CP-LAAO) Venom on Human Colon Cancer Cells. *Mol. 2018, Vol. 23, Page 1388* **23**, 1388 (2018).

142. Morais, I. C. O. *et al.* L-Aminoacid Oxidase from Bothrops leucurus Venom Induces Nephrotoxicity via Apoptosis and Necrosis. *PLoS One* **10**, e0132569 (2015).

143. Tavares, C. *et al.* l-Amino acid oxidase isolated from Calloselasma rhodostoma snake venom induces cytotoxicity and apoptosis in JAK2V617F-positive cell lines. *Rev. Bras. Hematol. Hemoter.* **38**, 128–134 (2016).

144. Burin, S. M. *et al.* CR-LAAO antileukemic effect against Bcr-Abl+ cells is mediated by apoptosis and hydrogen peroxide. *Int. J. Biol. Macromol.* **86**, 309–320 (2016).

145. Das, T. *et al.* Inhibition of leukemic U937 cell growth by induction of apoptosis, cell cycle arrest and suppression of VEGF, MMP-2 and MMP-9 activities by cytotoxin protein NN-32 purified from Indian spectacled cobra (Naja naja) venom. *Toxicon* **65**, 1–4 (2013).

146. Yang, S.-H., Chien, C.-M., Chang, L.-S. & Lin, S.-R. Cardiotoxin III-Induced Apoptosis Is Mediated by Ca 2+-Dependent Caspase-12 Activation in K562 Cells. *J Biochem Mol. Toxicol.* **22**, 209–218 (2008).

147. Tsai, C. H. *et al.* Mechanisms of cardiotoxin iii-induced apoptosis in human colorectal cancer colo205 cells. *Clin. Exp. Pharmacol. Physiol.* **33**, 177–182 (2006).

148. Chiou, J. T. *et al.* Naja atra Cardiotoxin 3 Elicits Autophagy and Apoptosis in U937 Human Leukemia Cells through the Ca2+/PP2A/AMPK Axis. *Toxins 2019, Vol. 11, Page 527* **11**, 527 (2019).

149. Gutiérrez, J. M. *et al.* Tissue pathology induced by snake venoms: How to understand a complex pattern of alterations from a systems biology perspective? *Toxicon* **55**, 166–170 (2010).

150. Pucca, M. B. *et al.* History of Envenoming Therapy and Current Perspectives. *Front. Immunol.* **10**, 1–13 (2019).

151. León, G. *et al.* Current technology for the industrial manufacture of snake antivenoms. *Toxicon* **151**, 63–73 (2018).

152. Gutiérrez, J. M. *et al.* Neutralization of local tissue damage induced by Bothrops asper (terciopelo) snake venom. *Toxicon* **36**, 1529–1538 (1998).

153. Gutiérrez, J. M., León, G., Lomonte, B. & Angulo, Y. Antivenoms for snakebite envenomings. *Inflamm. Allergy - Drug Targets* **10**, 369–380 (2011).

154. Harrison, R. A. *et al.* Research strategies to improve snakebite treatment: Challenges and progress. *J. Proteomics* **74**, 1768–1780 (2011).

155. Williams, D. J. *et al.* Ending the drought: New strategies for improving the flow of affordable, effective antivenoms in Asia and Africa. *J. Proteomics* **74**, 1735–1767 (2011).

156. Gutiérrez, J. M., Lomonte, B., Sanz, L., Calvete, J. J. & Pla, D. Immunological profile of antivenoms: Preclinical analysis of the efficacy of a polyspecific antivenom through antivenomics and neutralization assays. *J. Proteomics* **105**, 340–350 (2014).

157. Ratanabanangkoon, K. A Quest for a Universal Plasma-Derived Antivenom Against All Elapid Neurotoxic Snake Venoms. *Frontiers in Immunology* vol. 12 1363 at https://doi.org/10.3389/fimmu.2021.668328 (2021).

158. Dennis, E. A., Cao, J., Hsu, Y. H., Magrioti, V. & Kokotos, G. Phospholipase A2 enzymes: Physical structure, biological function, disease implication, chemical inhibition, and therapeutic intervention. *Chem. Rev.* **111**, 6130–6185 (2011).

159. Magrioti, V. & Kokotos, G. Phospholipase A2 inhibitors for the treatment of inflammatory diseases: a patent review (2010--present). *Expert Opin. Ther. Pat.* **23**, 333–344 (2013).

160. Serruys, P. W. & Garcia-Garcia, H. M. Phospholipase A2 inhibitors. *Curr. Opin. Lipidol.* **20**, 327–332 (2009).

161. Lewin, M., Samuel, S., Merkel, J. & Bickler, P. Varespladib (LY315920) appears to be a potent, broad-spectrum, inhibitor of snake venom phospholipase A2 and a possible pre-referral treatment for envenomation. *Toxins (Basel).* **8**, (2016).

162. Gutiérrez, J. M. *et al.* The search for natural and synthetic inhibitors that would complement antivenoms as therapeutics for snakebite envenoming. *Toxins (Basel).* **13**, 1–30 (2021).

163. Lewin, M. R. *et al.* Delayed oral LY333013 rescues mice from highly neurotoxic, lethal doses of papuan taipan (Oxyuranus scutellatus) venom. *Toxins (Basel).* **10**, 1–7 (2018).

164. Bryan-Quirós, W., Fernández, J., Gutiérrez, J. M., Lewin, M. R. & Lomonte, B. Neutralizing properties of LY315920 toward snake venom group I and II myotoxic phospholipases A2. *Toxicon* **157**, 1–7 (2019).

165. Xiao, H. *et al.* Inactivation of Venom PLA2 Alleviates Myonecrosis and Facilitates Muscle Regeneration in Envenomed Mice: A Time Course Observation. *Mol. 2018, Vol. 23, Page 1911* **23**, 1911 (2018).

166. Bittenbinder, M. A. *et al.* Coagulotoxic Cobras: Clinical Implications of Strong Anticoagulant Actions of African Spitting Naja Venoms That Are Not Neutralised by Antivenom but Are by LY315920 (Varespladib). *Toxins (Basel).* **10**, 516 (2018).

167. Hall, S. R. *et al.* Repurposed drugs and their combinations prevent morbidity-inducing dermonecrosis caused by diverse cytotoxic snake venoms. *Nat. Commun.* (2023) doi:10.1101/2022.05.20.492855.

168. Carter, R. W. *et al.* The BRAVO Clinical Study Protocol: Oral Varespladib for Inhibition of Secretory Phospholipase A2 in the Treatment of Snakebite Envenoming. *Toxins (Basel).* **15**, (2023).

169. Laustsen, A. *et al.* From Fangs to Pharmacology: The Future of Snakebite Envenoming Therapy. *Curr. Pharm. Des.* **22**, 5270–5293 (2016).

170. Jenkins, T. P. *et al.* Toxin neutralization using alternative binding proteins. *Toxins (Basel).* **11**, 1–28 (2019).

171. Rucavado, A., Escalante, T. & Gutiérrez, J. M. Effect of the metalloproteinase inhibitor batimastat in the systemic toxicity induced by Bothrops asper snake venom: Understanding the role of metalloproteinases in envenomation. *Toxicon* **43**, 417–424 (2004).

172. Rucavado, A. *et al.* Inhibition of local hemorrhage and dermonecrosis induced by Bothrops asper snake venom: Effectiveness of early in situ administration of the peptidomimetic metalloproteinase inhibitor batimastat and the chelating agent CaNa2EDTA. *Am. J. Trop. Med. Hyg.* **63**, 313–319 (2000).

173. Arias, A. S., Rucavado, A. & Gutiérrez, J. M. Peptidomimetic hydroxamate metalloproteinase inhibitors abrogate local and systemic toxicity induced by Echis ocellatus (saw-scaled) snake venom. *Toxicon* **132**, 40–49 (2017).

174. Howes, J. M., Theakston, R. D. G. & Laing, G. D. Neutralization of the haemorrhagic activities of viperine snake venoms and venom metalloproteinases using synthetic peptide inhibitors and chelators. *Toxicon* **49**, 734–739 (2007).

175. Albulescu, L. O. *et al.* Preclinical validation of a repurposed metal chelator as an early-intervention therapeutic for hemotoxic snakebite. *Sci. Transl. Med.* **12**, (2020).

176. Albulescu, L.-O. *et al.* Preclinical validation of a repurposed metal chelator as a community-based therapeutic for hemotoxic snakebite. *bioRxiv* 717280 (2019) doi:10.1101/717280.

177. Albulescu, L. O. *et al.* A therapeutic combination of two small molecule toxin inhibitors provides broad preclinical efficacy against viper snakebite. *Nat. Commun.* **11**, 1–14 (2020).

178. Sivaramakrishnan, V. *et al.* Viper venom hyaluronidase and its potential inhibitor analysis: a multipronged computational investigation. *J. Biomol. Struct. Dyn.* **35**, 1979–1989 (2017).

179. Casewell, N. R., Jackson, T. N. W., Laustsen, A. H. & Sunagar, K. Causes and Consequences of Snake Venom Variation. *Trends Pharmacol. Sci.* **41**, 570–581 (2020).

180. Roncolato, E. C. *et al.* Human antibody fragments specific for Bothrops jararacussu venom reduce the toxicity of other Bothrops sp. venoms. *J. Immunotoxicol.* **10**, 160–168 (2013).

181. Laustsen, A. H. *et al.* Pros and cons of different therapeutic antibody formats for recombinant antivenom development. *Toxicon* **146**, 151–175 (2018).

182. Lauridsen, L. H., Shamaileh, H. A., Edwards, S. L., Taran, E. & Veedu, R. N. Rapid One-Step Selection Method for Generating Nucleic Acid Aptamers: Development of a DNA Aptamer against α-Bungarotoxin. *PLoS One* **7**, e41702 (2012).

183. Chen, Y. J., Tsai, C. Y., Hu, W. P. & Chang, L. Sen. DNA Aptamers against Taiwan Banded Krait α-Bungarotoxin Recognize Taiwan Cobra Cardiotoxins. *Toxins (Basel).* **8**, (2016).

184. Lynagh, T. *et al.* Peptide Inhibitors of the α-Cobratoxin-Nicotinic Acetylcholine Receptor Interaction. *J. Med. Chem.* **63**, 13709–13718 (2020).

185. O'Brien, J., Lee, S. H., Gutiérrez, J. M. & Shea, K. J. Engineered nanoparticles bind elapid snake venom toxins and inhibit venom-induced dermonecrosis. *PLoS Negl. Trop. Dis.* **12**, 1–20 (2018).

186. Albulescu, L. O. *et al.* A decoy-receptor approach using nicotinic acetylcholine receptor mimics reveals their potential as novel therapeutics against neurotoxic snakebite. *Front. Pharmacol.* **10**, 1–15 (2019).

187. Otvos, R. A. *et al.* Analytical workflow for rapid screening and purification of bioactives from venom proteomes. *Toxicon* **76**, 270–281 (2013).

188. Palermo, G. *et al.* Acetylcholine-Binding Protein Affinity Profiling of Neurotoxins in Snake Venoms with Parallel Toxin Identification. *Int. J. Mol. Sci.* **24**, 16769 (2023).

189. Nakamoto, M., Escalante, T., Gutiérrez, J. M. & Shea, K. J. A Biomimetic of Endogenous Tissue Inhibitors of Metalloproteinases: Inhibition Mechanism and Contribution of Composition, Polymer Size, and Shape to the Inhibitory Effect. *Nano Lett.* **21**, 5663–5670 (2021).

190. Puzari, U., Fernandes, P. A. & Mukherjee, A. K. Pharmacological re-assessment of traditional medicinal plants-derived inhibitors as antidotes against snakebite envenoming: A critical review. *Journal of Ethnopharmacology* vol. 292 115208 at https://doi.org/10.1016/j.jep.2022.115208 (2022).

191. Lizano, S., Domont, G. & Perales, J. Natural phospholipase A2 myotoxin inhibitor proteins from snakes, mammals and plants. *Toxicon* **42**, 963–977 (2003).

192. Bastos, V. A., Gomes-Neto, F., Perales, J., Neves-Ferreira, A. G. C. & Valente, R. H. Natural inhibitors of snake venom metalloendopeptidases: History and current challenges. *Toxins (Basel).* **8**, (2016).

193. van Thiel, J. *et al.* Convergent evolution of toxin resistance in animals. *Biol. Rev.* **97**, 1823–1843 (2022).

194. Campos, P. C., de Melo, L. A., Dias, G. L. F. & Fortes-Dias, C. L. Endogenous phospholipase A2 inhibitors in snakes: A brief overview. *J. Venom. Anim. Toxins Incl. Trop. Dis.* **22**, 1–7 (2016).

195. Fortes-Dias, C. L. Endogenous inhibitors of snake venom phospholipases A2 in the blood plasma of snakes. *Toxicon* vol. 40 481–484 at https://doi.org/10.1016/S0041-0101(01)00274-4 (2002).

196. Neves-Ferreira, A.G.C.; Valente, R.H.; Perales, J. ; Domont, G. B. Natural inhibitors - Innate immunity to snake venoms. in *Handbook of Venoms and Toxins of Reptiles* (ed. Mackessy, S. P.) 259–284 (2010).

197. Mors, W. B., Célia Do Nascimento, M., Ruppelt Pereira, B. M. & Alvares Pereira, N. Plant natural products active against snake bite — the molecular approach. *Phytochemistry* **55**, 627–642 (2000).

198. Soares, A. M. *et al.* Medicinal Plants with Inhibitory Properties Against Snake Venoms. *Curr. Med. Chem.* **12**, 2625–2641 (2005).

199. Carvalho, B. M. A. *et al.* Snake Venom PLA 2 s Inhibitors Isolated from Brazilian Plants: Synthetic and Natural Molecules. *Biomed Res. Int.* **2013**, (2013).

200. Félix-Silva, J., Silva-Junior, A. A., Zucolotto, S. M. & Fernandes-Pedrosa, M. D. F. Medicinal Plants for the Treatment of Local Tissue Damage Induced by Snake Venoms: An Overview from Traditional Use to Pharmacological Evidence. *Evidence-based Complement. Altern. Med.* **2017**, (2017).

201. Zdenek, C. N. *et al.* A Taxon-Specific and High-Throughput Method for Measuring Ligand Binding to Nicotinic Acetylcholine Receptors. *Toxins (Basel).* **11**, 600 (2019).

202. Harris, R. J. *et al.* Assessing the binding of venoms from aquatic elapids to the nicotinic acetylcholine receptor orthosteric site of different prey models. *Int. J. Mol. Sci.* **21**, 1–13 (2020).

203. O'Brien, J., Lee, S. H., Onogi, S. & Shea, K. J. Engineering the Protein Corona of a Synthetic Polymer Nanoparticle for Broad-Spectrum Sequestration and Neutralization of Venomous Biomacromolecules. *J. Am. Chem. Soc.* **138**, 16604–16607 (2016).

204. De Oliveira, M. *et al.* Antagonism of myotoxic and paralyzing activities of bothropstoxin-I by suramin. *Toxicon* **42**, 373–379 (2003).

205. Murakami, M. T. *et al.* Inhibition of Myotoxic Activity of Bothrops asper Myotoxin II by the Anti-trypanosomal Drug Suramin. *J. Mol. Biol.* **350**, 416–426 (2005).

206. Salvador, G. H. M. *et al.* Structural and functional characterization of suramin-bound MjTX-I from Bothrops moojeni suggests a particular myotoxic mechanism. *Sci. Rep.* **8**, 1–15 (2018).

207. Lomonte, B., Moreno, E., Tarkowski, A., Hanson, L. A. & Maccarana, M. Neutralizing interaction between heparins and myotoxin II, a lysine 49 phospholipase A2 from Bothrops asper snake venom. Identification of a heparin-binding and cytolytic toxin region by the use of synthetic peptides and molecular modeling. *J. Biol. Chem.* **269**, 29867–29873 (1994).

208. Diccianni, M. B., Mistry, M. J., Hug, K. & Harmony, J. A. K. Inhibition of phospholipase A2 by heparin. *Biochim. Biophys. Acta (BBA)/Lipids Lipid Metab.* **1046**, 242–248 (1990).

209. Rocha, S. L. G. *et al.* Functional analysis of DM64, an antimyotoxic protein with immunoglobulin-like structure from Didelphis marsupialis serum. *Eur. J. Biochem.* **269**, 6052–6062 (2002).

210. Fernandes, C. A. H. *et al.* Structural Basis for the Inhibition of a Phospholipase A2-Like Toxin by Caffeic and Aristolochic Acids. *PLoS One* **10**, e0133370 (2015).

211. dos Santos, J. I. *et al.* Structural and Functional Studies of a Bothropic Myotoxin Complexed to Rosmarinic Acid: New Insights into Lys49-PLA2 Inhibition. *PLoS One* **6**, e28521 (2011).

212. Ticli, F. K. *et al.* Rosmarinic acid, a new snake venom phospholipase A2 inhibitor from Cordia verbenacea (Boraginaceae): antiserum action potentiation and molecular interaction. *Toxicon* **46**, 318–327 (2005).

213. Aung, H. T. *et al.* Biological and Pathological Studies of Rosmarinic Acid as an Inhibitor of Hemorrhagic Trimeresurus flavoviridis (habu) Venom. *Toxins 2010, Vol. 2, Pages 2478-2489* **2**, 2478–2489 (2010).

214. Chandra, V. *et al.* Structural Basis of Phospholipase A2 Inhibition for the Synthesis of Prostaglandins by the Plant Alkaloid Aristolochic Acid from a 1.7 Å Crystal Structure†,‡. *Biochemistry* **41**, 10914–10919 (2002).

215. Nakamoto, M., Zhao, D., Benice, O. R., Lee, S. H. & Shea, K. J. Abiotic Mimic of Endogenous Tissue Inhibitors of Metalloproteinases: Engineering Synthetic Polymer Nanoparticles for Use as a Broad-Spectrum Metalloproteinase Inhibitor. *J. Am. Chem. Soc.* **142**, 2338–2345 (2020).

216. Valente, R. H., Dragulev, B., Perales, J., Fox, J. W. & Domont, G. B. BJ46a, a snake venom metalloproteinase inhibitor isolation, characterization, cloning and insights into its mechanism of action. *Eur. J. Biochem.* **268**, 3042–3052 (2001).

217. Omori-Satoh, T., Sadahiro, S., Ohsaka, A. & Murata, R. Purification and characterization of an antihemorrhagic factor in the serum of Trimeresurus flavoviridis, a crotalid. *Biochim. Biophys. Acta - Protein Struct.* **285**, 414–426 (1972).

218. Srinivasa, V. *et al.* Novel Apigenin Based Small Molecule that Targets Snake Venom Metalloproteases. *PLoS One* **9**, e106364 (2014).

219. Preciado, L. M., Comer, J., Núñez, V., Rey-Súarez, P. & Pereañez, J. A. Inhibition of a Snake Venom Metalloproteinase by the Flavonoid Myricetin. *Mol. 2018, Vol. 23, Page 2662* **23**, 2662 (2018).

220. Bala, E., Hazarika, R., Singh, P., Yasir, M. & Shrivastava, R. A biological overview of Hyaluronidase: A venom enzyme and its inhibition with plants materials. *Mater. Today Proc.* **5**, 6406–6412 (2018).

221. Mio, K. & Stern, R. Inhibitors of the hyaluronidases. *Matrix Biol.* **21**, 31–37 (2002).

Bitis nasicornis

Chapter 3

Development of a high-throughput *in vitro* screening method for the assessment of cell-damaging activities of snake venoms

Mátyás A. Bittenbinder, Liliana Capinha, Daniel Da Costa Pereira, Julien Slagboom, Bas van de Velde, Nicholas R. Casewell, Paul Jennings, Jeroen Kool, Freek J. Vonk

PLOS Neglected Tropical Diseases, 2023

Abstract

Snakebite envenoming is a globally important public health issue that has devastating consequences on human health and well-being, with annual mortality rates between 81,000 and 138,000. Snake venoms may cause different pathological effects by altering normal physiological processes such as nervous transfer and blood coagulation. In addition, snake venoms can cause severe (local) tissue damage that may result in life-long morbidities, with current estimates pointing towards an additional 450,000 individuals who suffer from permanent disabilities such as amputations, contractions, and blindness. Despite such high morbidity rates, research to date has been mainly focused on the neurotoxic and haemotoxic effects of snake venoms and considerably less on venom-induced tissue damage. The molecular mechanisms underlying this pathology include membrane disruption and extracellular matrix degradation.

This research describes methods used to study the (molecular) mechanisms underlying venom-induced cell- and tissue damage. A selection of cellular bioassays and fluorescent microscopy were used to study cell-damaging activities of snake venoms in multi-well plates, using both crude and fractionated venoms. A panel of 10 representative medically relevant snake species, which cover a large part of the geographical regions most heavily affected by snakebite, was used. The study comprises both morphological data and quantitative data on cell metabolism and viability, which were measured over time. Based on this data, a distinction could be made in the ways by which viper and elapid venoms exert their effects on cells. We further made an effort to characterise the bioactive compounds causing these effects, using a combination of liquid chromatography methods followed by bioassaying and protein identification using proteomics. The outcomes of this study might prove valuable for better understanding venom-induced cell- and tissue-damaging pathologies and could be used in the process of developing and improving snakebite treatments.

3.1 Introduction

Snakebite is one of the most significant global health crises known to date, with severe implications for human health and well-being, especially in the tropical and subtropical countries of the developing world. Worldwide, snakebites are accountable for mortality rates ranging from 81.000 to 138.000 individuals each year [1]. As most cases of snakebite affect male agricultural workers and occur in developing countries in sub-Saharan Africa, South and Southeast Asia, and Latin America, the socioeconomic impact of snakebite on families and local economies can be substantial [1–5].

Snake venom is a highly variable mixture of dozens of enzymatic and non-enzymatic proteins, which may produce a range of local and systemic effects in bite victims, with some being life-threatening while others being permanently debilitating [1,6]. The clinical effects of snakebite envenoming can be divided into three main pathologies: haemotoxicity, neurotoxicity and tissue-damaging effects [1,7,8]. Although most life-threatening pathologies in snake bite victims result from the haemotoxic and neurotoxic effects, tissue-damaging activities are the leading cause of life-long disabilities such as blindness and amputations [1–3,9]. Although annual morbidity rates surpass 450,000 individuals, most research has been focusing on the haemotoxic and neurotoxic effects and considerably less on venom-induced tissue damage [1,10]. The cell- and tissue-damaging effects of snake venoms may result in a range of pathologies, including (local) haemorrhage, muscle and skin necrosis, oedema, and organ failure [1,8,11–13].

Tissue-damaging toxins can be loosely divided into two groups based on the mechanisms of action by which these toxins affect the cells. The first group consists of 'true' cytotoxins, as these directly affect the cells by disrupting cell membrane integrity. These include three-finger toxins (3FTxs), phospholipases A_2 (PLA_2s) and β-defensin-like toxins [1,7,12–17]. The second group of toxins could be considered to be indirectly cytotoxic and cause cell death as a secondary effect of the degradation of extracellular matrix (ECM) components, not by directly damaging the cells. This group consists of snake venom metalloproteinases (SVMPs) and hyaluronidases [11,18–20]. Other toxins that may cause cell- or tissue damage through alternative mechanisms include disintegrins, L-amino acid oxidases (LAAOs), and possibly C-type lectins [1,21–23].

In an attempt to study venom-induced cell damage and the toxins associated with it, we combined a panel of cell-based assays with nanofractionation analytics. First, a panel of cellular bioassays was used to study the effects of ten medically relevant snake venoms *in vitro* using an immortalised human renal proximal tubular cell line (RPTEC/TERT1). We investigated venom effects over time using an imaging fluorescent microscope, which was used to study both morphological alterations of the cells and quantification of the total live cell count and cell surface area. In addition, we performed assays to determine the metabolic activity and cell viability of the cells post-venom dosing. Based on these assays, a distinction could be made in the way by which the venoms of elapid and viper venoms affect the cells. The venoms of *N. mossambica* and *N. naja* affected the cell membrane, whereas all vipers (except *D. russelii*) caused detachment of the cell monolayer. The assays were then used for integration into nanofractionation analytics. In nanofractionation analytics, chromatographic separation of venom by HPLC (i.e., reversed-phase chromatography (RP-LC) or size-exclusion chromatography (SEC)) is followed by toxin fractionation on 96- or 384 microwell plates for subsequent (cellular) bioassaying and toxin identification [24–26]. This workflow allowed us to identify toxins with cytotoxic properties in the venom of the Mozambique spitting cobra (*Naja mossambica*) and West African carpet viper (*Echis ocellatus*). Subsequently, we used proteomics for detailed characterisation analysis whereby wells containing bioactive compounds were subjected to tryptic digestion followed by nanoLC-MS/MS for protein identification. Incorporation of the *in vitro* assays into the established analytical workflow allowed for the separation of the toxins, followed by bioactivity assessment in parallel with toxin identification (see Figure 1).

This approach allowed us to perform high-throughput profiling of cell- and tissue-damaging toxins in snake venoms. The outcomes of this study could benefit the future development of snakebite treatments against venom-induced tissue damage.

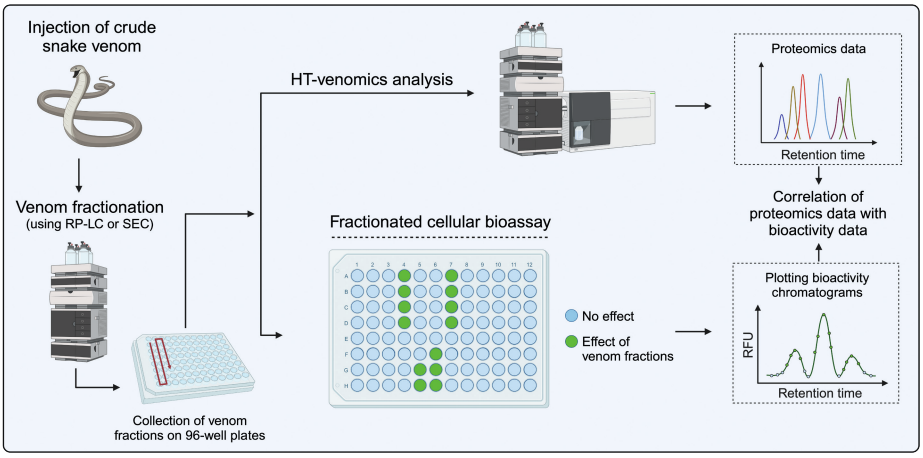

Figure 1. Graphical overview of the bioassay workflow. After injection of the venom, chromatographic separation is performed, followed by high-resolution fractionation on 96- or 384-well plates for subsequent cellular bioassaying and protein identification using proteomics, as described by Slagboom et al. [27]. Image created using www.biorender.com.

3.2 Methods

3.2.1 Venom preparation

Venoms were sourced from the extensive library of the Faculty of Science, BioAnalytical Chemistry, Vrije Universiteit Amsterdam (VU). This library contains samples obtained and subsequently provided by the Liverpool School of Tropical Medicine (LSTM), National University of Singapore (NUS) and captive breeders. The snake venoms used in this study came from the following viper (Viperidae) and elapid (Elapidae) species: *Bitis arietans* (puff adder, captive bred), *Bothrops jararaca* (jararaca, captive bred), *Bungarus multicinctus* (many-banded krait, locality unknown), *Calloselasma rhodostoma* (Malayan pitviper, Thailand), *Daboia russelii* (Russell's viper, locality unknown), *Echis carinatus* (Indian saw-scaled viper, India), *Echis ocellatus* (West African carpet viper, Nigeria), *Naja haje* (Egyptian cobra, captive bred), *Naja mossambica* (Mozambique spitting cobra, captive bred) and *Naja naja* (Indian cobra, captive bred). These species were selected as they represent some of the most medically relevant species across the geographical regions most heavily affected by snakebite (i.e., Latin America, Sub-Saharan Africa and Southeast Asia). Venoms from VU and NUS were lyophilised immediately after milking, then freeze-dried and stored at -80°C.

LSTM venoms were extracted, stored overnight at -20°C, then lyophilised and held at 4°C for the long term. Samples were reconstituted in Milli-Q-water (mQ) to the desired stock solutions, depending on the type of assay. These solutions were then aliquoted and subsequently snap-frozen in liquid nitrogen and stored at -80°C until use. All venoms were sourced in accordance with the Nagoya protocol, where applicable [28].

3.2.2 Cell culture

The RPTEC/TERT1 cell line was used to study the cell-damaging effects of our panel of medically relevant snake venoms. Cells were routinely cultured on 96-well flat bottom plates (Greiner Bio-One) according to a protocol by Jennings et al., 2009 [29].

Cells were exposed to increasing venom concentrations of ten medically relevant snake species for 3, 6, 12, 24 and 48 hours or 0.1% Triton T-100 as positive control. A five-point serial dilution was generated of decreasing venom concentrations: 100 µg/mL, 33.3 µg/mL, 11.1 µg/mL, 3.7 µg/m and 1.2 µg/mL. In each well, the concentration of the diluted venom relative to the medium was 1:9, and the negative control was accordingly incubated with a 1:9 dilution of mQ in the medium [30].

3.2.3 Fluorescent microscopy

Morphological data was collected using a confocal Operetta CLS high content imager (PerkinElmer) with 10X, 20X, or 63X objectives and a brightfield channel (white light), a digital phase contrast (DPC) channel, and two fluorescence channels. Although the brightfield channel is readily available in most microscopes, the limitation of this channel is the fact that the contrast is often poor, making visual cell analysis challenging [31]. Therefore, an additional channel was applied using digital phase contrast, which is a contrast-enhancing optical technique that can be used to produce high-contrast images of transparent subjects such as living cells. The combination of these four channels allowed us to closely follow the effects that the venoms had on the cells.

We employed several methods to quantify the cell-damaging activities caused by the venoms. In order to calculate the live cell count, we made use of two chromosome stains, Hoechst 33342 (H342) – a cell-permeable dye that is often

used for staining cell nuclei – and propidium iodide (PI), which is impermeable for live cells. The latter functions as a counterstain due to its inability to cross the intact plasma membrane and is an ideal marker for the destabilisation of the cell membrane. Once PI is bound, its fluorescence increases 20-30 fold [32]. H342 (Thermo Fisher Scientific) was used at a concentration of 1:20,000, and PI (Sigma-Aldrich) was used at 1:10,000; both stains were diluted in growth medium and protected from light. Cells were subsequently incubated for 15 minutes at 37°C with the medium containing both stains before the addition of the venoms. The cells were then imaged using two fluorescence channels: Ex355-385 nm Em430-500 (for H342) and Ex530-560 nm Em570-650 nm (for PI). Images were collected using Harmony software 4.8 (PerkinElmer). The software was used to quantify the total cell count (cells stained with H342) and the number of dead cells (stained with PI) (for details, see S8 Figure).

To obtain the live cell count, we subtracted the number of dead cells from the total cell count. We then divided the number of live cells by the negative control, yielding the percentage of live cells relative to the negative control.

For the venoms capable of disrupting the ECM and thereby detaching the cell monolayer from the bottom of the well, we used the brightfield channel to quantify the surface area of the cell monolayer. For this, we again used the Harmony software, this time to calculate the cell surface area relative to 'empty' areas in the wells in those spots where the monolayer was (partially) subtracted. The software was employed to differentiate cell populations from regions without cells (i.e., 'empty well area') using a simple learn-by-example approach (for details, see S9 Figure). The machine-learning technology available in the software was then used to generate an image analysis algorithm that enables quantification of cytotoxicity in terms of ECM degradation.

3.2.4 Resazurin reduction assay

Cell metabolism was studied by subjecting the cells to a colourimetric assay that uses the Alamar Blue reagent. This assay is used to quantify the number of cells with active metabolism and is based on the reduction of resazurin. This non-fluorescent indicator is metabolised to its fluorescent metabolite resorufin by viable cells in culture. At the end of the exposure time (i.e., 3, 6, 12, 24 or 48 hours), 5 µL of Alamar Blue (Thermo Fisher Scientific) was added to each well

and incubated for 1 hour. The fluorescence was subsequently measured using a CLARIOstar Plus reader (BMG Labtech) at 540 nm for excitation and 590 nm for emission. Cell metabolism was calculated by comparing the fluorescent values of the venom samples with those of the negative control (i.e., average signal without venom, where regular metabolic activity is expected).

3.2.5 ATP assay

Cell viability was quantified using ATP levels in cell lysates. As ATP is involved in a variety of enzymatic reactions and ATP levels decline rapidly when cells undergo necrosis or apoptosis, this assay is widely accepted as a valid marker of viable cells, as higher ATP concentrations indicate a higher number of living cells. This bioluminescent assay uses ATP from viable cells to generate photons of light. ATP levels were measured using the ATPlite kit from PerkinElmer (6016731) according to the manufacturer's instructions. After the cells were incubated with the venom for 24 or 48 hours, cells were subjected to this assay after the luminescence was measured on the CLARIOstar Plus reader. Cell viability was subsequently quantified by comparing the ATP levels in venom-incubated wells with the ATP levels of the negative control (where cells were 100% viable).

3.2.6 Liquid chromatography, nanofractionation and mass spectrometry

In order to investigate which venom toxins could potentially cause cell-damaging effects, we used advanced analytical methods to separate the crude venoms into their individual toxins. For this, we used the method developed by Slagboom et al. [33]. Section 1 in the S1 Methods provides a more elaborate description of this separation method.

3.2.7 Correlating bioassay data with toxin identification

For subsequent analysis of the fractions, we selected a representative species of each snake family of our panel of snake venoms. Three concentrations of crude venom were used for separation onto the 96-well plates: 0.5, 1.0, and 2.5 mg/mL. These plates were then subjected to the same panel of cell bioassays as described above. Venoms were separated with RP-LC, followed by fractionation on 96-well

plates for subsequent cellular bioassaying and toxin identification. The obtained bioactivity data was converted into bioactivity chromatograms by plotting the readout of each well on the y-axis against the elution time of each fraction in each well on the x-axis.

In order to analyse the bioactive fractions in *E. ocellatus* venom (for which the toxin activity was affected by our 'traditional' separation method), we applied an alternative approach using SEC with an eluent based on non-volatile salt buffers with PBS as the mobile phase. Two concentrations of *E. ocellatus* venom (i.e., 2.5 and 5.0 mg/mL) were fractionated onto 96-well plates. With this approach, we were able to collect the venom toxins in their native form. Section 2 in S1 Methods provides a more elaborate description of this method.

3.2.8 Identification of bioactive compounds by post-column proteomics

Following the identification of wells containing bioactive compounds, venom fractions were subjected to tryptic digestion in order to identify bioactive fractions using proteomics. For this, the proteomics approach developed by Slagboom et al. (2023), which was adapted to a 96-well plate, was used [27]. Section 3 of S1 Methods provides an extensive explanation of this workflow.

3.2.9 Quantification and statistical analysis

In general, data are represented by mean ±SD. Specific statistical tests used, p-value level definitions, and additional details are listed in figure legends.

3.3 Results & Discussion

The objective of this study was to assess the cell-damaging activities of 10 medically relevant venomous snake species from two snake families using fluorescent microscopy and a number of cellular assays commonly used for screening cytotoxic compounds. The effects of the respective species on RPTEC/TERT1 cells were evaluated with increasing venom concentrations and at varying exposure times. We subsequently combined the cellular bioassays with advanced analytical tools to characterise the compounds responsible for the observed cell-damaging activities of two distinct snake species.

3.3.1 Morphological assessment of venom effects

To provide an overview of the presence and level of activity within our panel of snake venoms, we collected representative brightfield, digital phase contrast, and immunofluorescence microscopy images, allowing us to study the morphology of the cells over time. Cells responded differently to the various types of venom, with morphological alterations of the cells depending on the snake species, the venom concentration and the duration of exposure.

After 3 hours of incubation, the effect of the venoms of *B. arietans, B. jararaca, C. rhodostoma, E. carinatus* and *E. ocellatu*s became visible. All four venoms caused detachment of the monolayer (which, under normal conditions, is attached to the bottom of the well). This detachment could be observed by the retraction of the monolayer, mainly from the corners inwards, after which the monolayer curled further upwards towards the middle of the well (see Figures 2 and 3 and S2-6 Figures). The level of detachment generally increased over time and with higher venom concentrations (see S1-6 Figures). After 24 hours, the top concentration of all viper species, excluding *D. russelii*, resulted in a more or less complete detachment of the cell monolayer (see Figure 2). At higher magnifications, the detachment of the monolayer was clearly visible, resembling a rolled-up sleeve (see Figure 3, S1 Movie). Time of exposure had a significant effect on the extent of monolayer detachment (see Figure 3 and S1-6 Figures). Interestingly, despite the striking effects in terms of monolayer detachment, membrane integrity was hardly affected, which could be deduced from the fact that PI was excluded from the cells, even after prolonged venom exposure (see Figure 2 and S6 Figure)

The venoms of *N. mossambica* and *N. naja* affected the cells in a completely different manner, with the monolayer being largely unaffected. These venoms seemed to affect the cell membranes instead, shown by the fact that PI entered the cells, staining the inside of the cell and the cell nucleus (see Figure 3 and S2 Movie). The number of PI-stained cells increased over time and with higher venom concentrations. The most striking effect was observed for 100 µg/mL of *N. mossambica* venom, reaching a maximum impact within the first 15 minutes post-venom addition (see Figure 3D, S2 Movie). For *B. multicinctus* and *N. haje* we observed little to no effect during the first 24 hours of incubation, even at higher concentrations (see Figure 2). Only after 48 hours at the highest concentration of *N. haje* venom an effect was observed, similar to that of *N. mossambica* and *N. naja* (see S6 Figure). Although cells that were exposed to the venoms of *B. multicinctus* and *N. haje* venoms did not show any apparent morphological alterations, we did observe a relatively large number of 'domes' in these cells compared to the negative control (see Figure 2A and S2-6 Figures). These are typical three-dimensional cellular structures in epithelial cells, which are characteristic of healthy cells.

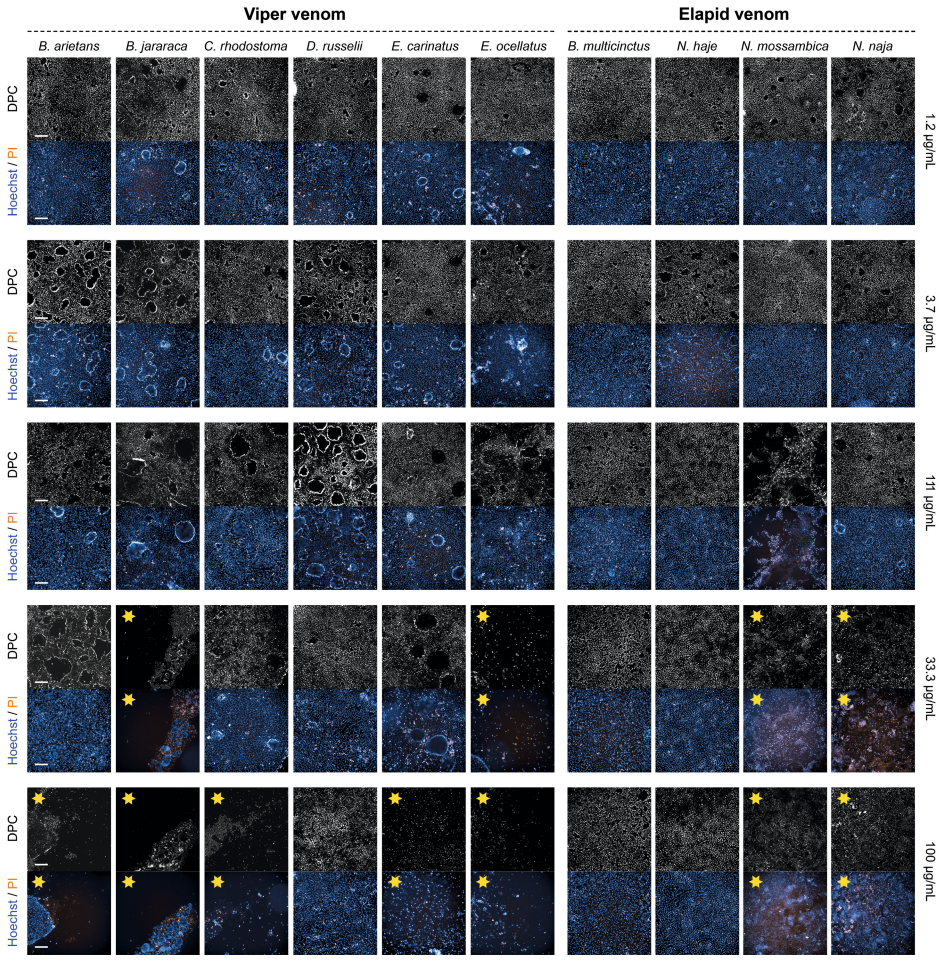

Figure 2. Digital phase contrast and immunofluorescent microscopy images showing the morphology of RPTEC/TERT1cells after 24 hours in the presence of ten medically relevant snake species at increasing venom concentrations. Both the DPC and fluorescent images were captured using confocal microscopy with 10X magnification. H342 staining is shown in blue, and PI in orange. All exposure settings were kept the same. The scale bar represents 200 µm. 0.1% Triton T-100 was used as a positive control. The images are scaled post-acquisition to the positive control. Yellow stars represent wells in which at least some activity was observed.

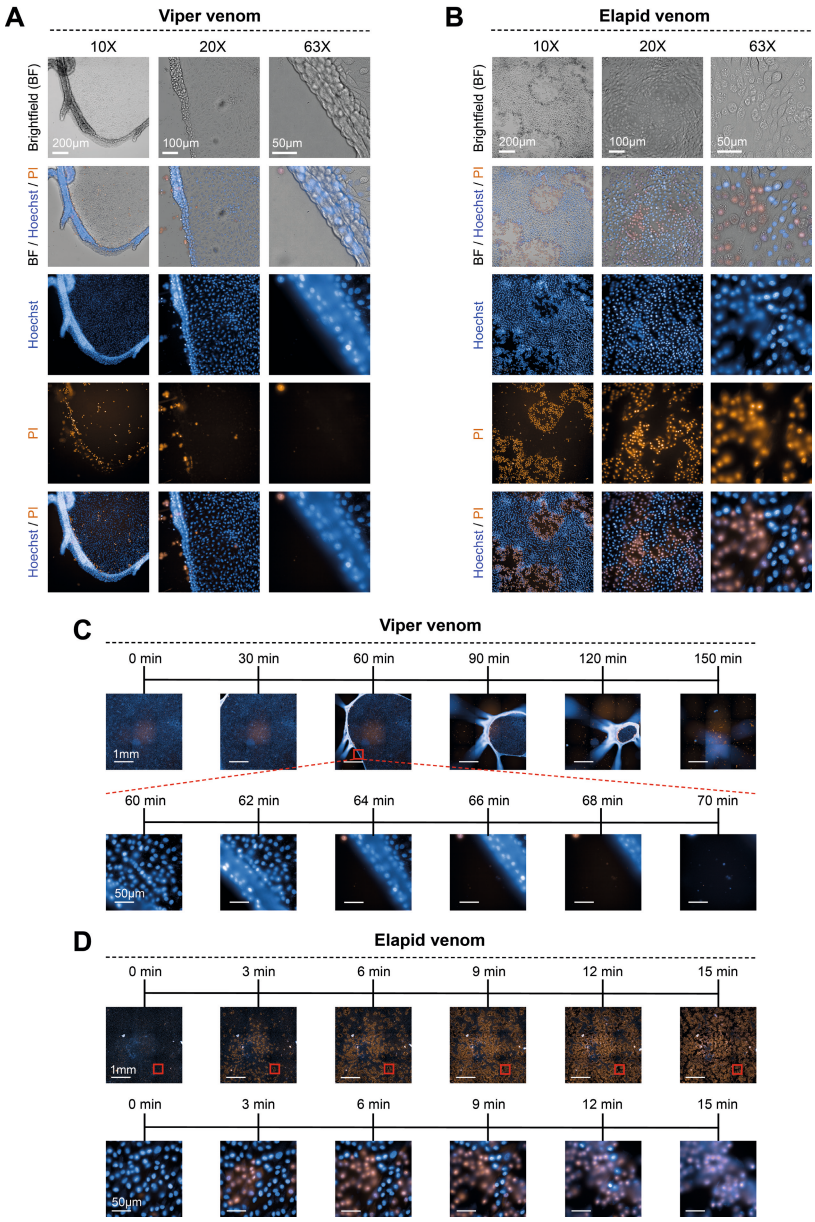

Figure 3. Brightfield and immunofluorescent microscopy images show the difference in morphology of RPTEC/TERT1 cells in the presence of two venoms with contrasting effects. (A) Cells exposed to 100 µg/mL *E. ocellatus* venom, with various channels (brightfield, Hoechst & PI) at 10X, 20X and 63X magnification. (B) Cells exposed to 100 µg/mL *N. mossambica* venom, with various channels (brightfield, Hoechst & PI) at 10X, 20X and 63X magnification. (C). Time series (0 – 150 min) of the effects of *E. ocellatus* venom (100 µg/mL), with a higher-magnification section (63X), clearly showing the monolayer detachment (60 – 70 min). (D). Time series (0 – 15 min) of the effects of *N. mossambica* venom (100 µg/mL) on cells, with a higher-magnification section (63X) showing the PI entering the cell (0 – 15 min). Scale bar lengths are represented in the images.

3.3.2 Quantitative assessment of venom effects

Live cell count (Hoechst / PI)

In order to complement the morphological data presented above, we used the same chromosome stains (i.e., H342 and PI), which provided both qualitative and quantitative data.

In cells incubated with viper venoms, PI was unable to cross the cell membrane even after prolonged incubation, resulting in low numbers of PI-stained cells. However, the quantitative data suggests differently. After 24 hours of incubation, all viper venoms (at 100 µg/mL) resulted in cell counts close to zero (see S7B Figure). This shows that live cell counts for the viper venom data should be interpreted with caution, as the morphological data clearly indicates that the cells did not become PI-permeable (see Figure 2 and S2-6 Figures). This observation will be further discussed in the section 'Matching morphological & quantitative data'.

The graphs representing the effects of *N. mossambica* and *N. naja* venoms show a potent cytotoxic effect for higher venom concentrations (see S7B Figure). This is in line with the qualitative data presented above, which accordingly showed that the highest venom concentrations heavily affected the permeability of the cells towards PI (see Figure 2 and S2-6 Figures). The graphs further show that the live cell count decreases with higher concentrations in a dose-dependent manner, as is the case for longer exposure times (see S7B Figure). For *B. multicinctus* and *N. haje* venoms, we did not observe any notable effects for the first 24 hours of exposure. After 48 hours of incubation, a decrease in the number of live cells relative to negative control for 100 µg/mL of *N. haje* venom could be seen (see S7B Figure).

Cell area quantification

As discussed above, quantification of the ratio of live cells relative to the total cell count proved to be challenging for those venoms that affected the cell monolayer in such a way that the total (live) cell count could not be determined appropriately. We, therefore, incorporated a method to quantify the level of activity in terms of their ability to destabilise the cell monolayer. This provided us with a valuable method of assessing the level of ECM-degrading activity.

For all viper venoms except *D. russelii*, subtraction of the monolayer was observed, with the magnitude of activity depending on the species, the venom concentration and the time of exposure (see Figure 2 and S2-6 Figures). The graphs closely match the morphology presented above. After 6 hours of exposure to 100 µg/mL of venom of *B. jararaca*, *C. rhodostoma* and *E. ocellatus, we observed near-to-*complete subtraction of the monolayer, which is represented by a cell surface area close to zero (see S8A Figure). When incubated for 12-24 hours, the graphs show potent activity for all viper venoms (excluding *D. russelii* venom), with *B. jararaca* and *E. ocellatus* being the most potent and the top two concentrations causing complete or near-to-complete subtraction of the monolayers. Maximal activity was observed after 48 hours of exposure, with all five viper venoms showing complete subtraction at 33.3 µg/mL and 100 µg/mL and with *E. ocellatus* causing potent monolayer destabilising activity at 11.1 µg/mL (see S8A Figure).

For *N. mossambica* and *N. naja* venoms, the graphs representing live cell count and cell surface area matched closely (see S8 Figure). After 48 hours of incubation, the graphs of *N. mossambica* and *N. naja* demonstrated a significant decrease in cell surface area for the top three concentrations of *N. mossambica*, and the two highest concentrations of *N. naja*, venom. The graphs associated with the venoms of *B. multicinctus* and *N. haje* match both the morphological and live cell count data (see S2-6 and S8 Figures), with little activity observed even at higher venom concentrations and prolonged exposure.

Resazurin reduction

Cell metabolism was monitored using the amount of resazurin reduction as a proxy for metabolic activity and cellular stress.

After 3 hours of incubation with viper venoms, the metabolic rate in the wells with the top concentrations increased substantially, which was most notable with the venom of *E. carinatus* (see S9A Figure). In the subsequent hours, the metabolic rates decreased to the level of the negative control, followed by a further decrease for the higher venom concentrations as the cells were incubated for over 24 hours. The only exception is *D. russelii*, for which the metabolic rate after an initial increase later resembles the negative control.

For *N. mossambica* and *N. naja*, a striking drop in the metabolic activity could be observed at all exposure times for the top two concentrations. A minimal

increase in metabolic activity was seen for *B. multicinctus* and *N. haje* venom (see S9B Figure). After 24 hours of incubation, there was a slight decrease for the cells incubated with 100 µg/mL of *N. haje* venom. This is in line with the minor effects of these venoms on the live cell count and cell surface area data discussed above.

ATP assay

In order to complement the data presented above, we further included cell viability in our panel of bioassays. For this, we investigated the cells that were incubated for 24 and 48 hours with the respective venoms, subsequently lysed the cells, and measured ATP levels.

For all viper species except *D. russelii,* we see lower levels of ATP relative to the negative control for the top concentrations of venom (see S10A Figure). After 48 hours of exposure, this decrease continued, with *B. jararaca* and *E. ocellatus* affecting cell viability at 3.7 µg/mL and 1.2 µg/mL (see S10A Figure). For *D. russelii,* we see a more subtle decrease in ATP levels for the top three concentrations but nothing substantial.

Similar levels of cell viability decrease were observed for *N. mossambica* and *N. naja* venoms, with the former being slightly more potent (see S10B Figure). After 48 hours, the viability for all five concentrations of both species has decreased, although only the top concentrations caused a steady drop in the ATP levels measured (see S10B Figure). Contrastingly, *B. multicinctus* and *N. haje* venom were not capable of causing a notable difference in cell viability except for the top concentrations of *N. haje* venom after a 48-hour incubation period, which resulted in a subtle drop in viability (see S10B Figure).

3.3.3 Matching morphological & quantitative data

Combining the data of the various bioassays allows us to quantify the level of cell-damaging activities, regardless of the mechanism involved. When comparing the morphological and quantitative data of the most potent viper venom in our panel (i.e., *E. ocellatus*), we see that the graphs representing live cell count and cell area match closely (see Figure 4A). As discussed, this observation suggests that the live cell counts for viper venoms should be interpreted with caution, as the morphological data clearly shows that the cells did not become PI-permeable. An explanation for this could be the fact that the detachment of the monolayer caused

the cells to move out of the focus of the microscope, hindering the cell count. Other methods were therefore needed to quantify the cell-damaging properties of the viper venoms properly. Calculation of the cell surface area provided a more suitable way of quantifying the activity of viper venoms, which could be easily calculated with any microscope with a camera mount and the appropriate software. The observed viper venom effects were less evident in the graphs for resazurin reduction compared to the graphs for live cell count and cell surface area (see Figure 4 and S7-S9 Figures). Also, an initial increase in resazurin metabolism was observed after 3 hours of incubation for higher concentrations of viper venom. As this assay is a measure for active metabolism and resazurin is generally postulated as being reduced by mitochondrial enzymes, the increase in metabolism could be the result of mitochondrial stress in response to the presence of the venom [34–37]. As these observations suggest that venom addiction may have caused an increase in metabolic activity, it was decided to also include the ATP assay as a direct measure of cell viability [38,39]. No proper trend could be observed for the ATP content in the lysates. This suggests that the viper venoms did not radically alter cell viability, as ATP levels tend to decline rapidly when cells undergo necrosis or apoptosis [38,39]. This observation is in line with the fact that for the first ~24 hours, except for the detachment of the monolayer, the cells were not affected. Only after prolonged incubation did the cells start to exhibit a significant loss in viability (see Figure 3 and S7 Figure). For the elapid venoms, the graphs show similar trends for all bioassays, regardless of the level of bioactivity (See Figure 4B and S7-S10 Figures).

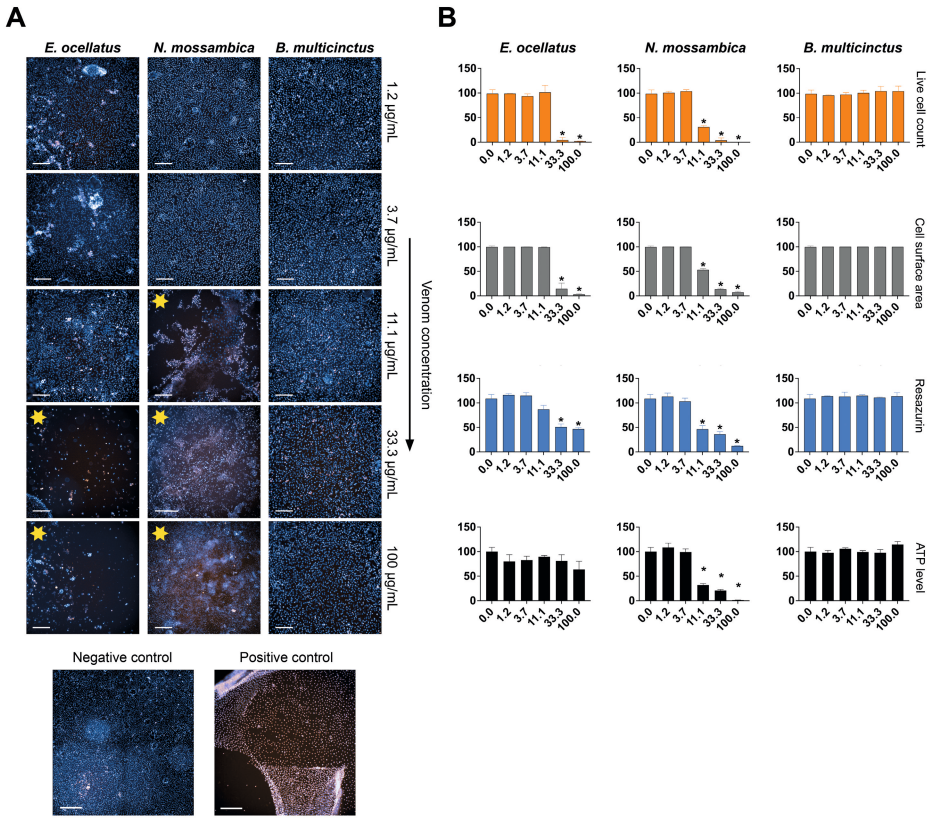

Figure 4. Comparison of morphological data and quantitative data for three venoms that have varying effects on the cells. (A) Immunofluorescent microscopy images showing the morphology of RPTEC/TERT1cells after 24 hrs of exposure. Images were captured using confocal microscopy with 10X magnification. H342 staining is shown in blue, and PI in orange. 0.1% Triton T-100 was used as a positive control. Yellow stars represent wells in which activity was observed. The scale bar represents 200 µm. (B) Quantitative data of four cellular bioassays are shown as bar graphs, with the activity of the venom described relative to negative control (0 µg/mL). Live cell count (orange); cell surface area (grey); resazurin reduction activity (blue); ATP level (black). Increasing venom concentrations on the x-axes (in µg/mL) and percentage relative to negative control on the y-axes. Measurements are presented as the mean of three individual experiments (N=3), error bars depict SD; '*' represents a statistically significant difference when compared to negative control, two-tailed test, $p < 0.05$ (Bonferroni-corrected).

3.3.4 Identification of bioactive compounds in fractionated venoms

To characterise the venom components responsible for the observed cell-damaging activity, we correlated the bioactivity peaks with proteomics data in order to improve the toxin identification obtained with the initial correlation analyses. The most potent venom of each snake family was selected for further

analysis using a similar nanofractionation approach as described by Slagboom et al. [33]. This was done in an attempt to identify the toxins responsible for the observed effect and to demonstrate the complete analytical workflow.

Correlation of bioactivity peaks with proteomics data

Venoms of *N. mossambica* and *E. ocellatus* at different concentrations (i.e., 0.5, 1.0 and 2.5 mg/mL) were fractionated using RP-LC. For all (bioactive) fractions of each species, the corresponding bioactivity chromatogram and proteomics data were acquired. For the bioassay chromatograms, the average y-axis signal at the beginning of each chromatogram represents the baseline (i.e., 'normal' cell activity). In contrast, the negative peaks (dips) correspond to the bioactive fractions in the wells. In order to try to improve the toxin identification obtained with the initial correlation, we performed tryptic digestion on the venom fractions, after which the proteomics data was correlated to the bioactivity data.

Identification of membrane-disrupting toxins in N. mossambica venom

The venoms of some of the elapids, including *N. mossambica,* were capable of affecting the membrane integrity, which was shown by the fact that PI could enter the cell (see Figure 3). As cell membrane integrity is crucial for the normal functioning of the cell, it is not surprising that certain toxin families act specifically on the cell membrane [7,8,40]. The destabilisation of cellular membranes can be caused by cytotoxic 3FTxs, PLA_2s, and ß-defensin-like toxins, which have different mechanisms of action [7,8].

For *N. mossambica,* activity was observed in a dose-dependent manner for all assays. At a concentration of 1.0 mg/mL, three bioactivity peaks were present between 14.2 and 19.4 minutes (see Figure 5). Within this bioactivity window, a total of 17 toxins could be identified using proteomics. Of these, 13 toxins were found to be part of the 3FTx toxin family and three to the PLA_2 family of toxins (see Figure 5, S1 Table). Assigning toxins to specific bioassay peaks was difficult, as for some toxins (e.g., 3SA5_NAJMO; 3SA1_NAJNA; 3SA4_NAJHA), there are multiple peaks present. Previous studies have argued that these peaks could be different toxins with sequence similarities that are not yet in the database and are therefore assigned to their closest homologue, as was described by Slagboom et al. [27,41]. According to the Uniprot database, the 3FTx proteins identified in this

study are 'showing cytolytic activity on many different cells by forming pores in lipid membranes' [42–48]. 3FTxs perform a variety of biological functions, including neuro-, haemo- and cytotoxicity, which is caused by a variety of mechanisms [16,17,49–54]. The exact mechanism by which these toxins execute their damaging effects on cells remains unclear, with competing hypotheses present, including pore formation and interactions with cell-surface proteins [17,55–60]. The venoms of *N. mossambica* and *N. naja* are particularly rich in 3FTxs, with relative abundances ranging from 63.8 – 80.5% (see S2 Table). Other toxins that were found within the bioactivity window were the PLA_2s, which were described in UniProt as 'showing several activities, including (in)direct haemolytic action, myonecrosis and strong anticoagulant activity' [61–63]. PLA_2s disrupt the plasma membrane by hydrolysing membrane phospholipids, resulting in the alteration of the membrane structure, whereas enzymatically inactive PLA_2s may act via direct perturbation of the membrane [13,64–67].

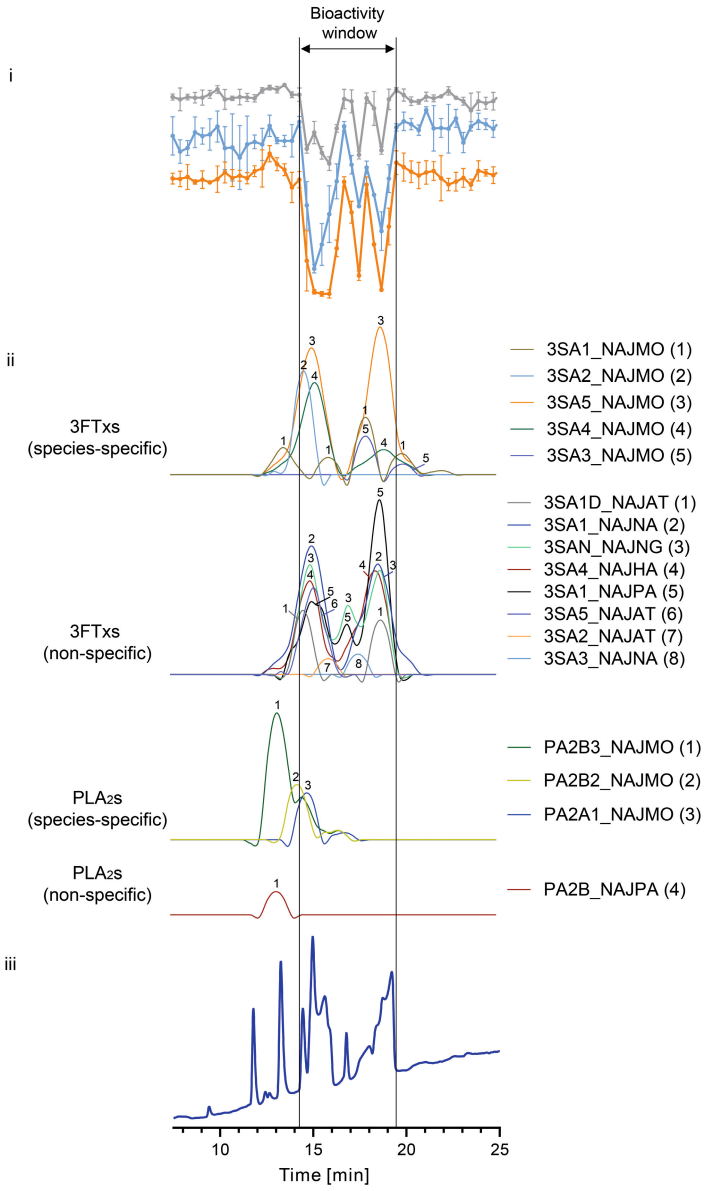

Figure 5. Identification of bioactive fractions of *N. mossambica* venom (1 mg/mL) by correlating bioactivity data with proteomics data. i: bioactivity chromatograms obtained by plotting the results of three bioassays: cell surface area (grey), resazurin reduction (blue), and live cell count (orange). The peaks with negative minima indicate the presence of bioactive fractions; ii: Graphs representing the protein score chromatograms (PSCs), showing the individual venom proteins found with Mascot database searching of the digested well fractions. iii: UV traces of the snake venoms at 220 nm obtained by RP-LC. The vertical outer lines mark the bioactivity window, which includes the prominent activity peaks and their corresponding PSC peaks and RP-LC UV chromatogram peaks. Measurements are presented as the mean of three individual experiments (N=3), and error bars depict SD.

Identification of toxins causing monolayer detachment in E. ocellatus venom

Incubation of cells with the venoms from all vipers (except *D. russelii*) resulted in the detachment and subsequent subtraction of the cell monolayer without affecting the cells directly (see Figures 2 and 4). This is further supported by the fact that cell viability and cell metabolism were less affected than observed for the venoms of *N. mossambica* and *N. naja*. This suggests that the viper venoms might affect the ECM, which is a macromolecular scaffold which attaches the cell monolayer to the bottom of the wells. The main components of the ECM are proteoglycans, glycoproteins and fibrous proteins such as collagen, elastin, fibronectin and laminin [11,40,68,69]. Certain toxin classes, such as SVMPs and hyaluronidases, are known to degrade ECM components proteolytically [1,11,20,25,70,71].

Surprisingly, the separated fractions of *E. ocellatus* did not show any bioactivity on either of the assays, even at higher concentrations (see S11B Figure). A possible explanation could be the fact that the responsible toxins were subject to denaturation as a result of the solvent conditions present during RP-LC separation. This is in line with previous studies on the effects of organic modifiers and acidifiers on protein stability [72–74]. In order to address this issue, we decided to use SEC as an alternative separation method, which uses an eluent based on non-volatile salt buffers with PBS as the mobile phase. The use of SEC allowed us to separate and collect the venom fractions in their native form. We then subjected the venom fractions to the same bioassays discussed above. The results demonstrate that the venom fractions separated using a non-volatile buffer retained their activities, showing effects similar to what was observed in the crude venoms (see Figure 6 and S12 Figure).

Fractions of *E. ocellatus* venom eluted between 8 and 13 minutes, with at least six peaks and a number of co-eluting peaks that can be observed in the SEC-UV chromatogram (see Figure 6). Bioactive fractions eluted from approx. 8.5 to 10.5 minutes. A total of 13 toxins could be identified, belonging to the following toxin classes: LAAOs (three toxins), SVMPs (six toxins), C-type lectins (two toxins) and renins (two toxins) (see Figure 6 and S3 Table). The LAAOs that were found (i.e., OXLA_ ECHOC, OXLA_ DABSI and OXLAB_ CERCA) belong to a family of toxins that are thought to be associated with the induction of oxidative stress, which may induce cell damage. These toxins may exhibit a

diverse array of biological activities, including haemorrhage, haemolysis and apoptosis of various cell types [21,75–79]. The SVMPs that were identified within the bioactivity window have been shown to be proteolytically active and exhibit haemorrhagic solid activity [80–82]. In addition to LAAO and SVMPs, we found two C-type lectins (SL1_ ECHOC; SL124_ECHOC) in the bioactive fractions, a family of toxins for which a diverse range of effects is described (including cytotoxicity), although the exact mechanisms have not been elucidated [83–86]. The other toxins represented in the graphs fall outside of the bioactivity window and are not known to exhibit proteolytic activity [1,7].

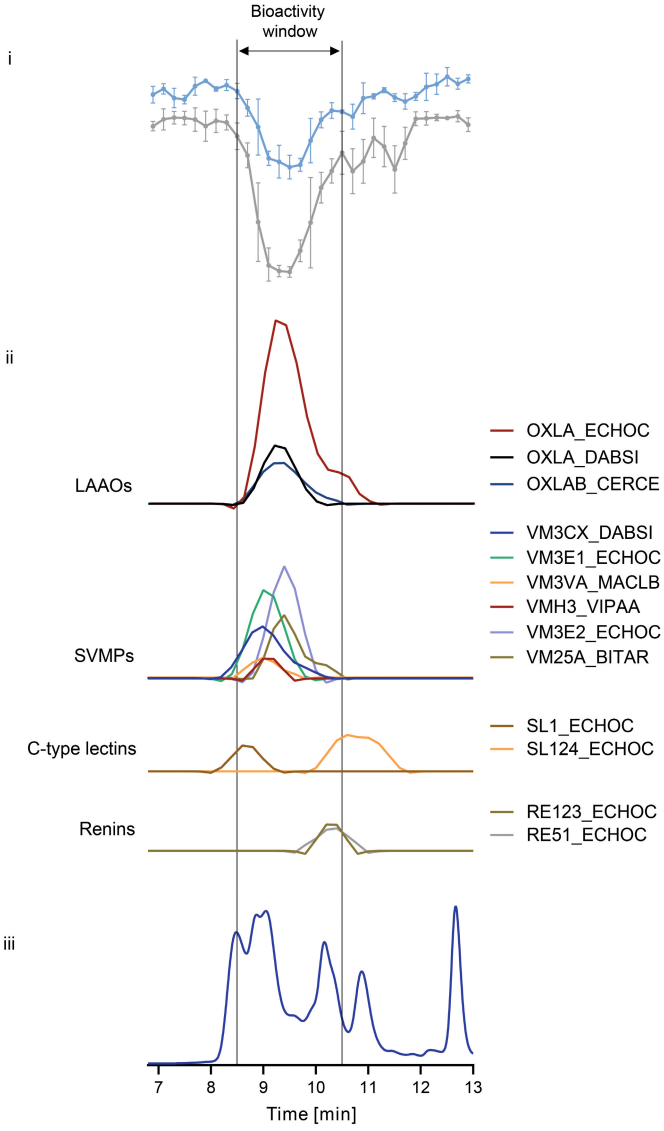

Figure 6. Identification of bioactive fractions of *E. ocellatus* venom (5 mg/mL) by correlating bioactivity data with proteomics data. i: bioactivity chromatograms obtained by plotting the results of two assays: resazurin reduction (blue) and cell surface area (grey). The live cell count was not included as the graphs do not accurately describe the number of live cells as a result of the detachment of the monolayer (see also above). The peaks with negative minima indicate the presence of bioactive fractions; ii: Graphs representing the protein score chromatograms (PSCs), showing the individual venom proteins found with Mascot database searching of the digested well fractions; iii: UV traces of the snake venoms at 220 nm obtained by SEC. The vertical outer lines mark the bioactivity window, which includes the prominent activity peaks and their corresponding PSC peaks and SEC-UV chromatogram peaks. Measurements are presented as the mean of three individual experiments (N=3), and error bars depict SD.

3.4 Concluding remarks

This study describes the development of a medium throughput approach for the identification of venom components associated with cell- and tissue-damaging effects. We used a set of 10 medically relevant species, which were screened on a panel of cellular bioassays. The results of this study revealed a notable difference in the way in which the venoms of elapids and vipers exert their effects on RPTEC/TERT1 cells. The venoms of *N. mossambica* and *N. naja* affected the integrity of the cell membrane (shown by the fact that PI was able to cross the cell membrane within minutes after incubation. The responsible toxins could, therefore, be considered 'true' cytotoxins, as these directly affect the cells by disrupting cell membrane integrity. Viper venoms, on the contrary, affect the substrates of the ECM scaffold, probably by proteolytic degradation of the matrix substrates. This resulted in the detachment of the cell monolayer, which is a secondary effect of degradation of the ECM. The RPTEC/TERT1 cell monolayer provided a suitable model for differentiating between the two distinct cell-damaging mechanisms of action, namely membrane disruption and ECM degradation. Although kidney cells used in this study might have different physiological properties as opposed to other cell types (e.g., endothelial cells), these cells can be used as a model to study the cell-damaging effect of snake venoms. The combination of RP-LC and SEC, post-column cellular bioassaying and proteomics allows for the parallel identification of membrane-disrupting and ECM-degrading venom components. The application of this approach could be valuable for better understanding venom-induced cell- and tissue damage. It could be used in the future development of snakebite therapeutics targeting (local) tissue damage caused by envenoming.

References

1. Gutiérrez, J. M. *et al.* Snakebite envenoming. *Nat. Rev. Dis. Prim.* **3**, (2017).
2. Chippaux, J. P. Snakebite envenomation turns again into a neglected tropical disease! *J. Venom. Anim. Toxins Incl. Trop. Dis.* **23**, 1–2 (2017).
3. Longbottom, J. *et al.* Vulnerability to snakebite envenoming : a global mapping of hotspots. *Lancet* **392**, 673–684 (2018).
4. Boyer, L.; Alagón, A.; Fry, B.G.; Jackson, T.N.W.; Sunagar, K.; Chippaux, J. P. S. Symptoms and Treatment of Envenomation. In Venomous Reptiles and Their Toxins: Evolution, Pathophysiology and Biodiscovery; Fry, B.G., Ed.; in *Oxford University Press: New York, NY, USA*, 32–60 (2015). doi:10.1017/CBO9781107415324.004.
5. Kasturiratne, A. *et al.* The global burden of snakebite: A literature analysis and modelling based on regional estimates of envenoming and deaths. *PLoS Med.* **5**, 1591–1604 (2008).
6. Gutiérrez, J. M., Escalante, T., Rucavado, A. & Herrera, C. Hemorrhage caused by snake venom metalloproteinases: A journey of discovery and understanding. *Toxins (Basel).* **8**, (2016).
7. Fry, B. G. *Venomous reptiles and their toxins: evolution, pathophysiology and biodiscovery*. *Oxford University Press, Oxford University Press.* (2015). doi:10.1016/0041-0101(71)90017-1.
8. Gopalakrishnakone, P., Inagaki, H., Vogel, C., Mukherjee, A. K. & Rahmy, T. R. *Snake Venoms*. (Springer Berlin, Germany., 2017).
9. Warrell, D. A. Guidelines of Management of Snake bite. *Lancet* **375**, 77–88 (2010).
10. Bénard-Valle, M. *et al.* Antivenom research and development. in *Venomous Reptiles and Their Toxins: Evolution, Pathophysiology and Biodiscovery; Fry, B.G., Ed.; Oxford University Press: New York, NY, USA* 61–72 (2015).
11. Gutiérrez, J. M., Escalante, T., Rucavado, A., Herrera, C. & Fox, J. W. A comprehensive view of the structural and functional alterations of extracellular matrix by snake venom metalloproteinases (SVMPs): Novel perspectives on the pathophysiology of envenoming. *Toxins (Basel).* **8**, (2016).
12. Montecucco, C., Gutiérrez, J. M. & Lomonte, B. Cellular pathology induced by snake venom phospholipase A2 myotoxins and neurotoxins: Common aspects of their mechanisms of action. *Cell. Mol. Life Sci.* **65**, 2897–2912 (2008).
13. Gasanov, S. E., Dagda, R. K. & Rael, E. D. Snake Venom Cytotoxins, Phospholipase A2 s, and Zn2+ -dependent Metalloproteinases: Mechanisms of Action and Pharmacological Relevance. *J. Clin. Toxicol.* **4**, (2014).
14. Hayashi, M. A. F. *et al.* Cytotoxic effects of crotamine are mediated through lysosomal membrane permeabilization. *Toxicon* **52**, 508–517 (2008).
15. Gutiérrez, J. M. & Ownby, C. L. Skeletal muscle degeneration induced by venom phospholipases A2: insights into the mechanisms of local and systemic myotoxicity. *Toxicon* **42**, 915–931 (2003).
16. Kini, R. M. & Doley, R. Structure, function and evolution of three-finger toxins: Mini proteins with multiple targets. *Toxicon* **56**, 855–867 (2010).

17. Sunagar, K. *et al.* Three-fingered RAVERs: Rapid Accumulation of Variations in Exposed Residues of snake venom toxins. *Toxins (Basel).* **5**, 2172–2208 (2013).

18. Escalante, T. *et al.* Role of collagens and perlecan in microvascular stability: Exploring the mechanism of capillary vessel damage by snake venom metalloproteinases. *PLoS One* **6**, (2011).

19. Markland, F. S. & Swenson, S. Snake venom metalloproteinases. *Toxicon* **62**, 3–18 (2013).

20. Girish, K. S., Jagadeesha, D. K., Rajeev, K. B. & Kemparaju, K. Snake venom hyaluronidase: An evidence for isoforms and extracellular matrix degradation. *Mol. Cell. Biochem.* **240**, 105–110 (2002).

21. Du, X. Y. & Clemetson, K. J. Snake venom L-amino acid oxidases. *Toxicon* **40**, 659–665 (2002).

22. Cesar, P. H. S., Braga, M. A., Trento, M. V. C., Menaldo, D. L. & Marcussi, S. Snake Venom Disintegrins: An Overview of their Interaction with Integrins. *Curr. Drug Targets* **20**, 465–477 (2018).

23. Eble, J. A. Structurally robust and functionally highly versatile—C-type lectin (-related) proteins in snake venoms. *Toxins (Basel).* **11**, (2019).

24. Mladic, M. *et al.* Rapid screening and identification of ACE inhibitors in snake venoms using at-line nanofractionation LC-MS. *Anal. Bioanal. Chem.* **409**, 5987–5997 (2017).

25. Slagboom, J., Kool, J., Harrison, R. A. & Casewell, N. R. Haemotoxic snake venoms: their functional activity, impact on snakebite victims and pharmaceutical promise. *Br. J. Haematol.* **177**, 947–959 (2017).

26. Zietek, B. M. *et al.* Liquid chromatographic nanofractionation with parallel mass spectrometric detection for the screening of plasmin inhibitors and (metallo)proteinases in snake venoms. *Anal. Bioanal. Chem.* **410**, 5751–5763 (2018).

27. Slagboom, J. *et al.* High-Throughput Venomics. *J. Proteome Res.* **22**, 1734–1746 (2023).

28. CBD Secretariat. Nagoya Protocol on Access To Genetic Resources and the Fair and Equitable Sharing of Benefits Arising from their Utilization to the convention on biological diversity - Text and annex. *Nagoya Protoc.* **12**, 1–320 (2011).

29. Jennings, P. *et al.* Inter-laboratory comparison of human renal proximal tubule (HK-2) transcriptome alterations due to Cyclosporine A exposure and medium exhaustion. *Toxicol. Vitr.* **23**, 486–499 (2009).

30. Aschauer, L. *et al.* Application of RPTEC/TERT1 cells for investigation of repeat dose nephrotoxicity: A transcriptomic study. *Toxicol. Vitr.* **30**, 106–116 (2015).

31. Selinummi, J. *et al.* Bright field microscopy as an alternative to whole cell fluorescence in automated analysis of macrophage images. *PLoS One* **4**, (2009).

32. Stiefel, P., Schmidt-Emrich, S., Maniura-Weber, K. & Ren, Q. Critical aspects of using bacterial cell viability assays with the fluorophores SYTO9 and propidium iodide. *BMC Microbiol.* **15**, (2015).

33. Slagboom, J. *et al.* High throughput screening and identification of coagulopathic snake venom proteins and peptides using nanofractionation and proteomics approaches. *PLoS Negl. Trop. Dis.* **14**, 1–26 (2020).

34. Nakayama, G. R., Caton, M. C., Nova, M. P. & Parandoosh, Z. Assessment of the Alamar Blue assay for cellular growth and viability in vitro. *J. Immunol. Methods* **204**, 205–208 (1997).

35. O'Brien, J., Wilson, I., Orton, T. & Pognan, F. Investigation of the Alamar Blue (resazurin) fluorescent dye for the assessment of mammalian cell cytotoxicity. *Eur. J. Biochem.* **267**, 5421–5426 (2000).

36. Perrot, S., Duterte-Catella, H., Martin, C., Rat, P. & Warnet, J. M. Resazurin metabolism assay is a new sensitive alternative test in isolated pig cornea. *Toxicol. Sci.* **72**, 122–129 (2003).

37. Hamid, R., Rotshteyn, Y., Rabadi, L., Parikh, R. & Bullock, P. Comparison of alamar blue and MTT assays for high through-put screening. *Toxicol. Vitr.* **18**, 703–710 (2004).

38. Castaño, A. & Tarazona, J. V. ATP assay on cell monolayers as an index of cytotoxicity. *Bull. Environ. Contam. Toxicol.* **53**, 309–316 (1994).

39. Riss, T. L. *et al.* Cell Viability Assays. *Assay Guid. Man.* 1–25 (2004).

40. Alberts, B. *et al. Essential cell biology: Fifth international student edition*. (WW Norton & Company., 2018).

41. Slagboom, J. *et al.* Analytical strategies in venomics. *Microchem. J.* **175**, 107187 (2022).

42. Uniprot.P25517 · 3SA5_NAJMO · Cytotoxin 5. https://www.uniprot.org/uniprotkb/P25517/entry.

43. Uniprot. P01452 · 3SA4_NAJMO · Cytotoxin 4. https://www.uniprot.org/uniprotkb/P01452/entry.

44. Uniprot. P01470 · 3SA3_NAJMO · Cytotoxin 3. https://www.uniprot.org/uniprotkb/P01470/entry.

45. Uniprot. P01447 · 3SA1_NAJNA · Cytotoxin 1. https://www.uniprot.org/uniprotkb/P01447/entry.

46. Uniprot. Q98958 · 3SA1D_NAJAT3 · Cytotoxin 1d/1e. https://www.uniprot.org/uniprotkb/Q98958/entry.

47. Uniprot. P01469 · 3SA2_NAJMO · Cytotoxin 2. https://www.uniprot.org/uniprotkb/P01469/entry.

48. Uniprot. P01467 · 3SA1_NAJMO · Cytotoxin 1. https://www.uniprot.org/uniprotkb/P01467/entry.

49. Dufton, M. J. & Hider, R. C. Conformational properties of the neurotoxins and cytotoxins isolated from Elapid snake venoms. *CRC Crit. Rev. Biochem.* **14**, 113–171 (1983).

50. Dufton, M.J., Hider, R. C. Structure and pharmacology of elapid cytotoxins. *Pharmacol Ther* **36**, 1–40 (1988).

51. Condrea, E. Membrane-active polypeptides from snake venom: Cardiotoxins and haemocytotoxins. *Exp. 1974 302* **30**, 121–129 (1974).

52. Harvey, A. L. Cardiotoxins from cobra venoms: Possible mechanisms of action. *Toxin Rev.* **4**, 41–69 (1985).

53. Méndez, I., Gutiérrez, J. M., Angulo, Y., Calvete, J. J. & Lomonte, B. Comparative study of the cytolytic activity of snake venoms from African spitting cobras (Naja spp., Elapidae) and its neutralization by a polyspecific antivenom. *Toxicon* **58**, 558–564 (2011).

54. Utkin, Y. N. Last decade update for three-finger toxins: Newly emerging structures and biological activities. *World J. Biol. Chem.* **10**, 17–27 (2019).

55. Bilwes, A., Rees, B., Moras, D., Ménez, R. & Ménez, A. X-ray structure at 1.55 Å of toxin γ, a cardiotoxin from Naja nigricollis venom: Crystal packing reveals a model for insertion into membranes. *Journal of Molecular Biology* vol. 239 122–136 at https://doi.org/10.1006/jmbi.1994.1357 (1994).

56. Forouhar, F. *et al.* Structural basis of membrane-induced cardiotoxin A3 oligomerization. *J. Biol. Chem.* **278**, 21980–21988 (2003).

57. Reeks, T. A., Fry, B. G. & Alewood, P. F. Privileged frameworks from snake venom. *Cell. Mol. Life Sci.* **72**, 1939–1958 (2015).

58. Dauplais, M., Neumann, J. M., Pinkasfeld, S., Ménez, A. & Roumestand, C. An NMR Study of the Interaction of Cardiotoxin γ from Naja nigricollis with Perdeuterated Dodecylphosphocholine Micelles. *Eur. J. Biochem.* **230**, 213–220 (1995).

59. Pucca, M. B. *et al.* Unity Makes Strength: Exploring Intraspecies and Interspecies Toxin Synergism between Phospholipases A2 and Cytotoxins. *Front. Pharmacol.* **11**, 1–10 (2020).

60. Utkin, Y. N. Last decade update for three-finger toxins: Newly emerging structures and biological activities. *World J. Biol. Chem.* **10**, 17–27 (2019).

61. Uniprot.P00603 · PA2B2_NAJMO · Basic phospholipase A2 CM-II. https://www.uniprot.org/uniprotkb/P00603/entry.

62. Uniprot.P00602 · PA2A1_NAJMO · Acidic phospholipase A2 CM-I. https://www.uniprot.org/uniprotkb/P00602/entry.

63. Uniprot.P00604 · PA2B3_NAJMO · Basic phospholipase A2 CM-III. https://www.uniprot.org/uniprotkb/P00604/entry.

64. Joubert, F. J. & van der Walt, S. J. Naja melanoleuca (Forest cobra) venom. Purification and some properties of phospholipases A. *BBA - Protein Struct.* **379**, 317–328 (1975).

65. Joubert, F. J. Naja mossambica mossambica venom Purification, some properties and the amino acid sequences of three phospholipases A (CM-I, CM-II and CM-III). *Biochim. Biophys. Acta - Protein Struct.* **493**, 216–227 (1977).

66. Kini, R. M. & Evans, H. J. Structure-function relationships of phospholipases. The anticoagulant region of phospholipases A2. *J. Biol. Chem.* **262**, 14402–14407 (1987).

67. Kini, R. M. Excitement ahead: Structure, function and mechanism of snake venom phospholipase A2 enzymes. *Toxicon* **42**, 827–840 (2003).

68. *Biology of Extracellular Matrix Series. Matrix Metalloproteinases* (Springer, 1998). doi:10.1016/b978-0-12-545090-4.50015-x.

69. Frantz, C., Stewart, K. M. & Weaver, V. M. The extracellular matrix at a glance. *J. Cell Sci.* **123**, 4195–4200 (2010).

70. Engmark, M. *et al.* High-throughput immuno-profiling of mamba (Dendroaspis) venom toxin epitopes using high-density peptide microarrays. *Sci. Rep.* **6**, 1–14 (2016).

71. Herrera, C. *et al.* Tissue Localization and Extracellular Matrix Degradation by PI, PII and PIII Snake Venom Metalloproteinases: Clues on the Mechanisms of Venom-Induced Hemorrhage. *PLoS Negl. Trop. Dis.* **9**, 1–20 (2015).

72. Gekko, K., Ohmae, E., Kameyama, K. & Takagi, T. Acetonitrile-protein interactions: Amino acid solubility and preferential solvation. *Biochim. Biophys. Acta - Protein Struct. Mol. Enzymol.* **1387**, 195–205 (1998).

73. Kony, D. B., Hünenberger, P. H. & van Gunsteren, W. F. Molecular dynamics simulations of the native and partially folded states of ubiquitin: Influence of methanol cosolvent, pH, and temperature on the protein structure and dynamics. *Protein Sci.* **16**, 1101–1118 (2007).

74. Wachtel, E. *et al.* Application of an Extracellular Matrix-Mimicking Fluorescent Polymer for the Detection of Proteolytic Venom Toxins. *Toxins (Basel).* **15**, (2023).

75. Suhr, S. M. & Kim, D. S. Identification of the snake venom substance that induces apoptosis. *Biochem. Biophys. Res. Commun.* **224**, 134–139 (1996).

76. Torii, S., Naito, M. & Tsuruo, T. Apoxin I, a Novel Apoptosis-inducing Factor with L-Amino Acid Oxidase Activity Purified from Western Diamondback Rattlesnake Venom. *J. Biol. Chem.* **272**, 9539–9542 (1997).

77. Uniprot. U6D7A7 · U6D7A7_NEOVI · L-amino-acid oxidase. https://www.uniprot.org/uniprotkb/U6D7A7/entry.

78. Uniprot.Q4F867 · OXLA_DABSI · L-amino acid oxidase. https://www.uniprot.org/uniprotkb/Q4F867/entry.

79. Uniprot.P0DQH9 · OXLAB_CERCE · L-amino acid oxidase. https://www.uniprot.org/uniprotkb/P0DQH9/entry.

80. Wagstaff, S. C., Sanz, L., Juárez, P., Harrison, R. A. & Calvete, J. J. Combined snake venomics and venom gland transcriptomic analysis of the ocellated carpet viper, Echis ocellatus. *J. Proteomics* **71**, 609–623 (2009).

81. UniProt. Q2UXR0 · VM3E1_ECHOC · Zinc Metalloproteinase-Disintegrin-Like Eoc1. https://www.uniprot.org/uniprotkb/Q2UXR0/entry.

82. UniProt. Q2UXQ5 · VM3E2_ECHOC · Zinc Metalloproteinase-Disintegrin-Like EoVMP2. https://www.uniprot.org/uniprotkb/Q2UXQ5/entry.

83. Tasoulis, T. & Isbister, G. K. A review and database of snake venom proteomes. *Toxins (Basel).* **9**, (2017).

84. Junqueira-de-Azevedo, I. L. M., Campos, P. F., Ching, A. T. C. & Mackessy, S. P. Colubrid Venom Composition: An -Omics Perspective. *Toxins (Basel).* **8**, 1–24 (2016).

85. Tasoulis, T., Pukala, T. L. & Isbister, G. K. Investigating Toxin Diversity and Abundance in Snake Venom Proteomes. *Front. Pharmacol.* **12**, (2022).

86. Uniprot.Q6X5T0 · SL1_ECHOC · Snaclec 1. https://www.uniprot.org/uniprotkb/Q6X5T0/entry.

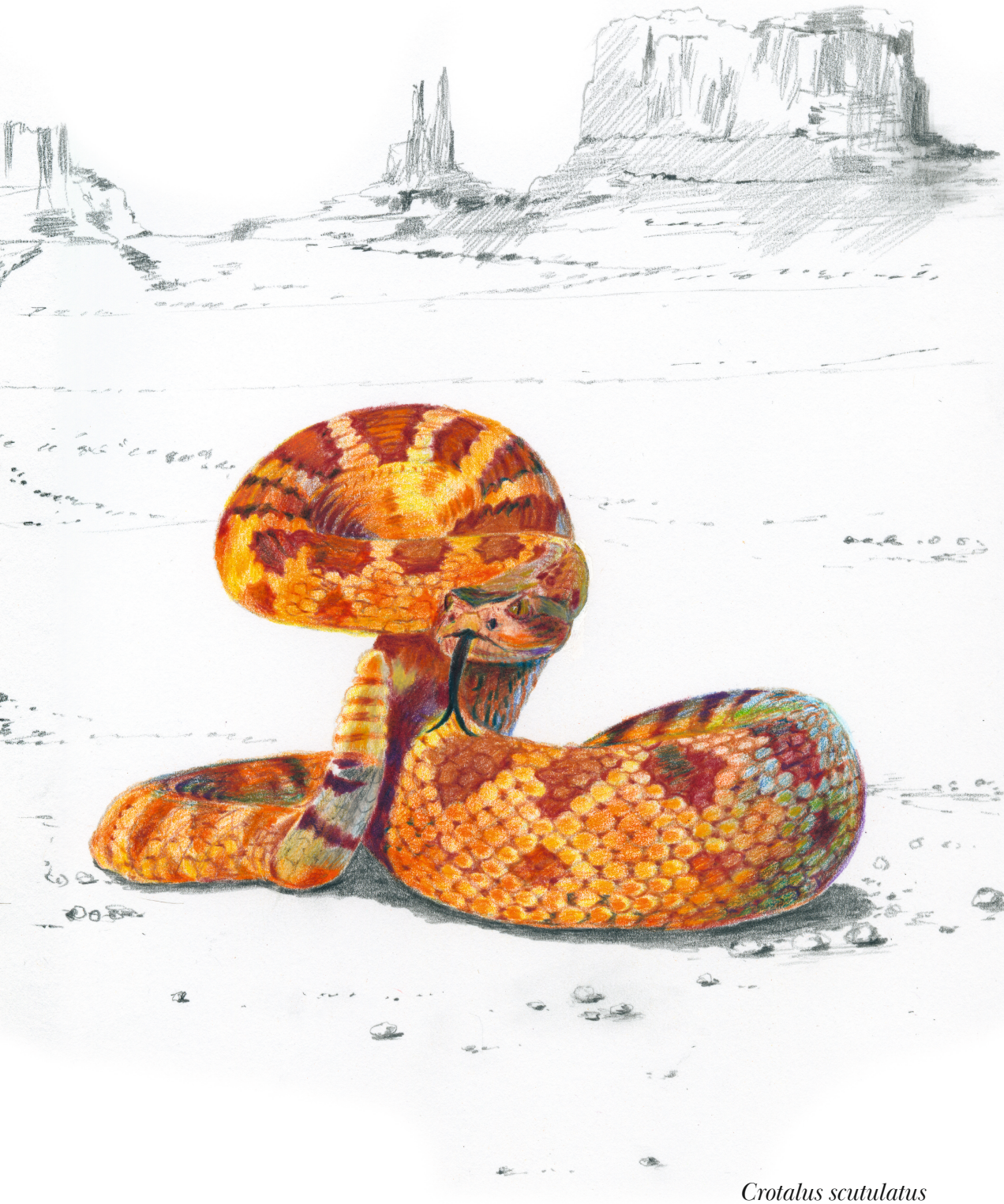

Crotalus scutulatus

Chapter 4

Monitoring snake venom-induced extracellular matrix degradation and identifying proteolytically active venom toxins using fluorescently labelled substrates

Mátyás A. Bittenbinder*, Nick D. Bergkamp*, Julien Slagboom, Jan Paul M. Bebelman, Nicholas R. Casewell, Marco H. Siderius, Martine J. Smit, Jeroen Kool, Freek J. Vonk

Biology, 12 (6), 2023

Abstract

Snakebite envenoming is an essential public health issue with devastating consequences and annual mortality rates that range between 81,000 and 138,000. Snake venoms may cause a range of pathophysiological effects affecting the nervous system and the cardiovascular system. Moreover, snake venom may have tissue-damaging activities that result in life-long morbidities such as amputations, muscle degeneration and organ malfunctioning. The tissue-damaging components in snake venoms comprise multiple toxin classes with various molecular targets, including cellular membranes and the extracellular matrix. In this study, we present multiple assay formats that enable the investigation of snake venom-induced extracellular matrix degradation using a variety of (dye-quenched, DQ) fluorescently labelled extracellular matrix components. Using a combinatorial approach, we were able to characterise different proteolytic profiles for other medically relevant snake venoms, followed by identification of the responsible components within the snake venoms. This workflow could provide valuable insights into the key mechanisms by which proteolytic venom components exert their effects and could, therefore, be helpful for the development of effective snakebite treatments against this severe pathology.

4.1 Introduction

Snakebite envenoming is a neglected tropical disease which causes 81.000 - 138.000 fatalities annually worldwide [1]. The pathological effects of snakebite envenoming, resulting from the hemotoxic, neurotoxic or cytotoxic properties of the venom, include tissue damage, paralysis, kidney failure and bleeding [1–4]. These effects are generally caused by proteins and peptides, which are highly abundant in snake venom (>90% dry weight) [5]. The four major toxin classes are represented by snake venom phospholipases A_2 (PLA_2s), three-finger toxins (3FTxs), snake venom serine proteases (SVSPs) and snake venom metalloproteinases (SVMPs). All other toxic components are classified as minor toxins [1,6]. PLA_2s, SVMPs, 3FTxs and some minor toxin classes cause tissue damage, resulting in myonecrosis, damage of capillaries, rhabdomyolysis and skin necrosis, which are evident in over 450,000 bite victims each year [1,4,7,8].

Tissue damage caused by snake venom toxins often involves the degradation of substrates of the extracellular matrix (ECM) and surrounding tissues. The ECM plays a vital role in providing structural support to cells and acts as a filtration barrier, preventing infiltrating cells and larger molecules from passing through [9–12]. The ECM is made up of the interstitial matrix and the basement membrane. The former consists of various types of collagen (i.e., collagen types I, III, VI, XII and XIV). In contrast, the latter consists of collagen types IV and VI, laminin, fibronectin, hyaluronic acid (HA), perlecan, and nidogen (see Figure 1A) [9–14]. Due to its pivotal role in cell viability, the ECM provides an excellent target for toxins known to degrade key substrates of the ECM, such as SVMPs [10,14–18]. The most clinically relevant role of SVMPs is the induction of local and systemic bleeding as a result of their proteolytic activity, destroying the ECM supporting the endothelial layer in capillary vessels [10–14].

Currently, only a limited number of studies have focused on the development of proteolytic assays that combine activity profiling with toxin identification [19–22]. In those cases where identification was performed via tryptic digestion followed by LC-MS/MS analysis, only a limited number of snake species was used [19,20]. In order to study the proteolytic activities of a selection of medically relevant snake venoms, here we used a variety of fluorescently labelled ECM-substrates (gelatin, collagen, elastin, fibronectin, laminin and hyaluronic acid).

Using SDS-PAGE, we were able to study the activity patterns of crude venoms over time and identify the venom components responsible for substrate cleavage via the application of tryptic digestion followed by nanoLC-MS/MS. Using inhibitors of SVMPs validated the vital role of these proteolytic toxins in ECM degradation. The data obtained in this study may prove particularly useful for the development of improved snakebite treatments, notably for those toxins that specifically target the proteolytic components.

4.2 Material and Methods

4.2.1 Venoms

Venoms were sourced from the extensive library of the Faculty of Science, BioAnalytical Chemistry, Vrije Universiteit Amsterdam (VU). This library contains samples obtained and subsequently provided by the Liverpool School of Tropical Medicine (LSTM), National University of Singapore (NUS) and captive breeders. The snake venoms used in this study came from the following viper (Viperidae) and elapid (Elapidae) species: *Bothrops jararaca* (jararaca, captive bred), *Calloselasma rhodostoma* (Malayan pitviper, Thailand), *Daboia russelii* (Russell's viper, locality unknown), *Deinagkistrodon acutus* (sharp-nosed viper, locality unknown); *Dendroaspis polylepis* (black mamba, captive bred), *Echis ocellatus* (West African carpet viper, Nigeria), *Naja mossambica* (Mozambique spitting cobra, captive bred) and *Naja naja* (Indian cobra, captive bred). These species were selected as they represent some of the most medically relevant species across the geographical regions most heavily affected by snakebite (i.e., Latin America, Sub-Saharan Africa and Southeast Asia). Venoms from VU and NUS were lyophilised immediately after milking, then freeze-dried and stored at -80°C. LSTM venoms were extracted, stored overnight at -20°C, then lyophilised and stored at 4°C for the long term. Samples were reconstituted in ultrapure (Milli-Q) H_2O to the desired stock solutions, depending on the type of assay. These solutions were then aliquoted and subsequently snap-frozen in liquid nitrogen and stored at -80°C until use. All venoms were sourced in accordance with the Nagoya protocol, where applicable [23].

4.2.2 Chemicals and reagents

Water was purified to Milli-Q (mQ) water grade using an in-house Milli-Q® Reference Water Purification System (Millipore). Gibco™ Dulbecco's phosphate-buffered saline (PBS) (no calcium, no magnesium, pH 7.07.3) was purchased from Sigma-Aldrich. Various substrates were used, including DQ™ gelatin from pig skin, fluorescein conjugate (Thermo Fisher Scientific); DQ™ collagen type I from bovine skin, fluorescein conjugate (Thermo Fisher Scientific); DQ™ elastin from bovine neck ligament, BODIPY FL conjugate (Thermo Fisher Scientific); rhodamine laminin from Engelbreth-Holm-Swarm mouse tumour (Cytoskeleton, Inc.); fibronectin from bovine plasma, HiLyte Fluor™ 488 labelled (Cytoskeleton, Inc.); fluorescein hyaluronic acid (Sigma-Aldrich). Positive controls included collagenase type IV from *Clostridium histolyticum* (Thermo Fisher Scientific), elastase from pig pancreas (Thermo Fisher Scientific), hyaluronidase from bovine testes Type IV-S (Sigma-Aldrich). For the inhibitor assays, two small molecule SVMP inhibitors were used, including marimastat (Sigma-Aldrich) and prinomastat (Sigma-Aldrich).

4.2.3 Detection of proteolytic activity of snake venoms

For profiling of ECM-substrate degradation patterns by different snake venoms, crude snake venoms were incubated with one of the fluorescent ECM-substrates (substrate diluted in PBS, concentration depending on the substrate) and incubated for 2 hours at 37°C. For kinetic measurements, DQ-gelatin (10 µg/mL) incubation with *C. rhodostoma* (10 µg/mL) was stopped at various time points. For DQ-gelatin inhibitor assays, *C. rhodostoma* (20 µg/mL, 2x pre-concentrated) was incubated with concentration-response curves (CRCs) of SVMP inhibitors marimastat or prinomastat for 30 minutes at 37°C, before addition of DQ-gelatin (10 µg/mL final concentration) and incubation for another 2 hours at 37°C. For marimastat single-point inhibition assays with all fluorescent substrates, the most potent snake venom (10 or 100 µg/mL) was incubated with or without marimastat (1 µM) for 30 minutes at 37°C. Subsequently, fluorescent substrates (final concentrations of 10 µg/mL for DQ-gelatin and DQ-collagen, 40 µg/mL for fluo-fibronectin and fluo-laminin, 50 µg/mL for fluo-HA and 100 µg/mL for DQ-elastin) were added to the mixtures, which were incubated for another 2 hours at 37°C. For all assays, incubation of snake venom with fluorescent

substrate was stopped by the addition of reducing Laemmli sample buffer (60 mM Tris-HCl, pH 6.8, 10% glycerol, 2% SDS, 0.01% bromophenol blue, 200 mM DTT) and subsequent heating of the samples for 5 minutes at 95°C. After loading 20 µL of each sample on gel and performing gel electrophoresis, gels were washed in PBS, and the proteolytic activity of snake venoms was visualised using the Azure 400 fluorescent imager (Azure Biosystems). Data was captured at 472 nm excitation for all fluorescent substrates, except fluo-laminin, for which 524 nm excitation was used.

4.2.4 Identification of proteolytically active proteins in venoms using in-gel (fluo-) zymography

For in-gel zymography, 20 µg of crude snake venom was mixed with non-reducing Laemmli sample buffer (60 mM Tris-HCl, pH 6.8, 10% glycerol, 2% SDS, 0.01% bromophenol blue) and loaded on an SDS-PAGE gel, co-polymerised with gelatin or collagen. For conventional zymography, a 7.5% SDS-PAGE with gelatin (1 mg/mL) or collagen 1 mg/mL) was used, whereas for fluorescent zymography a 10% polyacrylamide gel including DQ-gelatin (63 µg/mL) or DQ-collagen (63 µg/mL) was used. After gel electrophoresis, gels were washed 3x for 30 minutes with Triton X-100 (2.5%) to remove SDS and (partially) renature the venom proteins for recovery of their enzymatic activity. Gels were subsequently washed 3x for 10 minutes with mQ to remove Triton X-100 prior to incubation. Conventional zymography gels were then incubated overnight at 37°C in activity buffer (50 mM Tris-HCl, pH 7.5, 200 mM NaCl, 10 mM CaCl). After overnight incubation, these conventional zymography gels were stained for 2 hours using Coomassie Brilliant Blue solution and were de-stained using 40% ethanol / 10% acetic acid for 4x30 minutes. Proteolytic bands appeared as clear bands on a dark background, whereas highly abundant protein bands appeared as bands darker than the background. Fluo-zymography gels were also incubated in an activity buffer at 37°C, but proteolytic activity was monitored in real time during overnight incubation. Imaging of all gels was performed using the Azure 400 fluorescent imager. For fluorescence imaging, 472 nm was used as the excitation wavelength.

4.2.5 In-gel tryptic digestion of proteolytically active venom components

To identify the bioactive components in the snake venoms, in-gel fluo-zymography was performed as described above, with the exception that 100 µg of snake venom was loaded instead of 20 µg, protein bands of interest were carefully excised from the gels before being subjected to in-gel tryptic digestion. In order to make sure the correct bands were excised, a reference image of the gel, which was placed below the gel, was used. Gel bands were washed consecutively with washing buffer (25 mM ammonium bicarbonate pH = 8.2) and acetonitrile (ACN). After these washing steps, reduction buffer (0.05% β-mercaptoethanol in 25 mM ammonium bicarbonate, pH 8.2) was added, and the samples were incubated at 56°C for 30 minutes. Alkylation buffer (55 mM iodoacetamide) was then added, and the gel bands were incubated in the dark for 20 minutes. Subsequently, a stock solution of trypsin (1 µg/µL in 50 mM acetic acid) was diluted 50 times in 25 mM ammonium bicarbonate to a concentration of 0.02 µg/mL and added, after which the samples were incubated overnight at 37°C. The following day, the samples were centrifuged at 1000 rpm for 1 minute in an Eppendorf Centrifuge 5810 R, followed by adding 5% formic acid in order to quench the reaction.

4.2.6 Toxin identification using proteomics

By subjecting the bioactive components to our proteomics workflow, we were able to identify the proteolytically active toxins in the venoms. The samples were analysed using nanoLC-MS/MS (or stored at -20°C until analysis). Following the tryptic digestion, we performed nanoLC-MS/MS on the selected samples and used these samples for subsequent analysis. The samples were subjected to nano-LC separation on an UltiMate 3000 RSLCnano system (Thermo Fisher Scientific), followed by mass spectrometry. Mass spectrometry was performed on a maXis QTOF mass spectrometer (Bruker) carrying a Bruker Captive spray source that operates in positive-ion mode. Source parameters were: source temperature: 150°C; capillary voltage: 1.6 kV; dry gas flow: 3.0 L/min; nanoBooster pressure: 0.20 Bar. The spectral data was recorded at 2 Hz (in a 50 to 3000 m/z range). MS/MS spectra were collected using collision-induced dissociation (CID) in data-dependent mode, which uses 10-eV collision energy.

The data was processed using the Bruker DataAnalysis software, resulting in the identification of the proteins found in the individual venoms.

Using the data for the tryptic digests of the samples, toxin identification was performed using MASCOT (Matrix Science, London, United Kingdom) search against Swiss-Prot, NCBI and species-specific databases. The latter was generated from previously published transcriptomic data for all available species and was used to identify the components for which proteolytic activity was observed. A more elaborate description of the entire approach can be found in the paper of Slagboom et al. (2020) [24]. For each sample (activity-associated band), we used a cut-off of 100 for the protein score and subsequently selected the three toxins with the highest protein scores.

4.2.7 Statistical analysis

Data were analysed using GraphPad Prism, version 9.0.1 (GraphPad Software). Figures were made with Adobe Illustrator 2020 (Adobe Systems). The schematic figures illustrating assay formats were made using BioRender.

4.3 Results & Discussion

4.3.1 Profiling of proteolytic degradation using SDS-page gels

We set out to develop an SDS-PAGE-based method for the detection and profiling of snake venom-induced degradation of different ECM-substrates (see Figure 1A). For this, we used a panel of medically relevant snake venoms in combination with a selection of fluorescently labelled, commercially available ECM-substrates, aiming to maximise the accessibility of our newly developed method. Half of the fluorescent substrates, collagen type I, gelatin and elastin, are dye-quenched due to an excessive number of fluorophores and should, therefore, be essentially non-fluorescent in the absence of an active degrading enzyme. The other substrates, fibronectin, laminin and HA, are non-quenched (referred to as 'fluo-…') and display high levels of basal fluorescence. Upon pre-incubation with a substrate, the substrate-specific proteolytic activity in snake venom was expected to yield (smaller) fluorescent degradation products that could be visualised using a fluorescent imager after performing SDS-PAGE (see Figure 1B).

The panel of eight snake venoms used throughout this work (see S1 Figure) displayed differential degradation patterns for the six substrates (see Figure 1C, 1D). DQ-collagen type I and its derivative DQ-gelatin were entirely degraded by the crude venoms of *B. jararaca*, *C. rhodostoma*, *D. acutus*, *E. ocellatus* and *N. mossambica*, as illustrated by the appearance of a low-molecular-weight smear or more well-defined degradation product bands, respectively (see Figure 1C). *D. russelii*, *D. polylepis* and *N. naja* were unable to degrade DQ-gelatin. In contrast, partial degradation of DQ-collagen by these venoms was apparent. Unexpectedly, for the third dye-quenched substrate, DQ-elastin, the presence of low molecular weight fluorescence in the condition without snake venom treatment ('No SV') was observed, indicating some basal degradation (see Figure 1D). However, upon incubation with crude venoms from *B. jararaca*, *C. rhodostoma*, *D. acutus* and *E. ocellatus*, pronounced enhancement of basal fluorescence could be detected. Fluo-fibronectin was degraded into a venom-specific combination of smaller fluorescent products by all venoms. However, some residual intact substrate could be observed for *D. russelii* and *D. polylepis* (see Figure 1D). Fluo-laminin was visible as two high molecular weight fluorescent bands in the absence of snake venoms (see Figure 1D). Incubation with *B. jararaca, C. rhodostoma*, *D.*

acutus, *E. ocellatus* and *N. mossambica* resulted in (partial) proteolytic degradation of fluo-laminin, as evidenced by a reduction of the fluorescent starting material. The last substrate, fluo-HA, was most potently degraded by venom components of *D. polylepis*, to a lesser extent by those in *B. jararaca* and *D. russelii* venom and only marginally by *C. rhodostoma*, *D. acutus*, *N. mossambica* and *N. naja* venoms (see Figure 1D).

Next, we determined whether it was possible to simultaneously monitor the degradation of two fluorescent ECM-substrates with non-overlapping emission spectra. For this, we used C. rhodostoma, which is amongst the species with the broadest proteolytic profile (see Figure 1). In addition, we have used this species extensively in our previous studies, hence our particular interest in the activity patterns of- and the active components in the venom of this particular species. We compared single incubations of *C. rhodostoma* with fluo-laminin or fluo-fibronectin with co-incubations of *C. rhodostoma* with one of the green substrates, DQ-gelatin and with our only red substrate fluo-laminin, and measured fluorescence at 472 nm and 524 nm excitation (see S2 Figure). While the green fluo-fibronectin yielded a high amount of bleed-through in the red channel, this was not the case for DQ-gelatin. More importantly, due to size differences between intact DQ-gelatin and intact fluo-laminin as well as between degradation products of these two substrates, the co-incubation of these DQ-gelatin and fluo-laminin with *C. rhodostoma* venom allowed for the simultaneous detection of their proteolytic degradation. Hence, our new SDS-PAGE-based method provides for differentiation between snake venoms based on their ECM-substrate specificity and can be performed in a multiplexing fashion.

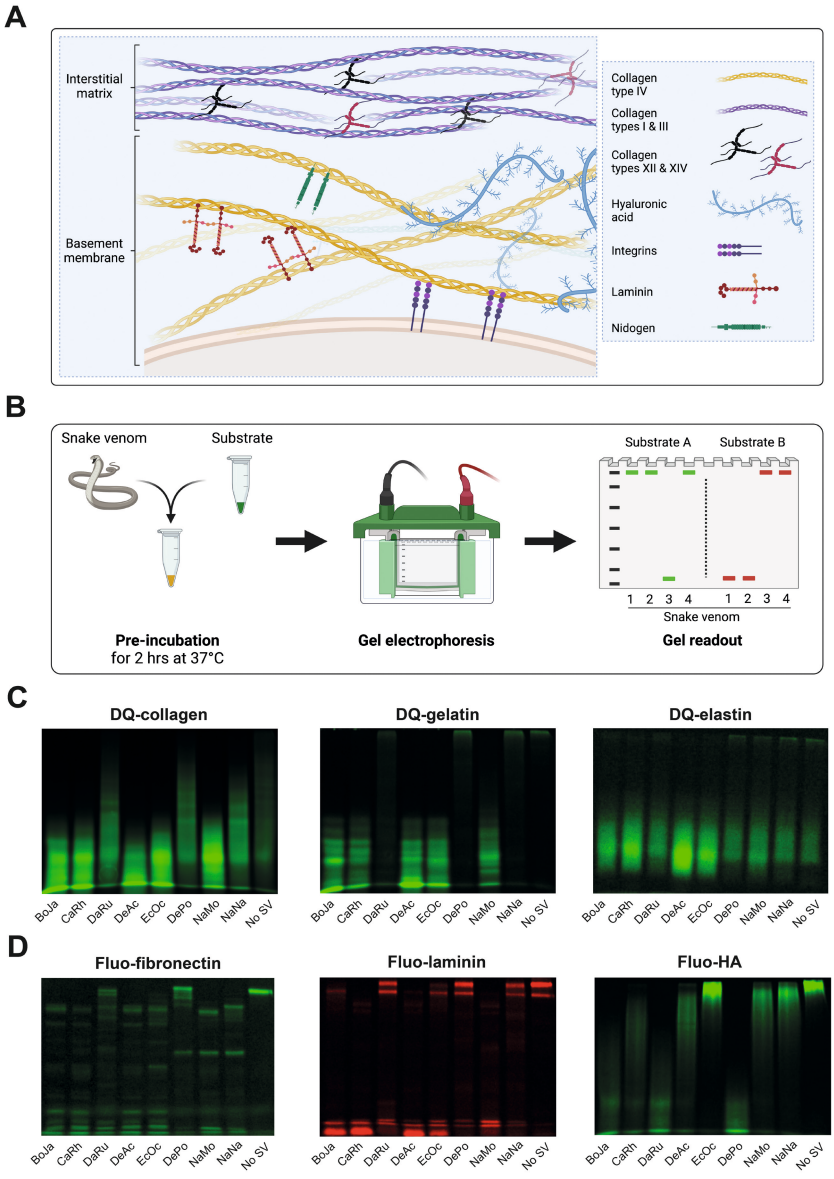

Figure 1. Different ECM components and SDS-PAGE-based fluorescence detection of snake venom-induced degradation thereof. A) Schematic representation of the ECM composition. **B**) Workflow used for the visualisation of fluorescent ECM-substrate degradation patterns by different snake venoms. **C, D**) SDS-PAGE-based visualisation of degradation of **C**) dye-quenched fluorescent substrates DQ-collagen (40 µg/mL), DQ-gelatin (10 µg/mL) and DQ-elastin (100 µg/mL) or **D**) non-dye-quenched ('fluo-') fluorescent substrates fluo-fibronectin (40 µg/mL), fluo-laminin (40 µg/mL) and fluo-HA (50 µg/mL), after incubation with indicated eight different snake venoms (10 µg/mL for DQ-collagen, DQ-gelatin, fluo-fibronectin and fluo-HA; 100 µg/mL for DQ-elastin and fluo-laminin) for 2 hrs at 37°C. Abbreviations: BoJa, *B. jararaca*; CaRh, *C. rhodostoma*; DaRu, *D. russelii*; DeAc, *D. acutus*; EcOc, *E. ocellatus*; DePo: *D. polylepis*; NaMo, *N. mossambica*; NaNa, *N. naja*.

4.3.2 Assessing potency and kinetics for degradation of fluorescent ECM components

Next, we assessed whether we could use the novel method to monitor the potency and kinetics for proteolytic degradation of fluorescent ECM-substrate by snake venoms. To test this, we used DQ-gelatin together with our model venom, *C. rhodostoma*. Increasing concentrations of *C. rhodostoma* venom yielded concentration-dependent degradation of DQ-gelatin but not unlabelled gelatin (see Figure 2A). A similar pattern was observed for the degradation of DQ-collagen by increasing concentrations of the same crude snake venom (see Figure 2B). Next, we tested whether different potencies were detectable using this method. Therefore, we pre-incubated fluo-HA with two snake venoms: *C. rhodostoma* and *D. polylepis*. Complete degradation of fluo-HA was observed by the positive control hyaluronidase-IV, and all concentrations of D. polylepis venom. In contrast, only incubation with the highest concentration of *C. rhodostoma* venom yielded partial degradation of fluo-HA (see Figure 2C). Subsequently, we used different incubation times of *C. rhodostoma* venom with DQ-gelatin to determine the time course of DQ-gelatin degradation. The results indicated the proteolytic degradation of DQ-gelatin by *C. rhodostoma* was a time-dependent, saturable process (see Figure 2D). Hence, the potency and kinetics of fluorescent ECM-substrate degradation by crude snake venoms can be assessed using the presented SDS-PAGE-based method. A clear limitation of the proposed approach is the low throughput, and much higher throughput for quantitative assessment of snake venom-induced degradation of ECM-substrates could be achieved using plate reader-based assays that rely on a change in total fluorescence. However, this requires the substrate to be dye-quenched in the absence of an active degrading enzyme. For non-quenched substrates, proteolytic activity does not increase total fluorescence. The SDS-PAGE-based evaluation we report here, albeit with a low throughput, allows for monitoring and quantification of degradation of these non-quenched substrates.

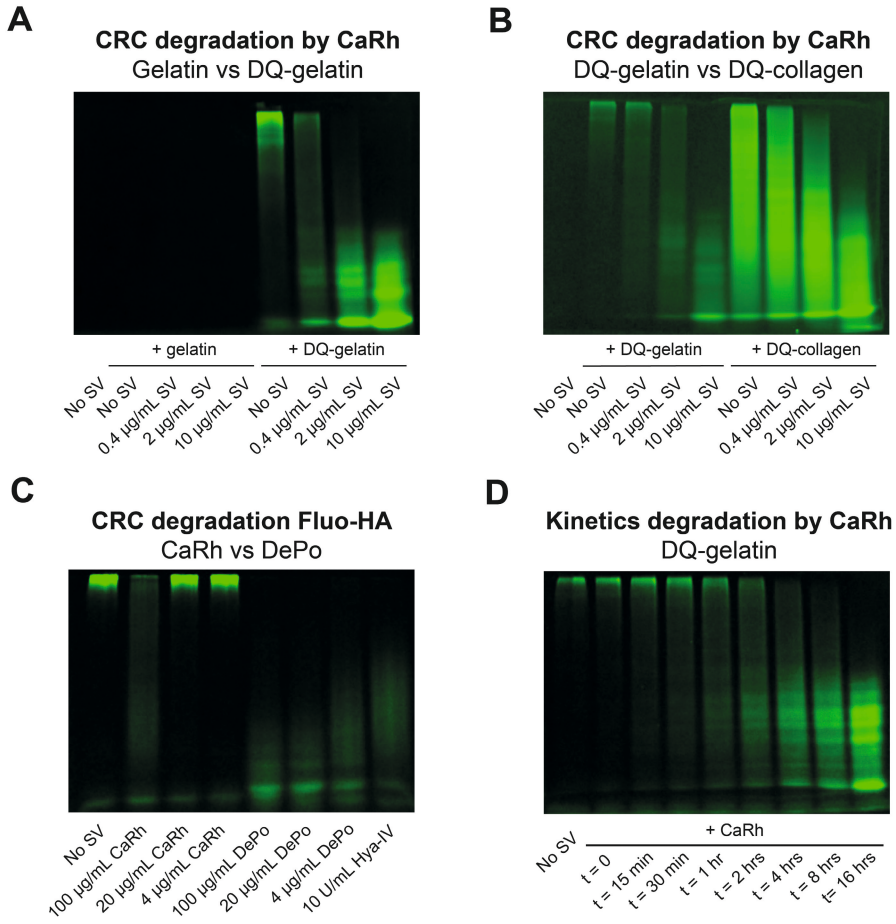

Figure 2. Assessing potency and kinetics for degradation of fluorescent ECM components. A) SDS-PAGE-based visualisation of gelatin (10 µg/mL, left) or DQ-gelatin (10 µg/mL, right) degradation by concentration-response curve (CRC) of *C. rhodostoma* (CaRh) venom. **B**) SDS-PAGE-based visualisation of DQ-gelatin (10 µg/mL, left) or DQ-collagen (10 µg/mL, right) degradation by CRC of *C. rhodostoma* venom. **C**) SDS-PAGE-based visualisation of fluo-HA (50 µg/mL) degradation by CRC of *C. rhodostoma* (left) or *D. polylepis* venom (right), with Hya-IV (10 U/mL) as a positive control (most right lane). **D**) SDS-PAGE-based visualisation of kinetics for proteolytic degradation of DQ-gelatin (10 µg/mL) by *C. rhodostoma* (10 µg/mL).

4.3.3 Extending the method to monitor substrate-specific inhibition of ECM degradation

ECM degradation by proteolytically active components in snake venoms is a key feature of the toxicity associated with snake bites. To prevent such toxicity, therapeutics that act as (non-) competitive enzyme inhibitors can be used. Given this, we assessed whether our new method, which combines SDS-PAGE with fluorescent ECM-substrates, allows for monitoring specific inhibition of snake venom-induced ECM degradation.

Pre-treatment of *C. rhodostoma* venom with increasing concentrations of two SVMP inhibitors, marimastat and prinomastat, resulted in dose-dependent inhibition of DQ-gelatin proteolysis (see Figure 3A). Marimastat ($logIC_{50}$ = -7.4 ± 0.3) displayed an almost ten-fold higher inhibitory potency compared to prinomastat ($logIC_{50}$ = -6.6 ± 0.2). To evaluate the specificity of the observed inhibition, we then tested the inhibitory effects of marimastat on the snake venom-induced degradation of all six fluorescent ECM-substrates. Although degradation of fluo-HA induced by the venom of *D. polylepis* remained largely unaffected by marimastat, snake venom-induced proteolytic degradation of all other substrates was found to be effectively inhibited by this inhibitor (see Figure 3B). This suggests that SVMPs are primarily responsible for the observed degradation of all ECM-substrates except HA. Hence, our method can be used to investigate the inhibitory potential and specificity of compounds targeting snake venom components. This could aid in the identification of new compounds with therapeutic potential against specific toxins found in different snake venoms.

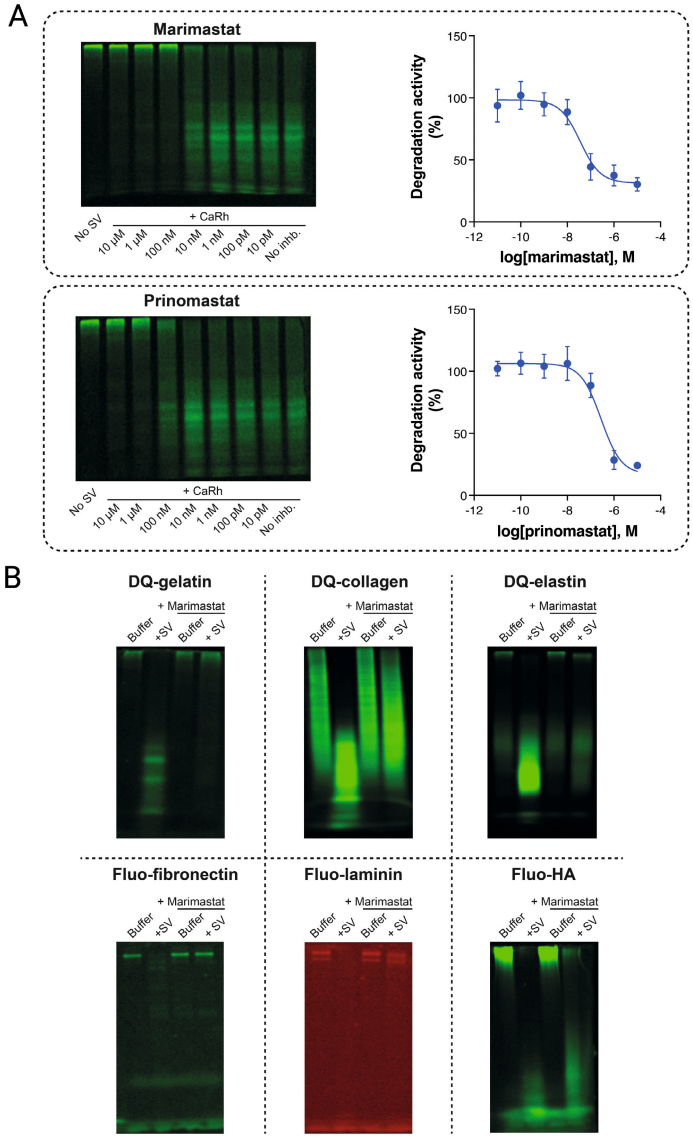

Figure 3. Extending the method to monitoring substrate-specific inhibition of ECM degradation. **A**) SDS-PAGE-based visualisation and quantification of the inhibition of snake venom (*C. rhodostoma*)-induced proteolytic degradation of DQ-gelatin (10 µg/mL) by inhibitory CRCs of SVMP inhibitors marimastat and prinomastat. Inhibition was quantified by measuring the intensity of the degradation products and normalising these values to the 'no SV' condition (0%) and 'SV no inhibitor' condition (100%). Gels are representative of four individual experiments. Graphs depict the mean degradation activity ± SEM of these four individual experiments. **B**) SDS-PAGE-based visualisation of snake venom-induced fluorescent substrate degradation inhibition by SVMP inhibitor marimastat. For each fluorescent ECM-substrate, the most potent snake venom was pre-treated with or without marimastat (1 µM). For DQ-gelatin, DQ-collagen, and fluo-fibronectin, this was C. rhodostoma; for DQ-Elastin and fluo-laminin, this was *D. acutus* and for fluo-HA = *D. polylepis*.

4.3.4 Identification of proteolytic components using (fluo-) zymography

In-gel zymography can be used to identify substrate-specific proteolytically active components within a mixture of proteins. Conventionally, non-fluorescent substrates, such as gelatin, are used for co-polymerisation with SDS-PAGE gels in order to obtain zymograms [21,22,25]. However, in an attempt to investigate whether it was possible to use dye-quenched fluorescent ECM-substrates in gel-zymography, which we named 'fluo-zymography'. In theory, this approach would allow for real-time detection of in-gel proteolytic activity, which is not possible with conventional zymography (see Figure 4A). For our panel of snake venoms, we performed in-gel conventional and fluo-zymography using (DQ-)gelatin as the co-polymerised substrate (see Figure 4B-C). In accordance with DQ-gelatin degradation profiles of the different snake venoms (see Figure 1C), we observed the highest abundance and intensity of proteolytically active bands for all viper venoms except *D. russelii* (see Figure 4B-4C). Despite a substrate concentration that was more than 15 times lower than that used for fluo-zymography and a shorter incubation time (2 hours vs 16 hours), a higher number of active bands were apparent using this novel method. This indicates a higher sensitivity of fluo-zymography than conventional zymography. Further comparison of conventional zymography and fluo-zymography gels revealed that the most abundant toxins (i.e., the bands that were most heavily stained with Coomassie Brilliant Blue) were not necessarily most active in terms of gelatin-degrading capacity (Figures 4B-C). While for (DQ-)collagen, almost no activity bands could be monitored with conventional zymography using unlabelled collagen, fluo-zymography revealed a more pronounced degradation pattern when using DQ-collagen (see S3A-B Figure). As expected, using two venoms with the highest DQ-gelatin degradation capacity (i.e., *B. jararaca* and *C. rhodostoma*) demonstrated that fluo-zymopgraphy allows for real-time monitoring of ECM-substrate proteolytic degradation (see Figure 4D). Interestingly, where for *C. rhodostoma,* most proteolytically active bands were visible directly after renaturation, for *B. jararaca,* the majority of proteolytically dynamic bands became apparent at later time points. In summary, the newly developed fluo-zymography approach 1) requires a lower ECM-substrate concentration for co-polymerisation in SDS-PAGE gels, 2) seems to give a higher sensitivity than conventional zymography (especially for collagen

zymography), and 3) can capture the contributions of individual components within snake venoms over time, in contrast to conventional zymography.

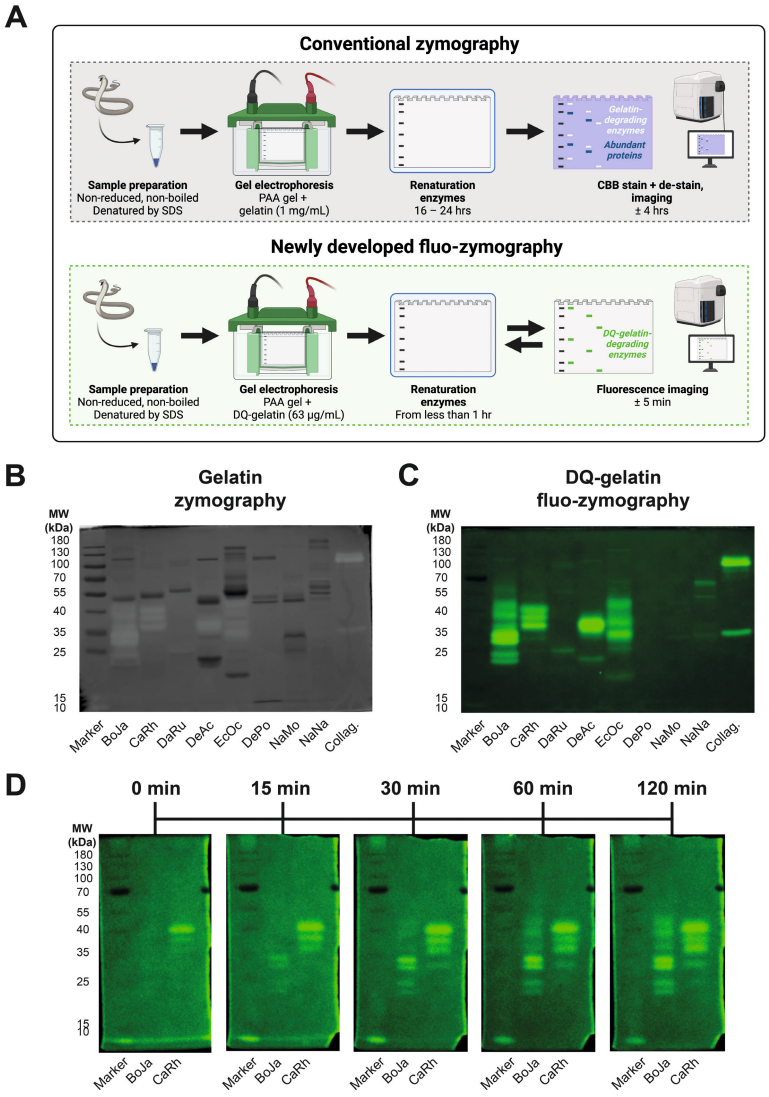

Figure 4. Assessing the proteolytic activity of snake venoms using (fluo-)zymography. A) Schematic representation of the workflow of the conventional zymography and the newly developed fluo-zymography methods. **B**) Activity profiles for the conventional in-gel zymography (1 mg/mL of gelatin) of our panel of snake venoms (20 µg) after 16 hrs of incubation. **C)** Activity profiles for the in-gel fluo-zymography (63 µg/mL of DQ-gelatin) of our panel of snake venoms (20 µg) after 2 hrs of incubation. **D**) Kinetics of fluorescent substrate degradation for the two most potent snake venoms (i.e., *B. jararaca* and *C. rhodostoma*). Abbreviations: BoJa, *B. jararaca*; CaRh, *C. rhodostoma*; DaRu, *D. russelii*; DeAc, *D. acutus*; EcOc, *E. ocellatus*; DePo: *D. polylepis*; NaMo, *N. mossambica*; NaNa, *N. naja*.

4.3.5 Validation of proteolytically active proteins within crude snake venoms using proteomics

In general, viper venoms demonstrated more activity on the substrates compared to the elapid venoms, with the exception of *D. russelii* venom (see Figure 4B-C). The (DQ-)gelatin degrading profile of all proteolytically-active vipers was characterised by low- to mid-weight compounds (i.e., 20 – 55 kDa), although some high mass compounds (i.e., > 70 – 130 kDa) were also present, albeit displaying lower proteolytic activity (see Figure 4C). The venom of *D. russelii* did not show a high level of substrate degrading capacity, except for a few minor bands at varying molecular weights (i.e., around 100 kDa, 55 kDa and 25 kDa). The elapid venoms showed considerably less activity, with *D. polylepis* venom being devoid of activity except for two minor bands around 40 – 55 kDa. The venoms of *N. mossambica* and *N. naja* showed somewhat higher activity, although the observed effect was lower when compared to the viper venoms. These findings were anticipated based on previous studies on proteolytic degradation by snake venoms [19,21,22,26].

For further analysis of those components responsible for the observed proteolytic activity, we combined fluo-zymography with advanced analytical techniques (see Figure 5A). For this, we excised all bands containing bioactive proteins, followed by tryptic digestion of each sample and subsequent MS/MS analysis for toxin identification (see Figure 5B). For each band, the three proteins with the highest protein score were selected.

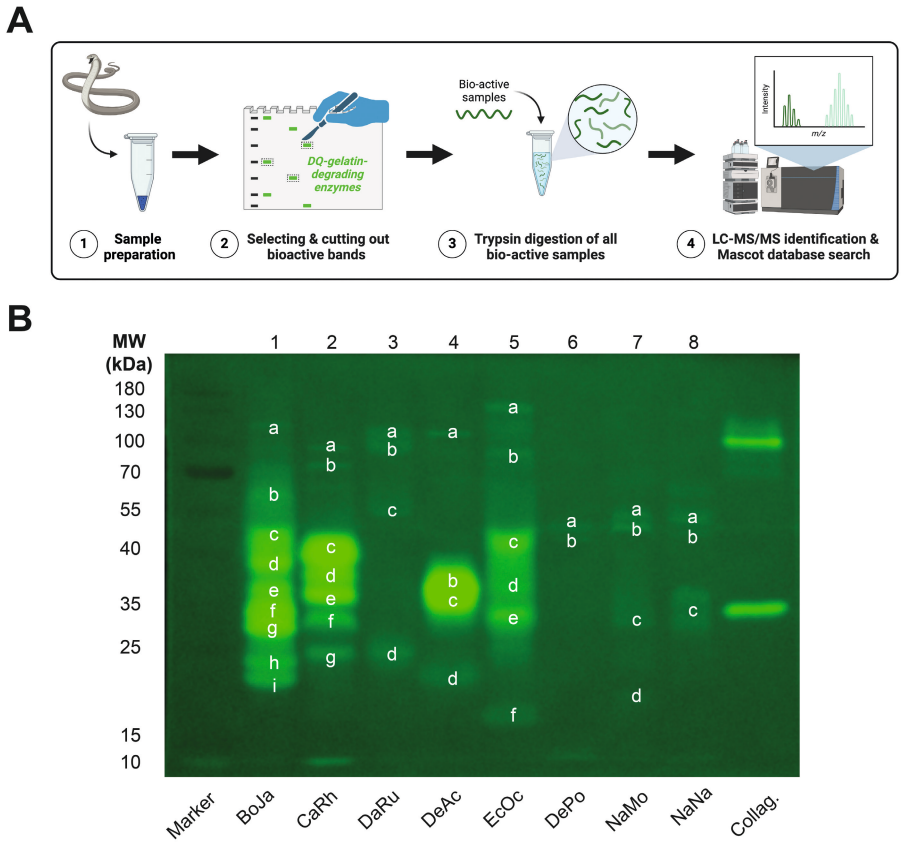

Figure 5. Proteomics of ECM-degrading components in crude snake venoms using fluo-zymography. A) Schematic representation of the workflow for the identification of proteolytic components within crude snake venoms using proteomics. **B**) Activity profiles for DQ-gelatin in-gel fluo-zymography of our panel of snake venoms (100 µg) and positive control collagenase (2 U) after 2 hrs of incubation. Letters depict bioactive bands in the venom of each species that were excised for subsequent toxin identification using proteomics. Abbreviations: BoJa, *B. jararaca*; CaRh, *C. rhodostoma*; DaRu, *D. russelii*; DeAc, *D. acutus*; EcOc, *E. ocellatus*; DePo: *D. polylepis*; NaMo, *N. mossambica*; NaNa, *N. naja*. The letters corresponding to each of the gel bands and the identified proteins can be found in Table S2.

The proteomics results demonstrated that for the venoms with high DQ-gelatin-degrading capacity, two toxin classes were more commonly represented, namely SVMPs and LAAOs. SVMPs form a class of enzymatic toxins that are found in all venomous snake families and which are subdivided into three groups (i.e., P-I to P-III) based on their domain structure [6,14,27]. The P-I group (~20 – 30 kDa) solely carry the metalloproteinase domain, whereas the P-II group (20 – 60 kDa) has an additional disintegrin domain, and the P-III group (60 – 100 kDa) has a disintegrin-like domain and another cysteine-rich domain [28,29].

In all viper venoms, we find SVMPs from all three subclasses. The substrate-degrading activity likely results from the SVMPs present in the venom, given the fact these toxins are highly abundant in the venoms (Table S1) and have the capacity to degrade specific substrates proteolytically [10,11,13]. This is in accordance with previous studies in which proteolytic activity of snake venoms was studied using zymogram gels [19,21,22,30–33]. Our inhibitor data (section 3.3) further suggests that SVMPs are likely to be responsible for the observed degradation of most ECM-substrates. Arguably, the most clinically relevant role of SVMPs is their induction of local and systemic bleeding by destruction of the ECM supporting the endothelial layer in capillary vessels [10,11,13]. SVMPs destabilise the interactions between endothelial cells and the basement membrane through the degradation of key components in the endothelial cell membrane and the basement membrane [10,11,14,34]. The basement membrane degradation by SVMPs further affects a variety of other cell types, including skeletal muscle cells, keratinocytes and kidney cells [1,10,35,36].

LAAOs are the second class of toxins that were regularly found in the viper venoms, and these are a group of enzymatic proteins made up of two subunits, each with a molecular weight of 50-70 kDa. The LAAOs are devoid of proteolytic activity and exert their cytotoxic effects by mechanisms unrelated to the degradation of vital components. The clinical impact of LAAOs includes haemolytic activity, bleeding, myotoxicity and induction of oedema in various tissues [37–40]. Other toxin classes present in some of the viper venoms included snake venom serine proteases (SVSPs), C-type lectin-related proteins (i.e., a group of toxins which is also known by the name 'snaclecs') and PLA_2s. These classes, however, have other activities and cannot cleave ECM-substrates [29,41–46].

Although the elapid venoms demonstrated much lower DQ-gelatin-degrading capacity on the fluo-zymograms compared to viper venoms, we did observe some proteolytic activity. For *N. mossambica* and *N. naja,* we found several P-III SVMPs, LAAOs, some cytotoxic 3FTxs and two cysteine-rich proteins. For *D. polylepis,* proteomics identified some SVMPs and a hyaluronidase, albeit these Mascot hits belonged to a different genus (i.e., *Bitis* and *Naja*) (Table S2 and S3).

4.4 Concluding remarks

This study describes the development of SDS-PAGE-based assay formats to visualise the proteolytic degradation of fluorescent ECM-substrates. These assays allowed the characterisation of the proteolytic activity in venoms of a selection of medically relevant snake species. Viper venoms were generally more proteolytically active than elapid venoms, except for *D. russelii* venom. Although the venoms of *D. russelii* and *D. polylepis* were largely devoid of proteolytic activity, the HA-degrading activities in these species were noticeably and perhaps unexpectedly potent. The use of fluorescently labelled ECM-substrates also facilitated the investigation of the kinetics of proteolytic degradation by toxin components. In contrast, the use of small molecule metalloproteinase inhibitors demonstrated that proteolysis could be readily inhibited in many cases, illustrating that the method could be implemented in efforts for the identification of novel snakebite therapeutics. By developing and using fluo-zymography, we were able to identify the proteins within the crude snake venoms that were responsible for the observed proteolytic degradation. An advantage of our newly developed method of fluo-zymography over conventional zymography is the low substrate concentration required for co-polymerisation, which enhances the sensitivity of the approach and could be helpful for ECM-substrates that cannot be dissolved to high concentrations. In combination with proteomics on all active venom components, this approach provided us with an extensive overview of the cleavage patterns, dose-dependency and kinetics of our panel of medically relevant species. Therefore, this workflow could be helpful in studying toxins that specifically target the proteolytic components responsible for causing snakebite morbidity.

References

1. Gutiérrez, J. M. *et al.* Snakebite envenoming. *Nat. Rev. Dis. Prim.* 3, (2017).
2. Kasturiratne, A. *et al.* The global burden of snakebite: A literature analysis and modelling based on regional estimates of envenoming and deaths. *PLoS Med.* 5, 1591–1604 (2008).
3. Habib, A. G. *et al.* Snakebite is Under Appreciated: Appraisal of Burden from West Africa. *PLoS Negl. Trop. Dis.* 9, 4–11 (2015).
4. Warrell, D. A. Guidelines of Management of Snake bite. *Lancet* 375, 77–88 (2010).
5. Waheed, H., Moin, S. F. & Choudhary, M. I. Snake Venom: From Deadly Toxins to Life-saving Therapeutics. *Curr. Med. Chem.* 24, 1874–1891 (2017).
6. Tasoulis, T. & Isbister, G. K. A review and database of snake venom proteomes. *Toxins (Basel).* 9, (2017).
7. Chippaux, J. P. Snakebite envenomation turns again into a neglected tropical disease! *J. Venom. Anim. Toxins Incl. Trop. Dis.* 23, 1–2 (2017).
8. Longbottom, J. *et al.* Vulnerability to snakebite envenoming : a global mapping of hotspots. *Lancet* 392, 673–684 (2018).
9. Alberts, B. *et al. Essential cell biology: Fifth international student edition*. (WW Norton & Company., 2018).
10. Gutiérrez, J. M., Escalante, T., Rucavado, A., Herrera, C. & Fox, J. W. A comprehensive view of the structural and functional alterations of extracellular matrix by snake venom metalloproteinases (SVMPs): Novel perspectives on the pathophysiology of envenoming. *Toxins (Basel).* 8, (2016).
11. Gutiérrez, J. M., Escalante, T., Rucavado, A. & Herrera, C. Hemorrhage caused by snake venom metalloproteinases: A journey of discovery and understanding. *Toxins (Basel).* 8, (2016).
12. Jayadev, R. & Sherwood, D. R. Basement membranes. *Curr. Biol.* 27, R207–R211 (2017).
13. Gutiérrez, J. M., Rucavado, A., Escalante, T. & Díaz, C. Hemorrhage induced by snake venom metalloproteinases: Biochemical and biophysical mechanisms involved in microvessel damage. *Toxicon* 45, 997–1011 (2005).
14. Takeda, S., Takeya, H. & Iwanaga, S. Snake venom metalloproteinases: Structure, function and relevance to the mammalian ADAM/ADAMTS family proteins. *Biochim. Biophys. Acta - Proteins Proteomics* 1824, 164–176 (2012).
15. Escalante, T. *et al.* Role of collagens and perlecan in microvascular stability: Exploring the mechanism of capillary vessel damage by snake venom metalloproteinases. *PLoS One* 6, (2011).
16. Markland, F. S. & Swenson, S. Snake venom metalloproteinases. *Toxicon* 62, 3–18 (2013).
17. Girish, K. S., Jagadeesha, D. K., Rajeev, K. B. & Kemparaju, K. Snake venom hyaluronidase: An evidence for isoforms and extracellular matrix degradation. *Mol. Cell. Biochem.* 240, 105–110 (2002).
18. Bala, E., Hazarika, R., Singh, P., Yasir, M. & Shrivastava, R. A biological overview of Hyaluronidase: A venom enzyme and its inhibition with plants materials. *Mater. Today Proc.* 5, 6406–6412 (2018).

19. Terra, R. M. S., Pinto, A. F. M., Guimarães, J. A. & Fox, J. W. Proteomic profiling of snake venom metalloproteinases (SVMPs): Insights into venom induced pathology. *Toxicon* 54, 836–844 (2009).

20. Mackessy, S. P. *et al.* Venom ontogeny in the mexican lance-headed rattlesnake (Crotalus polystictus). *Toxins (Basel).* 10, (2018).

21. Roldán-Padrón, O. *et al.* Snake venom hemotoxic enzymes: Biochemical comparison between Crotalus species from central Mexico. *Molecules* 24, 1–16 (2019).

22. Meléndez-Martínez, D. *et al.* Functional Mining of the Crotalus Spp. Venom Protease Repertoire Reveals Potential for Chronic Wound Therapeutics. *Mol. 2020, Vol. 25, Page 3401* 25, 3401 (2020).

23. CBD Secretariat. Nagoya Protocol on Access To Genetic Resources and the Fair and Equitable Sharing of Benefits Arising from their Utilization to the convention on biological diversity - Text and annex. *Nagoya Protoc.* 12, 1–320 (2011).

24. Slagboom, J. *et al.* High throughput screening and identification of coagulopathic snake venom proteins and peptides using nanofractionation and proteomics approaches. *PLoS Negl. Trop. Dis.* 14, 1–26 (2020).

25. Vandooren, J., Geurts, N., Martens, E., Van Den Steen, P. E. & Opdenakker, G. Zymography methods for visualizing hydrolytic enzymes. *Nature Methods* vol. 10 211–220 at https://doi.org/10.1038/nmeth.2371 (2013).

26. Bee, A., Theakston, R. D. G., Harrison, R. A. & Carter, S. D. Novel in vitro assays for assessing the haemorrhagic activity of snake venoms and for demonstration of venom metalloproteinase inhibitors. *Toxicon* 39, 1429–1434 (2001).

27. Tasoulis, T., Pukala, T. L. & Isbister, G. K. Investigating Toxin Diversity and Abundance in Snake Venom Proteomes. *Front. Pharmacol.* 12, (2022).

28. Fry, B. G. *Venomous reptiles and their toxins: evolution, pathophysiology and biodiscovery. Oxford University Press, Oxford University Press.* (2015). doi:10.1016/0041-0101(71)90017-1.

29. Gasanov, S. E., Dagda, R. K. & Rael, E. D. Snake Venom Cytotoxins, Phospholipase A2 s, and Zn2+ -dependent Metalloproteinases: Mechanisms of Action and Pharmacological Relevance. *J. Clin. Toxicol.* 4, (2014).

30. Bjarnason, J. B. & Fox, J. W. Characterization of two hemorrhagic zinc proteinases, toxin c and toxin d, from western diamondback rattlesnake (Crotalus atrox) venom. *Biochim. Biophys. Acta - Protein Struct. Mol. Enzymol.* 911, 356–363 (1987).

31. Antunes, T. C., Yamashita, K. M., Barbaro, K. C., Saiki, M. & Santoro, M. L. Comparative analysis of newborn and adult Bothrops jararaca snake venoms. *Toxicon* 56, 1443–1458 (2010).

32. Serrano, S. M. T., Shannon, J. D., Wang, D., Camargo, A. C. M. & Fox, J. W. A multifaceted analysis of viperid snake venoms by two-dimensional gel electrophoresis: An approach to understanding venom proteomics. *Proteomics* 5, 501–510 (2005).

33. Möller, C., Vanderweit, N., Bubis, J. & Mari, F. Comparative analysis of proteases in the injected and dissected venom of cone snail species. *Toxicon* 65, 59–67 (2013).

34. Gutiérrez, J. M. & Rucavado, A. Snake venom metalloproteinases: Their role in the pathogenesis of local tissue damage. *Biochimie* 82, 841–850 (2000).

35. Teixeira, C., Cury, Y., Moreira, V., Picolo, G. & Chaves, F. Inflammation induced by Bothrops asper venom. *Toxicon* 54, 67–76 (2009).

36. Sitprija, V. Animal toxins and the kidney. *Nat. Clin. Pract. Nephrol.* 4, 616–627 (2008).

37. Guo, C., Liu, S., Yao, Y., Zhang, Q. & Sun, M. Z. Past decade study of snake venom l-amino acid oxidase. *Toxicon* 60, 302–311 (2012).

38. Costal-Oliveira, F. *et al.* L-amino acid oxidase from Bothrops atrox snake venom triggers autophagy, apoptosis and necrosis in normal human keratinocytes. *Sci. Rep.* 9, (2019).

39. Izidoro, L. F. M. *et al.* Snake venom L-amino acid oxidases: Trends in pharmacology and biochemistry. *Biomed Res. Int.* 2014, (2014).

40. Ande, S. R. *et al.* Mechanisms of cell death induction by L-amino acid oxidase, a major component of ophidian venom. *Apoptosis* 11, 1439–1451 (2006).

41. Serrano, S. M. T. The long road of research on snake venom serine proteinases. *Toxicon* 62, 19–26 (2013).

42. Montecucco, C., Gutiérrez, J. M. & Lomonte, B. Cellular pathology induced by snake venom phospholipase A2 myotoxins and neurotoxins: Common aspects of their mechanisms of action. *Cell. Mol. Life Sci.* 65, 2897–2912 (2008).

43. Saikia, D. *et al.* Differential mode of attack on membrane phospholipids by an acidic phospholipase A2 (RVVA-PLA2-I) from Daboia russelli venom. *Biochim. Biophys. Acta - Biomembr.* 1818, 3149–3157 (2012).

44. Morita, T. Structures and functions of snake venom CLPs (C-type lectin-like proteins) with anticoagulant-, procoagulant-, and platelet-modulating activities. *Toxicon* 45, 1099–1114 (2005).

45. Clemetson, K. J. Snaclecs (snake C-type lectins) that inhibit or activate platelets by binding to receptors. *Toxicon* 56, 1236–1246 (2010).

46. Eble, J. A. Structurally robust and functionally highly versatile—C-type lectin (-related) proteins in snake venoms. *Toxins (Basel).* 11, (2019).

Tropidolaemus subannulatus

Chapter 5

Application of an extracellular matrix-mimicking fluorescent polymer for the detection of proteolytic venom toxins

Mátyás A. Bittenbinder*, Eric Wachtel*, Bas van de Velde, Julien Slagboom, Axel de Monts de Savasse, Luis L. Alonso, Nicholas R. Casewell, Freek J. Vonk, Jeroen Kool

Toxins, 15 (294), 2023

Abstract

Tissue-damaging effects caused by snake venoms are a serious medical problem that significantly contribute to the morbidity observed in snakebite patients. The cell- and tissue-damaging components found in snake venoms belong to a variety of toxin classes. They may exert their effects by targeting a range of molecular structures, including cellular membranes, the extracellular matrix and the cytoskeleton. Here, we present a high-throughput assay (384-well plate) that monitors extracellular matrix degradation by snake venom toxins via the application of fluorescent versions of model extracellular matrix substrates, specifically gelatin and collagen type I. Both crude venoms and fractionated toxins of a selection of medically relevant viperid and elapid species, separated via size-exclusion chromatography, were studied using the self-quenching, fluorescently labelled extracellular matrix polymer substrates. The viperid venoms showed significantly higher proteolytic degradation when compared to elapid venoms. However, the venoms with higher snake venom metalloproteinase content did not necessarily exhibit stronger substrate degradation than those with a lower one. Gelatin was generally more readily cleaved than collagen type I. In the viperid venoms, which were subjected to fractionation by size-exclusion chromatography, two (*B. jararaca* and *C. rhodostoma*, respectively) or three (*E. ocellatus*) active proteinases were identified. Therefore, the assay allows the study of proteolytic activity towards the ECM *in vitro* for crude and fractionated venoms.

5.1 Introduction

Snakebite envenoming is a severe health hazard and is listed as a Category A Neglected Tropical Disease (NTD) by the World Health Organization (WHO) [1,2]. An estimated 1.8–2.7 million snakebite cases occur annually, resulting in 81,000–138,000 fatalities and over 450,000 maimed victims. The regions that are most heavily affected include Southeast Asia, Sub-Saharan Africa, Latin America and Papua New Guinea, and snakebite disproportionally affects the rural, resource-poor communities in these regions [2–6]. Snake venoms consist of a broad range of protein families with numerous activities that may cause a variety of pharmacological effects. The pathophysiological effects caused by snake venoms can be broadly classified into neurotoxicity, haemotoxicity and tissue-damaging effects [2,4]. The latter is the least studied of all venom pathologies and may cause local tissue damage (e.g., necrosis), (striated) muscle damage, rhabdomyolysis, microvascular damage, oedema, blistering and pain [2,4,5,7].

Venom-induced tissue damage can be caused by a variety of toxins, both enzymatic and non-enzymatic. These include enzymatic toxins such as phospholipases A_2 (PLA_2s), snake venom metalloproteinases (SVMPs) and hyaluronidases and non-enzymatic toxins such as three-finger toxins (3FTxs) and β-defensin-like toxins [2,7–10]. Toxins with tissue-damaging properties can be loosely divided into two groups based on the way in which they affect the cells (and thus tissues). They may either destabilise the cellular membrane (i.e., these are 'true' cytotoxins as they directly affect cell viability) or degrade the extracellular matrix (ECM). However, some other toxins are known that are capable of modifying the cytoskeleton or inducing oxidative stress [2,7–12]. This study will focus mainly on ECM-degrading toxins. The ECM is a macromolecular scaffold made up of proteoglycans, including hyaluronic acid, fibrous proteins (mainly collagens, elastins, fibronectins and laminins) and glycoproteins [8,13]. The ECM consists of the interstitial matrix, which consists primarily of collagen I, III, VI, XII and XIV, and the basement membrane (BM), which is made up of collagen type IV and VI, laminin, perlecan and nidogen [13,14]. The latter plays a key scaffolding role in endothelial cells and other cell types [13,15].

Hyaluronidases and SVMPs are toxin classes capable of degrading ECM components [2,14,16,17]. The venoms of viperid snakes are particularly rich in SVMPs,

while the SVMP content in most elapid snake venoms is considerably lower [18,19]. While commonly only a minor venom component, hyaluronidases are seemingly ubiquitous across snake venoms, though the relative abundance of this toxin class is higher in viperid venoms [20,21]. SVMPs are divided into three groups (P-I, P-II and P-III) based on the presence or absence of non-catalytic disintegrin/disintegrin-like or cysteine-rich domains in the C terminal region [17,22–24]. The metalloproteinase domain is present in all three classes of SVMPs and hydrolyses vital components of the ECM, mainly in the BM, including collagen IV, VI and XV, laminin, fibronectin, perlecan and BM-specific heparan sulfate proteoglycan [2,14,15]. The proteolytic degradation of ECM-substrates leads to the loss of integrity of the BM, weakening the scaffolding structure of endothelial cells in capillary vessels and, therefore, increasing the distensibility of the microvessel wall [2,23].

In order to study the ECM-degrading activity of snake venoms, a variety of assays have been applied, ranging from *in vivo* wound exudate analysis by proteomics, immunochemical detection of ECM proteins in skin and exudates and various cell-based toxicity assays to *in vitro* low-throughput assays such as zymography (utilising non-fluorescent gelatin/collagen) and fluorometric assays assessing proteolytic activity with different fluorescently labelled peptide substrates (e.g., casein, rhodamine-110-peptide, desired peptide sequences) and self-quenched gelatin to determine proteinase activity [14,17,25–30]. These assays vary considerably in model complexity, specificity, throughput and costs. Neumann et al. (2020) developed a generic high-throughput screening assay for profiling snake venom proteinase activity after high-resolution chromatographic fractionation, using rhodamine-110-peptide as a substrate, while Biardi et al. (2011) used self-quenched, fluorescently labelled gelatin to study SVMP activity in crude snake venom and the effects of inhibitors on this activity [25,30]. The goal of this study was to establish a similar assay using 'true' ECM components, harnessing a polymeric, self-quenched ECM-component- and ECM-mimicking compound (such as the self-quenched gelatin used by Biardi et al. 2011) to investigate the proteinase activity of both crude venoms and fractionated toxins. Fluorescently labelled gelatin and collagen type I were used, both polymers that have already been used to study non-venom proteinases [31–35].

The assay was optimised using crude venom. The venoms were then separated by size utilising size-exclusion chromatography (SEC), followed by

nanofractionation analytics to assess the chromatographically separated and fractionated snake venom toxins for their ECM-degrading activity. Analytical SEC using a non-volatile phosphate buffer was performed, followed by characterisation of the proteolytic compounds using the high-throughput (HT) venomics approach by Slagboom et al. (2023) [36]. Our results demonstrated that the assay allowed the detection of ECM-degrading activity both in crude and fractionated venoms. The combination with nano-LC-MS/MS allowed the identification of the active compounds within the venoms. The SVMP assay presented here could prove valuable for better detecting and understanding venom-induced ECM degradation by snake venoms, which could be of importance for the process of improving snakebite treatments.

5.2 Material and methods

5.2.1 Chemicals and reagents

Water was purified to Milli-Q (mQ) water grade using an in-house Milli-Q® Reference Water Purification System (Millipore). Collagen–fluorescein (FITC) conjugate type I from bovine tendon was purchased from BioVision Inc. The EnzChek™ gelatinase/collagenase assay kit, containing DQTM gelatin from pig skin fluorescein conjugate, was obtained from InvitrogenTM by Thermo Fisher Scientific Inc. (lot 2,174,593 and 2,281,586). GibcoTM Dulbecco's phosphate-buffered saline (no calcium, no magnesium, pH 7.0 to 7.3; PBS) was purchased from Thermo Fisher Scientific Inc. Meanwhile, 2-propanol HPLC grade was purchased from VWR International. Acetonitrile HPLC-R (ACN), formic acid 99%, ULC/MS–CC/SFC (FA), and trifluoroacetic acid HPLC grade (TFA) were obtained from Biosolve B.V. Difluoroacetic acid for LC-MS (LiChropur, ≥97.5% (GC); DFA) was purchased from Sigma-Aldrich.

5.2.2 Venoms

Snake venoms were sourced from the venom library of the Faculty of Science, BioAnalytical Chemistry Division, Vrije Universiteit Amsterdam (VU). This library contains samples originally sourced from the Liverpool School of Tropical Medicine (LSTM), the National University of Singapore (NUS) and from captive

breeders. The snake venoms used in this study came from the following viper (Viperidae) and elapid (Elapidae) species: *Bothrops jararaca* (jararaca, captive-bred), *Calloselasma rhodostoma* (Malayan pit viper, Thailand), *Dendroaspis polylepis* (black mamba, captive-bred), *Echis ocellatus* (West African carpet viper, Nigeria), *Naja mossambica* (Mozambique spitting cobra, captive-bred) and *Naja naja* (Indian cobra, captive-bred). Venoms from NUS were lyophilised immediately after milking and then freeze-dried and stored at −80 °C. LSTM venoms were extracted, stored overnight at −20 °C and then lyophilised and stored at 4 °C for long-term use. Venoms extracted from snakes kept by private keepers were immediately flash-frozen and transported in liquid nitrogen, subsequently freeze-dried in the lab and stored at −80 °C. Samples were reconstituted in mQ to the desired stock solutions, depending on the type of assay. These solutions were then aliquoted and subsequently snap-frozen in liquid nitrogen and stored at −80 °C until use. All venoms were sourced prior to October 2014; therefore, these do not fall under the Nagoya Protocol [37].

5.2.3 High-throughput assays to study ECM degradation by crude snake venoms

The assays were based on a generic substrate degradation assay using fluorescently labelled gelatin (FG/gelatin) and collagen type I (FC/collagen I). Gelatin and collagen I were prepared as described by the manufacturer, protected from light and stored at −20 °C. Upon use, the substrates were diluted to the desired concentration with 1x reaction buffer. The 10x reaction buffer provided in the EnzChek™ assay kit (0.5 M Tris-HCl, 1.5 M NaCl, 50 mM CaCl2, 2 mM sodium azide, pH 7.6) was aliquoted and stored at −20 °C. Upon use, the buffer was diluted with sterile-filtered mQ to its final concentration. Collagenase type IV from *Clostridium histolyticum* (provided with the EnzChek™ gelatinase/collagenase assay kit) was used as a positive control at 1 U/mL and was dissolved in sterile mQ and further diluted in 1x reaction buffer. The proteolytic properties of the venoms of *B. jararaca*, *C. rhodostoma* and *E. ocellatus* were investigated using three concentrations of gelatin (10, 5 and 2 µg/mL) and collagen I (40, 20 and 10 µg/mL). The venoms of *D. polylepis*, *N. mossambica* and *N. naja* were tested with identical concentrations of gelatin (10, 5 and 2 µg/mL) and a single concentration of collagen I (40 µg/mL). The venoms were selected to cover a range of medically

significant species from the two snake families across a broad geographical range, covering regions significantly affected by snakebite.

Assays were performed in clear 384-well flat-bottom microwell plates (Greiner Bio One). Venoms were serially diluted in the well plate in reaction buffer: a 5-point dilution series was used for the elapid venoms (100; 33.3; 11.1; 3.7; 1.2 µg/mL), and a 9-point dilution series was performed with the viper venoms (100; 33.3; 11.1; 3.7; 1.2; 0.41; 0.14; 0.046; 0.015 µg/mL). Negative (45 µL 1x reaction buffer) and positive controls (40 µL 1x reaction buffer + 5 µL 10 U/mL collagenase solution) were included for each plate. Lastly, 5 µL of 10x gelatin or collagen I solution was added to the wells, resulting in a final well volume of 50 µL. Immediately after adding the substrate, the well plate was placed in a preheated (37 °C) Varioskan LUX Multimode Microplate Reader 3020-444 (ex. wavelength: 490 nm; em. wavelength: 525 nm), controlled by the SkanIt RE 4.1 software, and measured at 37 °C for 16 hours (first hour: one measurement every 5 minutes; remaining measurement time: one measurement every 15 minutes; measurement time: 1 sec/well). Fluorescence was measured in relative fluorescence units (RFU). Each sample and all controls were performed in triplicate. As the assay principle was based on self-quenching substrates, the higher the fluorescence readout, the greater the substrate cleavage. In addition to plotting RFU against time, the activity of the venoms relative to the positive control (1 U/mL collagenase) at 5 hours was calculated with the following equation:

$$\frac{RFU(venom) - RFU(neg.\ ctrl.)}{RFU(pos.\ ctrl.) - RFU(neg.\ ctrl.)} * 100 = relative\ activity\ [\%]$$

Relative activity [%] was then plotted against the venom concentration [µg/mL]. The negative control was subtracted for baseline correction. An overview of the workflow is visualised in the S6A Figure.

5.2.4 High-throughput assays to study ECM degradation by crude snake venoms

In order to study the proteolytic components in our panel of snake venoms, we used analytical SEC in HPLC mode for toxin separation based on size. We

employed SEC as a separation method to retain toxins in their native form and to avoid the potentially detrimental effects of separation on enzymatic protein activity. An overview of the complete workflow (SEC, fractionation, bioassay and proteomics) is visualised in the S6B Figure.

Effects of organic solvents, buffers and acidifiers on the proteolytic activity of snake venoms
Volatile eluents and acidifiers are usually used in liquid chromatography, as they allow optimal protein separation and post-column removal without leaving high salt concentrations in wells, which might negatively affect bioassays and would allow the direct coupling of SEC to MS if desired. Previous studies have shown that the use of volatile eluents (e.g., using ACN or methanol as the organic modifier and acidifiers such as TFA) negatively affects protein stability, including labile proteinases, by denaturing proteins through the destabilisation of the tertiary and quaternary protein structures [38–40]. To investigate the adverse effects of these components, we added *E. ocellatus* venom (5 mg/mL) to various concentrations of ACN (50, 40, 30, 20, 10, 5 and 0% in mQ) or the acidifiers FA, DFA or TFA (0.05, 0.01, 0.005, 0.001, 0.0005, 0.0001 and 0.0% in mQ, respectively) at a final venom concentration of 1 mg/mL. The venom was incubated at room temperature (RT) for 30 minutes, flash-frozen in liquid nitrogen and freeze-dried overnight. Upon use, the venom samples were reconstituted in 1x reaction buffer (final venom cons.: 1 mg/mL).

The incubation of *E. ocellatus* venom in PBS (80, 40, 20, 10, 5 and 0% in mQ) was performed by adding venom to the PBS solutions (final venom concentration: 1mg/mL) and it was incubated for 30 minutes at RT. These samples were not lyophilised and were added straight to the assay. All venom samples described above were subjected to the degradation assay with gelatin as a substrate to assess their activity (final concentrations: 100 µg/mL of *E. ocellatus* venom and 10 µg/mL of gelatin). A positive (collagenase [1 U/mL]) and negative control were added to the assay plate, and the assay was performed as described in Section 4.3.

Separation of venoms using SEC
The venoms of the species with the highest proteolytic activity (*B. jararaca*, *C. rhodostoma* and *E. ocellatus*) were fractionated using SEC on a Shimadzu HPLC system controlled with the Shimadzu Lab Solutions software. Venom stock

solutions of 5 mg/mL were diluted with ice-cold mQ to a concentration of 2.5 mg/mL. Samples were injected with a Shimadzu SIL 20AC Prominence autosampler utilising a 10 µL injection volume for venoms. Separation was performed on a Sepax Zenix SEC-300 column (300 Å, 5 µm, 4.6 mm × 300 mm) housed in a Shimadzu CTO-10AC VP column oven set to 27 °C. Solvent delivery was performed with a Shimadzu LC-10Ai pump set at a flow rate of 0.35 mL/min. The toxin elution from the column was monitored using a Shimadzu SPD-20A Prominence UV/Vis detector at 220 and 280 nm. The mobile phase consisted of 100% PBS with isocratic elution over 20 minutes. A solvent loop was added to the pump system using a solvent mixture of 20% 2-propanol and 80% mQ, which was used between each run to flush the system and ensure proper toxin separation during subsequent runs. Following the SEC column, there was an analytical post-column adjustable flow splitter with a splitting ratio set to 1:9. From the total flow, 90% was directed to a fraction collector. Samples were collected as 12-sec fractions in clear 384-well flat-bottom microwell plates (Greiner Bio-One) for a total of 18.0 minutes using a 6-minutes delay after the start of each run, resulting in 60 wells, each containing 62 µL collected eluent. For fractionation, a Gilson ASTED-XL autosampler rebuilt as a fraction collector was used, controlled by the Ariadne software (in-house written software, v1.08j). The plates were subsequently flash-frozen and stored at −20 °C until use.

Separation of venoms using 'reversed-phase chromatography'

RP-LC separation was performed as described by Arrahman et al. (2022) with minor modifications [41]. Gradient separation was performed on a Waters XBridge Peptide BEH C18 column (300 Å, 5 µm, 4.6 mm × 100 mm, 1K-15K, 1/pk) housed in a Shimadzu CTO-10AC VP column oven set to 30 °C. Mobile phases A and B contained either 0.1% TFA or no acidifier, respectively. The venoms (2.5 mg/mL in mQ) of *E. ocellatus* and *N. mossambica* were separated utilising the following gradients. *E. ocellatus*: Linear increase in solvent B from 0 to 30% over 5 minutes, followed by an increase from 30 to 50% of B in 25 minutes and a consecutive increase from 50 to 90% in 4 minutes, followed by 5-minute isocratic elution at 90% B and a subsequent decrease to 0% B in 1 minute with a 10-minute equilibration time at 0% B. *N. mossambica*: Linear increase in solvent B from 0 to 20% over 5 minutes, followed by an increase from 20 to 40% of B in

25 minutes. Solvent B was then increased from 40 to 90% in 4 minutes, followed by 5-minute isocratic elution at 90% B and a subsequent decrease to 0% B in 1 minute with a 10-minute equilibration time at 0% B. This set of experiments was performed prior to the proposed bioassays to rule out RP-LC as a viable option for toxin separation and fractionation.

Degradation of fluorescently labelled substrates by fractionated snake venom toxins using the proteinase assays

After separation, the fractionated venom toxins were subjected to the proteinase assays under conditions similar to those for the crude venoms (see Section 4.3), with minor modifications. Each well contained 35 µL of 1x reaction buffer, 10 µL of the respective venom fraction transferred from a plate with fractionated venom (in a selected time frame) and 5 µL gelatin or collagen I solution, resulting in a final substrate concentration of 10 µg/mL. Controls were added to each plate as described in Section 4.3. Plates were incubated for 4 hours at 37 °C, followed by measuring the plates in the preheated plate reader at 37 °C. For these analyses, end-point measurements (0.5 sec/well) were performed (in triplicate) in order to reduce the plate reader measurement time needed per plate.

5.2.5 High-throughput in-well tryptic digestion and nano-LC-MS/MS analysis for proteomics

In parallel with the bioactivity assays, following the analytical SEC separation, we performed proteomic analysis of the respective venom fractions. For this, we used the so-called 'high-throughput venomics' methodology recently described by Slagboom et al. (2023) [36]. After venom fractionation (see Section 4.4.2), 10 µL of sample from each well was pipetted into an empty 384-well plate. To each well, 25 µL of reduction buffer (25 mM ammonium bicarbonate and 0.05% β-mercaptoethanol; pH 8.2) was added using a pipetting robot (ThermoFisher Multidrop). The plates were then incubated at 95 °C for 15 minutes in the oven of a Hewlett Packard HP 6890 GC System. They were allowed to cool down to RT, after which 10 µL of alkylating agent was added (12.5 mM Iodoacetamide) using the same Multidrop. After this step, the plates were incubated in the dark for 30 minutes at RT. A stock solution of trypsin (1 µg/µL in 50 mM acetic acid) was subsequently diluted 100 times in 25 mM ammonium bicarbonate to

a concentration of 0.01 µg/µL, of which 10 µL was added using the Multidrop, and the plates were incubated overnight at 37 °C. The plates were centrifuged at 1000 rpm for 1 minute in an Eppendorf Centrifuge 5810 R, followed by adding 10 µL of 1.25% formic acid to the plates. Finally, the plates were analysed using nano-LC-MS/MS (or stored at −20 °C until analysis) as described by Slagboom et al. (2023) [36]. Venom samples were digested using trypsin and then subjected to nano-LC separation on an UltiMate 3000 RSLCnano system (Thermo Fisher Scientific), followed by mass spectrometry. Mass spectrometry was performed on a maXis QTOF mass spectrometer (Bruker Daltonics), and the data was processed using the Bruker DataAnalysis software, resulting in the identification of the proteins found in the individual venoms. Protein scores from each of the venom proteins were plotted against the corresponding retention times (x-axis) in order to generate so-called protein score chromatograms (PSCs) [36].

5.3 Results and Discussion

We set out to establish high-throughput proteinase assays to enable the *in vitro* study of ECM-degrading venoms and the identification of venom toxins that mediate this activity. To do so, we used fluorescently labelled gelatin and collagen type I as substrates in 384-well plate assays. The assays developed were used to study both crude venoms and fractionated venom toxins.

5.3.1 Degradation of Gelatin and Collagen Type I by Crude Snake Venoms

The venoms of all six snake species included in this study degraded gelatin, a widely used, readily available and affordable standard polymer that mimics collagen. The three viperid venoms (*B. jararaca*, *C. rhodostoma* and *E. ocellatus*) were capable of cleaving gelatin at a high rate at venom concentrations of ≥33.3 µg/mL, even surpassing the proteolytic activity of the positive control (see Figure 1 and S1–S3 Figures). For all viper venoms tested in this study, gelatin degradation detection limits were venom concentrations of ≥0.046 µg/mL (10 µg/mL gelatin), ≥0.14 µg/mL (5 µg/mL gelatin) and ≥0.41 µg/mL (2 µg/mL gelatin) (see Figure 1 and S1 Figure). A profound decrease in fluorescence (RFU) was observed at a

venom concentration of 100 µg/mL for all gelatin and collagen I concentrations for the viper venoms after 6 - 10 hours, indicating less cleavage (explanation see below). The elapid venoms (*D. polylepis*, *N. mossambica* and *N. naja*) cleaved gelatin at a lower rate than the viper venoms and the positive control (see Figure 1 and S1–S3 Figures). The lowest concentration of 2 µg/mL gelatin failed to give satisfactory results regarding sensitivity (see Figure 1 and S1 Figure).

Depending on the species, viper venom concentrations as low as 0.015–0.046 µg/mL at 10–40 µg/mL collagen I could be distinguished from the negative control (0.0 µg/mL) (see S2 Figure). As with gelatin, the high concentrations of viper venoms also gave a higher cleavage rate of collagen I than the positive control (see S2 and S3 Figures). For elapid venoms, a high concentration of collagen I (40 µg/mL) was required to achieve proper performance of the assay, and even with this substrate concentration, only tested elapid venom concentrations of 1.2 µg/mL and higher were distinguishable from the negative control (i.e., 11.1 µg/mL for *D. polylepis*, 3.7 µg/mL for *N. naja* and 1.2 µg/mL for *N. mossambica*) (see S2 Figure). As for gelatin, collagen I was degraded at a higher rate by the viper venoms than the elapid venoms. These experiments further revealed that, for collagen I, higher substrate concentrations (10–40 µg/mL) were needed than for gelatin (2–10 µg/mL) (see Figure 1 and S1 and S2 Figures).

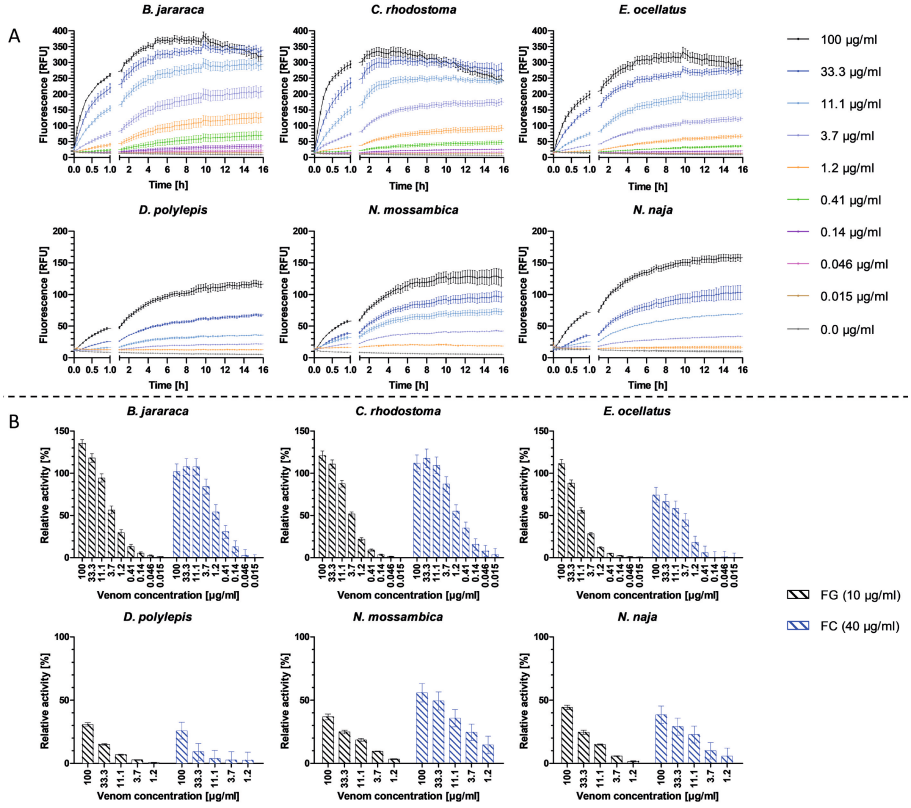

Figure 1. Degradation of fluorescent gelatin and collagen type I by crude snake venoms and relative activity of venoms, normalised with collagenase type IV. (A) The degradation of gelatin by snake venoms was monitored over 16 hrs, at 37 °C, at a substrate concentration of 10 µg/mL gelatin, with nine concentrations of viper venoms (100—0.015 µg/mL) or five concentrations of elapid venoms (100—1.2 µg/mL), compared to the negative control (0.0 µg/mL). (B) Relative activity of snake venoms towards gelatin (FG) (black) and collagen (FC) (blue) normalised with positive control (100% activity); negative control was subtracted for baseline correction. Activity was measured after 5 hrs of incubation at 37 °C. (C) Direct comparison of relative activity between species of the six snake venoms towards gelatin (FG, left) and collagen I (FC, right), respectively. The three viper species show the highest relative activity compared to the elapid venoms for both substrates. Graphs are colour-coded and numbered. Graphs are normalised with positive control (100% activity); negative control was subtracted for baseline correction. Activity was measured after 5 hrs of incubation at 37 °C. Each sample was measured in triplicate. Error bars show standard deviation.

Overall, the higher the substrate concentration, the greater the separation of individual curves and overall higher fluorescence output, leading to higher sensitivity, which allowed for the more sensitive detection of the fluorescence increase as a result of substrate degradation (see Figure 1 and S1 and S2 Figures). Fluorescent substrate concentrations of ≥2 µg/mL gelatin and ≥10 µg/mL collagen I for viper venoms and ≥5 µg/mL gelatin and ≥40 µg/mL

collagen I for elapid venoms were selected as suitable substrate concentrations to ensure robust assay sensitivity. Fluorescence plateaued at all substrate and venom concentrations for both substrates after approximately 5 hours. Further, for some vipers, at the highest venom concentrations, decreases in fluorescence were observed after about 5 hours (see Figure 1 and S1-S2 Figures). This could be due to substrate depletion in combination with light-induced and chemical fluorescent product degradation or due to buffer concentration increases resulting in a pH change caused by evaporation during the measurement (visual inspection of the plates post-measurement revealed reduced volumes in the wells). As fluorescein fluorescence properties are highly pH-dependent, this could lead to the observed fluorescence decrease [42]. Regardless, based on these combined observations, a measurement time of 5 hours was selected for use. Plotting the relative fluorescence (relative to the positive control) against the venom concentration allows the direct comparison of the cleavage activity of different venoms towards the respective substrate. It enables the identification of particularly potent venoms. The degradation of the two substrates varied significantly between both families for gelatin and collagen I, respectively (gelatin: t (0.995, 16) = 2.29, p = 1.81−12, Cohen's d size = 7.61; collagen I: t (0.995, 16) = 2.29, p = 4.26−6, Cohen's d size = 3.03). Both the viper and elapid venoms showed similar relative activity within their respective family, with viper venoms exhibiting higher overall activity (see Figure 1 and Table 1).

Table 1. Maximum relative degradation activity of venoms towards gelatin and collagen I (compared to Figure 1B). Relative activity was calculated against positive control (equivalent to 100% activity). Error is in standard deviation.

Viperidae						
	B. jararaca		*C. rhodostoma*		*E. ocellatus*	
	Gelatin	Collagen I	Gelatin	Collagen I	Gelatin	Collagen I
Sub. conc. [µg/mL]	100	33.3	100	33.3	100	100
Max. rel. activity [%]	135.2 ± 4.9	108.1 ± 9.4	121.0 ± 5.5	117.8 ± 11.1	111.3 ± 5.1	74.3 ± 9.0
Elapidae						
	D. polylepis		*N. mossambica*		*N. naja*	
	Gelatin	Collagen I	Gelatin	Collagen I	Gelatin	Collagen I
Sub. conc. [µg/mL]	100	100	100	100	100	100
Max. rel. activity [%]	30.9 ± 1.4	25.9 ± 6.7	36.9 ± 2.3	55.9 ± 7.3	44.4 ± 1.7	38.5 ± 6.9

The necessity of a four-fold higher collagen I concentration than gelatin, in addition to higher relative activity towards gelatin, indicates that gelatin is more susceptible to degradation by these venoms than collagen type I, which is a finding supported by the literature [43]. The difference between collagen I and gelatin degradation was the highest in *E. ocellatus* and *B. jararaca* venom, followed by *N. naja* and *D. polylepis* venom. The difference in degradation of the two substrates is the smallest in *C. rhodostoma* venom, which shows an almost equally high cleavage rate for both substrates (see Figure 1 and Table 1). One exception to this is that the venom of *N. mossambica* exhibited higher relative activity towards collagen I than gelatin (Figure 1 and Table 1). Collagens (e.g., collagen type I) are key structural proteins found in the ECM, as opposed to gelatin, which is thermally denatured or disintegrated collagen type I [44]. This denaturing by hydrolysation leads to a loss of the triple-helix organisation, which makes gelatin more susceptible to degradation by proteinases. At the same time, collagen is more resistant and requires specific metalloproteinases, such as collagenases or SVMPs, for its degradation [14,17,44]. Collagen I, therefore, provides a better representation of the ECM-degrading potential of venoms, whereas gelatin could be a more suitable model for monitoring overall proteolytic activity [44].

The venoms of the three viper species included in this study are known to cause local tissue necrosis, oedema and blistering, as well as systemic effects such as bleeding and coagulopathy [45–47]. These are pathologies that are caused by SVMPs, among other toxins [14,48,49]. The venoms of the three viper species tested contain a relatively high abundance of SVMPs, with *E. ocellatus* venom being particularly rich in SVMPs (34.8–72.4%), with animals from Nigeria housed at LSTM containing 66.5% SVMPs in their venom according to Wagstaff et al. (2009) [18,45,50]. The venom of *C. rhodostoma* consists of 35.7–46.5% SVMPs (venom from Thai specimens (Bangkok) contain 46.28% SVMPs in their venom, according to Tang et al. (2019)), while the venom of *B. jararaca* contains between 10.3% and 42.8%, depending on the locality [18,47,51–54]. Contrastingly, SVMPs are typically minor components of elapid venom, representing 0.9–16.2% of total toxins in *N. naja* venom and 2.6% and 3.2% of the venom proteome of *N. mossambica* and *D. polylepis*, respectively [18,55–59]. These data seem likely to explain the lower degradation of gelatin and collagen I by the three elapid venoms compared to the viper venoms (see Figure 1).

The results also indicate that venoms that are particularly rich in SVMPs might not necessarily have higher gelatin and collagen I cleavage capacity compared to venoms with lower SVMP content within the respective family. As the locality of the snakes that the venoms were collected from is not known (with the exception of *E. ocellatus* and *C. rhodostoma*), it is unknown how high the actual SVMP share of the individual venoms is. It thereby remains inconclusive whether the SVMP abundance is the sole property affecting the activity detected in the developed bioassay. While there are clear distinctions between SVMP-rich viper and SVMP-deficient elapid venoms, data within these families indicate that overall higher SVMP content does not necessarily coincide with higher proteolytic activity (see Figure 1 and S1 Table). Therefore, it is not possible to confirm with certainty whether the SVMP content affects the venom potency in the assay. The ability of SVMPs to degrade ECM components is thought to be linked to their haemorrhagic activity, which varies between the SVMP subgroups (P-I, P-II and P III) [8,15,17]. Correlating the presented *in vitro* data with actual ECM degradation *in vivo* remains challenging. Therefore, the assays presented in this study solely provide an indication of ECM degradation by snake venoms.

5.3.2 Effects of organic solvents and acidifiers on the proteolytic activity of snake venoms

Organic solvents and acidifiers are commonly used in HPLC, especially RP-LC. The effect of using an organic solvent (e.g., ACN) for SEC separation was compared to the non-organic buffer PBS, generally used for analytical SEC. Concentrations of up to 20% ACN did not have significant effects on the proteolytic activity of *E. ocellatus* venom. Concentrations higher than 20% resulted in a noticeable decrease in venom activity, with 50% ACN resulting in around half the activity of 0% ACN (see S4 Figure). PBS, even at higher concentrations (≥40%), had less impact on protein activity than ACN, with higher proteolytic activity remaining at all concentrations. At PBS concentrations above 80% and at longer assay run times (≥10 hours), the activity started to decrease. However, it was still not noticeably lower when compared to other PBS concentrations (see S4 Figure). Therefore, the inhibitory effect on the protein activity of PBS is negligible, especially with a 5-hour assay runtime.

When the effects of the three acidifiers (e.g., FA, DFA and TFA) on the proteolytic activity of *E. ocellatus* venom were investigated, the outcomes were considerably different from those obtained with PBS. The presence of any of the three acidifiers tested resulted in a significant decrease in protein activity at concentrations of ≥0.005%, indicating that a 0.1% acidifier concentration, often used in 'conventional' RP-LC separations of proteins (and also in analytical SEC), would likely result in an enormously detrimental effect on the proteolytic venom activity, which also applied for ACN concentrations ≥30% (see S4 Figure). Completely excluding acidifiers from the mobile phase for RP-LC and SEC separations of venom into constituents resulted in deficient separation quality (see S5 Figure). The observed decrease in activity in the presence of solvents and/or acidifiers is consistent with the observed effects in previous studies investigating protein stability when using volatile eluents [38–40]. Therefore, we chose to revert to an alternative SEC separation method with an eluent based on non-volatile salt buffers (see Section 4.4.2). This necessary approach comes at the cost of no direct MS compatibility.

5.3.3 Separation of venoms using analytical SEC, followed by bioactivity profiling in parallel with HT venomics

Analytical SEC with PBS as the mobile phase and post-column fractionation were performed, as described in Section 4.4.2, to separate and collect venom toxins in their native forms. Actual toxin identification was performed in parallel to the post-column bioassays using the recently described HT venomics methodology by Slagboom et al. (2023) [36]. Gelatin and collagen I were used as the substrates to investigate their suitability for use in post-separation bioassaying using nanofractionation analytics. For this, the three most proteolytically active venoms were used, namely *B. jararaca*, C. *rhodostoma* and *E. ocellatus*. Bioassay chromatograms for all three venoms were plotted using the post-column recorded bioassay data of the collected fractions (see Figures 2–4).

Bioassaying and profiling of B. jararaca venom after SEC

Toxins in the venom of *B. jararaca* eluted over a time window between minutes 7 and 14, with the SEC-UV chromatogram showing two smaller peaks (1 and 5), one small split peak (4a + b) and three major peaks (2, 3 and 6). Peak 3 is split

into the main peak (3a) and a shoulder appearing after the main peak (3b)—peaks 1 and 5 eluted shortly before peaks 2 and 6 and partly co-eluted, respectively. Bioactive toxins eluted between 7.8 and 9.7 minutes, with the central bioactivity peak corresponding to peak 2 and peak 1 matching the minor activity shortly before the main bioassay peak (see Figure 2). This observation suggests at least two proteolytic compounds are present in the venom. A total of 18 compounds belonging to six toxin classes were identified. These included SVSPs (two toxins), SVMPs (two toxins and four toxin fragments), snaclecs (six toxin subunits and one subunit fragment), disintegrins (one toxin fragment), snake venom vascular endothelial growth factors (SV VEGFs; one toxin) and bradykinin-potentiating peptides (BPPs; one toxin) (see Figure 2 and Table 2). Part of the bioassay peak profile overlapped well with the PSCs of the identified SVMPs and snaclecs. For the bioactivity peak profile, the PSC peaks for SVSPs and SV VEGFs coincided partially (see Figure 2). In terms of their proteolytic activity, SVMPs are known to degrade ECM components, indicating that they are responsible for the observed activity, as the other toxin classes identified are usually not associated with ECM degradation [2,17,29]. One specific P-III SVMP, namely zinc metalloproteinase-disintegrin-like bothropasin (VM3BP_BOTJA), correlated perfectly with the bioassay activity peak profile for both gelatin and collagen I and peak 2 of the SEC chromatogram (see Figure 2) [46]. A second P-III SVMP, zinc metalloproteinase-disintegrin-like jararhagin (VM3JA_BOTJA), appeared to correlate in PSC peak shape and retention time with the shoulder of the bioactivity peaks seen in both the gelatin and collagen I assay as well as with peak 1 of the SEC-UV chromatogram (see Figure 2) [60,61]. As this toxin eluted before bothropasin, it is likely responsible for the observed shoulder in the bioactivity peak. As jararhagin is known to hydrolyse collagen, it was likely responsible for the observed substrate degradation preceding the main bioassay peak (see Figure 2). However, the main activity detected was most likely caused by bothropasin, as it correlated with the main bioassay peak. This also shows that not all SVMPs in the venom are capable of cleaving both substrates, as only two of the six identified SVMPs exhibited this activity. This could be due to variations in the quantities of each of the SVMP toxins in the venom, with some perhaps eliciting insufficient substrate degradation activity or not showing proteolytic activity towards the substrates.

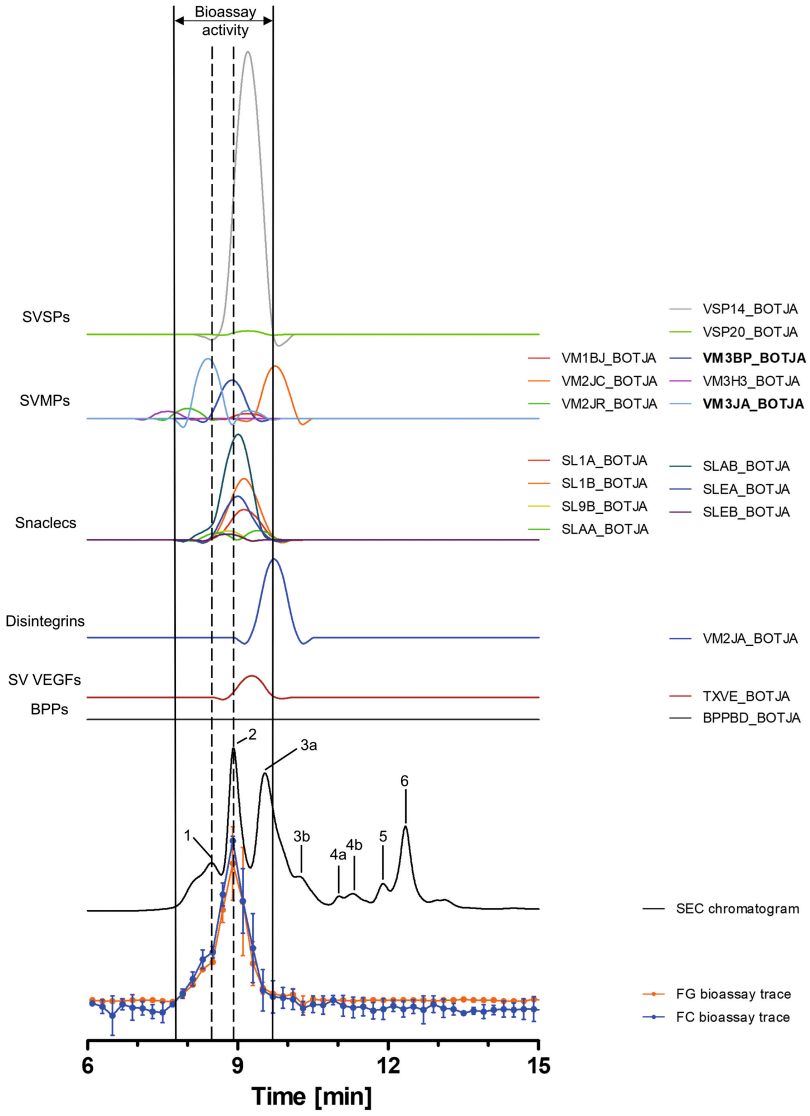

Figure 2. Identification of gelatin- and collagen type I-degrading activity by proteolytic compounds in *B. jararaca venom*. The upper graphs show the protein score chromatograms (PSCs), which represent the individual venom proteins found with the Mascot database searching for the digested toxin content in the wells. The eluting toxins were detected at 220 nm, resulting in the SEC-UV chromatogram (black line). The lower two lines represent the bioassay traces (orange for gelatin (FG) and blue for collagen I (FC)). The vertical bold outer lines mark the area in which bioactivity has been detected, and the vertical dashed lines mark the main activity peaks and their correlating SEC-UV chromatogram and PSC peaks. Bioactive toxins eluted between 7.8 and 9.7 min, with the main bioactivity peak corresponding to peaks 1 and 2 in the SEC-UV chromatogram. In total, 18 toxins from six toxin classes were identified from the proteomics data (for which the corresponding information can be found in Table 2), with two toxins (jararhagin (VM3JA_BOTJA) and bothropasin (VM3BP_BOTJA)) being identified as the likely active compounds (highlighted with bold lettering). Bioactivity data was measured in triplicate; error bars show standard deviation.

Bioassaying and profiling of C. rhodostoma venom after SEC

Toxins in *C. rhodostoma* venom eluted between ~7.5 and 13.5 minutes, with the SEC-UV chromatogram showing one major (4) and four smaller peaks (1, 2, 3 and 5). Peaks 3 and 4 seemed to correlate with both peaks in the bioassay chromatograms (see Figure 3). The bioactive toxins eluted between 8.7 and 11.1 minutes, with the main activity being recorded between 9.7 and 11.1 minutes (peak 4), while the first activity peak (8.7–9.7 minutes) exhibited a lower intensity (see Figure 3). HT venomics identified a total of six compounds from four different toxin classes, including SVMPs (two toxins), SVSPs (two toxins), snaclecs (one toxin subunit) and L-amino-acid oxidases (LAAOs; one toxin). The two SVMPs, snake venom metalloproteinase kistomin (CALRH_VM1K) and zinc metalloproteinase rhodostoxin/disintegrin rhodostomin (CALRH_VM2RH), matched with the bioactivity peaks of both the substrates, correlating with peaks 3 (rhodostoxin/disintegrin rhodostomin) and 4 (kistomin and rhodostoxin/disintegrin rhodostomin) of the SEC-UV chromatogram (see Figure 3 and Table 2). Kistomin is a P-I class SVMP and was found in the fractions causing the proteolytic activity corresponding to SEC-UV peak 4 only. This toxin has been shown to degrade fibrinogen and GP1b, as well as prolong the latent period of platelet aggregation, blocking vWF-induced platelet activation and inhibiting the ATP secretion of human-washed platelets [47]. The zinc metalloproteinase rhodostoxin/disintegrin rhodostomin was found in fractions aligning with both activity peaks (peaks 3 and 4). While the disintegrin domain rhodostomin does not affect the proteolytic activity but is known to act as a potent platelet aggregation inhibitor, rhodostoxin, a P-II SVMP and the main haemorrhagic toxin in *C. rhodostoma* venom, is known to cause potent dermal haemorrhagic effects and has shown proteolytic activity [47,62]. On the upslope of the first bioassay peak, a small shoulder was visible, which correlated with peak 2 of the SEC-UV chromatogram. This peak overlapped with the two SVSP peaks, thrombin-like enzyme ancrod and ancrod-2 (CALRH_VSPF1 and CALRH_VSPF2). They are known to be involved in venom-induced consumption coagulopathy by catalysing the release of fibrinopeptides from fibrinogen. Apparently, our assays picked up this proteolytic activity. It is important to note, however, that SVSPs are usually not associated with ECM degradation *in vivo.* Still, as they are proteinases, they could express proteolytic activity in this assay [47,62,63]. From this data, we suggested

that, most likely, kistomin and rhodostoxin are the main toxins responsible for the proteolytic activity in *C. rhodostoma* venom.

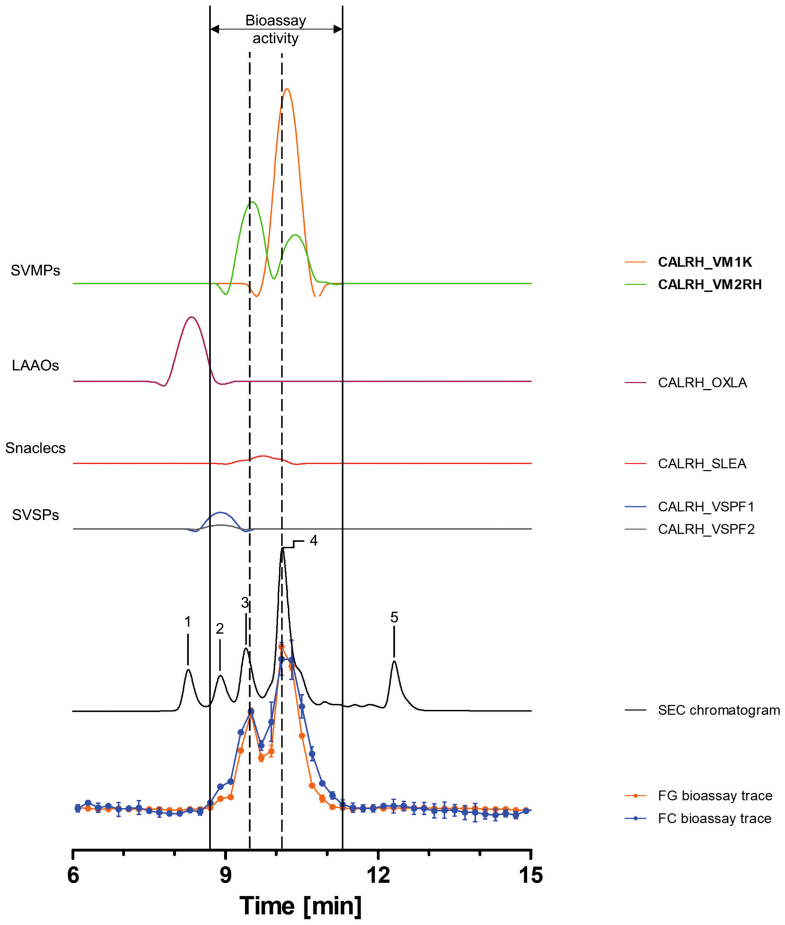

Figure 3. Identification of gelatin- and collagen type I-degrading activity by proteolytic compounds in *C. rhodostoma* venom. The upper graphs show the protein score chromatograms (PSCs), which represent the individual venom proteins found with the Mascot database searching for the digested content in the wells. The eluting toxins were detected at 220 nm, resulting in the SEC chromatogram (black line). The lower two lines represent the bioassay traces (orange for gelatin (FG) and blue for collagen I (FC)). The vertical bold outer lines mark the area in which bioactivity has been detected, and the vertical dashed lines mark the main activity peaks and their correlating SEC-UV chromatogram and PSC peaks. Bioactive toxins were eluted between 8.7 and 11.1 min, with the bioactivity peaks corresponding to peaks 3 and 4 of the SEC chromatogram. In total, six toxins from four toxin classes were identified from the proteomics data (for which the corresponding information can be found in Table 2), with two toxins (i.e., kistomin (CALRH_VM1K) and rhodostoxin/disintegrin rhodostomin (CALRH_VM2RH)) being identified as the likely active compounds (highlighted with bold lettering). Bioactivity data was measured in triplicate. Error bars show standard deviation.

Bioassaying and profiling of E. ocellatus venom after SEC

Toxins in the venom of *E. ocellatus* eluted between 7 and 14 minutes, with four major peaks (1, 3, 4 and 6), one co-eluting twin peak (2a + b) and one smaller peak (5) observed in the SEC-UV chromatogram. Peak 1 was the most prominent, exhibiting a shoulder (1a) before the main peak (1b) (see Figure 4). Bioactive toxins eluted from 7.7 to 10.9 minutes, with two distinct peaks between 7.7 and 8.9 minutes and 10.1 and 10.9 minutes and a third, broader peak around ~9–10 minutes. The first bioactivity peak correlated largely with peak 1b in the SEC-UV chromatogram, the second bioactivity peak with SEC-UV-peaks 2a and 2b, and the third peak in the bioassay chromatogram correlated with SEC-UV peak 4. In total, eight toxins belonging to the toxin classes SVMPs (three toxins), disintegrins (two toxins), LAAOs (one toxin) and snaclecs (two toxins) were identified (see Figure 4 and Table 2). Zinc metalloproteinase-disintegrin-like Eoc1 (ECHOC_VM3E1), a P-III SVMP corresponding to peak 1b, has been shown to hydrolyse azocasein and the α- and β-chains of fibrinogen. Additionally, it inhibits endothelial cell adhesion to ECM proteins such as fibrinogen and collagen I [45,64]. Zinc metalloproteinase-disintegrin-like EoVMP2 (ECHOC_VM3E2) overlapped with peaks 2a and 2b and is known to exhibit strong haemorrhagic activity and inhibit collagen-induced platelet aggregation [65]. This haemorrhagic activity is caused by degradation of capillary basement membrane components such as collagen IV, laminin and fibronectin [65]. The final SVMP zinc metalloproteinase Eoc6/disintegrin ocellatusin (ECHOC_VM2OC), which corresponds to SEC-UV peak 4, is a P-II SVMP consisting of a metalloproteinase and disintegrin domain [45,66]. The disintegrin domain ocellatusin, which is proteolytically processed, is known to inhibit platelet aggregation and is not considered to have proteolytic activity [45,66]. The zinc metalloproteinase Eoc6, however, is capable of impairing haemostasis *in vivo* and has been shown to have proteolytic activity [66]. The other toxins overlapping with these bioactivity peaks (disintegrins, snaclecs and LAAOs) are not known to exhibit proteolytic activity [2,8].

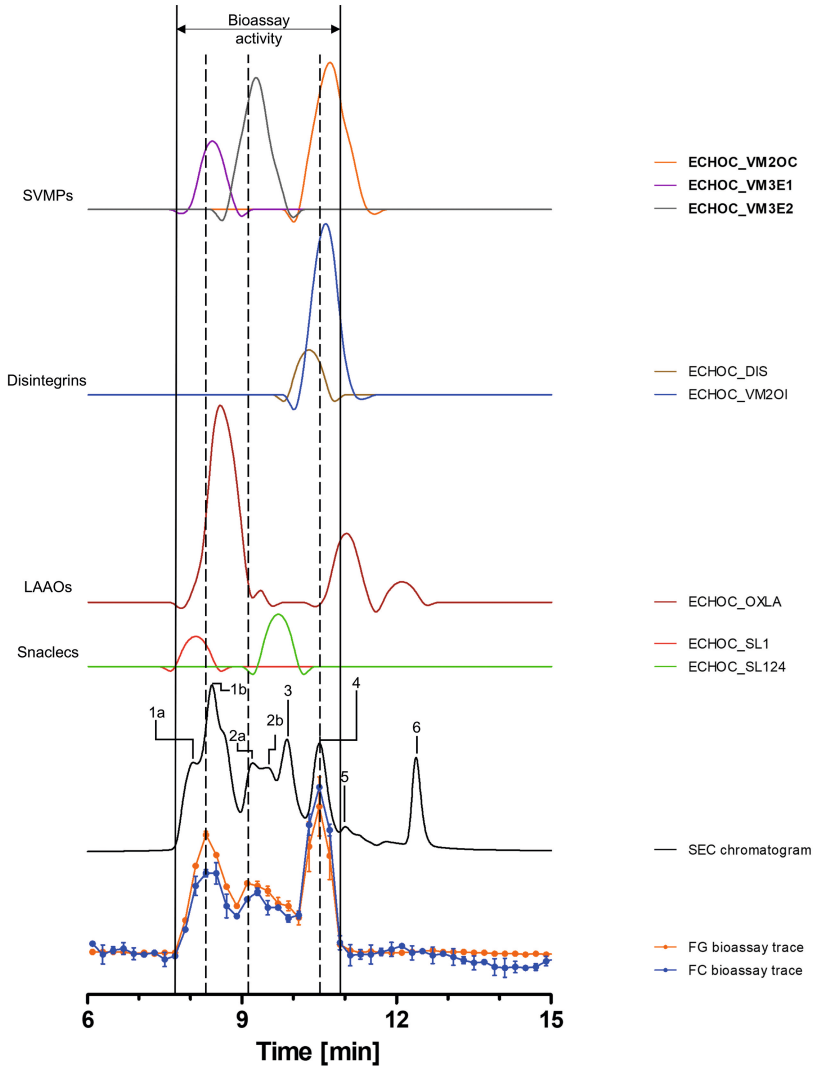

Figure 4. Identification of gelatin- and collagen type I-degrading activity by proteolytic compounds in *E. ocellatus* venom. The upper graphs show the protein score chromatograms (PSCs), which represent the individual venom proteins found with the Mascot database searching for the digested content in the wells. The eluting toxins were detected at 220 nm, resulting in the SEC chromatogram (black line). The lower two lines represent the bioassay traces (orange for gelatin (FG) and blue for collagen I (FC)). The vertical bold outer lines mark the area in which bioactivity has been detected, and the vertical dashed lines mark the main activity peaks and their correlating SEC-UV chromatogram and PSC peaks. Bioactive toxins eluted between 7.7 and 10.9 min, with two distinct and one broad bioactivity peak corresponding to peaks 1b and 4, plus peaks 2a + b of the SEC chromatogram. Eight toxins from four different toxin classes were identified from the proteomics data (for which the corresponding information can be found in Table 2), with three toxins (Eoc1 (ECHOC_VM3E1), EoVMP2 (ECHOC_VM3E2) and Eoc6 (ECHOC_VM2OC)) being identified as the likely active compounds (highlighted with bold lettering). Bioactivity data was measured in triplicate. Error bars show standard deviation.

Table 2. Toxins identified by nano-LC-MS/MS following tryptic digestion of fractionated toxins from the venoms of *B. jararaca*, *C. rhodostoma*, and *E. ocellatus*. Toxins identified as the bioactive compounds, which correlated with bioactive peaks observed in the bioactivity chromatograms from the gelatin and collagen I degradation bioassays, are marked in bold. Names and molecular weights (kDa) are according to the UniProt database (www.uniprot.org (accessed on 15 January 2023)). ***** Correlating SEC chromatogram peak (between b/w). The remaining proteomics data are provided in Excel files in the Supplementary Information.

Species	Protein Class	Toxin	prot_acc	kDa	Peak *
B. jararaca	SVSP	Snake venom serine protease HS114	VSP14_BOTJA	27.834	3a
		Venom serine protease-like HS120	VSP20_BOTJA	27.815	3a
	SVMP	Snake venom metalloproteinase bothrojaractivase (Fragments)	VM1BJ_BOTJA	7.166	b/w 2 & 3a
		Zinc metalloproteinase/disintegrin (Fragment)	VM2JC_BOTJA	17.555	3a
		Zinc metalloproteinase-disintegrin jararin (Fragment)	VM2JR_BOTJA	16.835	before 1
		Zinc metalloproteinase-disintegrin-like bothropasin	**VM3BP_BOTJA**	**68.213**	**2**
		Zinc metalloproteinase-disintegrin-like HF3	VM3H3_BOTJA	67.695	before 1
		Zinc metalloproteinase-disintegrin-like jararhagin (Fragment)	**VM3JA_BOTJA**	**63.983**	**1**
	Snaclec	Snaclec bothrojaracin subunit alpha	SLAA_BOTJA	17.577	1 & 3a
		Snaclec bothrojaracin subunit beta	SLAB_BOTJA	17.292	2
		Snaclec botrocetin subunit alpha	SLEA_BOTJA	15.215	2
		Snaclec botrocetin subunit beta	SLEB_BOTJA	15.037	2
		Snaclec coagulation factor IX/ factor X-binding protein subunit B (Fragment)	SL9B_BOTJA	3.582	2
		Snaclec GPIB-binding protein subunit alpha	SL1A_BOTJA	16.720	b/w 2 & 3a
		Snaclec GPIB-binding protein subunit beta	SL1B_BOTJA	14.298	b/w 2 & 3a
	Dis-integrin	Disintegrin jarastatin (Fragment)	VM2JA_BOTJA	9.323	3a
	SV VEGF	Snake venom vascular endothelial growth factor toxin	TXVE_BOTJA	16.377	b/w 2 & 3a
	BPP	Bradykinin-potentiating peptide 11d	BPPBD_BOTJA	1.112	?

Table 2. (continued)

Species	Protein Class	Toxin	prot_acc	kDa	Peak *
C. rhodostoma	SVSP	Thrombin-like enzyme ancrod	CALRH_VSPF1	26.570	2
		Thrombin-like enzyme ancrod-2	CALRH_VSPF2	29.145	2
	SVMP	**Snake venom metalloproteinase kistomin**	**CALRH_VM1K**	**47.446**	**4**
		Zinc metalloproteinase rhodostoxin/disintegrin rhodostomin	**CALRH_VM2RH**	**54.006**	**3 & 4**
	Snaclec	Snaclec rhodocetin subunit alpha	CALRH_SLEA	15.962	b/w 3 & 4
	LAAO	L-amino-acid oxidase	CALRH_OXLA	58.221	1
E. ocellatus	SVMP	**Zinc metalloproteinase Eoc6/ disintegrin ocellatusin**	**ECHOC_VM2OC**	**55.165**	**4**
		Zinc metalloproteinase-disintegrin-like Eoc1	**ECHOC_VM3E1**	**68.751**	**1b**
		Zinc metalloproteinase-disintegrin-like EoVMP2	**ECHOC_VM3E2**	**69.426**	**2a & b**
	Snaclec	Snaclec 1	ECHOC_SL1	16.601	1a
		Snaclec CTL-Eoc124	ECHOC_SL124	16.882	2b & 3
	Dis-integrin	Disintegrin ocellatusin	ECHOC_DIS	14.076	b/w 3 & 4
		Disintegrin ocellatin	ECHOC_VM2OI	5.526	4
	LAAO	L-amino-acid oxidase	ECHOC_OXLA	56.523	1b, 2a, 5 & 6

5.4 Concluding remarks

The goal of this study was to develop and establish high-throughput screening assays that allow the high-throughput analysis of the proteolytic degradation of ECM-substrates by (fractionated) snake venoms. Traditional zymography approaches using non-fluorescent gelatin and/or collagen as substrates, which are qualitative and semi-quantitative, and the 96-well-plate-based quantitative assay described by Biardi et al. (2011), are mainly suitable for low- to mid-throughput bioassays [25,67]. In order to validate the applicability of this high-throughput approach, the activity of a selection of medically relevant viperid and elapid venoms was investigated. For this, both crude venoms and fractionated toxins separated by analytical SEC were taken into account. Our approach using fluorescently labelled substrates allowed the post-column bioassaying of SEC-separated venom components. It used only a low amount of venom sample and a low substrate concentration in a 384-well plate, making it a high-throughput method. Overall, the developed bioassays provide a framework for sensitive measurements of gelatin and collagen degradation due to their fluorescein-labelled self-quenched conjugates, which yield highly fluorescent fragments when cleaved. The developed assay also allows the parallel identification of proteolytic venom components by the application of methodologies such as HT venomics. We foresee that the application of this bioassay could be valuable for a better understanding of venom-induced ECM-degrading effects and could be used in the process of developing new and improving existing snakebite treatments to better neutralise these toxin components that contribute to envenoming pathology.

References

1. Chippaux, J. P. Snakebite envenomation turns again into a neglected tropical disease! *J. Venom. Anim. Toxins Incl. Trop. Dis.* **23**, 1–2 (2017).
2. Gutiérrez, J. M. *et al.* Snakebite envenoming. *Nat. Rev. Dis. Prim.* **3**, (2017).
3. Arias, A. S., Rucavado, A. & Gutiérrez, J. M. Peptidomimetic hydroxamate metalloproteinase inhibitors abrogate local and systemic toxicity induced by Echis ocellatus (saw-scaled) snake venom. *Toxicon* **132**, 40–49 (2017).
4. Slagboom, J., Kool, J., Harrison, R. A. & Casewell, N. R. Haemotoxic snake venoms: their functional activity, impact on snakebite victims and pharmaceutical promise. *Br. J. Haematol.* **177**, 947–959 (2017).
5. Warrell, D. A. Snake bite. *Lancet* **375**, 77–88 (2010).
6. Chippaux, J.-P. Snake-bites: appraisal of the global situation. *Bull. World Health Organ.* **76**, 515–524 (1998).
7. Selistre-De-Araujo, H. S., Pontes, C. L. S., Montenegro, C. F., Carolina, A. & Martin, B. M. Snake Venom Disintegrins and Cell Migration. *Toxins (Basel).* **2**, 2606–2621 (2010).
8. Fry, B. G. *Venomous reptiles and their toxins: evolution, pathophysiology and biodiscovery. Oxford University Press, Oxford University Press.* (2015). doi:10.1016/0041-0101(71)90017-1.
9. Gopalakrishnakone, P., Inagaki, H., Vogel, C., Mukherjee, A. K. & Rahmy, T. R. *Snake Venoms*. (Springer Berlin, Germany., 2017).
10. Gasanov, S. E., Dagda, R. K. & Rael, E. D. Snake Venom Cytotoxins, Phospholipase A2 s, and Zn2+ -dependent Metalloproteinases: Mechanisms of Action and Pharmacological Relevance. *J. Clin. Toxicol.* **4**, (2014).
11. Costal-Oliveira, F. *et al.* L-amino acid oxidase from Bothrops atrox snake venom triggers autophagy, apoptosis and necrosis in normal human keratinocytes. *Sci. Rep.* **9**, (2019).
12. Guo, C., Liu, S., Yao, Y., Zhang, Q. & Sun, M. Z. Past decade study of snake venom l-amino acid oxidase. *Toxicon* **60**, 302–311 (2012).
13. Frantz, C., Stewart, K. M. & Weaver, V. M. The extracellular matrix at a glance. *J. Cell Sci.* **123**, 4195–4200 (2010).
14. Gutiérrez, J. M., Escalante, T., Rucavado, A., Herrera, C. & Fox, J. W. A comprehensive view of the structural and functional alterations of extracellular matrix by snake venom metalloproteinases (SVMPs): Novel perspectives on the pathophysiology of envenoming. *Toxins (Basel).* **8**, (2016).
15. Gutiérrez, J. M., Escalante, T., Rucavado, A. & Herrera, C. Hemorrhage caused by snake venom metalloproteinases: A journey of discovery and understanding. *Toxins (Basel).* **8**, (2016).
16. Gutiérrez, J. M., Rucavado, A., Escalante, T. & Díaz, C. Hemorrhage induced by snake venom metalloproteinases: Biochemical and biophysical mechanisms involved in microvessel damage. *Toxicon* **45**, 997–1011 (2005).

17. Herrera, C. *et al.* Tissue Localization and Extracellular Matrix Degradation by PI, PII and PIII Snake Venom Metalloproteinases: Clues on the Mechanisms of Venom-Induced Hemorrhage. *PLoS Negl. Trop. Dis.* **9**, 1–20 (2015).

18. Tasoulis, T. & Isbister, G. K. A review and database of snake venom proteomes. *Toxins (Basel).* **9**, (2017).

19. Tasoulis, T., Pukala, T. L. & Isbister, G. K. Investigating Toxin Diversity and Abundance in Snake Venom Proteomes. *Front. Pharmacol.* **12**, (2022).

20. Girish, K. S., Jagadeesha, D. K., Rajeev, K. B. & Kemparaju, K. Snake venom hyaluronidase: An evidence for isoforms and extracellular matrix degradation. *Mol. Cell. Biochem.* **240**, 105–110 (2002).

21. Girish, K., Kemparaju, K., Nagaraju, S. & Vishwanath, B. Hyaluronidase Inhibitors: A Biological and Therapeutic Perspective. *Curr. Med. Chem.* **16**, 2261–2288 (2009).

22. Baldo, C., Jamora, C., Yamanouye, N., Zorn, T. M. & Moura-da-Silva, A. M. Mechanisms of vascular damage by hemorrhagic snake venom metalloproteinases: Tissue distribution and in Situ hydrolysis. *PLoS Negl. Trop. Dis.* **4**, (2010).

23. Escalante, T., Rucavado, A., Fox, J. W. & Gutiérrez, J. M. Key events in microvascular damage induced by snake venom hemorrhagic metalloproteinases. *J. Proteomics* **74**, 1781–1794 (2011).

24. Anai, K., Sugiki, M., Yoshida, E. & Maruyama, M. Neutralization of a snake venom hemorrhagic metalloproteinase prevents coagulopathy after subcutaneous injection of Bothrops jararaca venom in rats. *Toxicon* **40**, 63–68 (2002).

25. Biardi, J. E., Nguyen, K. T., Lander, S., Whitley, M. & Nambiar, K. P. A rapid and sensitive fluorometric method for the quantitative analysis of snake venom metalloproteases and their inhibitors. *Toxicon* **57**, 342–347 (2011).

26. Conlon, J. M. *et al.* Cytotoxic activities of [Ser49]phospholipase A2 from the venom of the saw-scaled vipers Echis ocellatus, Echis pyramidum leakeyi, Echis carinatus sochureki, and Echis coloratus. *Toxicon* **71**, 96–104 (2013).

27. Escalante, T. *et al.* Wound exudate as a proteomic window to reveal different mechanisms of tissue damage by snake venom toxins. *J. Proteome Res.* **8**, 5120–5131 (2009).

28. Hayashi, M. A. F. *et al.* Cytotoxic effects of crotamine are mediated through lysosomal membrane permeabilization. *Toxicon* **52**, 508–517 (2008).

29. Kalogeropoulos, K. *et al.* Protease activity profiling of snake venoms using high-throughput peptide screening. *Toxins (Basel).* **11**, 1–23 (2019).

30. Neumann, C. *et al.* Development of a generic high-throughput screening assay for profiling snake venom protease activity after high-resolution chromatographic fractionation. *Toxicon* **178**, 61–68 (2020).

31. Fisher, G. J. *et al.* Collagen fragmentation promotes oxidative stress and elevates matrix metalloproteinase-1 in fibroblasts in aged human skin. *Am. J. Pathol.* **174**, 101–114 (2009).

32. Naqvi, T. *et al.* Relaxin's induction of metalloproteinases is associated with the loss of collagen and glycosaminoglycans in synovial joint fibrocartilaginous explants. *Arthritis Res. Ther.* **7**, (2005).

33. Saito, S., Katoh, M., Masumoto, M., Matsumoto, S. I. & Masuho, Y. Involvement of MMP-1 and MMP-3 in collagen degradation induced by IL-1 in rabbit cartilage explant culture. *Life Sci.* **62**, PL359–PL365 (1998).

34. Ugarte-Berzal, E., Vandooren, J., Bailón, E., Opdenakker, G. & García-Pardo, A. Inhibition of MMP-9-dependent Degradation of Gelatin, but Not Other MMP-9 Substrates, by the MMP-9 Hemopexin Domain Blades 1 and 4. *J. Biol. Chem.* **291**, 11751–11760 (2016).

35. Vandooren, J. *et al.* Gelatin degradation assay reveals MMP-9 inhibitors and function of O-glycosylated domain. *World J. Biol. Chem.* **2**, 14–24 (2011).

36. Slagboom, J. *et al.* High-Throughput Venomics. *J. Proteome Res.* **22**, 1734–1746 (2023).

37. CBD Secretariat. Nagoya Protocol on Access To Genetic Resources and the Fair and Equitable Sharing of Benefits Arising from their Utilization to the convention on biological diversity - Text and annex. *Nagoya Protoc.* **12**, 1–320 (2011).

38. Gekko, K., Ohmae, E., Kameyama, K. & Takagi, T. Acetonitrile-protein interactions: Amino acid solubility and preferential solvation. *Biochim. Biophys. Acta - Protein Struct. Mol. Enzymol.* **1387**, 195–205 (1998).

39. Kony, D. B., Hünenberger, P. H. & van Gunsteren, W. F. Molecular dynamics simulations of the native and partially folded states of ubiquitin: Influence of methanol cosolvent, pH, and temperature on the protein structure and dynamics. *Protein Sci.* **16**, 1101–1118 (2007).

40. Lau, S. Y. M., Taneja, A. K. & Hodges, R. S. Synthesis of a Model Protein of Defined Secondary and Quaternary Structure. *J. Biol. Chem.* **259**, 13253–13261 (1984).

41. Arrahman, A. *et al.* A Combined Bioassay and Nanofractionation Approach to Investigate the Anticoagulant Toxins of Mamba and Cobra Venoms and Their Inhibition by Varespladib. *Toxins (Basel).* **14**, 736 (2022).

42. Sjöback, R., Nygren, J. & Kubista, M. Absorption and fluorescence properties of fluorescein. *Spectrochim. Acta Part A Mol. Spectrosc.* **51**, (1995).

43. Maruyama, M., Sugiki, M., Yoshida, E., Shimaya, K. & Mihara, H. Broad substrate specificity of snake venom fibrinolytic enzymes: Possible role in haemorrhage. *Toxicon* **30**, 1387–1397 (1992).

44. Gorgieva, S. & Kokol, V. Collagen- vs. Gelatine-Based Biomaterials and Their Biocompatibility: Review and Perspectives. *Biomater. Appl. Nanomedicine* (2011) doi:10.5772/24118.

45. Wagstaff, S. C., Sanz, L., Juárez, P., Harrison, R. A. & Calvete, J. J. Combined snake venomics and venom gland transcriptomic analysis of the ocellated carpet viper, Echis ocellatus. *J. Proteomics* **71**, 609–623 (2009).

46. Antunes, T. C., Yamashita, K. M., Barbaro, K. C., Saiki, M. & Santoro, M. L. Comparative analysis of newborn and adult Bothrops jararaca snake venoms. *Toxicon* **56**, 1443–1458 (2010).

47. Tang, E. L. H., Tan, C. H., Fung, S. Y. & Tan, N. H. Venomics of Calloselasma rhodostoma, the Malayan pit viper: A complex toxin arsenal unraveled. *J. Proteomics* **148**, 44–56 (2016).

48. Gutiérrez, J. M. & Rucavado, A. Snake venom metalloproteinases: Their role in the pathogenesis of local tissue damage. *Biochimie* **82**, 841–850 (2000).

49. Jiménez, N., Escalante, T., Gutiérrez, J. M. & Rucavado, A. Skin pathology induced by snake venom metalloproteinase: Acute damage, revascularization, and re-epithelization in a mouse ear model. *J. Invest. Dermatol.* **128**, 2421–2428 (2008).

50. Dingwoke, E. J. *et al.* Venom proteomic analysis of medically important Nigerian viper Echis ocellatus and Bitis arietans snake species. *Biochem. Biophys. Reports* **28**, 101164 (2021).

51. Gonçalves-Machado, L. *et al.* Combined venomics, venom gland transcriptomics, bioactivities, and antivenomics of two Bothrops jararaca populations from geographic isolated regions within the Brazilian Atlantic rainforest. *J. Proteomics* **135**, 73–89 (2016).

52. Nicolau, C. A. *et al.* An in-depth snake venom proteopeptidome characterization: Benchmarking Bothrops jararaca. *J. Proteomics* **151**, 214–231 (2017).

53. Sousa, L. F., Nicolau, C. A., Peixoto, P. S., Bernardoni, J. L. & Oliveira, S. S. Comparison of Phylogeny, Venom Composition and Neutralization by Antivenom in Diverse Species of Bothrops Complex. *PLoS Negl Trop Dis* **7**, 2442 (2013).

54. Tang, E. L. H., Tan, N. H., Fung, S. Y. & Tan, C. H. Comparative proteomes, immunoreactivities and neutralization of procoagulant activities of Calloselasma rhodostoma (Malayan pit viper) venoms from four regions in Southeast Asia. *Toxicon* **169**, 91–102 (2019).

55. Ainsworth, S. *et al.* The medical threat of mamba envenoming in sub-Saharan Africa revealed by genus-wide analysis of venom composition, toxicity and antivenomics profiling of available antivenoms. *J. Proteomics* **172**, 173–189 (2018).

56. Dutta, S. *et al.* Proteomic analysis to unravel the complex venom proteome of eastern India Naja naja: Correlation of venom composition with its biochemical and pharmacological properties. *J. Proteomics* **156**, 29–39 (2017).

57. Laustsen, A. H., Lomonte, B., Lohse, B., Fernández, J. & Gutiérrez, J. M. Unveiling the nature of black mamba (Dendroaspis polylepis) venom through venomics and antivenom immunoprofiling: Identification of key toxin targets for antivenom development. *J. Proteomics* **119**, 126–142 (2015).

58. Petras, D. *et al.* Snake venomics of African spitting cobras: Toxin composition and assessment of congeneric cross-reactivity of the Pan-African EchiTAb-Plus-ICP antivenom by antivenomics and neutralization approaches. *J. Proteome Res.* **10**, 1266–1280 (2011).

59. Senji Laxme, R. R. *et al.* Biogeographical venom variation in the indian spectacled cobra (Naja naja) underscores the pressing need for pan-india efficacious snakebite therapy. *PLoS Negl. Trop. Dis.* **15**, 1–28 (2021).

60. Escalante, T. *et al.* Pulmonary hemorrhage induced by jararhagin, a metalloproteinase from Bothrops jararaca snake venom. *Toxicol. Appl. Pharmacol.* **193**, 17–28 (2003).

61. Moura-da-Silva, A. M. & Baldo, C. Jararhagin, a hemorrhagic snake venom metalloproteinase from Bothrops jararaca. *Toxicon* **60**, 280–289 (2012).

62. Tan, N. H., Ponnudurai, G. & Chung, M. C. M. Proteolytic specificity of rhodostoxin, the major hemorrhagin of Calloselasma rhodostoma (Malayan pit viper) venom. *Toxicon* **35**, 979–984 (1997).

63. Matsui, T., Fujimura, Y. & Titani, K. Snake venom proteases affecting hemostasis and thrombosis. *Biochim. Biophys. Acta - Protein Struct. Mol. Enzymol.* **1477**, 146–156 (2000).

64. UniProt. Q2UXR0 · VM3E1_ECHOC · Zinc Metalloproteinase-Disintegrin-Like Eoc1. https://www.uniprot.org/uniprotkb/Q2UXR0/entry.

65. Howes, J. M., Wilkinson, M. C., Theakston, R. D. G. & Laing, G. D. The purification and partial characterisation of two novel metalloproteinases from the venom of the West African carpet viper, Echis ocellatus. *Toxicon* **42**, 21–27 (2003).

66. UniProt. Q14FJ4 · VM2OC_ECHOC · Zinc metalloproteinase Eoc6/ Disintegrin Ocellatusin. https://www.uniprot.org/uniprotkb/Q14FJ4/entry.

67. Ricci, S., D'Esposito, V., Oriente, F., Formisano, P. & Di Carlo, A. Substrate-zymography: A still worthwhile method for gelatinases analysis in biological samples. *Clin. Chem. Lab. Med.* **54**, 1281–1290 (2016).

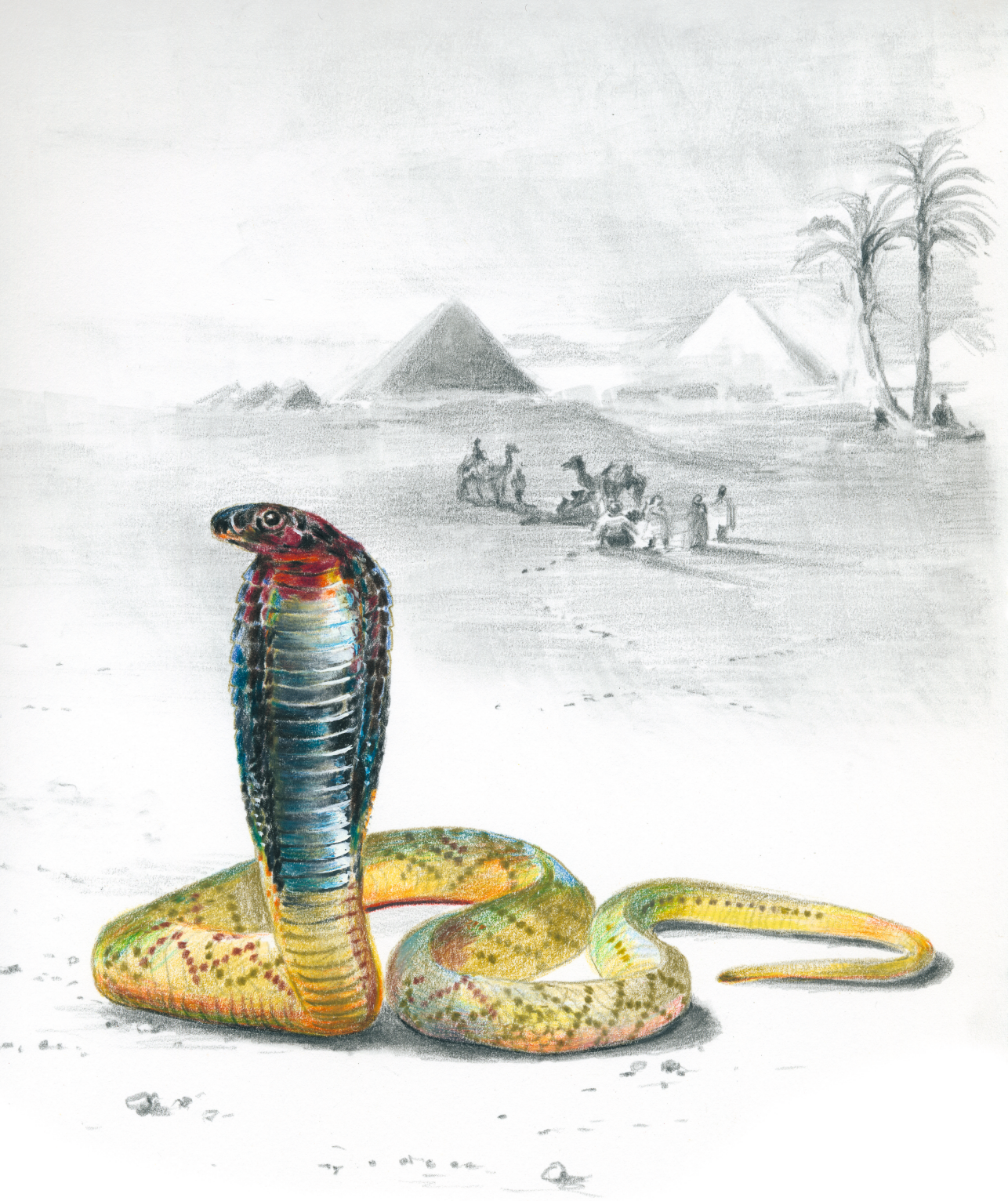

Naja haje

Chapter 6

Development of a membrane-disruption assay using phospholipid vesicles as a proxy for the detection of cellular membrane degradation

Mátyás A. Bittenbinder, Eric Wachtel, Daniel Da Costa Pereira, Julien Slagboom, Nicholas R. Casewell, Paul Jennings, Jeroen Kool, Freek J. Vonk

Toxicon: X, (100197)

Abstract

Snakebite envenoming is a global health issue that affects millions of people worldwide and that causes morbidity rates surpassing 450,000 individuals annually. Patients suffering from snakebite morbidities may experience permanent disabilities such as pain, blindness and amputations. The (local) tissue damage that causes these life-long morbidities is the result of cell- and tissue-damaging toxins present in the venoms. These compounds belong to a variety of toxin classes and may affect cells in various ways, for example, by affecting the cell membrane. In this study, we have developed a high-throughput *in vitro* assay that can be used to study membrane disruption caused by snake venoms using phospholipid vesicles from egg yolk as a substrate. The resuspended chicken egg yolk was used to form these vesicles, which were fluorescently stained to allow monitoring of the degradation of egg yolk vesicles on a plate reader. The assay proved to be suitable for studying phospholipid vesicle degradation of crude venoms and was also tested for its applicability for neutralisation studies of varespladib, which is a PLA_2 inhibitor. We additionally made an effort to identify the responsible toxins with liquid chromatography, followed by post-column bioassaying and protein identification using high-throughput venomics. We successfully identified various toxins in the venoms of *C. rhodostoma* and *N. mossambica*, which are likely to be involved in the observed vesicle-degrading effect. This indicates that the assay can be used for screening the membrane-degrading activity of both crude and fractionated venoms as well as for neutralisation studies.

6.1 Introduction

An estimated 1.8-2.7 million snakebites occur annually, resulting in over 100,000 fatalities and more than 450,000 victims suffering from permanent physical damage [1]. Snake venoms are complex mixtures containing numerous toxins from various protein families, which possess a variety of activities and clinical effects. The three main pathologies in snakebite victims include haemotoxicity, neurotoxicity and tissue-damaging activities [1–4]. Although the latter is not the most life-threatening, the tissue-damaging effects are one of the leading causes of life-long morbidities [1,4–6]. Therefore, it is surprising that considerably less research has been performed on the tissue-damaging effects compared to the research that has been done on the haemotoxic and neurotoxic venom effects [1,7]. The cell- and tissue-damaging activities of snake venoms are caused by a variety of toxins. These include hydrolytic enzymes (e.g., phospholipases A_2 (PLA_2), snake venom metalloproteinases (SVMPs) and hyaluronidases), as well as β-defensins, C-type lectin-like proteins (CTLs), disintegrins and cytotoxic three-finger toxins (3FTxs) [1,8,9]. These toxins possess various mechanisms by which they affect cells and tissues. These include 'direct' cytotoxins, which affect the cells by disrupting or destabilising the plasma membrane, and toxins that affect the cells 'indirectly' by damaging the extracellular matrix [1,10–15]. The plasma membrane performs an essential role in normal cell functioning and forms an integral part of the cell [16]. This could explain the fact that various toxin families target the cell membrane to achieve their cell-damaging effects.

Several assays have been developed over the years that can be used to study the membrane-degrading activity of snake venoms. Cell-culturing assays are used to study the effect of certain toxins on cell membrane integrity and cell viability. In addition to cell-based assays, a number of methods exist that have been used to study the activity of toxins targeting the cell membrane. Some of these assays rely on the release of free fatty acids as a result of the hydrolysis of phospholipids, resulting in an acidification of the reaction mixture [17–19]. Others include turbidity assays that use egg yolk emulsions, in which a decrease in turbidity is used as a measure for membrane-degrading activity [20–23]. With the latter, a decrease in turbidity is caused by the fact that certain venoms and their toxins degrade the egg yolk vesicles. The lipid vesicles structurally resemble the membrane of living

cells and could, therefore, be used as a proxy for membrane-degrading activity [20,24]. Although practical, these turbidity assays were used primarily for studying crude venoms and require relatively large sample volumes [20–22,25].

In this study, we describe the development of a low assay volume high-density well plate (i.e., 384-wells) based vesicle degradation (VD) assay that uses fluorescently dyed phospholipid vesicles to study membrane degradation of both crude snake venoms and fractionated venom toxins. The size of the vesicles created by resuspending the egg yolk was not formally characterised and probably contains multiple forms of phospholipid vesicles, including micelles and liposomes [26–29]. By fluorescently staining these vesicles, we were able to quantify the membrane-degrading activity in terms of a decrease in fluorescence signal, which was done in a high-throughput manner on a fluorescence plate reader. After optimisation and validation of the assay using crude venoms, the assay was integrated into nanofractionation analytics. With nanofractionation analytics, the venoms are subjected to chromatographic separation using reversed-phase chromatography (RP-LC) [30–32]. This is followed by toxin fractionation on 384-well plates for subsequent bioassaying and toxin identification with high-throughput (HT) venomics [33,34]. Although some studies have investigated the membrane-degrading effect of purified toxins on egg yolk vesicles, this study involves the fractionation of multiple venoms followed by post-column bioassaying of fractionated toxins for their membrane-degrading activity [23,35].

The assay was optimised by evaluating various parameters, including egg yolk concentration, well volumes, egg yolk buffer preparation methods, microwell plate types and plate reader types. After optimisation, the assay was validated using the venoms of a panel of medically relevant venomous snake species. The results show that the assay could be used to study vesicle degradation by crude venoms, and it was also tested for its applicability in neutralisation studies. After studies with crude venoms, we set out to identify the bioactive compounds that were capable of vesicle degradation. These data showed a substantial decrease in fluorescence signal (i.e., indicating degradation of the vesicles) by specific venom components. Subsequent toxin characterisation by HT venomics revealed that the responsible venom components were likely to be phospholipase A_2s (PLA_2s). This suggests that the assay could be used to screen both crude and fractionated

venoms, making it suitable for studying venom effects and for screening for possible inhibitory candidates for membrane-degrading activities.

6.2 Material and methods

6.2.1 Chemicals and reagents

Milli-Q (mQ) water was obtained through purification using a Milli-Q® Reference Water Purification System (Millipore). Dulbecco's phosphate buffered saline (no calcium, no magnesium, pH 7.07.3; PBS) was purchased from Thermo Fisher Scientific Inc. Tris-HCl buffer (50 mM, pH 7.4) was prepared with Trizma® base in mQ water and the pH was as adjusted using 1.0 M HCl. Egg yolk from chicken (powder), Trizma® base (≥99.9 %), hydrochloric acid (ACS reagent, 37 %; HCl) and Triton™ X-100 (BioXtra) were obtained from Sigma-Aldrich. Hoechst 33342 (trihydrochloride, trihydrate - 10 mg/mL solution in water; Hoechst) nucleic acid stain was obtained from Invitrogen™ by Thermo Fisher Scientific Inc., Gibco™. For the neutralisation assays, varespladib (Sigma-Aldrich) was used as a PLA_2 inhibitor. Acetonitrile HPLC-R (ACN) and trifluoroacetic acid HPLC grade (TFA) were obtained from Biosolve B.V.

6.2.2 Venoms

Snake venoms were sourced from the venom library of the Faculty of Science, BioAnalytical Chemistry division, Vrije Universiteit Amsterdam (VU). This library contains samples from, amongst others, the Liverpool School of Tropical Medicine (LSTM), the National University of Singapore (NUS), and private keepers. The snake venoms used in this study came from the following viper (Viperidae) and elapid (Elapidae) species: *Bothrops jararaca* (jararaca, captive bred), *Bungarus multicinctus* (many-banded krait, locality unknown), *Calloselasma rhodostoma* (Malayan pitviper, Thailand), *Daboia russelii* (Russell's viper, locality unknown), *Dendroaspis polylepis* (black mamba, captive bred), *Echis ocellatus* (West African carpet viper, Nigeria), *Naja mossambica* (Mozambique spitting cobra, captive bred) and *Naja naja* (Indian cobra, captive bred). These species were selected as they represent some of the most medically relevant species across the geographical regions most heavily affected by snakebite (i.e., Latin America,

Sub-Saharan Africa and Southeast Asia). Venoms were stored at -80°C. Venom samples were reconstituted in mQ water to the desired concentrations. These solutions were then aliquoted and subsequently snap-frozen in liquid nitrogen and stored at -80°C until use. All venoms used are in accordance with the Nagoya protocol, where applicable [36].

6.2.3 Method development

The assay is based on the principle that the fluorescent signal decreases in the presence of phospholipid vesicle-degrading proteins (e.g., snake venom toxins). This is caused by the fact that the fluorescence dye that was trapped in the vesicles is now released into the buffer solution, which results in lower fluorescence.

The formation of egg yolk vesicles is thought to occur due to the self-assembly of amphiphilic molecules in an aqueous solution. In these vesicles, the hydrophobic tails are shielded from the water while the hydrophilic heads interact with the aqueous environment [24,37]. In an attempt to better visualise the vesicle-degrading effect, we used Hoechst 33342 (Hoechst), which is known as a nucleic acid stain [38,39]. Although Hoechst is generally used for cellular staining, we noticed that the vesicles were much better visible in the presence of this stain (data not shown). Although the exact mechanisms are unknown, Hoechst (due to its lipophilic nature) probably gets entrapped in the lipid bilayer, thereby 'dyeing' the vesicles [38,39]. This allowed us to measure the vesicle-degrading activity in terms of a decrease in fluorescence signal, which could be done in a high-throughput manner on a fluorescence plate reader.

For the initial experiments, a transparent 96-well F-bottom plate (Greiner Bio-One) was used. We first added 10 µL of sample to the wells (i.e., 10 µL of mQ as a negative control, 10 µL of 20% Triton X-100 as a positive control or 10 µL venom), followed by adding 90 µL of egg yolk buffer. The egg yolk buffer was made by resuspending egg yolk from chicken (i.e., egg yolk powder) in PBS or Tris-HCl buffer to make a stock solution of 11 mg/mL egg yolk buffer (i.e. so that the final assay concentration would become ~10 mg/mL). Prior to resuspending the egg yolk in PBS or Tris-HCl, Hoechst was added to this buffer (diluted 1:20,000). The egg yolk buffer was homogenised by shortly shaking the emulsion prior to pipetting into a microwell plate. For these experiments, we used

the venoms of four snake species (i.e., *B. jararaca*, *E. ocellatus*, *D. polylepis* and *N. mossambica*) at 100 µg/mL. The effects on the egg yolk vesicles were subsequently imaged using one of the fluorescence channels of the Operetta CLS high content imager (i.e., Ex: 355- 385 nm, Em: 430-500).

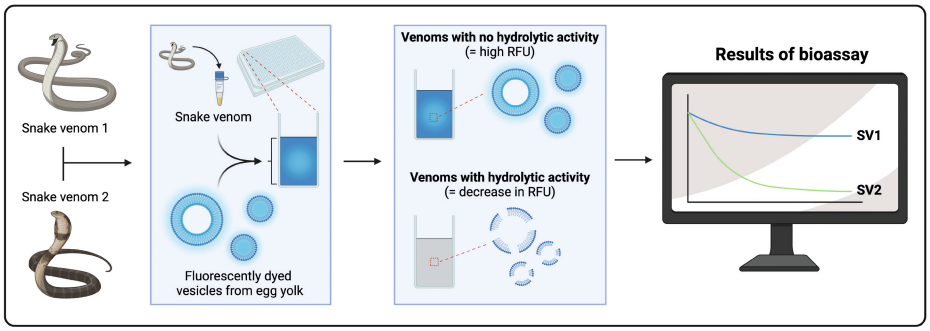

Figure 1. The concept of using fluorescently dyed phospholipid vesicles as a proxy for membrane disruption. Graphical overview of the concept of the VD assay. RFU = relative fluorescence units. Image created using

6.2.4 Method optimisation

Egg yolk vesicle degradation was quantified using the decrease in fluorescence in response to venoms with membrane-disrupting activity. Degradation of the vesicle membrane would result in a decrease in relative fluorescence, which was monitored using a fluorescence plate reader (Varioskan™ LUX Multimode Microplate Reader 3020-444, controlled by SkanIt RE 4.1 software). The signal decrease was used as a proxy to monitor the membrane-degrading activity of the respective venom analysed. In order to make the assay usable for plate reader format, we evaluated various parameters, including egg yolk concentration, assay well volumes, egg yolk buffer preparation methods, microwell plate types and different plate reader types. The fluorescence signal was captured using an excitation wavelength of 355 nm and an emission wavelength of 460 nm. The degradation of egg yolk vesicles was monitored at 37°C for 120 minutes (data captured every 2 minutes). Fluorescence was measured over time, and membrane-disrupting activity was expressed in relative fluorescence units (RFU). Triton X-100 was used as the positive control, and PBS was used as a negative control. For a detailed overview of the parameters that were assessed during optimisation, see Section 1 of the S1 Methods.

After optimisation, we continued further assaying with a total well volume of 50 µL by combining 5 µL of venom (at a concentration that is 10x pre-concentrated so that the final concentration would be 10x lower) with 45 µL of egg yolk buffer (final concentration ~10 mg/mL). For both controls, either 5 µL of 20% Triton X-100 (i.e., so that the final percentage of Triton X-100 was 2%) or 5 µL of PBS was used, followed by adding 45 µL egg yolk buffer. Measurements were done on 384-well V-bottom plates (Greiner Bio-One) with the CLARIOstar PLUS Microplate reader (using bottom optic reading).

6.2.5 Validation of the VD assay using crude venoms

The assay was subsequently used to study the membrane-disrupting effects of a selection of eight snake venoms. For this, a serial dilution of each of the venoms was made (i.e., final concentrations of 100, 33.3, 11.1, 3.7, 1.2 and 0.4 µg/mL). These experiments were performed using the 384-well V-bottom plate. Each condition (positive control, negative control, and venom dilutions) was tested in triplicate. Plates were then measured at 37°C, with data being captured every 10 minutes for a total of 12 hours.

6.2.6 Testing the ability of the assay to be used for neutralisation studies

In order to test the applicability of the assay for neutralisation studies, we tested the neutralising capacities of varespladib, a PLA_2 inhibitor which is known for its capacity to neutralise both the enzymatic and catalytically inactive variants of PLA_2s [40–42]. A serial dilution of the venoms was made (400, 133.3, 44.4, 14.8, 4.9, 1.6 µg/mL, 4x concentrated), which was added to varespladib (4 µM, 4x concentrated) in a 1:1 ratio. This mixture was incubated for 30 minutes at 37 °C. We then pipetted 25 µL of the venom-varespladib mixture into a 384-V bottom plate and added 25 µL of egg yolk buffer (20 mg/mL, 2x concentrated). This resulted in final concentrations of 100, 33.3, 11.1, 3.7, 1.2 and 0.4 µg/mL for the venom, 1 µM for varespladib and 10 mg/mL for the egg yolk buffer. Next, the measurement on the CLARIOstar Plus Microplate reader was started at 37 °C. Data was captured every 10 minutes for a total of 12 hours.

6.2.7 Identification of bioactive compounds in fractioned venoms

To elucidate which venom toxins were possibly associated with the degradation of the vesicle membranes, we used nanofractionation analytics to separate crude venoms into their individual toxins [32,43]. We selected the venoms of the most potent species from each snake family, which were used for subsequent analysis (i.e., *C. rhodostoma* from the Viperidae family and *N. mossambica* from the Elapidae family). The nanofractionation approach includes chromatographic separation of the venom by RP-LC, followed by the post-column VD assay in parallel with toxin identification using the HT venomics approach developed by Slagboom et al. [33]. Section 2.1 of the S1 Methods provides a more elaborate description of chromatographic separation and HT venomics.

After fractionation, the plates were evaporated overnight using a Christ Rotational Vacuum Concentrator RVC 2-33 CD plus (Salm en Kipp). The plates were subsequently stored at −20 °C. Upon use, the fractions in each well were reconstituted in 50 µL of egg yolk buffer (10 mg/mL) by robotic pipetting using a ThermoFisher Multidrop. The plates were centrifuged at 1500 rpm at 20 °C for 60 seconds in a 5810 R centrifuge (Eppendorf AG). Each plate was then sealed (i.e., using Thermo Scientific Sealing Tape for 96-well plates) to avoid evaporation, and the plates were subsequently incubated at 37 °C. The well plates were then measured on the CLARIOstar Plus microplate reader at various time points (i.e., after 0, 2, 4, 8 and 16 hours of incubation). Bioactivity chromatograms were generated by plotting the fluorescence readouts (in RFU) of the fractions on the y-axis against the retention time of fractionation on the x-axis. The baseline signal (i.e., showing no vesicle-degrading effect) is represented on the y-axis at the beginning of each chromatogram, whereas the negative peaks (dips) correspond to bioactive fractions.

In an attempt to identify the toxins responsible for the negative peaks (i.e., representing membrane-degrading activity), we performed the HT venomics method described by Slagboom et al. [33] on both venoms that were fractionated on separate 384 V-bottom plates. Tryptic digestion was performed directly on the microwell plates, followed by MicroLC-MS/MS, which yielded proteomics data for each well. This data was converted into MGF files using ProteoWizard's msConvert (for details, see section 2.4 of the S1 Methods). Database searching was performed using the UniProt database, which contained only Serpentes (i.e.,

snake) accessions. Using multiple in-house written scripts, the database searches were first exported as comma-separated values (CSV) files (containing all information obtained from the database search). The relevant information from these files was then merged into a single Excel file containing the information of all toxins found in each well (e.g., protein accession numbers, protein scores, sequence coverages, and protein descriptions). Then, so-called protein score chromatograms (PSCs) were generated by plotting the protein score (y-axis) against the retention time (x-axis) for each toxin found in the wells. Sections 2.2 – 2.4 of the S1 Methods provide a complete overview of the HT venomics workflow. For additional information on the scripts and data processing steps for HT venomics, see Slagboom et al. [33]. Lastly, the PSCs were then superimposed with the bioactivity chromatograms in order to correlate the bioactivity peaks with each snake venom fraction based on retention time and matching peak shapes. Graphs were drawn using GraphPad Prism version 9 (GraphPad Software, Inc.). We have previously described a similar workflow in more detail [34].

6.2.8 Statistical analysis

All data was measured in triplicate and is represented by mean ±SD. For the neutralisation studies, the differences between venoms with and without inhibitors were assessed using a one-tailed test. Statistical analysis was performed using GraphPad Prism 9. Specific statistical tests used, p-value level definitions, and additional details are listed in the respective figure legends.

6.3 Results and discussion

6.3.1 Method development

In order to test the applicability of the vesicle degradation assay principle, we studied the vesicle-degrading activity of the venoms of *B. jararaca*, *E. ocellatus*, *D. polylepis* and *N. mossambica*. Using a microscope with a fluorescence channel for Hoechst (i.e., Ex: 355- 385 nm, Em: 430-500 nm) provided insights into how the vesicles were affected in the presence of venom. The addition of the venoms of *B. jararaca*, *E. ocellatus* and *N. mossambica*, for example, resulted in a clear decrease in the number of vesicles (see S1 and S2 Figures). For *D. polylepis,* however, no visual reduction of vesicles was observed, even not after prolonged incubation (i.e., 2 hours). This suggests that the venoms of *B. jararaca*, *E. ocellatus* and *N. mossambica* could have a membrane-degrading activity, which results in the degradation of the vesicle membrane. A clear difference could further be observed when using PBS as a buffer compared to Tris-HCl buffer. With the latter, the contrast between wells in which the vesicles were affected was less apparent (see S1 and S2 Figures).

6.3.2 Optimisation of the VD assay

As the vesicle-degrading effects of certain venoms were clearly visible under the fluorescence microscope, we set out to see whether this decrease in fluorescence could also be measured on a fluorescence plate reader. For optimisation of the VD assay, a range of parameters was tested to make the assay reliable, robust and suitable for high-throughput screening of snake venoms on high-density, low-volume microwell plates. As the first parameters, we tested the concentration of the egg yolk emulsion and the appropriate well plate type. We compared seven concentrations of egg yolk emulsion (i.e., final concentrations of 20, 10, 5, 2.5, 1.25, 0.63 and 0 mg/mL) and three microwell plate types (i.e., clear 96-well flat-bottom, 384-well flat-bottom and 384-well V-bottom, for details see S1 Table). For the concentrations of the egg yolk emulsion, we observed that an egg yolk concentration of 10 mg/mL provided the highest RFU and the largest assay window (i.e., the difference in RFU between negative and positive control) (see S3 Figure).

In addition to the variation in RFU when using different egg yolk concentrations, apparent differences in RFUs for the assay windows between the controls could be observed between the three types of microwell plates. The data obtained from the 96-well F-bottom plate resulted in larger error bars compared to both 384-well plates tested (see S3 Figure). The 384-well F-bottom plate produced a minor background noise, although the assay window between both controls was smaller than with the other two microwell plates (see S3b Figure). In addition to showing smaller error bars compared to the other two plate types, the 384-well V-bottom plate gave the largest assay window between positive and negative control (see S3c Figure). This well plate type was used for further assay optimisation.

To determine the optimal way of preparing the egg yolk buffer (i.e., to investigate whether various preparation methods would influence the assay window between negative and positive control), various ways of preparing the egg yolk buffer were tested. Slow shaking for 10 – 60 seconds once the egg yolk powder and PBS were combined gave the best results in terms of the homogeneity of the egg yolk emulsion and provided the smallest error bars and largest assay window between positive and negative control (for an overview of the effect of various preparation methods on the assay window see S5 Figure). Fast shaking, vortexing (for >30 seconds), or sonification, on the other hand, seriously reduced the assay window between positive and negative control (see S5 Figure). Slow shaking for ~10 seconds was found to provide the best results (i.e., this gave the largest assay window). The advantage of using this method for preparing the egg yolk emulsion is that it is straightforward and can be easily used when preparing larger stock solutions (e.g., more than 50 mL). We, therefore, continued the assay development using this preparation method.

The reaction volume was the following parameter that was optimised. In order to test this, end volumes of 10 – 100 µL were investigated, and measurements were done kinetically for 1 hour at 37°C. Reaction volumes of 30 – 50 µL gave the largest assay window when negative and positive controls were compared (see S4 Figure). For further optimisation, we selected 50 µL as the optimal assay volume, as this volume gave a proper assay window and because larger volumes will require more reagents.

As a final step in optimisation, in an effort to increase the assay window and minimise signal variation, we compared the differences in the results of two types of fluorescence plate readers. For this, we repeated the assay (positive vs. negative) on a 384-well V-bottom at 37°C with all optimised parameters as mentioned above. We compared the readouts of the Varioskan™ microplate reader to that of the CLARIOstar Plus Microplate reader 430-4478 (BMG LABTECH), which is coupled to MARS data analysis software. For the CLARIOstar, we further compared top optic and bottom optic readings (as this option was only available to us in our CLARIOstar Plus), in addition to a number of other settings (i.e., focal height and gain). The largest window between positive and negative control was found when using the bottom reading on the CLARIOstar (see S6 Figure). To summarise, for further experiments, we used the following parameters: 1) final concentration of 10 mg/mL egg yolk in a buffer on a 384 V-bottom microwell plate; 2) slow shaking for ~10 seconds as a preparation method; 3) assay volume of 50 µL; 4) bottom reading on the CLARIOstar microplate reader.

6.3.3 Validation of the VD assay using crude venoms

To validate the proposed assay method for screening the effects of snake venoms on the vesicles, we selected venoms from a panel of medically relevant venomous snake species. This was done to validate that a dose-dependent assay signal reduction could be obtained for cytotoxic snake venoms. The venoms of eight different snake species were selected to validate the VD assay. Each venom was tested at six concentrations (i.e., final concentrations of 100 – 0.4 µg/mL) and kinetically measured for the duration of 12 hours at 37°C.

All venoms except that of *D. polylepis* showed a notable egg yolk vesicle-degrading effect (see Figure 2). In particular, the two highest concentrations of *B. jararaca* and the three highest concentrations of *C. rhodostoma* gave a decrease in signal similar to that of the positive control. The venom of *D. russelii* was also potent in this regard, and although the total signal reduction was less compared to *B. jararaca* and *C. rhodostoma*, the reduction could be observed for all concentrations, not exclusively the highest venom concentrations. A similar effect was observed for the venoms of *B. multicinctus*, *N. mossambica* and *N. naja*. Of the elapid species that were tested, *N. mossambica* clearly had the highest effect in terms of vesicle degradation (see Figure 2).

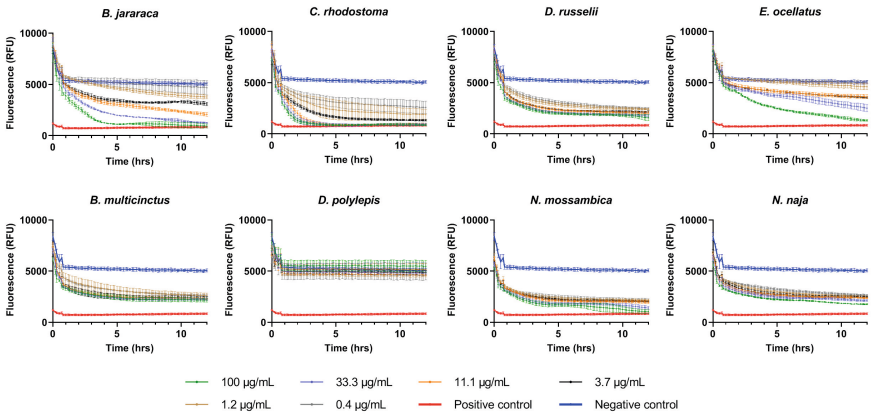

Figure 2. Assay validation using a panel of snake venoms to study vesicle degradation. The degradation of egg yolk vesicles was monitored over 12 hrs (data captured every 10 min) at 37°C, with six concentrations of venom (100 – 0.4 µg/mL). mQ water was added as a negative control, and 2% Triton-X was added as a positive control. Readings were performed on a CLARIOstar Plus Microplate reader (using bottom optic reading); data was measured in triplicate; error bars show standard deviation.

6.3.4 Testing the ability of the assay to be used for neutralisation studies

In an attempt to test the versatility of the VD assay, we assessed the possible use of the assay for neutralisation studies. To do so, we tested the neutralising capacities of varespladib, as it is known for its ability to neutralise the hydrolysing effect of PLA_2s in snake venoms, which could be causing the observed egg yolk vesicle-degrading effects. Varespladib acts as a potent inhibitor of venom PLA_2s, thereby preventing the breakdown of phospholipids in cell membranes [44,45].

For all venoms that showed egg yolk vesicle-degrading activity, we saw a significant reduction in the activity when venom was pre-incubated with 20 µM of varespladib (for an overview of the neutralising effects of varespladib compared to venom controls, see Figure 3 and S7 Figure). Vesicle-degrading activity can be observed for the highest concentrations of *B. jararaca*, *D. russelii*, *B. multicinctus* and *N. mossambica*, although to a much lesser extent. These outcomes suggest that PLA_2s are likely involved in egg yolk vesicle degradation observed without the inhibitor varespladib (see Figure 2). This is in line with previous studies focusing on the membrane-disrupting effect of PLA_2s in snake venoms. These toxins disrupt the membrane by hydrolysis of the phospholipids (in the

case of enzymatically active toxins). In contrast, the enzymatically inactive PLA_2 homologs exert their effects via perturbation of the plasma membrane [13,46].

These findings are further supported by looking at the relative abundances of PLA_2s in each of the venoms. Although the venoms of *B. jararaca* and *C. rhodostoma* showed a higher potency at higher concentrations compared to *D. russelii*, the latter was consistently potent at all concentrations, with a slight increase in potency upon increasing venom concentration. When looking at the relative PLA_2 abundance in these venoms, we observed that *D. russelii* has the highest abundance of PLA_2s (32.8 – 35%) compared to the other viper venoms based on literature (S2 Table). For the elapid venoms, we see that for *D. polylepis*, which contains <0.1% PLA_2s, no significant egg yolk vesicle-degrading activity is observed (S2 Table). In contrast, for the other elapid species, which do contain much larger abundances of PLA_2s, we clearly see the egg yolk vesicle-degrading activity that is neutralised by the PLA_2 inhibitor varespladib (see Figure 3).

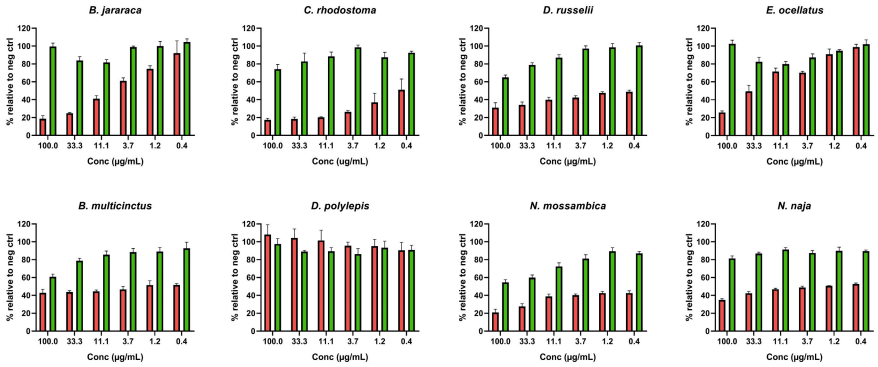

Figure 3. Overview of the neutralising effects of varespladib on vesicle degradation evoked by different snake venoms, relative to the negative control. The degradation of egg yolk vesicles after 12 hrs of incubation at 37°C, in absence of varespladib (red) and in presence of varespladib (green). Results for each venom are represented in a graph, in which the vesicle degradation of six venom concentrations (100 – 0.4 µg/mL) is given for which the venoms are either pre-incubated with 20 µM of varespladib or, in the absence of varespladib. Negative control values were 5078 ± 145 RFU (i.e., no venom, no varespladib) and 4795 ± 43 RFU (i.e., no venom, with varespladib control). Readings were performed on a CLARIOstar microplate reader (using bottom optic reading). Data was measured in triplicate; error bars show standard deviation.

6.3.5 Identification of bioactive compounds in fractioned venoms

In an effort to identify the venom components responsible for the observed vesicle-degrading activity, we separated and fractionated the venoms of *C. rhodostoma* and *N. mossambica*, followed by post-column bioassaying and characterisation using HT venomics. We selected these two species as their venoms proved to be the most potent on the VD assay (see Figures 2 and 3). For parallel identification of the bioactive toxins after fractionation and bioassaying, we applied the HT venomics approach developed by Slagboom et al. [33]. The VD assay was carried out on the fractionated toxins (on the 384 V-bottom plates) after vacuum freeze-drying these overnight. The plates were measured at various time points (i.e., 0, 2, 4, 8 and 16 hours), and bioassay chromatograms were generated for all time points (see Figure 4, Figure 5 and S8 Figure). The baseline signal (i.e., no vesicle-degrading effect) is provided on the y-axis, whereas the negative peaks (dips) correspond to bioactive fractions.

Figure 4 shows the bioactivity chromatograms (see Figure 4i) and bioactive fractions (see Figures 4 ii and iii) for *C. rhodostoma* after 8 hours of incubation. Two bioactivity peaks could be observed between 15.1 and 19.1 minutes. When looking at the HT venomics data (see Figures 4ii and 4iii), we identified a total of 11 toxins that matched in the retention time profile with the bioactivity peak(s) and, as such, could be identified within this bioactivity window. Of these toxins, three were found to be part of the PLA_2 family, and eight were part of other families (see Figure 4, S3 Table). According to the Uniprot database, the following PLA_2s could be identified within this time frame: PA2A_BOTPC, PA2AA_CALRH, PA2A4_BOTAL. These are acidic PLA_2s with hydrolytic activity that are capable of degrading lipid membranes [47–49]. Snake venom PLA_2s can be divided into two groups based on their structural characteristics, with the PLA_2s in the viper family being classified as Group II PLA_2 [50]. Within this group, two mechanisms of action can be found, with enzymatically active PLA_2s being capable of hydrolysing membrane phospholipids. In contrast, the enzymatically inactive toxins exert their effect via (in)direct perturbation of the plasma membrane [13,46,51]. VM1K_CALRH is another toxin that was identified, which is part of the SVMP family of toxins. According to Uniprot, this toxin 'inhibits platelet aggregation' but is devoid of any membrane-disrupting activity [52–54]. Other toxins that were found within the bioactivity window include

several snake venom serine proteases (i.e., VSPF2_CALRH and VSPP_Trist and A0A2I7YS44_CROCT) capable of affecting haemostasis but are lacking any membrane-disrupting activity [55–58]. Similarly, the snaclecs (snake C-type lectins) that were identified (SLED_CALRH; SLYB_CALRH; SL_DEIAC and A0A077LA68_PROEL) are capable of affecting normal blood coagulation, although a range of other effects (including cytotoxicity on various cancer cell lines) have been described [59,60,69,61–68]. Most of the toxins not belonging to the family of venom PLA_2s are likely, not active in the egg yolk vesicle bioassay and coeluted with the tentatively identified PLA_2s.

Figure 5 shows the bioactivity chromatograms (Figure 5i) and bioactive fractions (Figures 5 ii and iii) for *N. mossambica* after 8 hours of incubation. Egg yolk vesicle-degrading activity was observed between 15.1 – 19.1 minutes, and within this bioactivity window, a total of 12 toxins were found from HT venomics. Three toxins were found to be part of the PLA_2s family, four toxins belong to the 3FTxs family, and five were found to be nerve growth factors (see Figure 5, S4 Table). According to Uniprot, these PLA_2s are 'capable of hydrolysing phospholipids and have several activities including (in)direct haemolytic action, myonecrosis and strong anticoagulant activity' [70–72]. In addition, the 3FTx proteins found are known, according to Uniprot, for their 'cytolytic activity on different cell types by forming pores in lipid membranes'. However, the exact mechanisms by which these toxins exert their effects remain unclear [73–76]. The observed effects could, therefore, also be (partially) caused by cytotoxic 3FTxs, in addition to the activity caused by PLA_2 toxins or by a synergistic effect between both toxin classes, which potentiates the cytotoxic effects of PLA_2s [77–83]. However, taking into account the vesicle-degrading activity was completely neutralised by varespladib, it is also possible that PLA_2s are exclusively responsible for the observed effect. A third group of toxins identified within the bioactivity peak area of the venom analysed was the group of nerve growth factors. Although their exact relevance in snake venom is not yet elucidated, their role in membrane disruption seems limited [84–87] , and these toxins were likely non-active and coeluting with the other bioactive toxins identified.

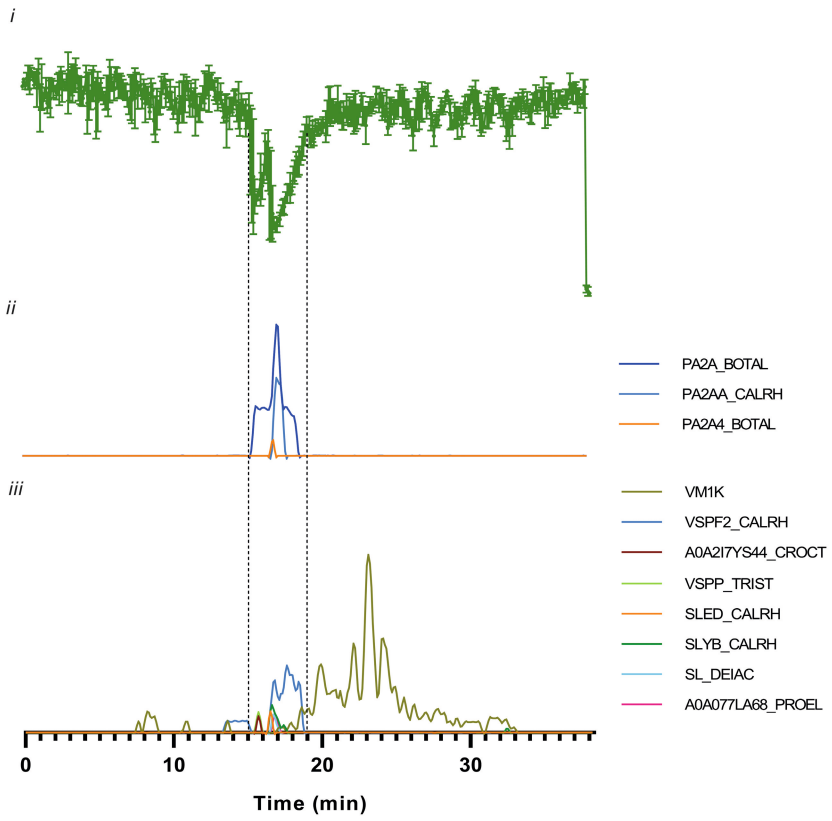

Figure 4. Identification of bioactive fractions of *C. rhodostoma* venom (1 mg/mL injected) by correlating bioactivity data with high throughput venomics data. i: bioactivity chromatograms of the VD assay after 8 hrs of incubation of egg yolk emulsions with venom fractions at 37 °C. Peaks with negative minima indicate the presence of bioactive fractions; ii and iii: Graphs representing the protein score chromatograms (PSCs), showing the individual venom proteins found with Mascot database searching of the tryptically digested and bottom-up proteomics analysed well fractions. NB. The PSCs in ii represent PLA_2s correlating in retention time frame with the bioactivity peaks, and the PSCs in iii represent other protein hits. The two vertical dotted lines mark the bioactivity window, which includes the main activity peaks and their corresponding PSC peaks. The last three data points (38.1 – 38.3 min) show the positive control (2% Triton-X). Measurements represented by the bioactivity chromatograms were performed in triplicate; error bars show standard deviation. The corresponding CSV and Excel files can be found in the Supplementary Information folders "CSV files" and "Excel files".

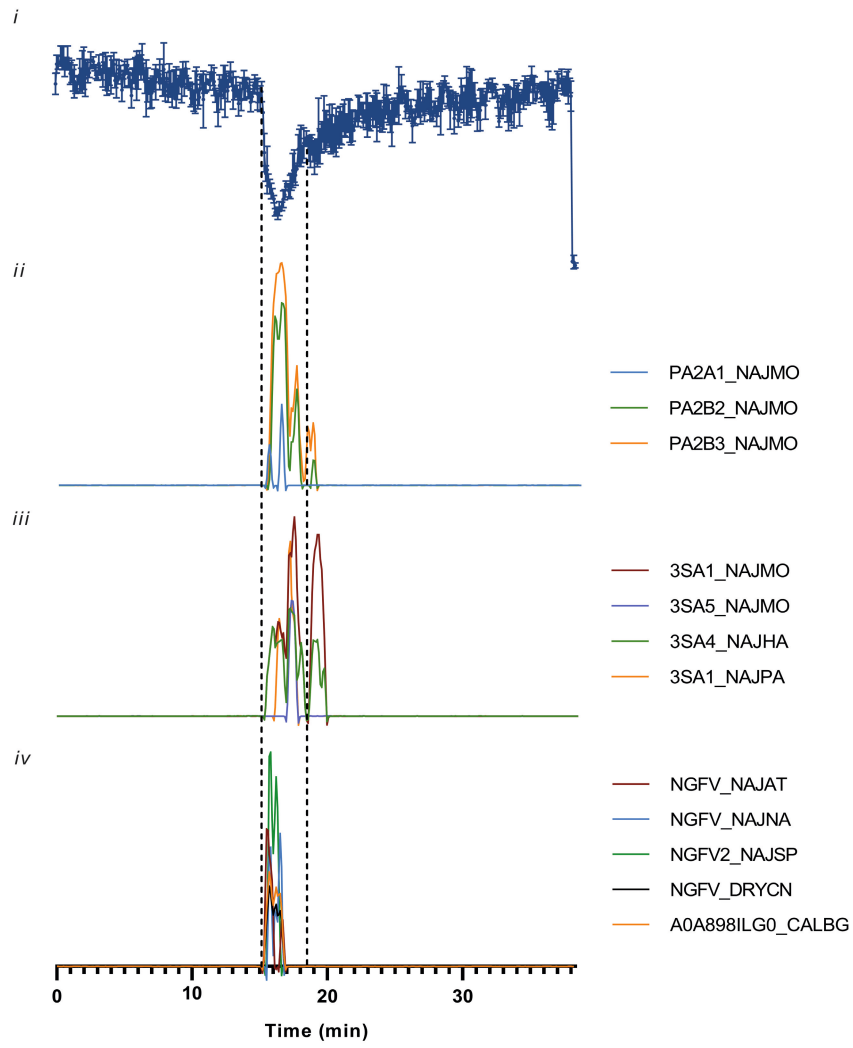

Figure 5. Identification of bioactive fractions of *N. mossambica* venom (1 mg/mL injected) by correlating bioactivity data with high throughput venomics data. i: bioactivity chromatograms of the VD assay after 8 hrs of incubation of egg yolk emulsions with venom fractions at 37 °C. Peaks with negative minima indicate the presence of bioactive fractions; ii - iii: Graphs representing the protein score chromatograms (PSCs), showing the individual venom proteins found with Mascot database searching of the tryptically digested and bottom-up proteomics analysed well fractions. NB. The PSCs in ii represent PLA_2s hits, iii these represent 3FTx correlating in retention time frame with the bioactivity peak, and in iv these represent other protein hits. The two dotted lines mark the bioactivity window, which includes the main activity peaks and their corresponding PSC peaks. The last three data points (38.1 – 38.3 min) show the positive control (2% Triton-X). Measurements represented by the bioactivity chromatograms were performed in triplicate; error bars show standard deviation. The corresponding CSV and Excel files can be found in the Supplementary Information folders "CSV files" and "Excel files".

6.4 Concluding remarks

In this study, we describe the development of a screening assay that can be used to assess membrane-degrading activities of (snake) venoms. Our goal was to develop an assay that uses a low assay volume on high-density well plates (i.e., 384 wells) and which can be used to monitor membrane degradation of crude snake venoms and fractionated venom toxins. By fluorescently dyeing the vesicles, we were able to both visualise the degradation under a fluorescence microscope and quantify the membrane-degrading activity on a fluorescence plate reader. For optimisation of the VD assay, we evaluated various parameters, including the concentration of the egg yolk emulsion, well volumes, egg yolk buffer preparation methods, microwell plate types and plate reader types. Validating the assay with serial dilutions of venoms of a panel of medically relevant snake species showed that the assay could indeed be used for evaluating membrane-disrupting effects of snake venoms. The results showed a dose-dependent egg yolk vesicle-degrading activity for all cytotoxic venoms investigated. The non-cytotoxic venom of *D. polylepis* did not show any activity in the bioassay. We further noticed that elapid venoms, in general, were potent across all concentrations, whereas the viper venoms showed only higher potency at the highest venom concentrations tested. Further experiments which focused on the applicability of the VD assay for neutralisation studies showed that micromolar concentrations of the PLA_2 inhibitor varespladib resulted in near-complete neutralisation of the observed membrane-disrupting effects for all cytotoxic venoms tested. This suggests that the observed vesicle-degrading effect could be caused exclusively by PLA_2s. This could mean that the vesicle degradation assay would be suitable for specifically monitoring PLA_2 activity.

This is further supported when we take into account the HT venomics data. When looking at the toxins identified in the venom of *C. rhodostoma*, we see that PLA_2s are likely to be responsible for the vesicle-degrading activity, as the other toxins found are devoid of any membrane-disrupting activities. For the venom of *N. mossambica,* we expect a similar role for the PLA_2s, although 3FTxs might also be responsible for the vesicle-degrading effect, either alone or in synergy with PLA_2s. However, given the fact that the activity in crude venom is almost completely abrogated in the presence of the PLA_2 inhibitor varespladib, it might

well be that the vesicle-degrading activity is exclusively caused by PLA_2s. Despite these findings, it is not possible to say with complete certainty that the VD assay is specific for monitoring the vesicle-degrading activities of PLA_2s exclusively.

The cell- and tissue-damaging effects of snake venom toxins play a major role in morbidities caused by snakebites. Therefore, it is important to develop straightforward and high-throughput assays that can be used to study these effects and for future neutralisation studies. This study was an effort to contribute new bioassaying tools for this endeavour.

References

1. Gutiérrez, J. M. *et al.* Snakebite envenoming. *Nat. Rev. Dis. Prim.* **3**, (2017).
2. Kasturiratne, A. *et al.* The global burden of snakebite: A literature analysis and modelling based on regional estimates of envenoming and deaths. *PLoS Med.* **5**, 1591–1604 (2008).
3. Habib, A. G. *et al.* Snakebite is Under Appreciated: Appraisal of Burden from West Africa. *PLoS Negl. Trop. Dis.* **9**, 4–11 (2015).
4. Warrell, D. A. Guidelines of Management of Snake bite. *Lancet* **375**, 77–88 (2010).
5. Longbottom, J. *et al.* Vulnerability to snakebite envenoming : a global mapping of hotspots. *Lancet* **392**, 673–684 (2018).
6. Chippaux, J. P. Snakebite envenomation turns again into a neglected tropical disease! *J. Venom. Anim. Toxins Incl. Trop. Dis.* **23**, 1–2 (2017).
7. Bénard-Valle, M. *et al.* Antivenom research and development. in *Venomous Reptiles and Their Toxins: Evolution, Pathophysiology and Biodiscovery; Fry, B.G., Ed.; Oxford University Press: New York, NY, USA* 61–72 (2015).
8. Fry, B. G. *Venomous reptiles and their toxins: evolution, pathophysiology and biodiscovery*. *Oxford University Press, Oxford University Press.* (2015). doi:10.1016/0041-0101(71)90017-1.
9. Gopalakrishnakone, P., Inagaki, H., Vogel, C., Mukherjee, A. K. & Rahmy, T. R. *Snake Venoms*. (Springer Berlin, Germany., 2017).
10. Bittenbinder, M. A. *et al.* Development of a high-throughput in vitro screening method for the assessment of cell-damaging activities of snake venoms. *PLoS Negl. Trop. Dis.* **17**, e0011564 (2023).
11. Markland, F. S. & Swenson, S. Snake venom metalloproteinases. *Toxicon* **62**, 3–18 (2013).
12. Gutiérrez, J. M., Escalante, T., Rucavado, A., Herrera, C. & Fox, J. W. A comprehensive view of the structural and functional alterations of extracellular matrix by snake venom metalloproteinases (SVMPs): Novel perspectives on the pathophysiology of envenoming. *Toxins (Basel).* **8**, (2016).
13. Montecucco, C., Gutiérrez, J. M. & Lomonte, B. Cellular pathology induced by snake venom phospholipase A2 myotoxins and neurotoxins: Common aspects of their mechanisms of action. *Cell. Mol. Life Sci.* **65**, 2897–2912 (2008).
14. Gasanov, S. E., Dagda, R. K. & Rael, E. D. Snake Venom Cytotoxins, Phospholipase A2 s, and Zn2+ -dependent Metalloproteinases: Mechanisms of Action and Pharmacological Relevance. *J. Clin. Toxicol.* **4**, (2014).
15. Sunagar, K. *et al.* Three-fingered RAVERs: Rapid Accumulation of Variations in Exposed Residues of snake venom toxins. *Toxins (Basel).* **5**, 2172–2208 (2013).
16. Alberts, B. *et al. Essential cell biology: Fifth international student edition*. (WW Norton & Company., 2018).
17. Condrea, E., De Vries, A., Mager, J. Action of snake-venom phospholipase a on free and lipoprotein-bound phospholipids. *Biochim. Biophys. Acta* **58**, 389–397 (1962).
18. Still, K. B. M. *et al.* Development of high-throughput screening assays for profiling snake venom phospholipase A2 activity after chromatographic fractionation. *Toxicon* **184**, 28–38 (2020).

19. Price, J. A. A colorimetric assay for measuring phospholipase A2 degradation of phosphatidylcholine at physiological pH. *J. Biochem. Biophys. Methods* **70**, 441–444 (2007).

20. Marinetti, G. V. The action of phospholipase A on lipoproteins. *Biochim. Biophys. Acta (BBA)/Lipids Lipid Metab.* **98**, 554–565 (1965).

21. Joubert, F. J. & Taljaard, N. Purification, Some Properties and Amino-Acid Sequences of Two Phospholipases A (CM-II and CM-III) from Naja naja kaouthia Venom. *Eur. J. Biochem.* **112**, 493–499 (1980).

22. Senji Laxme, R. R. *et al.* Beyond the 'Big four': Venom profiling of the medically important yet neglected Indian snakes reveals disturbing antivenom deficiencies. *PLoS Negl. Trop. Dis.* **13**, e0007899 (2019).

23. Doley, R., King, G. F. & Mukherjee, A. K. Differential hydrolysis of erythrocyte and mitochondrial membrane phospholipids by two phospholipase A2 isoenzymes (NK-PLA 2-I and NK-PLA2-II) from the venom of the Indian monocled cobra Naja kaouthia. *Arch. Biochem. Biophys.* **425**, 1–13 (2004).

24. Monteiro, N., Martins, A., Reis, R. L. & Neves, N. M. Liposomes in tissue engineering and regenerative medicine. *J. R. Soc. Interface* **11**, (2014).

25. Senji Laxme, R. R. *et al.* Biogeographical venom variation in the indian spectacled cobra (Naja naja) underscores the pressing need for pan-india efficacious snakebite therapy. *PLoS Negl. Trop. Dis.* **15**, 1–28 (2021).

26. Oladimeji, B. M. & Gebhardt, R. Physical Characteristics of Egg Yolk Granules and Effect on Their Functionality. *Foods* **12**, (2023).

27. Abeyrathne, E. D. N. S., Nam, K. C., Huang, X. & Ahn, D. U. Egg yolk lipids: separation, characterization, and utilization. *Food Sci. Biotechnol.* **31**, 1243–1256 (2022).

28. Strixner, T., Sterr, J., Kulozik, U. & Gebhardt, R. Structural Study on Hen-egg Yolk High Density Lipoprotein (HDL) Granules. *Food Biophys.* **9**, 314–321 (2014).

29. Dennis, E. A., Cao, J., Hsu, Y. H., Magrioti, V. & Kokotos, G. Phospholipase A2 enzymes: Physical structure, biological function, disease implication, chemical inhibition, and therapeutic intervention. *Chem. Rev.* **111**, 6130–6185 (2011).

30. Mladic, M. *et al.* Rapid screening and identification of ACE inhibitors in snake venoms using at-line nanofractionation LC-MS. *Anal. Bioanal. Chem.* **409**, 5987–5997 (2017).

31. Slagboom, J., Kool, J., Harrison, R. A. & Casewell, N. R. Haemotoxic snake venoms: their functional activity, impact on snakebite victims and pharmaceutical promise. *Br. J. Haematol.* **177**, 947–959 (2017).

32. Zietek, B. M. *et al.* Liquid chromatographic nanofractionation with parallel mass spectrometric detection for the screening of plasmin inhibitors and (metallo)proteinases in snake venoms. *Anal. Bioanal. Chem.* **410**, 5751–5763 (2018).

33. Slagboom, J. *et al.* High-Throughput Venomics. *J. Proteome Res.* **22**, 1734–1746 (2023).

34. Palermo, G. *et al.* Acetylcholine-Binding Protein Affinity Profiling of Neurotoxins in Snake Venoms with Parallel Toxin Identification. *Int. J. Mol. Sci.* **24**, 16769 (2023).

35. Fernandes, F. F. A. *et al.* Counteraction of Bothrops snake venoms by Combretum leprosum root extract and arjunolic acid. *J. Ethnopharmacol.* **155**, 552–562 (2014).

36. CBD Secretariat. Nagoya Protocol on Access To Genetic Resources and the Fair and Equitable Sharing of Benefits Arising from their Utilization to the convention on biological diversity - Text and annex. *Nagoya Protoc.* **12**, 1–320 (2011).

37. Nsairat, H. *et al.* Liposomes: structure, composition, types, and clinical applications. *Heliyon* vol. 8 at https://doi.org/10.1016/j.heliyon.2022.e09394 (2022).

38. Lalande, M. E., Ling, V. & Miller, R. G. Hoechst 33342 dye uptake as a probe of membrane permeability changes in mammalian cells. *Proc. Natl. Acad. Sci. U. S. A.* **78**, 363–367 (1981).

39. Bucevičius, J., Lukinavičius, G. & Gerasimaite, R. The Use of Hoechst Dyes for DNA Staining and Beyond. *Chemosens. 2018, Vol. 6, Page 18* **6**, 18 (2018).

40. Salvador, G. H. M. *et al.* Structural basis for phospholipase A2-like toxin inhibition by the synthetic compound Varespladib (LY315920). *Sci. Rep.* **9**, 1–13 (2019).

41. Bryan-Quirós, W., Fernández, J., Gutiérrez, J. M., Lewin, M. R. & Lomonte, B. Neutralizing properties of LY315920 toward snake venom group I and II myotoxic phospholipases A2. *Toxicon* **157**, 1–7 (2019).

42. Lewin, M. R. *et al.* Varespladib in the Treatment of Snakebite Envenoming: Development History and Preclinical Evidence Supporting Advancement to Clinical Trials in Patients Bitten by Venomous Snakes. *Toxins (Basel).* **14**, 1–21 (2022).

43. Mladic, M. *et al.* At-line nanofractionation with parallel mass spectrometry and bioactivity assessment for the rapid screening of thrombin and factor Xa inhibitors in snake venoms. *Toxicon* **110**, 79–89 (2016).

44. Lewin, M., Samuel, S., Merkel, J. & Bickler, P. Varespladib (LY315920) appears to be a potent, broad-spectrum, inhibitor of snake venom phospholipase A2 and a possible pre-referral treatment for envenomation. *Toxins (Basel).* **8**, (2016).

45. Gutiérrez, J. M. *et al.* The search for natural and synthetic inhibitors that would complement antivenoms as therapeutics for snakebite envenoming. *Toxins (Basel).* **13**, 1–30 (2021).

46. Lomonte, B. Lys49 myotoxins, secreted phospholipase A2-like proteins of viperid venoms: A comprehensive review. *Toxicon* **224**, 107024 (2023).

47. Uniprot.Q9I8F8 · PA2A_BOTPC · Acidic phospholipase A2. https://www.uniprot.org/uniprotkb/Q9I8F8/entry.

48. Uniprot. Q9PVF1 · PA2AA_CALRH · Acidic phospholipase A2 S1E6-a. https://www.uniprot.org/uniprotkb/Q9PVF1/entry.

49. Uniprot. P86456 · PA2A4_BOTAL · Acidic phospholipase A2 SpII RP4.

50. Arni, R. K. & Ward, R. J. Phospholipase A2—a structural review. *Toxicon* **34**, 827–841 (1996).

51. Kini, R. M. Excitement ahead: Structure, function and mechanism of snake venom phospholipase A2 enzymes. *Toxicon* **42**, 827–840 (2003).

52. Escalante, T., Rucavado, A., Fox, J. W. & Gutiérrez, J. M. Key events in microvascular damage induced by snake venom hemorrhagic metalloproteinases. *J. Proteomics* **74**, 1781–1794 (2011).

53. Herrera, C. *et al.* Tissue Localization and Extracellular Matrix Degradation by PI, PII and PIII Snake Venom Metalloproteinases: Clues on the Mechanisms of Venom-Induced Hemorrhage. *PLoS Negl. Trop. Dis.* **9**, 1–20 (2015).

54. Uniprot. P0CB14 · VM1K_CALRH · Snake venom metalloproteinase kistomin. https://www.uniprot.org/uniprotkb/P0CB14/entry.

55. Serrano, S. M. T. The long road of research on snake venom serine proteinases. *Toxicon* **62**, 19–26 (2013).

56. Uniprot.P47797 · VSPF2_CALRH · Thrombin-like enzyme ancrod-2. https://www.uniprot.org/uniprotkb/P47797/entry.

57. Uniprot.Q71QH7 · VSPP_TRIST · Snake venom serine protease PA. https://www.uniprot.org/uniprotkb/Q71QH7/entry.

58. Uniprot. A0A2I7YS44 · A0A2I7YS44_CROCT · Serine endopeptidase. https://www.uniprot.org/uniprotkb/A0A2I7YS44/entry.

59. De Carvalho, D. D., Schmitmeier, S., Novello, J. C. & Markland, F. S. Effect of BJcuL (a lectin from the venom of the snake Bothrops jararacussu) on adhesion and growth of tumor and endothelial cells. *Toxicon* **39**, 1471–1476 (2001).

60. Sarray, S. *et al.* Lebectin and lebecetin, two C-type lectins from snake venom, inhibit α5β1 and αv-containing integrins. *Matrix Biol.* **26**, 306–313 (2007).

61. Pires, W. L. *et al.* Effect of BjcuL, a lectin isolated from Bothrops jararacussu, on human peripheral blood mononuclear cells. *Toxicol. Vitr.* **41**, 30–41 (2017).

62. Sartim, M. A. & Sampaio, S. V. Snake venom galactoside-binding lectins: A structural and functional overview. *J. Venom. Anim. Toxins Incl. Trop. Dis.* **21**, 1–11 (2015).

63. Nunes, E. S. *et al.* Cytotoxic effect and apoptosis induction by Bothrops leucurus venom lectin on tumor cell lines. *Toxicon* **59**, 667–671 (2012).

64. Pathan, J., Mondal, S., Sarkar, A. & Chakrabarty, D. Daboialectin, a C-type lectin from Russell's viper venom induces cytoskeletal damage and apoptosis in human lung cancer cells in vitro. *Toxicon* **127**, 11–21 (2017).

65. Cummings, R. D. & McEver, R. P. C-type Lectins. in *Essentials of Glycobiology. Cold Spring Harbor Laboratory Press* (Cold Spring Harbor Laboratory Press, 2009).

66. Uniprot. D2YW40 · SLED_CARLH · Snaclec rhodocetin subunit delta. https://uniprot.org/uniprotkb/D2YW40/entry.

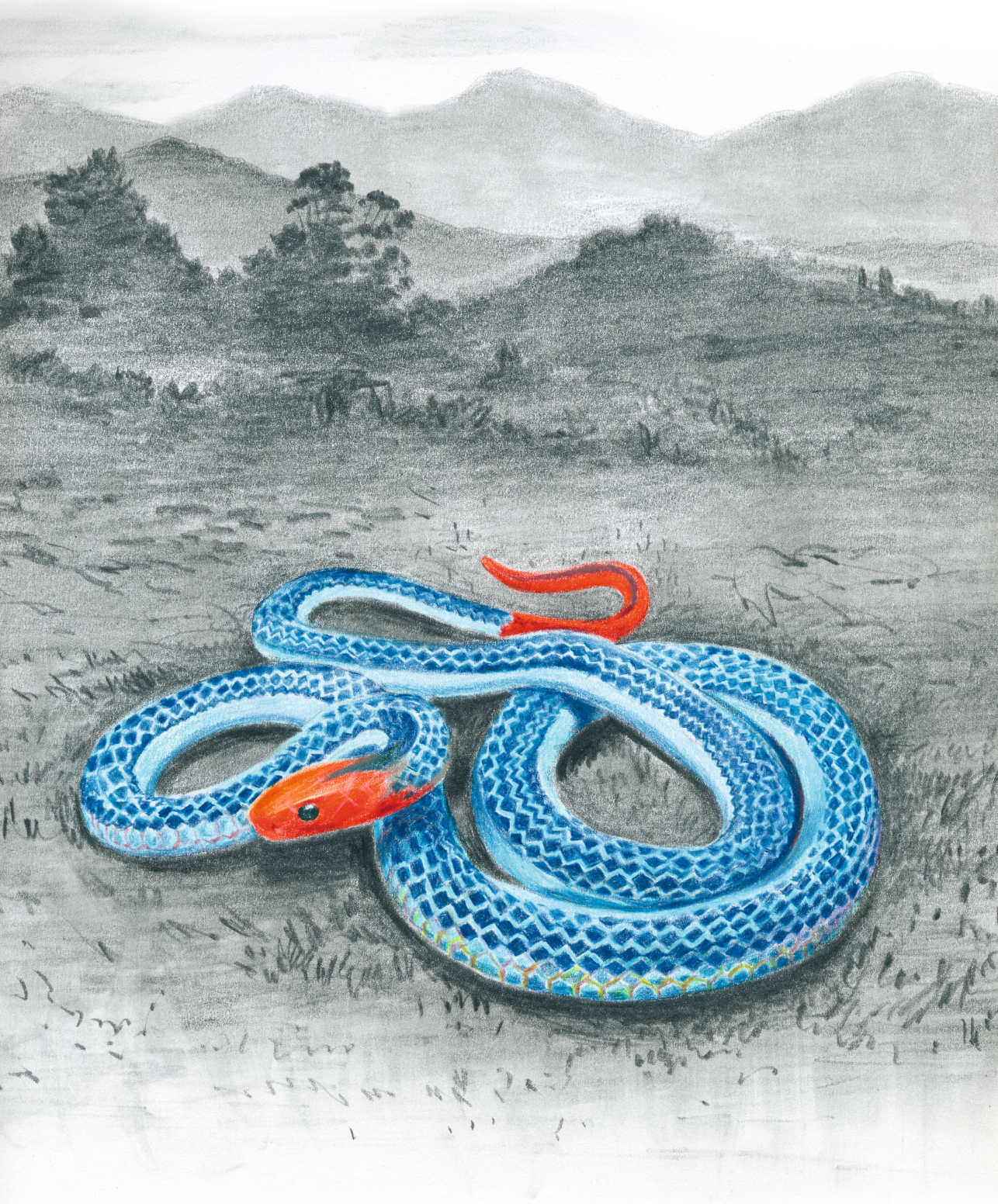

Calliophis bivirgatus

Chapter 7

Bloody insights: using organ-on-a-chip technology to study haemorrhagic activities of snake venoms on endothelial tubules

Mátyás A. Bittenbinder*,
Flavio Bonanini*, Dorota Kurek,
Paul Vulto, Jeroen Kool, Freek J. Vonk

Scientific Reports, 14 (11157)

Abstract

Snakebite envenomation is a major public health issue which causes severe morbidity and mortality, affecting millions of people annually. Of a diverse range of clinical manifestations, local and systemic haemorrhage are of particular relevance, as this may result in ischemia, organ failure and even cardiovascular shock. Thus far, in *vitro* studies have failed to recapitulate the haemorrhagic effects observed *in vivo*. Here, we present an organ-on-a-chip approach to investigate the effects of four different snake venoms on a perfused microfluidic blood vessel model. We assess the impact of the venoms of four snake species on epithelial barrier function, cell viability, and contraction/delamination. Our findings reveal two different mechanisms by which the microvasculature is being affected, either by disruption of the endothelial cell membrane or by delamination of the endothelial cell monolayer from its matrix. The use of our blood vessel model may shed light on the key mechanisms by which tissue-damaging venoms exert their effects on the capillary vessels, which could be helpful for the development of effective treatments against snakebites.

7.1 Introduction

Snakebite is one of the leading global health crises known to date, which claims between 81,000 and 138,000 lives annually, particularly in the (sub)tropical regions of this world [1,2]. Snake venom is comprised of a complex mixture of proteins and peptides, which poses a substantial threat to human life, causing significant morbidity and mortality. Snakebite morbidity, which is mainly caused by the toxins that directly or indirectly destroy cells, may cause permanent disability, which includes severe tissue loss (i.e. muscle and skin), chronic renal diseases and blindness [1,3–6]. Morbidity is estimated to occur in at least 450,000 snake bite victims annually [1,2,5,7].

Many venoms have tissue-damaging activities that may result in a range of pathologies, including muscle and skin necrosis, acute kidney injury and haemorrhage [1,7–9]. The most medically relevant pathology caused by the tissue-damaging components in snake venoms is local and systemic bleeding [1,10]. Local and systemic haemorrhage may further promote ischemia, which may cause acute kidney injury and organ failure and could even lead to cardiovascular shock [1,11,12]. Haemorrhage is a rapid event *in vivo* with capillary endothelial cells showing drastic structural alterations within minutes [13,14].

However, the same tissue-damaging components do not necessarily induce rapid toxicity to endothelial cells *in vitro*. The discrepancy between these two observations may arise from the fact that traditional *in vitro* systems do not take into account the mechanical action of haemodynamic forces acting on the endothelial cells, as is the case with *in vivo* systems [12,15,16]. To date, the study of tissue-damaging effects of snake venom toxins has been primarily based on two-dimensional cell culture models. These do not have the tubular morphology of vasculature found *in vivo* and lack important environmental cues from the cellular microenvironment, such as interaction with an extracellular matrix (ECM) and exposure to flow [17,18]. In an attempt to address this discrepancy, innovative approaches are required that advance our understanding of venom-induced haemorrhage and can be utilised to develop effective treatments. The development of snakebite treatments focusing on the neutralisation of the haemorrhagic effects of snake venom components relies on robust and quantitative *in vitro* models of blood vessels.

Organ-on-a-chip is an emerging technology that utilises microengineering to create three-dimensional (3D) models in microfluidic channel networks. In contrast to cells grown in 2D, blood vessels grown in microfluidic channels enable the inclusion of several important physiological parameters during cell culture, such as 3D tubular morphology, fluid perfusion, inclusion of ECM and exposure to biochemical gradients [19]. Organ-on-a-chip assays have been successfully used for the formation of perfused vascular models, including angiogenesis [20,21], T-cell migration [22], monocyte adhesion [23], vascularisation of spheroids [24] and real-time methods to study vascular barrier function [25]. In this latter study, organ-on-a-chip is combined with high-content imaging systems that enable direct monitoring of vascular barrier, viability and morphology.

In this study, we aimed to use a human blood vessel model grown in an organ-on-a-chip platform to simulate the haemorrhagic effect of different snake venoms while assessing their direct toxicity to endothelial cells. For this, we exposed microfluidic human blood vessels to a panel of four venoms from four different snake species. We used fluorescent tracer molecules and image analysis to assess endothelial barrier function and monitor vascular leakage following venom exposure. Furthermore, we assessed cellular viability and vessel morphology to evaluate the tissue-damaging activities of the snake venoms comprehensively. This allowed us to differentiate between different mechanisms of action by which venoms cause blood vessel disruption.

We found two distinct mechanisms by which the blood vessel is being affected: delamination of the endothelial cell monolayer from its matrix and disruption of the endothelial cell membrane. The workflow presented here could be utilised in the routine assessment of snake toxicity and its tissue-damaging and proteolytic effects and will be helpful for the development of effective snakebite treatments.

7.2 Materials & Methods

7.2.1 Venoms

Venoms were sourced from the library of the Faculty of Science, BioAnalytical Chemistry, Vrije Universiteit Amsterdam (VU). This library contains samples obtained and subsequently provided by the Liverpool School of Tropical

Medicine (LSTM), National University of Singapore (NUS) and captive breeders. The snake venoms used in this study came from the following viper (Viperidae) and elapid (Elapidae) species: *Echis ocellatus* (West African carpet viper, Nigeria), *Bungarus multicinctus* (many-banded krait, locality unknown), *Naja mossambica* (Mozambique spitting cobra, captive bred) and *Naja naja* (Indian cobra, captive bred). Venoms from VU and NUS were lyophilised immediately after milking, then freeze-dried and stored at -80 °C. LSTM venoms were extracted, stored overnight at -20 °C, then lyophilised and stored at 4 °C for the long term. Samples were reconstituted in Milli-Q (mQ) water to the desired stock solutions, depending on the type of assay. These solutions were then aliquoted and subsequently snap-frozen in liquid nitrogen and stored at -80 °C until use. All venoms were sourced in accordance with the Nagoya protocol, where applicable [26].

7.2.2 OrganoPlate culture

OrganoReady Blood Vessel HUVEC 3-lane 64 plates (Mimetas B.V, MI-OR-BV-02) were cultured according to the manufacturer's instructions. The medium was replaced on the day of receiving to OrganoMedium HUVEC-BM (Mimetas B.V.) on the day of receiving the plates. OrganoReady Blood Vessel HUVEC 3-lane 64 are ready-to-use HUVEC tubes in OrganoPlates that follow a similar process for ECM seeding (rat tail collagen 1 at 4mg/mL), endothelial cell seeding and establishment of perfusion through the tubules as described by Duinen et al. for the OrganoPlate 3-lane 40 [19]. The perfusion flow was maintained by placing the plate on an OrganoFlow rocker (Mimetas B.V., MI-OFPR-L) set at 14 degrees with 8-minute intervals optimised for the 3-lane 64 in a humidified incubator (37 °C, 5 % CO_2). This allows the perfusion of the medium through the endothelial tube in an intermittent, bi-directional flow profile with peaks of shear stress of approximately 0.17 Pa. Plates were kept in a humidified incubator (37 °C, 5 % CO_2) for 5 days prior to venom exposure with a complete medium change (50 µL in each in-and outlets) every 2-3 days.

7.2.3 Vascular leakage assessment

A mixture of 10 µg/mL, 1 µg/mL snake venom or 1:100 mQ water (as vehicle control) was prepared in OrganoMedium HUVEC-BM with 0.25 mg/mL

TRITC-labelled 150 kDa Dextran (Sigma, T1287). The medium was then aspirated from all wells of the OrganoPlate, and 20 µl HBSS (Thermo, 14025092) was added to the left channel wells (see A1 and B1 in Figure 1A). 20 µl of venom or control solution was added to the bottom well of the right channel (see B3 in Figure 1A), followed by 40 µl in the top well of the right channel (see A3 in Figure 1A) in a total of four different chips/condition. The plate was then quickly introduced in an ImageXpress Micro XLS microscope (Molecular Devices) with temperature control set at 37 °C. Fluorescent images were acquired every 2 minutes for 30 minutes. The plate was then placed back in a humidified incubator (37 °C, 5 % CO_2) on the OrganoFlow rocker. Additional single timepoint images were acquired 60 minutes and 90 minutes after venom addition. Fluorescence intensity was quantified as average intensity from the gel channel adjacent to the endothelial tubule using Fiji [27].

7.2.4 Assessment of endothelial tubules morphology

A staining solution was prepared in OrganoMedium HUVEC-BM with 2 drops/mL Propidium Iodide Ready Flow™ Reagent (Thermo, R37169), 1:500 SPY650-FastAct™ (reconstituted following manufacturer's instructions), 1:500 Calcein-AM (Thermo, C3099) and 1:1000 Hoechst (Thermo, H3570). Medium from all wells was removed and replaced with 50 µl of staining solution and incubated in an incubator for 1 hour prior to snake venom addition. Bright-field and fluorescent images were acquired using an ImageXpress Micro XLS microscope with a 10X objective. Then, a mixture of 10 µg/mL, 1 µg/mL snake venom or 1:100 mQ (as vehicle control) was prepared in a staining solution. The staining solution was aspirated from the left channel wells of the OrganoPlate (see A1 and B1 in Figure 1A) 20 µl of venom or control solution was then added to the bottom well of the right channel (see B3 in Figure 1A), followed by 40 µL in the top well of the right channel (see A3 in Figure 1A) in a total of three different chips/condition. The plate was placed back on the rocker in the incubator, and images were again acquired after 90 minutes of incubation. For time-lapse acquisition, venom was diluted to 100 µg/mL in a staining solution, and single-slice images were acquired every 10 seconds for 300 seconds using a Micro XLS-C confocal microscope (Molecular Devices) set at 37 °C.

7.2.5 Viability quantification

The propidium iodide (PI) and Hoechst signals were thresholded to a black-and-white image using Fiji. Watershed was applied to segment overlapping nuclei, which were counted in each channel using the built-in analyse particle function. Viability was then expressed as a percentage of the total number of nuclei minus PI-positive nuclei.

7.2.6 Statistical analysis

Significant differences between control and experimental groups without multiple factors were assessed using 1-way ANOVA. Statistical analysis was performed using GraphPad Prism 6.

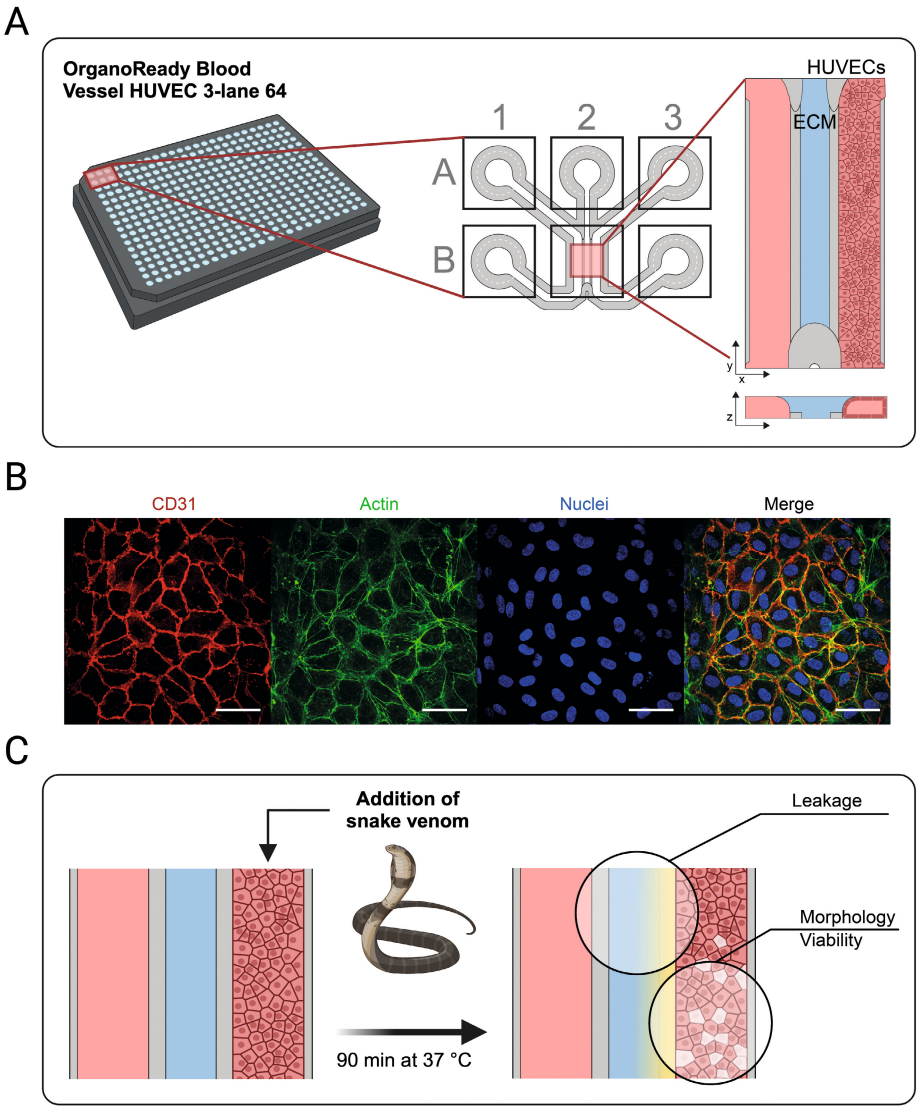

Figure 1. Set-up for studying haemorrhagic activities in the OrganoPlate 3-lane 64. (A) Schematic of the channel arrangement of one culture chip within the OrganoPlate 3-lane 64. (B) Brightfield image of a HUVEC blood vessel grown against the collagen-I-filled middle channel. The scale bar represents 200 µm. (C) Immunofluorescent microscopy images showing the expression of platelet cell adhesion molecule CD31, actin and nuclei of the grown blood vessel. The scale bar represents 50 µm. (D) Schematic overview of the experimental setup. Snake venom is added in combination with fluorescent tracers and live imaging dyes. Live microscopy is used to assess endothelial leakage, morphology and viability.

7.3 Results

7.3.1 Assessment of barrier integrity (i.e., venom-induced vascular leakage)

Figure 1 shows the setup used to assess haemorrhagic effects of snake venoms. A blood vessel was grown in a microfluidic channel by seeding HUVECs against an extracellular matrix, forming a perfused lumenised tubule after 5 days of culture (see Figure 1A). The resulting blood vessel consists of a dense endothelial layer with extensive cell junctions between adjacent cells, as indicated by the expression of CD31 (see Figure 1B). The lumen of the vessel structure was exposed to snake venom, a fluorescent tracer molecule and live imaging dyes for toxicity and morphological assessment (see Figure 1C). Barrier function of the blood vessel was assessed by observing leakage of the fluorescent tracer (FITC-dextran, 150 kDa) to the lumen and measuring leakage into the adjacent gel channel (see S1 Figure).

Figure 2 shows the impact on blood vessel barrier function from a panel of snake venoms. Snake venom of *E. ocellatus* induced extensive leakage within minutes in both 1 and 10 µg/mL concentrations (see Figure 2A, left). Tubule leakage continued to increase at 60 and 90 minutes after venom addition (see Figure 2A, right). *N. mossambica* did not induce vascular leakage during the first 30 minutes (see Figure 2B, left), but significant outflux of dextran was observed after 60 and, in particular, 90 minutes of exposure (see Figure 2B, right). *B. multicinctus* caused significant leakage at 60 and 90 minutes of exposure, but not in a dose-dependent manner (see Figure 2C). *N. naja* at 10 µg/mL induced significant leakage after 30 and 60 minutes, and at 90 minutes, both tested concentrations caused significant dextran leak (see Figure 2D).

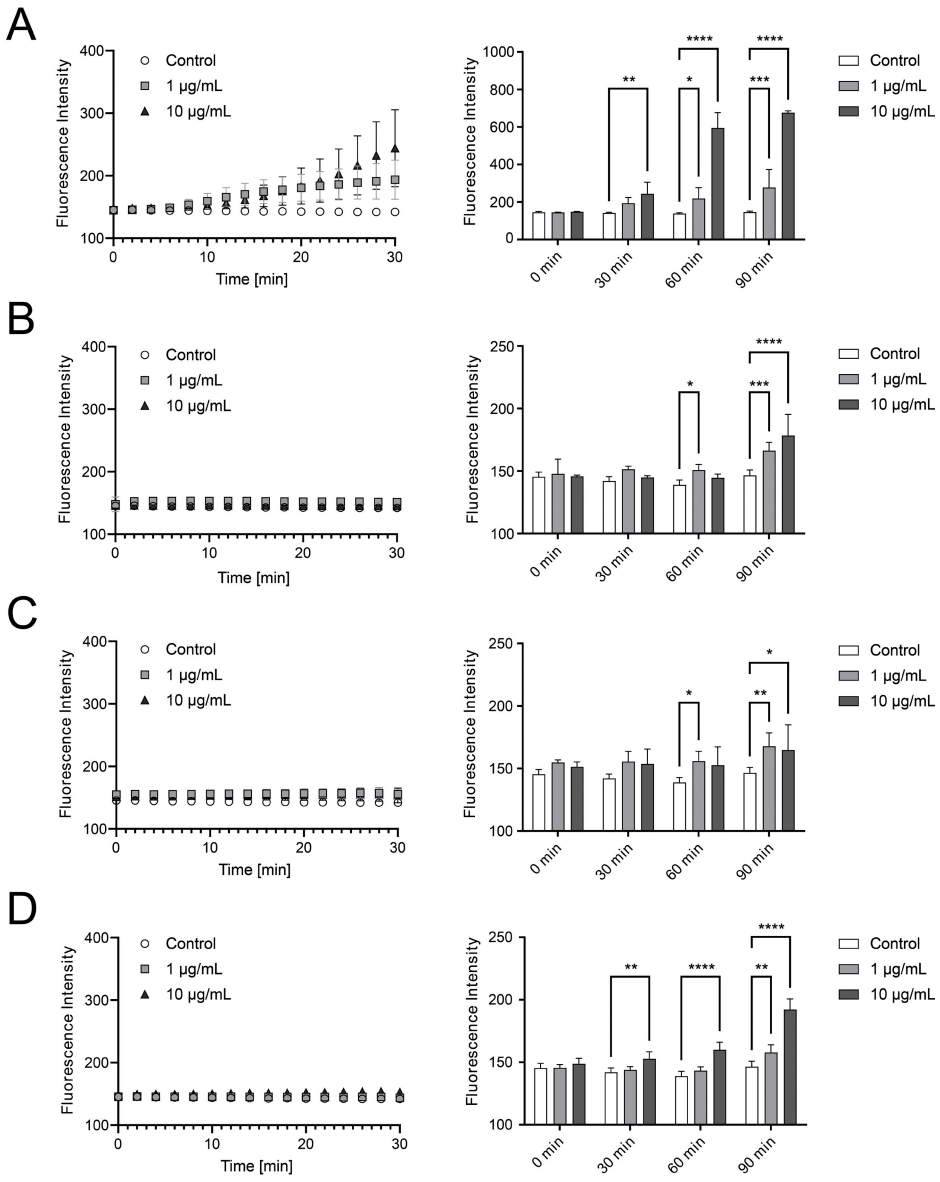

Figure 2. Assessment of venom-induced vascular leakage. Fluorescence intensity was quantified as the average intensity measured from the middle ECM channel as an indication of vascular leakage. The left panel shows the time course of vascular leakage for the first 30 min after venom addition, and the right panel shows fluorescence intensity at 0, 30, 60 and 90 min after venom addition of (A) *E. ocellatus* (B) *N. mossambica* (C) *B. multicinctus* (D) *N. naja*. Measurements are presented as the mean of three individual experiments (N=4); mean ± SD; *p < 0.05, **p < 0.01, ***p < 0.001, ****p < 0.001, 1-way ANOVA, venom exposed vs control).

7.3.2 Morphological assessment of venom exposure to endothelial tubules

We assessed the effect of the venoms on the morphology and structure integrity of the endothelial tubes by microscopy. Endothelial tubes were incubated for 90 minutes with venoms in combination with Calcein-AM, PI and a live actin probe (see Figure 3). We observed drastic structural disruptions for tubes exposed to 10 µg/mL *E. ocellatus* as indicated by delamination and collapse of the structure. In contrast, 1 µg/mL caused smaller, localised gaps in the endothelial layer. The other venoms did not seem to induce the same general structural damage to the endothelial tubules. Still, we observed marked vessel disruption in tubules exposed to 10 µg/mL, as indicated by an extensive loss of Calcein-AM and actin signal in parts of the cell layer. Notably, we observed an increase in actin signal in the remaining cells compared to the control.

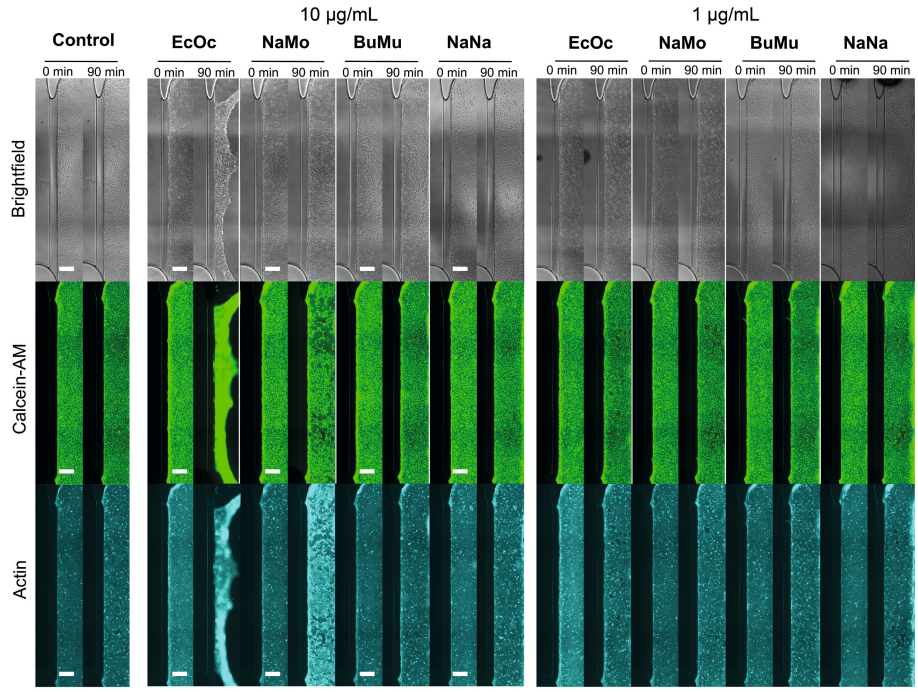

Figure 3. Morphological assessment of endothelial tubules after 90 minutes of snake venom exposure. Brightfield and immunofluorescent microscopy images show the morphology of the endothelial vessels at 0 minutes and 90 minutes after exposure to 1 and 10 µg/mL of snake venom, compared to control. The scale bar represents 200 µm. Abbreviations: EcOc, *E. ocellatus*; NaMo, *N. mossambica*; BuMu, *B. multicinctus*; NaNa, *N. naja*.

7.3.3 Assessment of direct cytotoxic activity

We then assessed whether venoms had a direct cytotoxic effect (i.e., toxins that have a toxic effect directly on the cells) or an indirect cytotoxic effect (e.g., by affecting the ECM, which could eventually lead to cell injury) on the endothelial cells.

To distinguish direct cytotoxicity from indirect effects (matrix remodelling, contraction), we performed a viability assessment by staining and quantifying the number of total and dead cells using Hoechst and PI, respectively (see Figure 4A). 90 minutes after 1 µg/mL venom exposure, we observed a slight but significant reduction in viability for *E. ocellatus* (93%), *N. mossambica* (94%) and *N. naja (*95%), but no change in viability was observed for *B. multicinctus* compared to control (see Figure 4B). Similarly, 10 µg/mL caused a decrease in viability for *N. mossambica* (70%) and *N. naja* (92%). For exposure to *E. ocellatus*, viability could not be determined as tubule contraction prevented from quantifying individual nuclei (see Figure 4B).

At the cellular level, notable differences emerge between the toxic effects of the different venoms in terms of cell morphology. Although at 10 µg/mL, *E. ocellatus* caused complete collapse of the endothelial vessels, 1 µg/mL was sufficient to cause apparent gaps in the Calcein-AM and actin stain of the endothelial layer (see Figure 5). Interestingly, dead cells were observed at the edges of these voids but not within them. Similarly, 10 µg/mL *N. mossambica* caused significant disruption of the cell layer, but, in contrast to *E. ocellatus*, dead cells were clearly visible inside these spaces. Although visibly less potent, we observed a similar pattern for *N. naja* while *B. multicinctus* did not seem to alter the cell layer's morphology to any significant extent.

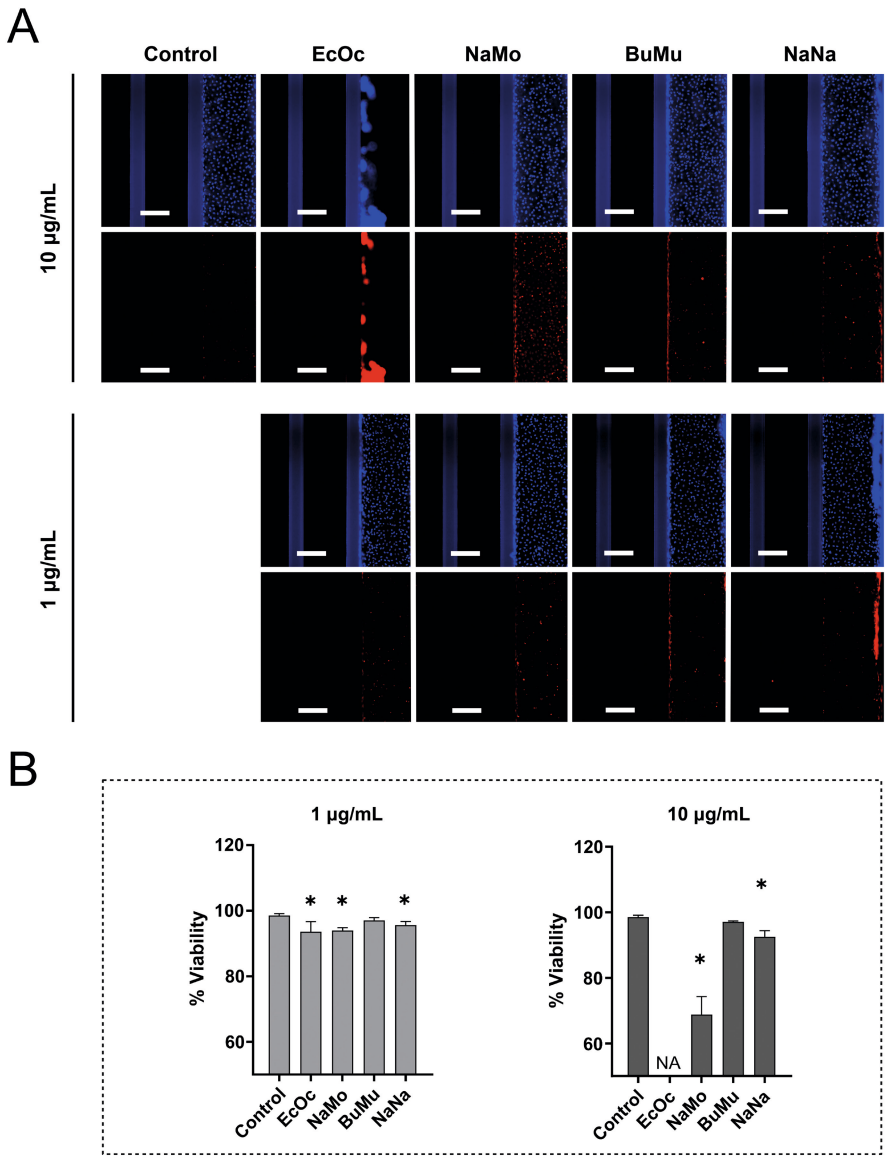

Figure 4. Viability assessment 90 minutes after snake venom exposure. (A) Immunofluorescent microscopy images showing the difference in morphology of the endothelial vessels 90 minutes after exposure to 1 µg/mL and 10 µg/mL of snake venom, compared to control. Hoechst staining is shown in blue (top panels) and PI in red (lower panels). The scale bar represents 200 µm. (B) Quantitative assessments of four species at 1 µg/mL and 10 µg/mL are shown as bar graphs. Measurements are presented as the mean of three Individual experiments (N=4); mean ± SD; *p < 0.05, 1-way ANOVA, venom exposed vs control). Abbreviations: EcOc, *E. ocellatus*; NaMo, *N. mossambica*; BuMu, *B. multicinctus*; NaNa, *N. naja*.

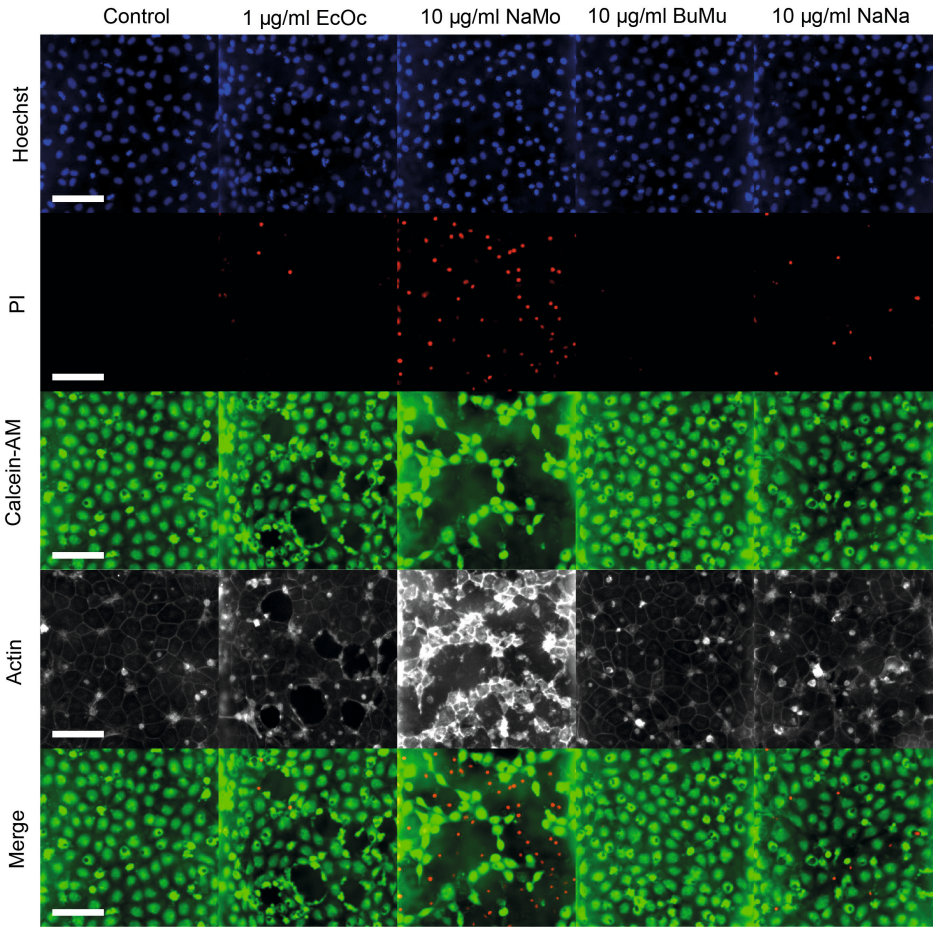

Figure 5. Morphological assessment of direct cytotoxic activity. Immunofluorescent microscopy images showing the difference in morphology of the endothelial vessels after 90 minutes of exposure to snake venom (1 µg/mL or 10 µg/mL), compared to control. Hoechst staining is shown in blue, PI in red, Calcein-AM in green and live-actin in white. The lower panels represent an image in which all four channels are merged. The scale bar represents 100 µm. Abbreviations: EcOc, *E. ocellatus*; NaMo, *N. mossambica*; BuMu, *B. multicinctus*; NaNa, *N. naja*.

To further characterise and confirm the morphological changes at the cellular level as a result of venom exposure, we performed live imaging of endothelial tubules exposed to a higher concentration of 100 µg/mL of venom for 300 seconds. We observe that *E. ocellatus* delaminates the endothelial tubules without inducing significant cell death (see Figure 6, Supplementary Video). In line with previous observations, *N. mossambica* caused direct cytotoxicity, as indicated by a simultaneous loss of Calcein-AM stain and emergence of PI signal in the

nucleus. Notably, cell death seemed to occur preferentially in cells adjacent to already dead cells, which could be a distinct front of cell death propagation. *N. naja* exposure also led to direct cytotoxicity, although to a lesser magnitude compared to *N. mossambica*, and no apparent cell death propagation was observed at this concentration.

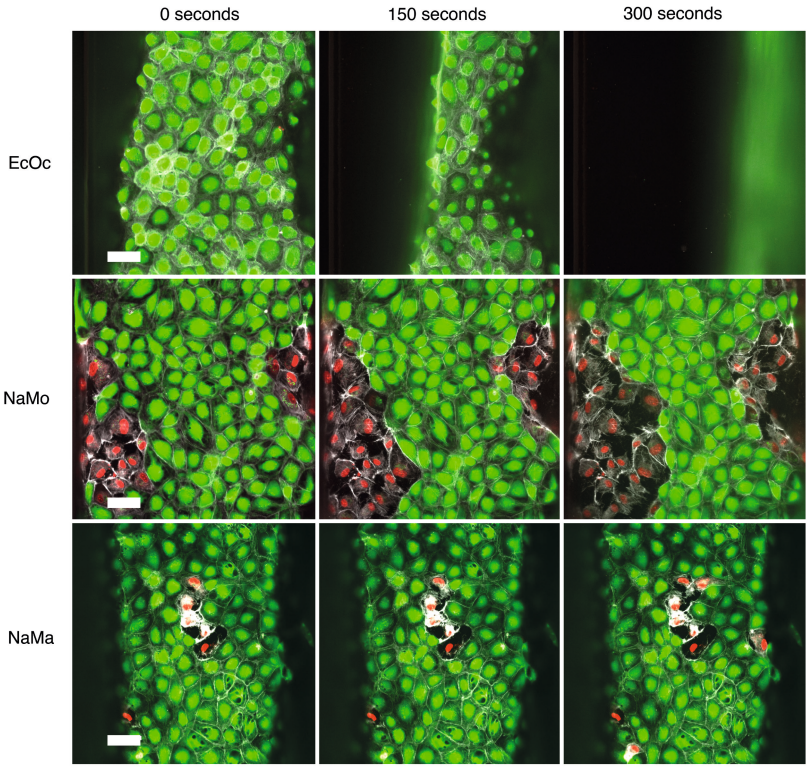

Figure 6. Timelapse of high venom dose exposure on endothelial tubules Immunofluorescent microscopy images show the difference in morphology of the endothelial vessels after 0, 150, and 300 sec of exposure to 100 µg/mL of snake venom compared to the control. PI is shown in red, Calcein-AM is shown in green, and live-actin is shown in white. The scale bar represents 50 µm. Abbreviations: EcOc, *E. ocellatus*; NaMo, *N. mossambica*; BuMu, *B. multicinctus*; NaNa, *N. naja*.

7.4 Discussion

In this study, we utilised an "organ-on-a-chip" approach to study the effect of a panel of snake venoms on a microfluidic blood vessel model that mimics perfused conditions. This was done in an effort to create a model that could predict the effects of these venoms on epithelial barrier function, cell viability and contraction/delamination. The morphological and quantitative data presented in this study show that at least two distinct mechanisms exist by which the endothelial cells are affected by snake venom. The ways by which the endothelial cells are affected by the venoms can be either 'direct' (e.g., affect the cells directly, for example, by disrupting the cellular membrane) or indirect (e.g. by affecting the ECM, which could eventually lead to cell injury). Regardless of the mechanisms of endothelial cell damage, this may lead to vascular leakage (see Figure 7) [6,12,28–30].

The first includes degradation of the ECM, which is observed as the detachment of the cell monolayer from the surrounding tube. The ECM is made up of the interstitial matrix and the basement membrane, which consist of glycoproteins, proteoglycans and fibrous proteins such as collagen and laminin. The ECM is a macromolecular structure that is important for providing structural support to a variety of cell types [29,31–33]. Because of its pivotal role, the ECM provides an important target for various toxin classes with tissue-damaging activities, including snake venom s and hyaluronidases [16,29,34,35]. Degradation of the ECM may affect various cell types, including (skeletal) muscle cells, keratinocytes, kidney cells, and endothelial cells [1,28,29,36–40]. Hydrolysis of the ECM surrounding the capillary endothelial weakens the capillary wall and may ultimately result in vascular leakage [12,13,15,16,29]. This is in line with the observations in this study, in which the detachment of the vessel from its surroundings is accompanied by vascular leakage, which can be seen as the endothelial cells delaminate, as is the case for *E. ocellatus*. In this process, the cell membrane remains intact, shown by the fact that PI is not entering the cell, nor is Calcein-AM leaking out of the cell. The observed effect can, therefore, be considered an indirect cytotoxic effect, which means that cell death occurs as a secondary effect resulting from the ECM degradation and not by directly destroying the endothelial cells [6,12,15]. Initially, proteolytic enzymes degrade the basement membrane and adhesion proteins,

thus weakening the capillary wall and perturbing the interactions between endothelial cells and the basement membrane. The pathological effects described in these cells *in vivo* are therefore argued to be a result of the mechanical action of haemodynamic forces secondarily to the weakening of the basement membrane [12,13,15,29,41,42]. The venoms of *N. mossambica* and *N. naja* did affect the integrity of the vessel to some extent (i.e., lesions can be observed in the top section of the vessel wall and extensive loss of Calcein-AM), the venoms did not seem to affect the ECM of the endothelial cells.

The second mechanism likely involves disruption of the cellular membrane, which can be deduced from the fact that the cell membrane becomes permeable to both PI and Calcein-AM. The destabilisation of the cell membrane is associated with a number of snake venom toxins, including cytotoxic phospholipases A_2, cytotoxic three-finger toxins and β-defensin-like toxins [43,44]. Cellular membranes obviously play a crucial role in normal cell functioning and, therefore, are an optimal target for a variety of toxin classes. These 'true' cytotoxins deploy their effects by altering membrane integrity, in particular, the plasma membrane [45]. Disruption of the membrane may occur via hydrolysis of membrane phospholipids, direct perturbation of the membrane, pore formation and other cell-penetrating mechanisms [43,46–54]. As the venoms of *N. mossambica* and *N. naja* indeed affected cell viability in combination with Calcein-AM leakage from the cells, we can conclude that these venoms have a direct cytotoxic effect. This is in line with observations from previous studies [28]. As cell death occurs preferentially in cells adjacent to apoptotic cells, there might be a mechanism in play that propagates cell death. A possible explanation might be ATP-release secondary to toxin-induced cytotoxicity, which may lead to cell death pathways of neighbouring cells [55–58]. However, future studies on isolated toxins should focus on the exact mechanisms by which these venoms execute their damaging effects on cells.

The venoms of *E. ocellatus* and *B. multicinctus* did not seem to have much impact on membrane stability, as PI uptake and Calcein-AM leakage were similar to negative control. However, the delamination of endothelial tubes for *E. ocellatus* made assessment of cell viability impossible.

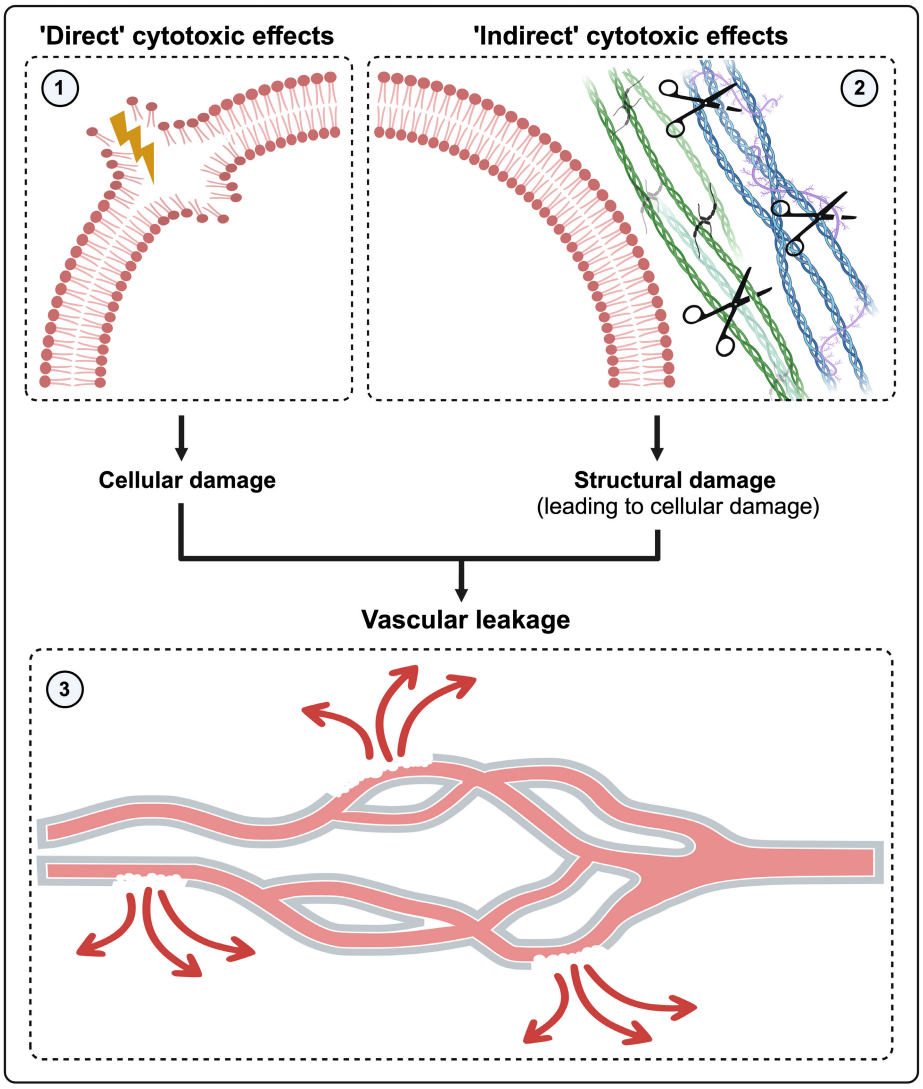

Figure 7. Schematic overview showing the mechanisms by which tissue-damaging toxins exert their effects. (1) 'Direct' cytotoxic effects cause cellular damage by acting directly on the endothelial cells (e.g., by affecting the membrane integrity). (2) The indirect cytotoxic effects (i.e., degradation of various ECM components) cause structural damage, which may contribute to cellular damage indirectly by affecting the stability of endothelial cells. (3) Both mechanisms may ultimately lead to vascular leakage. Image created using www.biorender.com.

7.5 Concluding remarks

In this study, we presented a method to investigate the impact of snake venom on *in vitro*-grown perfused endothelial tubules that are in direct contact with an ECM. This allowed us to study the molecular and cellular mechanisms underlying venom-induced tissue damage in a way that closely resembled conditions in the human body. The use of a microfluidic device replicating the complex physiological micro-environment of the capillary vessel allowed for an accurate, sensitive and real-time study of the tissue-damaging effects of snake venoms on barrier integrity. We studied the impact of four medically relevant snake venoms using this platform and identified two mechanisms by which these venoms affected the microvasculature. The 'direct' cytotoxic effects of *N.mossambica* and *N. naja* venoms affected the cells by disrupting the cellular membrane, whereas the 'indirect' effects of *E. ocellatus* venom affected the ECM, leading to delamination and contraction or collapse of the blood vessel. Based on the findings in this study, the cellular effects of *B. multicinctus* seem to be minimal.

The organ-on-a-chip approach could provide valuable insights into the pathogenesis of haemorrhagic activities of snake venoms and could be used to assess the neutralising capabilities of snakebite treatments in real-time and in near-native conditions. The approach will thus contribute to the development of better, more effective strategies to mitigate snakebite morbidity while reducing the number of survival studies needed on mice.

References

1. Gutiérrez, J. M. *et al.* Snakebite envenoming. *Nat. Rev. Dis. Prim.* **3**, (2017).
2. Longbottom, J. *et al.* Vulnerability to snakebite envenoming : a global mapping of hotspots. *Lancet* **392**, 673–684 (2018).
3. Gutiérrez, J. M., Theakston, R. D. G. & Warrell, D. A. Confronting the neglected problem of snake bite envenoming: The need for a global partnership. *PLoS Med.* **3**, 0727–0731 (2006).
4. Williams, D. J. *et al.* Ending the drought: New strategies for improving the flow of affordable, effective antivenoms in Asia and Africa. *J. Proteomics* **74**, 1735–1767 (2011).
5. Chippaux, J. P. Snakebite envenomation turns again into a neglected tropical disease! *J. Venom. Anim. Toxins Incl. Trop. Dis.* **23**, 1–2 (2017).
6. Bittenbinder, M. A. *et al.* Tissue damaging toxins in snake venoms: mechanisms of action , pathophysiology and treatment strategies. *Commun. Biol.* **7**, (2024).
7. Warrell, D. A. Guidelines of Management of Snake bite. *Lancet* **375**, 77–88 (2010).
8. Kasturiratne, A. *et al.* The global burden of snakebite: A literature analysis and modelling based on regional estimates of envenoming and deaths. *PLoS Med.* **5**, 1591–1604 (2008).
9. Habib, A. G. *et al.* Snakebite is Under Appreciated: Appraisal of Burden from West Africa. *PLoS Negl. Trop. Dis.* **9**, 4–11 (2015).
10. Slagboom, J., Kool, J., Harrison, R. A. & Casewell, N. R. Haemotoxic snake venoms: their functional activity, impact on snakebite victims and pharmaceutical promise. *Br. J. Haematol.* **177**, 947–959 (2017).
11. Sitprija, V. & Sitprija, S. Renal effects and injury induced by animal toxins. *Toxicon* **60**, 943–953 (2012).
12. Gutiérrez, J. M., Escalante, T., Rucavado, A. & Herrera, C. Hemorrhage caused by snake venom metalloproteinases: A journey of discovery and understanding. *Toxins (Basel).* **8**, (2016).
13. Escalante, T., Rucavado, A., Fox, J. W. & Gutiérrez, J. M. Key events in microvascular damage induced by snake venom hemorrhagic metalloproteinases. *J. Proteomics* **74**, 1781–1794 (2011).
14. Ownby, C. L., Fletcher, J. E. & Colberg, T. R. Cardiotoxin 1 from cobra (Naja naja atra) venom causes necrosis of skeletal muscle in vivo. *Toxicon* **31**, 697–709 (1993).
15. Gutiérrez, J. M., Rucavado, A., Escalante, T. & Díaz, C. Hemorrhage induced by snake venom metalloproteinases: Biochemical and biophysical mechanisms involved in microvessel damage. *Toxicon* **45**, 997–1011 (2005).
16. Escalante, T. *et al.* Role of collagens and perlecan in microvascular stability: Exploring the mechanism of capillary vessel damage by snake venom metalloproteinases. *PLoS One* **6**, (2011).
17. Duinen, V. Van *et al.* Perfusable vasculature on a High-Throughput Microfluidic Platform. 3.
18. Wevers, N. R. *et al.* A perfused human blood-brain barrier on-a-chip for high-throughput assessment of barrier function and antibody transport. *Fluids Barriers CNS* **15**, 1–12 (2018).
19. van Duinen, V. *et al.* Perfused 3D angiogenic sprouting in a high-throughput in vitro platform. *Angiogenesis* **22**, 157–165 (2019).

20. van Duinen, V. *et al.* Robust and scalable angiogenesis assay of perfused 3D human ipsc-derived endothelium for anti-angiogenic drug screening. *Int. J. Mol. Sci.* **21**, 1–9 (2020).

21. Van Duinen, V. *et al.* 96 Perfusable Blood Vessels To Study Vascular Permeability in Vitro. *Sci. Rep.* **7**, 1–11 (2017).

22. de Haan, L. *et al.* A Microfluidic 3D Endothelium-on-a-Chip Model to Study Transendothelial Migration of T Cells in Health and Disease. *Int. J. Mol. Sci.* **22**, (2021).

23. Poussin, C. *et al.* 3D human microvessel-on-a-chip model for studying monocyte-to-endothelium adhesion under flow - application in systems toxicology. *ALTEX* **37**, 47–63 (2020).

24. Bonanini, F. *et al.* In vitro grafting of hepatic spheroids and organoids on a microfluidic vascular bed. *Angiogenesis* **25**, 455–470 (2022).

25. Ehlers, H. *et al.* Vascular inflammation on a chip: A scalable platform for trans-endothelial electrical resistance and immune cell migration. *Front. Immunol.* **14**, 1118624 (2023).

26. CBD Secretariat. Nagoya Protocol on Access To Genetic Resources and the Fair and Equitable Sharing of Benefits Arising from their Utilization to the convention on biological diversity - Text and annex. *Nagoya Protoc.* **12**, 1–320 (2011).

27. Schindelin, J. *et al.* Fiji: an open-source platform for biological-image analysis. *Nat. Methods 2012 97* **9**, 676–682 (2012).

28. Bittenbinder, M. A. *et al.* Development of a high-throughput in vitro screening method for the assessment of cell-damaging activities of snake venoms. *PLoS Negl. Trop. Dis.* **17**, e0011564 (2023).

29. Gutiérrez, J. M., Escalante, T., Rucavado, A., Herrera, C. & Fox, J. W. A comprehensive view of the structural and functional alterations of extracellular matrix by snake venom metalloproteinases (SVMPs): Novel perspectives on the pathophysiology of envenoming. *Toxins (Basel).* **8**, (2016).

30. Reeks, T. A., Fry, B. G. & Alewood, P. F. Privileged frameworks from snake venom. *Cell. Mol. Life Sci.* **72**, 1939–1958 (2015).

31. *Biology of Extracellular Matrix Series. Matrix Metalloproteinases* (Springer, 1998). doi:10.1016/b978-0-12-545090-4.50015-x.

32. Alberts, B. *et al. Essential cell biology: Fifth international student edition*. (WW Norton & Company., 2018).

33. Frantz, C., Stewart, K. M. & Weaver, V. M. The extracellular matrix at a glance. *J. Cell Sci.* **123**, 4195–4200 (2010).

34. Markland, F. S. & Swenson, S. Snake venom metalloproteinases. *Toxicon* **62**, 3–18 (2013).

35. Girish, K. S., Jagadeesha, D. K., Rajeev, K. B. & Kemparaju, K. Snake venom hyaluronidase: An evidence for isoforms and extracellular matrix degradation. *Mol. Cell. Biochem.* **240**, 105–110 (2002).

36. Teixeira, C., Cury, Y., Moreira, V., Picolo, G. & Chaves, F. Inflammation induced by Bothrops asper venom. *Toxicon* **54**, 67–76 (2009).

37. Sitprija, V. Animal toxins and the kidney. *Nat. Clin. Pract. Nephrol.* **4**, 616–627 (2008).

38. Jiménez, N., Escalante, T., Gutiérrez, J. M. & Rucavado, A. Skin pathology induced by snake venom metalloproteinase: Acute damage, revascularization, and re-epithelization in a mouse ear model. *J. Invest. Dermatol.* **128**, 2421–2428 (2008).

39. Baldo, C., Jamora, C., Yamanouye, N., Zorn, T. M. & Moura-da-Silva, A. M. Mechanisms of vascular damage by hemorrhagic snake venom metalloproteinases: Tissue distribution and in Situ hydrolysis. *PLoS Negl. Trop. Dis.* **4**, (2010).

40. Herrera, C. *et al.* Tissue Localization and Extracellular Matrix Degradation by PI, PII and PIII Snake Venom Metalloproteinases: Clues on the Mechanisms of Venom-Induced Hemorrhage. *PLoS Negl. Trop. Dis.* **9**, 1–20 (2015).

41. Clemetson, K. J., Lu, Q. & Clemetson, J. M. Snake C-type lectin-like proteins and platelet receptors. *Pathophysiol. Haemost. Thromb.* **34**, 150–155 (2006).

42. Rucavado, A. *et al.* Inhibition of local hemorrhage and dermonecrosis induced by Bothrops asper snake venom: Effectiveness of early in situ administration of the peptidomimetic metalloproteinase inhibitor batimastat and the chelating agent CaNa2EDTA. *Am. J. Trop. Med. Hyg.* **63**, 313–319 (2000).

43. Fry, B. G. *Venomous reptiles and their toxins: evolution, pathophysiology and biodiscovery. Oxford University Press, Oxford University Press.* (2015). doi:10.1016/0041-0101(71)90017-1.

44. Gopalakrishnakone, P., Inagaki, H., Vogel, C., Mukherjee, A. K. & Rahmy, T. R. *Snake Venoms.* (Springer Berlin, Germany., 2017).

45. Powell, R. Snakes. in *Encyclopedia of Toxicology* 57–60 (Elsevier, 2005).

46. Montecucco, C., Gutiérrez, J. M. & Lomonte, B. Cellular pathology induced by snake venom phospholipase A2 myotoxins and neurotoxins: Common aspects of their mechanisms of action. *Cell. Mol. Life Sci.* **65**, 2897–2912 (2008).

47. Hayashi, M. A. F. *et al.* Cytotoxic effects of crotamine are mediated through lysosomal membrane permeabilization. *Toxicon* **52**, 508–517 (2008).

48. Kini, R. M. Excitement ahead: Structure, function and mechanism of snake venom phospholipase A2 enzymes. *Toxicon* **42**, 827–840 (2003).

49. Sunagar, K. *et al.* Three-fingered RAVERs: Rapid Accumulation of Variations in Exposed Residues of snake venom toxins. *Toxins (Basel).* **5**, 2172–2208 (2013).

50. Kini, R. M. & Doley, R. Structure, function and evolution of three-finger toxins: Mini proteins with multiple targets. *Toxicon* **56**, 855–867 (2010).

51. Utkin, Y. N. Last decade update for three-finger toxins: Newly emerging structures and biological activities. *World J. Biol. Chem.* **10**, 17–27 (2019).

52. Pucca, M. B. *et al.* Unity Makes Strength: Exploring Intraspecies and Interspecies Toxin Synergism between Phospholipases A2 and Cytotoxins. *Front. Pharmacol.* **11**, 1–10 (2020).

53. Forouhar, F. *et al.* Structural basis of membrane-induced cardiotoxin A3 oligomerization. *J. Biol. Chem.* **278**, 21980–21988 (2003).

54. Kerkis, I., Silva, F. D. S., Pereira, A., Kerkis, A. & Rádis-Baptista, G. Biological versatility of crotamine a cationic peptide from the venom of a South American rattlesnake. *Expert Opin. Investig. Drugs* **19**, 1515–1525 (2010).

55. Zhang, C., Medzihradszky, K. F., Sánchez, E. E., Basbaum, A. I. & Julius, D. Lys49 myotoxin from the Brazilian lancehead pit viper elicits pain through regulated ATP release. *Proc. Natl. Acad. Sci. U. S. A.* **114**, E2524–E2532 (2017).

56. Cintra-Francischinelli, M. *et al.* Bothrops snake myotoxins induce a large efflux of ATP and potassium with spreading of cell damage and pain. *Proc. Natl. Acad. Sci. U. S. A.* **107**, 14140–14145 (2010).

57. Bours, M. J. L., Swennen, E. L. R., Di Virgilio, F., Cronstein, B. N. & Dagnelie, P. C. Adenosine 5′-triphosphate and adenosine as endogenous signaling molecules in immunity and inflammation. *Pharmacol. Ther.* **112**, 358–404 (2006).

58. Di Virgilio, F. Liaisons dangereuses: P2X7 and the inflammasome. *Trends Pharmacol. Sci.* **28**, 465–472 (2007).

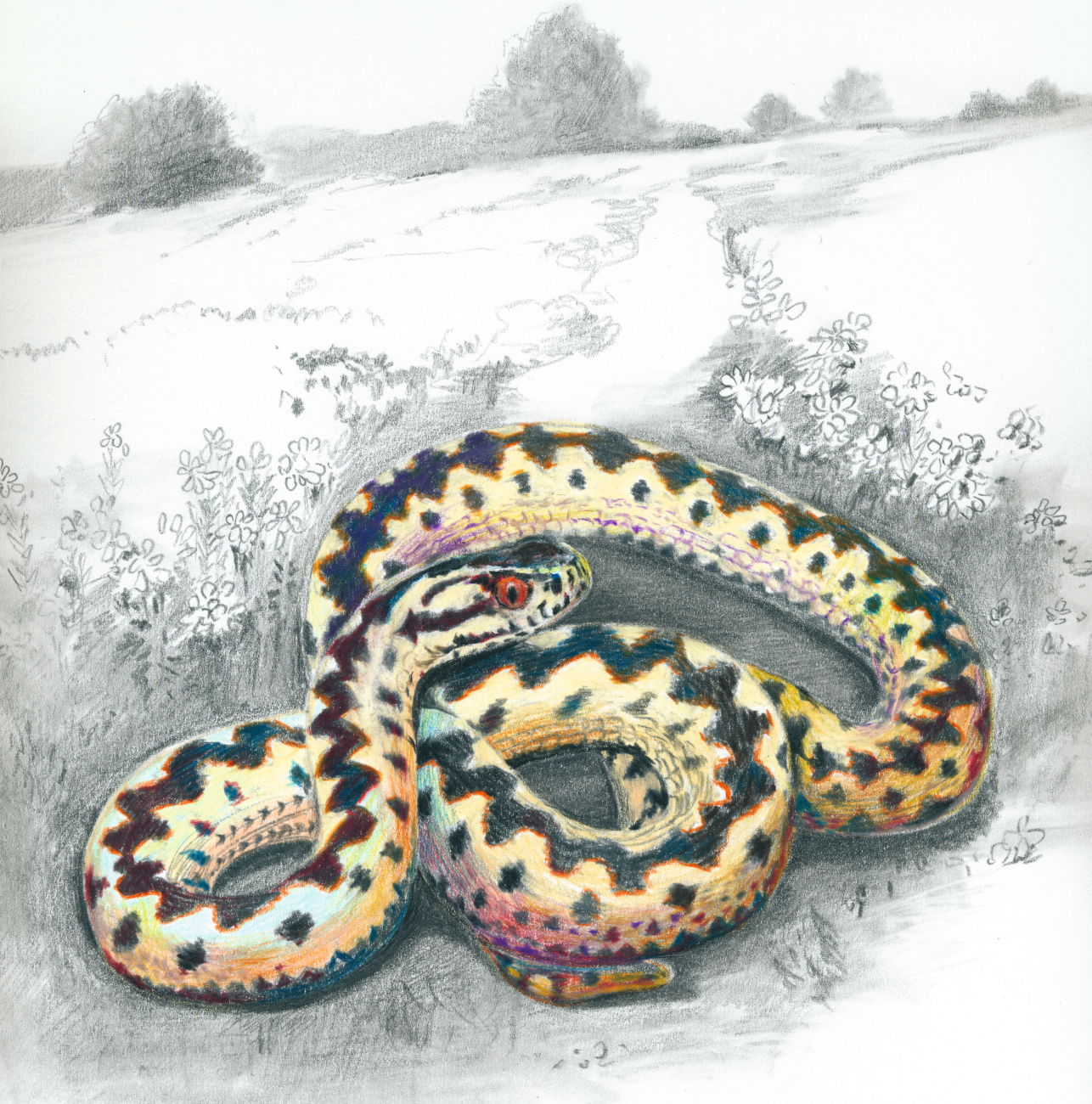

Vipera berus

Chapter 8

Discussion, future perspectives & concluding remarks

8.1 Discussion and future perspectives

The research presented in this thesis has hopefully contributed to a better understanding of various aspects of cell- and tissue-damaging snake venoms. Combining multiple *in vitro* assays allowed the detailed study of the cell-damaging effects of a panel of medically relevant snake venoms.

8.1.1 Why study venom-induced tissue damage?

The first chapter of the thesis starts with a general introduction to venomous snakes, followed by an overview of snakebite envenoming, emphasising its global health impact. The chapter then discusses haemotoxicity and neurotoxicity and focuses specifically on venom-induced cell- and tissue damage. The tissue-damaging effects are the primary cause of morbidity, resulting in (long-term) disabilities, including local and systemic tissue loss, (acute) kidney injuries, haemorrhage, blistering, and other debilitating pathologies. Despite the fact that the tissue-damaging activities in snake venoms affect an estimated 450,000 individuals annually, research on these effects has been relatively limited compared to neurotoxic and haemotoxic effects. The reason for this could be the fact that the neurotoxic and haemotoxic effects often lead to rapid and severe symptoms, including respiratory failure or bleeding disorders.

In contrast, some of the tissue-damaging effects, such as local tissue damage, pain, and swelling, are not immediately life-threatening and may, therefore, have received less attention from a research perspective. However, the tissue-damaging toxins may also cause life-threatening systemic effects such as rhabdomyolysis (i.e., systemic muscle necrosis), leading to acute kidney failure and cardiovascular shock (as a result of systemic bleeding and plasma extravasation). This underpins the relevance of studying the mechanical aspects that are the basis for these pathologies.

8.1.2 A shift in the nomenclature of tissue-damaging toxins

The traditional categorisation of toxin (sub)classes is primarily based on the tissue these toxins predominantly affect, such as myotoxins (i.e., toxins targeting target skeletal muscle cells) or cardiotoxins (i.e., toxins that target cardiomyocytes). This, however, oversimplifies the complexity of these toxins

and does not take into account their mechanical aspects, which is also the case for cell- and tissue-damaging toxins. Chapter 2, therefore, provides a new way of classifying the tissue-damaging toxins into 'true' cytotoxins (directly affecting cells) and extracellular matrix (ECM)-degrading enzymes (indirectly causing cell death). The work further provides an overview of the pathological impacts of tissue-damaging toxins and potential treatment options. This chapter thereby contributes to our understanding of the bioactivity associated with tissue-damaging toxins in snake venoms.

8.1.3 Assessing cell-damaging activities of snake venoms using a high-throughput *in vitro* screening method

In order to gain more knowledge on the mechanical aspects of cell- and tissue damage caused by snake venoms, a panel of cell-based assays was used and integrated in nanofractionation analytics. For this, a number of established cellular bioassays were combined with fluorescence microscopy, which was used to assess cell-damaging actions of the venoms of a selection of medically relevant snake species. This showed that two distinct mechanisms were involved, which were more or less specific for each of both families of venomous snakes (i.e., Viperidae or Elapidae). The viper venoms affected the cell monolayer in such a way that it would detach from its surroundings. This effect is likely caused by the proteolytic activities of specific venom components that cause the degradation of extracellular matrix components. This ultimately results in the partial or complete detachment of the cell monolayer. The venoms of elapids did not affect the ECM but rather exerted their effects by disrupting the cell membrane integrity. In an attempt to identify which toxin families were causing the observed activities, the *in vitro* assays were then integrated into nanofractionation analytics. This involves LC separation of a venom followed by bioassaying and protein identification through high throughput (HT) venomics. A venom of each snake family was fractionated using reversed-phase chromatography (RP-LC) and size-exclusion chromatography (SEC). A challenge remains when using the 'standard' RP-LC separation, in which some toxin classes are subject to denaturation as a result of the solvent conditions, resulting in a loss in bioactivity. This is similar to what previous studies have found on the effects of organic modifiers and acidifiers on protein stability. To overcome this problem, SEC was tested for

separating the viper venom, as this separation method uses non-denaturing salt buffers as eluent. This approach demonstrated that venom fractions separated with a non-denaturing buffer retained activity, showing effects comparable to what was observed in the crude venom. These outcomes indicate that the stability of certain toxins classes should be taken into account when choosing the optimal LC separation method for bioactivity profiling. However, although SEC offers separation of the toxins in their native form, the resolution with this chromatographic method is lower. Future studies should, therefore, look at alternative separation methods that combine the advantages of both approaches, such as ion exchange chromatography (IEX) and hydrophobic interaction chromatography (HIC).

Although this study offers a methodology based on a single cell type, it effectively distinguished between membrane disruption and ECM degradation caused by venom. This study, thereby, is valuable for better understanding venom-induced cell- and tissue damage and offers an excellent basis for the development of other *in vitro* assays for studying (local) tissue damage. In future studies, it would be interesting to see whether the observed effects are similar for different cell types (e.g., muscle cells or keratinocytes) or whether these cells respond differently. It is essential to consider the fact that venom-induced pathologies often involve multiple tissues and that different tissues (and thus cell types) may have varying susceptibility to specific venom components. By testing various cell types, a more comprehensive understanding of the mechanisms underlying venom-induced tissue damage can be achieved.

8.1.4 Developing *in vitro* assays for studying ECM degradation

To look further into the mechanisms responsible for the detachment of the cell monolayer, the thesis then focused on studying ECM degradation in more detail. The ECM consists of various polymers such as collagen, laminin and fibronectin and is critical for cellular support and barrier function. The ECM, therefore, is a prime target for proteolytic venom components such as SVMPs. Chapter 4 described the development of a new screening assay that uses a range of fluorescent ECM components to study the proteolytic activity of snake venoms. The study used polyacrylamide gel electrophoresis to assess the degradation of fluorescent ECM-substrates over time by a panel of medically

relevant snake species, some with known ECM-degrading activity and some that were expected to be devoid of any proteolytic activity. The first part of the research used fluorescently labelled ECM-substrates (i.e., gelatin, collagen I, elastin, fibronectin, laminin and hyaluronic acid), which were incubated with venom to assess overall proteolytic activity. This clearly showed that although some venoms had potent proteolytic activities on all substrates, other venoms were specific for a particular ECM component (e.g., hyaluronic acid), others were completely devoid of any activity.

The study successfully showed that this setup could be used to monitor potency and kinetics for the degradation of fluorescent ECM-substrates by specific snake venoms. In addition, the use of small-molecule metalloproteinase inhibitors demonstrated that proteolytic activity could be inhibited, thereby illustrating that this method could also be used for the identification of novel snakebite therapeutics. Lastly, in-gel zymography was used to identify proteolytically active components with substrate-specific activities. In conventional zymography, non-fluorescent substrates (e.g., gelatin) are co-polymerised with the gel in order to obtain zymograms of the venom proteins with proteolytic activity. As a next step, it was investigated whether it was possible to use dye-quenched fluorescent ECM-substrates in a principle that was named 'fluo-zymography'. Each of the fluorescent substrates (i.e., gelatin, collagen type I, and elastin) consists of a fluorophore (i.e., dye) linked to a quencher molecule, causing the fluorescence to be quenched or suppressed. When the substrate is intact, the quencher suppresses the fluorescence emitted by the dye. However, as soon as the substrate is cleaved or degraded by proteolytic enzymes, the fluorophore and quencher are separated, leading to a significant increase in fluorescence. This fluorescence increase can then be used as a measurable signal indicating proteolytic activity.

This approach allowed the real-time study of in-gel proteolytic activity, which is impossible with conventional zymography. As a last step, the identification of bioactive toxins was done using in-gel tryptic digestion, followed by proteomics analysis of the resulting tryptic digests for toxin identification. The substrate-degrading activity was likely the result of the SVMPs, as these were identified after in-gel tryptic digestion followed by nanoLC-MS/MS. In addition, SVMPs are relatively abundant in the venoms and are known for their proteolytic activities on specific ECM-substrates. The use of SVMP inhibitors validated the

vital role of these proteolytic toxins in ECM degradation. Although effective, this approach however requires manual selection and cutting of proteolytically active fractions from the gel, which makes this an assay with a limited throughput. This is a serious challenge when the goal is to study the activity of dozens of proteolytically active toxins from a range of different snake venoms.

The efforts to study proteolytic degradation in a medium- to high-throughput fashion required the development of an assay for proteolytic activity that can be measured on a plate reader. Chapter 5 describes the development of a fluorometric-based assay to study proteolytic degradation by snake venom toxins using two dye-quenched ECM-substrates (i.e., gelatin and collagen type I). Similar to the approach described above, the increase in fluorescence emitted from the dye-quenched substrates in response to a particular venom is measured. The intensity of the fluorescence directly correlates with the degree of substrate degradation, providing a quantitative measure of the proteinase activity. To validate the assay, the proteolytic activity of a panel of medically relevant snake species was measured kinetically. The viper venoms showed a high level of gelatin and collagen I degradation, even surpassing the positive control at higher venom concentrations. The elapid venoms exhibited lower proteolytic activities compared to the viper venoms. These results suggest that venoms rich in SVMPs do not necessarily have a higher proteolytic activity than venoms with less SVMPs. Although a clear difference can be observed between SVMP-rich viper (i.e., SVMP-rich venoms) and elapid venoms (i.e., relatively low in SVMP content), data within these families indicate that overall higher SVMP contents do not have to coincide with higher proteolytic activity. The next step in this study was to try and identify the toxins responsible for proteolytic activity, which again was done by combining the assay with nanofractionation analytics. In order to maintain proteolytic activity, SEC was used, followed by post-column fractionation to collect the toxins for further bioassaying and HT venomics (i.e., done in parallel). The results demonstrated that this combined approach could be used successfully for the detection of ECM-degrading activities in crude and fractionated snake venoms. However, as discussed in Chapter 3, the use of SEC in this study could be more optimal in terms of its chromatographic resolution, and future studies should, therefore also consider alternative separation methods.

8.1.5 Developing an *in vitro* assay for studying membrane disruption

Chapter 6 describes the development of an assay that can be used to study venom-induced membrane degradation and that is suitable for high-throughput screening of crude and fractionated venoms. The assay used fluorescently dyed phospholipid vesicles from egg yolk as a substrate. This allowed the study of vesicle degradation using a fluorescence plate reader. The first part of the study describes the development and optimisation of the assay, which is followed by validation of the assay using venoms of a number of medically relevant snake species. As a next step, neutralisation studies were performed using varespladib, which is a dedicated phospholipase A_2 (PLA_2) inhibitor. This data suggested that the responsible toxins were likely to be part of the PLA_2 family. To further substantiate this claim, the last part of the study used RP-LC to separate and fractionate two venoms, after which the fractionated venom toxins were bioassayed using the vesicle degradation assay. The reason for using RP-LC instead of SEC is the fact that previous observations (see Chapter 3) indicated that the toxins responsible for the membrane-disrupting effects are not affected by the volatile buffers used with RP-LC. Parallel to post-column fractionation for the bioassay, HT venomics was performed on the fractionated venoms in an attempt to characterise the bioactive toxins. Analysis of the bioactive fractions revealed the presence of PLA_2s, indicating a role in the observed vesicle degradation. Neutralisation studies using a specific PLA_2 inhibitor (i.e., varespladib) further supported this observation, which suggests that the observed vesicle-degrading effect could be caused exclusively by PLA_2s. This would indicate that the vesicle-degradation assay could be used for specifically monitoring PLA_2 activity, although further research should be done to substantiate this claim.

8.1.6 Advancing the way in which we use cell-based assays to study tissue-damaging effects of snake venoms

Chapter 7 focused on investigating the tissue-damaging effects of snake venoms on microvasculature. This was done in an attempt to better understand the mechanisms underlying local and systemic haemorrhage, which can be a severe and sometimes life-threatening result of tissue-damaging toxins. This study utilised an 'organ-on-a-chip' model to study the effect of a panel of snake venoms

on a microfluidic blood vessel model that resembles *in vivo* conditions. This was done in an effort to create a model that could predict the effects of these venoms on epithelial barrier function, cell viability, and contraction/delamination. The approach can be used to investigate the tissue-damaging effects of snake venoms on *in vitro* perfused endothelial tubules, thereby mimicking the complex conditions of human capillary vessels. This offers insights into the molecular and cellular mechanisms underlying venom-induced tissue damage. Based on the outcomes of the study, two distinct mechanisms of action could be identified, which show similarities with the activities observed in Chapter 2. The viper venoms affected the ECM, resulting in vessel delamination and contraction, whereas the venoms of two elapids exhibited direct cytotoxic effects by disrupting cellular membranes. The use of a 3D-microvessel model replicating the complex physiological micro-environment of the capillary vessel allowed for an accurate, sensitive and real-time study of the tissue-damaging effects of snake venoms on barrier integrity. The findings of this study could be used to better understand the venom activities leading to haemorrhage. This three-dimensional blood vessel model may contribute to the development of better, more effective strategies to mitigate snakebite morbidity. At the same time, it may reduce the number of survival studies needed on mice. Future studies could be used to examine in more detail the effects on endothelial microvasculature and the molecular pathways in which the venom toxins exert their effects. The model offers excellent potential for follow-up studies, such as studying the impact of isolated SVMPs on this model to see whether there is a difference in proteolytic activity between the various subfamilies of SVMPs.

8.2 Concluding remarks

The research presented in this thesis aimed to explore the various facets of venom-induced cell- and tissue damage. The study encompasses a comprehensive examination of the underlying molecular mechanisms contributing to this pathology, which affects at least 450,000 people per year. This thesis has focused on various aspects of the cell- and tissue-damaging activities of snake venoms and set out to combine bioactivity profiling with toxin identification. The

ultimate goal was to develop bioassays that could be used to study either the ECM-degrading and membrane-disrupting effects of snake venoms or combine this with nanofractionation analytics for high-throughput screening of tissue-damaging snake venoms. This approach involves LC separation followed by mass spectrometry analysis in parallel with collecting high-resolution fractions in microwell plates. By directly combining bioassays and by performing MS detection, the toxins of interest can be directly identified from the MS data that was acquired in parallel (i.e., LC-MS and/or toxin proteomics data).

Future studies should also investigate alternative chromatographic methods that combine the advantages of good chromatographic resolution and separation of the toxins in their native form. These include ion exchange chromatography (IEX) and hydrophobic interaction chromatography (HIC). The former uses the interactions between charged molecules in a sample (i.e., snake venom) and charged sites on a solid support matrix to separate the molecules based on their charge. HIC separates molecules based on their hydrophobicity along a salt gradient. Molecules with higher hydrophobicity interact more strongly with the stationary phase and are retained longer, which leads to a slower elution from the column. Both methods have their advantages and disadvantages; however, these methods fall outside of the scope of this study.

Future research could further expand the study of snake venom-induced cell damage by incorporating various cell types beyond kidney cells and endothelial cells. This is crucial because different cell types, such as muscle cells, keratinocytes, and endothelial cells, may exhibit distinct responses to venom toxins. Understanding these differences will provide a more comprehensive picture of venom-induced pathologies, which often involve multiple tissues.

Although outside the scope of this thesis, future work could further focus on the molecular pathways involved in venom-induced cytotoxicity, particularly those leading to cell death and tissue damage. Additionally, there is a need to bridge the gap in understanding the *in vivo* effects of venom toxins, particularly regarding inflammatory responses and other endogenous processes in cell- and tissue damage. By doing this, clinical outcomes of envenomation could be better predicted, which could be used to improve targeted therapies to mitigate the devastating effects of venom-induced tissue damage.

Lastly, it is essential to incorporate neutralisation studies and explore the use of novel inhibitory compounds, such as small-molecule inhibitors. However, the challenge remains that a single inhibitor may not effectively neutralise all toxin classes, therefore suggesting the need for a combination approach for a broad-spectrum treatment against snakebites.

By addressing all the above, future studies will achieve a deeper understanding of the mechanisms underlying venom-induced tissue damage and improve therapeutic strategies for snakebite victims.

8

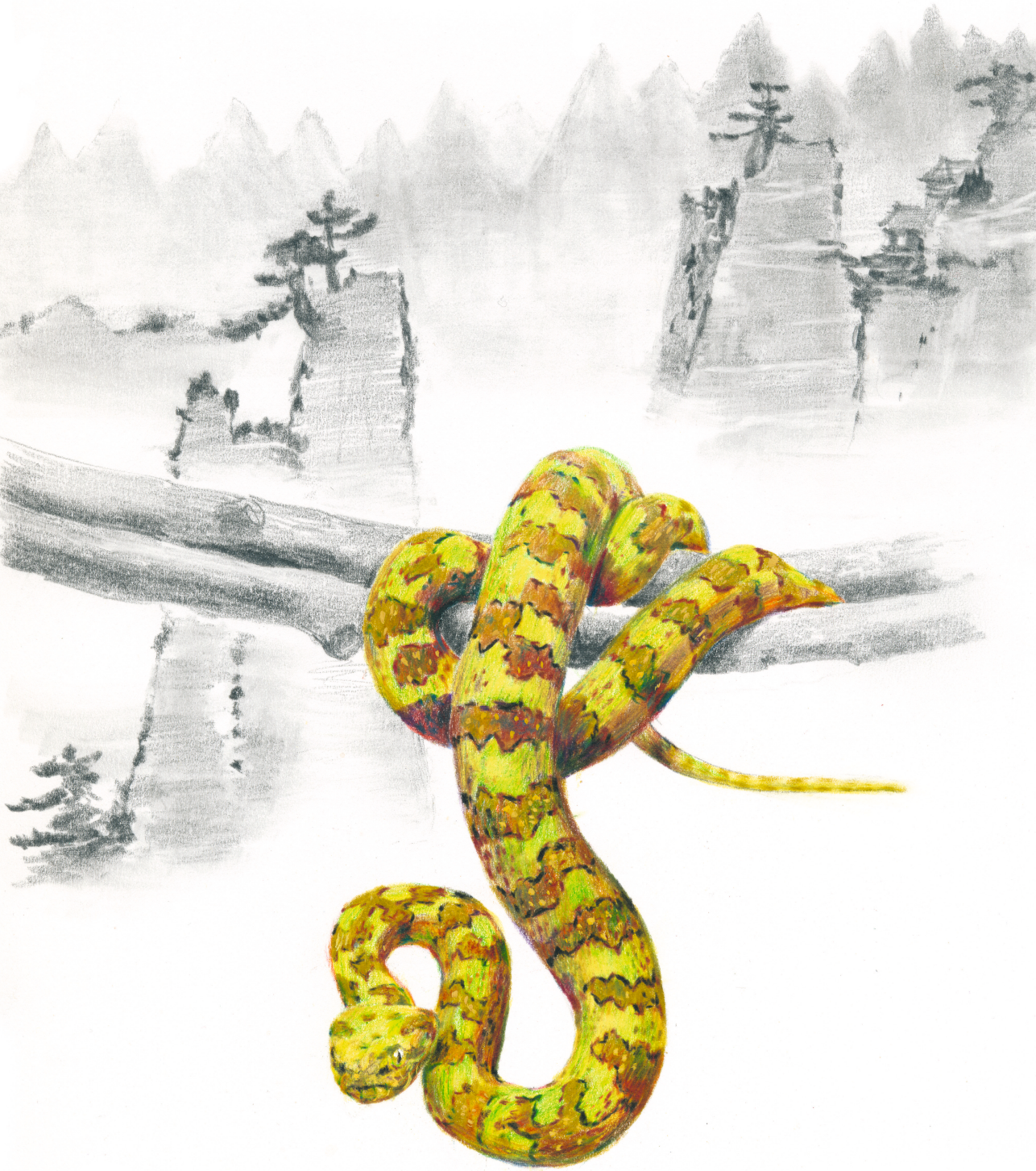

Protobothrops mangshanensis

Chapter 9

Scientific summaries (in English & Dutch)
and popular scientific summary (in Dutch)

9.1 Summary in English

Snakebite envenomation is an important public health issue that has long had tremendous implications for human health and well-being. An estimated 1.8-5.4 million people per year fall victim to snakebites, with mortality rates surpassing 100,000 individuals. Although most life-threatening pathologies from venomous snakebites result from neurotoxic and haemotoxic effects, tissue-damaging activities are a significant cause of life-long disabilities. These morbidities include tissue necrosis, amputations, renal damage and blindness. Despite the fact that venom-induced tissue damage affects over 450,000 people annually, research efforts on this pathology are limited compared to neurotoxicity or haemotoxicity. The research in this work, therefore, focuses on elucidating the mechanisms of venom-induced cell- and tissue damage.

The relevance of further research on venom-induced cell- and tissue damage is clarified in Chapter 1. This chapter provides an introduction to venomous snakes, discussing their historical and cultural significance and unique characteristics. The first section of this chapter further discusses the taxonomy of venomous snakes. It characterises the morphology of venom delivery systems, highlighting the variations between the various families of venomous snakes. The same chapter describes the global impact of snakebite envenoming, which affects at least 1.8 million people per year, especially in certain regions in Latin America, sub-Saharan Africa, and Southeast Asia. The main focus of Chapter 1 is on snake venom composition and the diverse pathological effects. It categorises these effects into neurotoxicity, haemotoxicity, and tissue-damaging effects and emphasises venom-induced tissue damage. The next section of this chapter provides an overview of the various assays that exist to study tissue-damaging venoms, both *in vivo* and *in vitro.* These include assays focusing on cell viability, membrane degradation, and molecular mechanisms underlying cell damage.

The chapter then discusses the relevance of elucidating venom composition and points out why separating venoms into their individual components (i.e., their toxins) is essential. This section further provides an overview of the various liquid chromatography (LC) techniques used to separate venoms into their components and stresses the importance of 'nanofractionation analytics' and 'high-throughput (HT) venomics'. By combining bioactivity profiling and mass spectrometry (MS),

the toxins of interest (i.e., the bioactive toxins measured with the bioassay used) can directly be identified from the MS data (i.e., LC-MS and/or toxin proteomics data) that is collected in parallel.

As previously mentioned, relatively limited research has been done on venom-induced tissue damage, partially due to the complicated nature of this pathology. What further complicates this matter is that the traditional classification of tissue-damaging venom components is confusing and oversimplifies the complexity of these toxins. Chapter 2 proposes an alternative classification for the tissue-damaging toxins, which is based on their mechanical aspects. The chapter also provides an overview of the molecular mechanisms associated with venom-induced tissue damage, which include direct cytotoxicity and extracellular matrix (ECM) degradation. Lastly, the chapter discusses pathophysiological aspects and gives an overview of potential treatment strategies.

The research in Chapter 3 presents the development of a cell-based workflow that could be used to study the molecular mechanisms associated with venom-induced tissue damage. In this study, a selection of cellular bioassays was combined with fluorescence microscopy in microwell plates in order to study venom effects. First, crude venoms of a selection of medically relevant snake species were used. This showed that at least two distinct ways exist in which cells are affected, either by disrupting the cellular membrane or by degradation of the cell monolayer. In an attempt to identify the responsible venom components, these bioassays were combined post-column with two liquid chromatography methods to separate, fractionate and bioassay the fractionated venom toxins, followed by toxin identification HT venomics. As separation with reversed-phase liquid chromatography (RP-LC) resulted in a complete loss of proteolytic activity, the separation was repeated using size-exclusion chromatography (SEC). This demonstrated that the use of denaturing eluents (i.e., when performing RP-LC) resulted in a loss of activity, while the use of non-denaturing SEC eluents allowed them to separate and collect the venom fractions in their native form. The outcomes of this chapter form the basis for chapters 4-8.

Chapters 4 and 5 describe the development of *in vitro* assays that can be used to study the venom components that induce ECM degradation. The goal of these studies was to develop assays that could be used to investigate the effect of proteolytic venom components in both crude and fractionated venoms.

Chapter 4 describes the development of an assay using sodium dodecyl sulphate-polyacrylamide gel electrophoresis (SDS-PAGE) to visualise the degradation of various fluorescent ECM-substrates by snake venoms. This method used in-gel zymography, which is used to identify substrate-specific proteolytically active components within a mixture of proteins, such as snake venom. After the separation of the toxins based on molecular weight, the bioactive protein toxins were identified using in-gel tryptic digestion followed by nanoLC-MS/MS of the tryptic digests. Although this method proved successful, the assay's low throughput makes it less suitable for large-scale screening of proteolytic venom components. In Chapter 5, the development of a plate reader-based fluorometric assay is described, which allows the study of the proteolytic activity of snake venom components in high throughput. The assay was first validated using a panel of medically relevant snake species. In an attempt to identify the proteolytically active toxins, the venoms were separated using SEC with post-column fractionation in microwell plates for subsequent bioassaying and parallel HT venomics.

Chapter 6 describes the development of a high-throughput *in vitro* bioassay that can be used to study snake-venom-induced membrane disruption using phospholipid vesicles from egg yolk as a substrate. Chicken egg yolk was used to create phospholipid vesicles, which were fluorescently stained and used to monitor the degradation of these vesicles on a plate reader. The principle of the assay is that venoms with membrane-degrading activities cause the degradation of the phospholipid vesicles, which can be observed as a decrease in fluorescence signal. After initial assay optimisation and validation, the assay was tested for its applicability for neutralisation studies using varespladib, which is a phospholipase A_2 (PLA_2) inhibitor. These experiments were performed in an effort to identify the toxins responsible for the observed membrane-disrupting effects. The analytical workflow was first executed by separating the toxins in a given venom using LC with post-column nanofractionation. This was then followed by post-column bioassaying in the presence of varespladib. In parallel, identification of the eluted toxins was done using HT venomics. Two venoms were analytically separated, fractionated, and post-column bioassayed using the membrane disruption assay. From these results, it was found that of the fractionated toxins, PLA_2s were identified in the bioactive areas of the bioassay chromatograms plotted from the

plate reader bioassay data. This confirmed that the venom PLA_2s are likely to be involved in the observed membrane-disrupting effects.

The last part of this thesis focuses on one of the most critical clinical impacts of venom-induced tissue damage: local and systemic haemorrhage following snakebite, which may lead to life-threatening clinical conditions such as organ failure and cardiovascular shock. Chapter 7 described the use of an advanced, three-dimensional blood vessel model to study the effects of tissue-damaging snake venoms on a system that mimics *in vivo* conditions. This innovative approach advances traditional cell culturing methods by replicating human microvasculature. The advantage of using such a blood vessel model is that it includes several important physiological parameters, such as tubular morphology and interaction with an ECM. The use of this model may shed light on how tissue-damaging venoms affect capillary vessels.

Finally, Chapter 8 provides the concluding remarks on the work covered in Chapters 1-7, discusses several important aspects of venom-induced tissue damage and provides future perspectives.

9.2 Samenvatting in het Nederlands

Slangenbeten vormen een belangrijk probleem dat al sinds mensenheugenis grote gevolgen heeft voor de gezondheid en het welzijn van mensen. Naar schatting worden jaarlijks tussen de 1,8 en 5,4 miljoen mensen slachtoffer van een slangenbeet, met meer dan 100.000 doden tot gevolg. Hoewel de levensbedreigende effecten voor het grootste deel het gevolg zijn van de neuro- en hemotoxines, spelen de giftoxines die weefselschade veroorzaken de belangrijkste oorzaak van levenslange aandoeningen. Deze omvatten weefselsterfte, amputaties, nierschade en blindheid. Ondanks het feit dat door slangengif veroorzaakte weefselschade jaarlijks meer dan 450.000 mensen treft, wordt hier aanzienlijk minder onderzoek gedaan dan naar de neuro- en hemotoxische effecten. Het onderzoek in dit proefschrift richt zich daarom op het ophelderen van de mechanismen van door slangengif veroorzaakte cel- en weefselschade.

De relevantie van nader onderzoek wordt toegelicht in Hoofdstuk 1. Dit hoofdstuk geeft een overzicht van de verschillende families van gifslangen en bespreekt hun bijzondere kenmerken en cultuurhistorische betekenis. Het eerste deel van dit hoofdstuk behandelt de taxonomie van gifslangen en de morfologie van gifklier en giftanden, waarbij ook de variatie tussen de verschillende families van giftige slangen wordt beschreven. Dit hoofdstuk behandelt daarnaast de wereldwijde impact van gifslangenbeten, een probleem dat jaarlijks meer dan 1,8 miljoen mensen treft, vooral in Latijns-Amerika, sub-Sahara Afrika en Zuidoost-Azië. De nadruk van Hoofdstuk 1 ligt op het beschrijven van de samenstelling van slangengif en de diverse pathologische effecten ervan. Het classificeert de lichamelijke effecten in neurotoxiciteit, hemotoxiciteit en richt zich hierbij met name op weefselschade. Het volgende deel van dit hoofdstuk geeft een overzicht van de verschillende proefopstellingen die bestaan om cel- en weefselschade te bestuderen, zowel *in vivo* als *in vitro*. Dit omvat proeven die zich richten op het kwantificeren van het aantal levende cellen, membraandegradatie en de moleculaire mechanismen die ten grondslag liggen aan cel- en weefselschade. Het hoofdstuk bespreekt vervolgens de relevantie van het ophelderen van de samenstelling van gif en beargumenteert waarom het scheiden van slangengif in afzonderlijke componenten (toxinen) relevant is. Het hoofdstuk geeft tot slot een overzicht van beschikbare chromatografietechnieken die worden gebruikt

om slangengiffen te scheiden en benadrukt het belang van 'nanofractionation analysis' en 'high-throughput (HT) venomics'. Door bioactiviteitsprofielen en massaspectrometriedata (MS-data) te combineren, werd het mogelijk om relevante toxines rechtstreeks te identificeren.

Ondanks de hoge morbiditeitscijfers is er beperkt onderzoek gedaan naar weefselschade die door slangengif wordt veroorzaakt, mede door de gecompliceerde aard van deze toxiciteit. Wat dit onderzoek verder bemoeilijkt is het feit dat de traditionele classificatie van toxines die weefselschade veroorzaken verwarrend is, waardoor de complexiteit van deze gifcomponenten vaak onnodig versimpeld wordt. Hoofdstuk 2 beschrijft daarom een alternatieve classificatie voor toxines die weefselschade veroorzaken, gebaseerd op de werkingsmechanismen van deze toxines. Het hoofdstuk geeft daarnaast een overzicht van de moleculaire mechanismen die geassocieerd zijn met door gif veroorzaakte weefselschade, waaronder directe celtoxiciteit en degradatie van de extracellulaire matrix (ECM). Ten slotte bespreekt het hoofdstuk pathofysiologische aspecten en geeft het een overzicht van mogelijke behandelingsstrategieën.

Het onderzoek in Hoofdstuk 3 beschrijft de ontwikkeling van een methode die gebruik maakt van celkweken om de moleculaire mechanismen te bestuderen die samenhangen met door gif veroorzaakte weefselschade. Een selectie van cellulaire bioanalyses werd hiervoor uitgevoerd op microtiterplaten en met gebruik van fluorescentiemicroscopie, om de effecten van gif te bestuderen. Eerst werd het gif van een selectie van medisch relevante slangensoorten getest. Dit liet zien dat er minstens twee verschillende manieren zijn waarop cellen worden aangevallen, namelijk door verstoring van het celmembraan of door degradatie van de monolaag van cellen. In een poging om de verantwoordelijke gifcomponenten te identificeren, werden deze bioanalyses gecombineerd met twee vloeistofchromatografie-methoden om het gif te scheiden, om het vervolgens te fractioneren en de biologische activiteit van de toxines te bepalen. Dit werd gevolgd door identificatie van de relevante toxines met behulp van proteomicadata. Met proteomica kunnen de eiwitten in een (deel van) een organisme (bijvoorbeeld in het gif) in kaart worden gebracht. Omdat scheiding met *reverse-phased* chromatografie (RP-LC) resulteerde in een volledig verlies van activiteit, werd de scheiding herhaald met behulp van *size-exclusion chromatografie* (SEC). Dit toonde aan dat het gebruik van denaturerende eluentia (NB. die

gebruikt zijn bij het uitvoeren van RP-LC) resulteerde in een verlies van biologische activiteit, terwijl het gebruik van niet-denaturerende SEC-eluenten het mogelijk maakte om de gifcomponenten te scheiden en te verzamelen in hun natieve conformatie. De resultaten van dit hoofdstuk vormden de basis voor hoofdstukken 4-8.

Hoofdstukken 4 en 5 beschrijven de ontwikkeling van *in vitro* analyses die gebruikt kunnen worden om de gifcomponenten te bestuderen die de degradatie van de extracellulaire matrix veroorzaken. Het doel van deze hoofdstukken was om analyses te ontwikkelen die kunnen worden gebruikt om het effect van proteolytische gifcomponenten te onderzoeken in zowel niet-gefractioneerde als gefractioneerde giffen. Hoofdstuk 4 beschrijft de ontwikkeling van een analyse met behulp van natriumdodecylsulfaat-polyacrylamidegelelektroforese (SDS-PAGE) om de degradatie van verschillende fluorescerende ECM-substraten door slangengiffen te visualiseren. Deze methode maakt gebruik van in-gel zymografie, die wordt gebruikt om substraat-specifieke en proteolytisch-actieve componenten te identificeren binnen een mengsel van eiwitten, zoals slangengif. Na scheiding van de toxines op basis van moleculair gewicht, werden de bioactieve eiwitten geïdentificeerd met behulp van in-gel digestie met trypsine (NB. trypsine splitst eiwitten door bindingen van basische aminozuren te verbreken in een eiwitmolecuul) gevolgd door nanoLC-MS/MS van de digesties. Hoewel deze methode succesvol bleek te zijn, maakt de lage doorvoer deze minder geschikt voor grootschalige *screening* van proteolytische gifcomponenten. In Hoofdstuk 5 wordt daarom de ontwikkeling van een fluorometrische analyse beschreven die gebaseerd is op *plate readers*, waarmee de proteolytische activiteit van slangengifcomponenten kan worden bestudeerd. De analyse werd eerst gevalideerd met behulp van een panel van medisch relevante slangensoorten. In een poging om de proteolytisch actieve toxines te identificeren, werden de giffen gescheiden met SEC, gevolgd door fractionatie in microtiterplaten voor daaropvolgende biologische analyses en HT venomics.

Hoofdstuk 6 beschrijft de ontwikkeling van een hoge doorvoer *in vitro* bioanalyse die kan worden gebruikt om membraanverstoring veroorzaakt door slangengif te bestuderen met behulp van fosfolipideblaasjes afkomstig van eigeel als substraat. Kippeneigeel werd gebruikt om fosfolipideblaasjes te creëren, die fluorescerend werden gekleurd en werden gebruikt om de degradatie van

fosfolipideblaasjes op een *plate reader* te volgen. Het principe van de analyse is dat giffen met membraanafbrekende activiteiten de fosfolipideblaasjes kunnen degraderen, wat kan worden waargenomen als een afname in fluorescent signaal. Na optimalisatie en validatie van deze methode, werd deze getest op zijn toepasbaarheid voor neutralisatiestudies met behulp van varespladib, wat een phospholipase A_2 (PLA_2) -remmer is. Dit werd gevolgd door een poging om de verantwoordelijke toxines te identificeren met behulp van RP-LC gevolgd door bioanalyses en eiwitidentificatie met behulp van HT venomics. Twee giffen werden analytisch gescheiden, gefractioneerd en getest met behulp van de ontwikkelde analyse. Uit deze resultaten bleek dat de PLA_2s die met HT venomics geïdentificeerd zijn, gevonden werden in het gedeelte van de microtiterplaten waar bioactiviteit te zien was. Dit bevestigde dat de PLA_2s in het slangengif waarschijnlijk betrokken zijn bij de membraanverstorende effecten.

Het laatste deel van het proefschrift richt zich op een van de belangrijkste klinische gevolgen van door gif veroorzaakte weefselschade lokale en systemische bloeding na een slangenbeet, wat kan leiden tot levensbedreigende klinische aandoeningen zoals orgaanfalen en cardiovasculaire shock. Hoofdstuk 7 beschrijft het gebruik van een geavanceerd, driedimensionaal bloedvatmodel om de effecten van weefselschadelijke slangengiffen te bestuderen op een systeem dat *in vivo* omstandigheden nabootst. Deze innovatieve aanpak verbetert traditionele celkweekmethoden door menselijke microvasculatuur na te bootsen. Het voordeel van het gebruik van zo'n bloedvatmodel is dat het rekening houdt met verschillende belangrijke fysiologische parameters, zoals tubulaire morfologie en interactie met een ECM. Het gebruik van dit model kan inzicht geven in hoe weefselschadelijke giffen capillaire vaten beïnvloeden.

Tot slot geeft hoofdstuk 8 een concluderend overzicht met betrekking tot het werk in hoofdstukken 1-7. Daarnaast worden verschillende belangrijke aspecten van door gif veroorzaakte weefselschade besproken, en wordt er een toekomstperspectief geschetst voor het gifonderzoek.

9.3 Populair-wetenschappelijke samenvatting

Slangen zijn er in alle soorten en maten. Van de groene anaconda die meer dan zes meter lang en 200 kilo zwaar kan worden, tot piepkleine draadwormslangetjes die nog geen 11 centimeter lang zijn. Wereldwijd bestaan meer dan 4000 soorten slangen in alle kleuren van de regenboog, met allerlei specialisaties en bijzonderheden. Ik ben dan ook niet voor niets als kind volledig in de ban geraakt van deze unieke wezens. Ongeveer 2500 slangensoorten zijn 'technisch' gezien giftig, 500-600 daarvan kunnen gevaarlijk zijn voor mensen. We noemen deze soorten slangen vaak 'medisch significant', met andere woorden: als je gebeten wordt door een van deze slangen heb je een groot probleem. Gifslangenbeten hebben gigantische gevolgen voor de gezondheid en het welzijn van mensen. Naar schatting worden jaarlijks tussen de 1,8 en 5,4 miljoen mensen gebeten door een giftige slang en opgeteld maken slangenbeten jaarlijks meer dan 100.000 dodelijke slachtoffers. De meeste slangenbeten vinden plaats in tropische en subtropische gebieden in Afrika, Azië en Latijns-Amerika. Het is belangrijk om te beseffen dat slangenbeten zowel een oorzaak als een gevolg van armoede zijn. In landen met een minder goede gezondheidszorg en schaarse medische bronnen is dit probleem natuurlijk het grootste. Slangenbeten worden ook wel een 'ziekte van de armen genoemd'. Met name de plattelandsbevolking loopt het grootste risico op een slangenbeet, en door gebrek aan (en bereikbaarheid van) goede medische zorg en antigif lopen zij ook de meeste kans om eraan te overlijden. Het is daarom van groot belang dat we onderzoek doen naar slangengif en daardoor beter begrijpen hoe het slangengif effect heeft op het (menselijk) lichaam.

Slangengif kan worden beschouwd als een soort cocktail van tientallen tot meer dan honderd bioactieve moleculen die we toxines noemen. Deze giftige cocktails zijn door evolutie in honderdduizenden tot miljoenen jaren ontwikkeld tot de extreem nauwkeurige en krachtige giffen die het vandaag de dag zijn. De toxines in het gif hebben maar één doel: het lichaam volledig ontregelen. Een prachtig staaltje evolutie, dat je misschien nog wel het beste kunt zien als een soort biochemisch clusterbombardement. Alsof je tegelijkertijd een overdosis pijnstillers, rattengif en bloedverdunners toegediend krijgt. Het lichaam kan op verschillende manieren door (slangen)gif worden ontregeld. Zo hebben de neurotoxines in het gif effect op het zenuwstelsel, waarbij de ademhaling wordt

stilgelegd of het hart het begeeft. Hemotoxines daarentegen, richten zich op het bloed en de bloedstolling. Deze gifcomponenten veroorzaken bijvoorbeeld ontelbare kleine bloedpropjes in het lichaam, of doen juist het tegenovergestelde en zorgen ervoor dat het bloed niet goed meer kan stollen. Ook kan door het gif de bloeddruk enorm snel dalen, wat kan leiden tot een hypovolemische *shock*, waarbij het hart niet langer in staat is om het bloed rond te pompen. Alhoewel de meest levensbedreigende effecten het gevolg zijn van de neurotoxische en hemotoxische effecten, zijn de weefselbeschadigende activiteiten een belangrijke oorzaak van levenslang lichamelijk letsel. Denk hierbij aan weefselsterfte, amputaties, nierschade en blindheid. Deze effecten maken jaarlijks meer dan 450.000 slachtoffers, die een beet weliswaar overleven maar er levenslang schade aan overhouden

Bij het grootste deel van het werelwijde onderzoek naar slangengif ligt de nadruk op de neurotoxische en hemotoxische effecten, waardoor de cel- en weefselbeschadigende effecten relatief onderbelicht zijn gebleven. Vandaar dat dit onderzoek zich juist heeft gericht op de laatste vorm van toxiciteit, om deze relevante pathologieën te onderzoeken en daarmee de onderliggende mechanismen van weefselschade beter te begrijpen. In dit proefschrift ligt daarom de nadruk vooral op het beter begrijpen van de mechanismen van door slangengif veroorzaakte cel- en weefselschade.

Eén van de belangrijkste aspecten van dit onderzoek was het bestuderen van de samenstelling van slangengif en hoe de verschillende componenten daarvan schade aanrichten aan cellen en weefsels. Hiervoor hebben mijn collega's en ik methodes ontwikkeld om precies te kunnen zien hoe de verschillende soorten slangengif werken. We namen bijvoorbeeld celkweken waarbij we gebruik maakten van een geavanceerde microscoop en van minuut tot minuut konden bestuderen hoe levende cellen reageerden op het slangengif. Hierbij zagen we duidelijk verschil in de manier waarop bepaalde slangengiffen hun effect hadden op de cellen. Bij de Mozambikaanse spugende cobra bijvoorbeeld zagen we dat het celmembraan van de cellen werd geperforeerd, waardoor de cellen als het ware 'lek' raakten. Bij de familie van de adders zagen we een heel ander effect, namelijk dat het gif de cellulaire matrix leek te vernietigen. Omdat deze celmatrix een soort componentenlijm is die de cellen bij elkaar houdt, raken de cellen los van elkaar en van hun omgeving, waardoor deze giffen

ook grote schade kunnen veroorzaken in het lichaam. In de eerste plaats keken we hierbij naar de effecten van het gif in z'n geheel, om daarna specifiek te kijken naar de afzonderlijke componenten in het gif. Voor dat laatste hebben we gebruik gemaakt van verschillende analytische scheidingsmethoden zoals chromatografie en massa spectrometrie. Deze technieken hebben ons geholpen bij het scheiden en analyseren van de toxines in het gif, zodat we een beter beeld hebben van de gifcomponenten die verantwoordelijk zijn voor de cellulaire schade. Tot slotte hebben we gebruik gemaakt van een 'orgaan-op-een-chip model' dat een menselijk bloedvat nabootst. In een dergelijke *chip* die bestaat uit een plastic plaat met ingebouwde 'microkanaaltjes', groeien bloedvatcellen in een omgeving die het lichaam nabootst. Deze microkanaaltjes zijn vergelijkbaar met een traditionele petrischaal waarin cellen worden gekweekt. In dit geval kunnen de cellen zich echter aan alle kanten van het buisje kunnen hechten – driedimensionaal dus – waarbij de bloedvatcellen een soort 3D-imitatiebloedvat vormen dat een menselijk bloedvat nabootst. Dit model helpt ons beter te begrijpen hoe de giftoxines bloedingen kunnen veroorzaken, zonder daarbij proefdieren te gebruiken.

In de kern draagt dit onderzoek bij aan een beter begrip van hoe slangengif werkt, hoe weefselschade wordt veroorzaakt en hoe we deze schade beter kunnen behandelen. De uitkomsten van dit onderzoek gaan in de toekomst hopelijk een rol spelen bij de oplossing van het probleem van gifslangenbeten.

9

Pseudocerastes urarachnoides

Chapter 10

Appendices

Appendix A. Supporting Information Chapter 2
Appendix B. Supporting Information Chapter 3
Appendix C. Supporting Information Chapter 4
Appendix D. Supporting Information Chapter 5
Appendix E. Supporting Information Chapter 6
Appendix F. Supporting Information Chapter 7

Appendix A. Supporting Information Chapter 2

Supporting Information available via the DOI below or by scanning the QR code.

Adapted from: Mátyás A. Bittenbinder et al., (2024). Tissue-damaging toxins in snake venoms: mechanisms of action, pathophysiology and treatment strategies. *Communications Biology, 7* (358). DOI: 10.1038/s42003-024-06019-6

Appendix B. Supporting Information Chapter 3

Supporting Information available via the DOI below or by scanning the QR code.

Adapted from: Mátyás A. Bittenbinder et al., (2023). Development of a high-throughput *in vitro* screening method for the assessment of cell-damaging activities of snake venoms. *PLOS Neglected Tropical Disease.* DOI: 10.1371/journal.pntd.0011564

Appendix C. Supporting Information Chapter 4

Supporting Information available via the DOI below or by scanning the QR code.

Adapted from: Mátyás A. Bittenbinder et al., (2023). Monitoring snake venom-induced extracellular matrix degradation and identifying proteolytically active venom toxins using fluorescently labelled substrate. *Biology, 12* (6). DOI: 10.3390/biology12060765

Appendix D. Supporting Information Chapter 5

Supporting Information available via the DOI below or by scanning the QR code.

Adapted from: Mátyás A. Bittenbinder et al., (2023). Application of an extracellular matrix-mimicking fluorescent polymer for the detection of proteolytic venom toxins. *Toxins, 15* (294). DOI: 10.3390/toxins15040294

Appendix E. Supporting Information Chapter 6

Supporting Information available via the DOI below or by scanning the QR code.

Adapted from: Mátyás A. Bittenbinder et al., 2024. Development of a membrane-disruption assay using phospholipid vesicles as a proxy for the detection of cellular membrane degradation. *Toxicon: X* (100197). DOI: 10.1016/j.toxcx.2024.100197

Appendix F. Supporting Information Chapter 7

Supporting Information available via the DOI below or by scanning the QR code.

Adapted from: Mátyás A. Bittenbinder et al., (2024). Bloody insights: using organ-on-a-chip technology to study haemorrhagic activities of snake venoms on endothelial tubules. *Scientific Reports, 14* (11157). DOI: 10.1038/s41598-024-60282-5

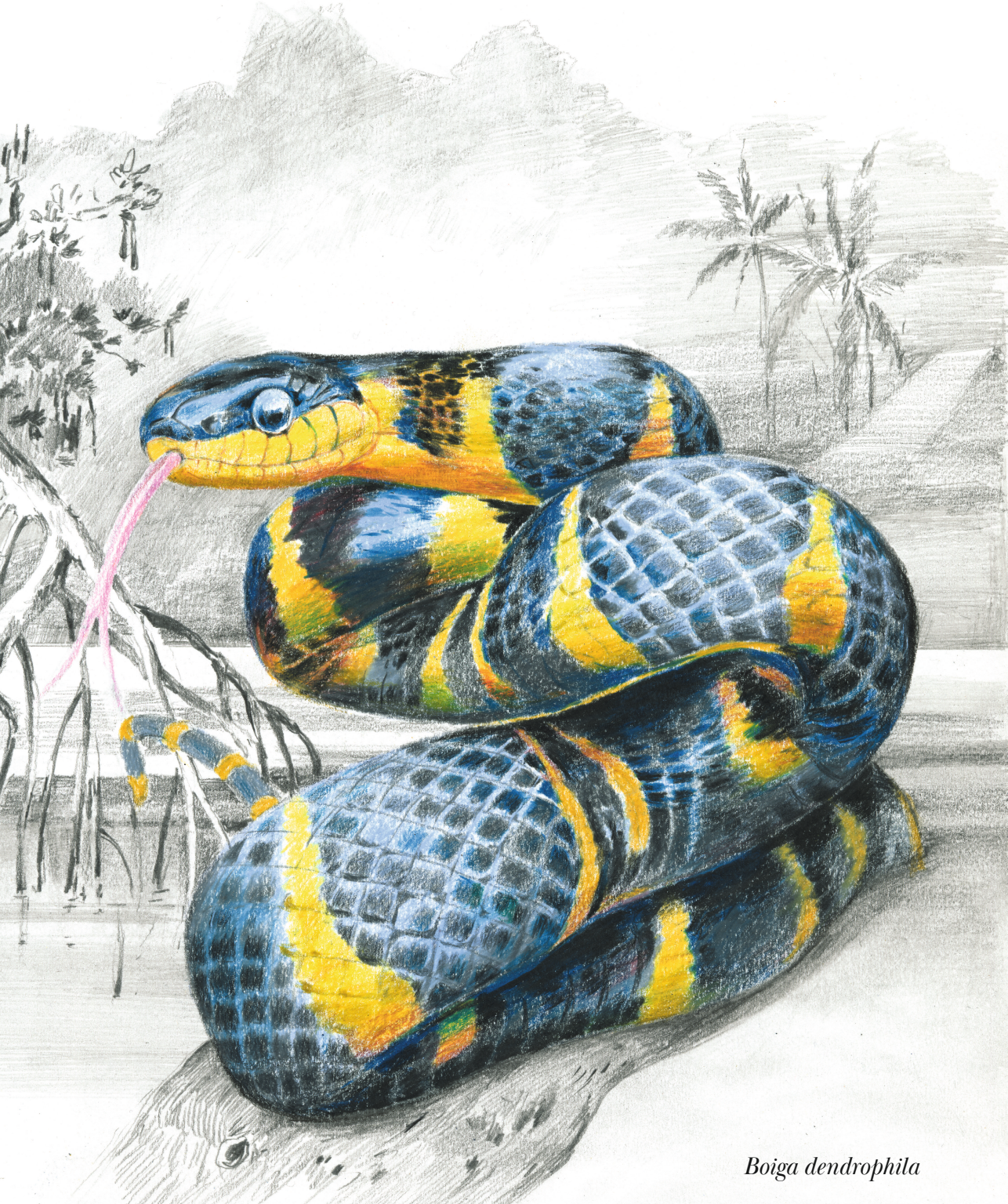

Boiga dendrophila

Chapter 11

Sundries

11.1 Scientific output

Journal papers included in this thesis

1) **Mátyás A. Bittenbinder,** Jory van Thiel, Fernanda C. Cardoso, Nicholas R. Casewell, José-María Gutiérrez[§,#], Jeroen Kool[§,#], Freek J. Vonk[§] (2024). Tissue-damaging toxins in snake venoms: mechanisms of action, pathophysiology and treatment strategies. ***Communications Biology***, ***7*** (358)

[§]These authors jointly supervised this work
[#]Corresponding authors

2) **Mátyás A. Bittenbinder**, Liliana Capinha, Daniel Da Costa Pereira, Julien Slagboom, Bas van de Velde, Nicholas R. Casewell, Paul Jennings, Jeroen Kool[§,#], Freek J. Vonk[§] (2023). Development of a high-throughput *in vitro* screening method for the assessment of cell-damaging activities of snake venoms. ***PLOS Neglected Tropical Diseases***.

[§]These authors jointly supervised this work
[#]Corresponding author

3) **Mátyás A. Bittenbinder**[*], Nick D. Bergkamp[*], Julien Slagboom, Jan Paul M. Bebelman, Nicholas R. Casewell, Marco H. Siderius, Martine J. Smit, Jeroen Kool[§,#], Freek J. Vonk[§] (2023). Monitoring snake venom-induced extracellular matrix degradation and identifying proteolytically active venom toxins using fluorescently labelled substrates. ***Biology***, ***12*** (6)

[*]These authors contributed equally to this work
[§]These authors jointly supervised this work
[#]Corresponding author

4) **Mátyás A. Bittenbinder*,** Eric Wachtel[*], Bas van de Velde, Julien Slagboom, Axel de Monts de Savasse, Luis L. Alonso, Nicholas R. Casewell, Freek J. Vonk[§], Jeroen Kool[§,#] (2023). Application of an extracellular matrix-mimicking fluorescent polymer for the detection of proteolytic venom toxins. ***Toxins***, ***15*** (294)

[*]These authors contributed equally to this work
[§]These authors jointly supervised this work
[#]Corresponding author

5) **Mátyás A. Bittenbinder**, Eric Wachtel, Daniel, Daniel Da Costa Pereira, Julien Slagboom, Nicholas R. Casewell, Paul Jennings, Jeroen Kool[§,#], Freek J. Vonk[§] (2024). Development of a membrane-disruption assay using phospholipid vesicles as a proxy for the detection of cellular membrane degradation. ***Toxicon: X*** (100197).

[§]These authors jointly supervised this work
[#]Corresponding author

6) **Mátyás A. Bittenbinder***, Flavio Bonanini*, Dorota Kurek, Paul Vulto, Jeroen Kool[§,#], Freek J. Vonk[§] (2024). Bloody insights: using organ-on-a-chip technology to study haemorrhagic activities of snake venoms on endothelial tubules. ***Scientific Reports, 14*** (11157).

*These authors contributed equally to this work
[§]These authors jointly supervised this work
[#]Corresponding author

Journal papers not included in this thesis

7) Julien Slagboom, Abigail H. Lewis, Wietse M. Schouten, Rien van Haperen, Mieke Veltman, **Mátyás A. Bittenbinder**, Freek J. Vonk, Nicholas R. Casewell, Frank Grosveld, Dubravka Drabek, Jeroen Kool (2024). High throughput identification of human monoclonal antibodies and heavy-chain-only antibodies to treat snakebite. ***Toxicon: X***, (100185).

8) Ronald Vlasblom, Jory van Thiel, **Mátyás A. Bittenbinder,** Jon-Ruben van Rhijn, Rinske Drost, Lotte Muis, Julien Slagboom, Daniela Salvatori, Jeroen Kool, Robert Jan Veldman (2024). Distinct cardiotoxic effects by venoms of a spitting cobra (*Naja pallida*) and a rattlesnake (*Crotalus atrox*) revealed using an ex vivo Langendorff heart model. ***Toxicon***, ***240*** (107637).

9) Sedef Terzioglu, **Mátyás A. Bittenbinder**, Julien Slagboom, Bas van de Velde, Nicholas R. Casewell, Jeroen Kool (2023). Analytical size-exclusion chromatography coupled to nanofractionation analytics for coagulopathic venom profiling. ***Toxins, 15*** (9).

10) **Mátyás A. Bittenbinder***, Freek J. Vonk*, Harald M.I. Kerkkamp*, Dwin G.B. Grashof, John P. Archer, Sandra Afonso, Michael K. Richardson, Jeroen Kool, Arie van der Meijden (2021). A non-lethal method for studying scorpion venom gland transcriptomes, with a review of potentially suitable taxa to which it can be applied. ***PLoS ONE, 16***.
*These authors contributed equally to this work

11) Timothy P. Jenkins, **Mátyás A. Bittenbinder*,** Shirin Ahmadi*, Trenton K. Stewart, Dilber E. Akgun, Melissa Hale, Nafiseh N. Nasrabadi, Darian S. Wolff, Freek J. Vonk, Jeroen Kool, Andreas H. Laustsen (2021). Venomous animals and the envenomings they cause in the Middle East and North Africa. ***PLoS Neglected Tropical Diseases, 15*** (12).
*These authors contributed equally to this work

12) Jens Puschhof, Yorick Post, Joep Beumer, Harald M. Kerkkamp, **Mátyás A. Bittenbinder**, Freek J. Vonk, Nicholas R. Casewell, Michael K. Richardson, Hans Clevers. Derivation of snake venom gland organoids for in vitro venom production (2021). ***Nature Protocols, 16*** (3).

13) Chunfang Xie, **Mátyás A. Bittenbinder**, Julien Slagboom, Arif Arrahman, Sven Bruijns, Govert W Somsen, Freek J. Vonk, Nicholas R. Casewell, Juan J. García-Vallejo, Jeroen Kool (2021). Erythrocyte haemotoxicity profiling of snake venom toxins after nanofractionation. ***Journal of Chromatography B***, 1176.

14) Chunfang Xie, Laura-Oana Albulescu, **Mátyás A. Bittenbinder**, Govert W. Somsen, Freek J. Vonk, Nicholas R. Casewell, Jeroen Kool (2020). Neutralizing effects of small molecule inhibitors and metal chelators on coagulopathic Viperinae snake venom toxins ***Biomedicines, 8*** (9).

15) **Mátyás A. Bittenbinder**, James S. Dobson, Christina N. Zdenek, Bianca op den Brouw, Arno Naude, Freek J. Vonk, Bryan G. Fry (2019). Differential destructive (non-clotting) fibrinogenolytic activity in Afro-Asian elapid snake venoms and the links to defensive hooding behavior. ***Toxicology in Vitro, 60***.

16) Nicholas J. Youngman, Christina N. Zdenek, James S. Dobson, **Mátyás A. Bittenbinder**, Amber Gillettb, Brett Hamilton, Nathan Dunstan, Luke Allen, Andrew Veary, Elle Veary, Bryan G. Fry (2019). Mud in the blood: Documentation of novel potent anticoagulant coagulotoxicity in the venoms of the Australian elapid snake genus *Denisonia* (mud adders) and relative antivenom efficacy. ***Toxicology Letters, 302***.

17) **Mátyás A. Bittenbinder**, Christina N. Zdenek, Bianca Op den Brouw, Nicholas J. Youngman, James S. Dobson, Arno Naude, Freek J. Vonk, Bryan G. Fry (2018). Clinical implications of strong anticoagulant actions of African spitting *Naja* venoms not neutralized by antivenom but are by LY315920 (varespladib). ***Toxins, 10*** (12).

18) Philippe J.R. Kok, **Mátyás A. Bittenbinder**, Joris K. van den Berg, Sergio Marques-Souza, Pedro M. Sales Nunes, Alexandra E. Laking, Mauro Teixeira Jr, Antoine Fouquet, D. Bruce Means, Ross D. MacCulloch, Miguel Trefaut Rodrigues (2018). Integrative taxonomy of the gymnophthalmid lizard *Neusticurus rudis* Boulenger, 1900 identifies a new species in the eastern Pantepui region, north-eastern South America. ***Journal of Natural History, 52*** (13-16).

Journal papers in preparation

19) Jeroen Kool, Anniek X. Verstegen, Jorg Sander, Radja M. Kosasih, Tanno J. van Herpen, Luis L. Alonso, Julien Slagboom, Freek J. Vonk, Timothy N.W. Jackson, **Mátyás A. Bittenbinder**. Bloody Australians: Venom variation in procoagulant and anticoagulant activities of Australian elapids in the genus *Pseudonaja* and *Oxyuranus*. *(In preparation).*

20) **Mátyás A. Bittenbinder***, Nick D. Bergkamp*, Marco H. Siderius, Martine J. Smit, Freek J. Vonk, Nicholas R. Casewell, Jeroen Kool, Rachel H. Clare. Monitoring hyaluronidase activity using a high-throughput screening method. *(In preparation).*

*These authors contributed equally to this work

21) **Mátyás A. Bittenbinder**, Nanne N. Paauw, Nicole N. van der Wel, Freek J. Vonk, Jeroen Kool. Studying morphological changes in endothelial cells and keratinocytes following venom exposure using scanning electron microscopy. *(In preparation).*

22) Haifeng Xu, **Mátyás A. Bittenbinder**, Julien Slagboom, Nicholas R. Casewell, Paul Jennings, Jeroen Kool. Assessing the cell-damaging activities of elapid venoms on a selection of cell types using a high-throughput *in vitro* screening method. *(In preparation).*

23) Haifeng Xu, **Mátyás A. Bittenbinder**, Julien Slagboom, Nicholas R. Casewell, Paul Jennings, Jeroen Kool. Assessing the cell-damaging activities of viper venoms on a selection of cell types using a high-throughput *in vitro* screening method. *(In preparation).*

24) Mrinalini Walter, Nicholas R. Casewell, S. Yahya Anvar, Juan J. Calvete, Eivind Undheim, **Mátyás A. Bittenbinder**, Arnold Binta, Nalini Puniamoorthy, Manjunatha R. Kini, Michael K. Richardson, Freek J. Vonk. Genomic insights into the evolution of venom toxins and developmental patterning genes in the Malayan pitviper, *Calloselasma rhodostoma*. *(In preparation).*

11.2 Overview of co-authors' contributions

Chapter 1. Introduction

Mátyás A. Bittenbinder	Wrote the chapter
Jeroen Kool	Reviewed, edited and provided feedback for improvements
Freek J. Vonk	Reviewed, edited and provided feedback for improvements

Chapter 2 – Tissue-damaging toxins in snake venoms: mechanisms of action, pathophysiology and treatment strategies

Mátyás A. Bittenbinder	Wrote the manuscript; edited and corrected the manuscript; discussed the scientific content; prepared the figures
Jory van Thiel	Wrote the manuscript; edited and corrected the manuscript; discussed the scientific content
Fernanda C. Cardoso	Edited and corrected the manuscript; discussed the scientific content
Nicholas R. Casewell	Edited and corrected the manuscript; discussed the scientific content
José-María Gutiérrez	Wrote the manuscript; edited and corrected the manuscript and discussed the scientific content
Jeroen Kool	Edited and corrected the manuscript and discussed the scientific content
Freek J. Vonk	Edited and corrected the manuscript and discussed the scientific content

Chapter 3 – Development of a high-throughput *in vitro* screening method for the assessment of cell-damaging activities of snake venom

Mátyás A. Bittenbinder	Conceptualisation; methodology; investigation; software; data curation; formal analysis; validation; visualisation; writing of the original draft; review and editing
Liliana Capinha	Methodology; data curation; formal analysis
Daniel Da Costa Pereira	Methodology; data curation; formal analysis
Julien Slagboom	Methodology; data curation
Bas van de Velde	Data curation; formal analysis
Nicholas R. Casewell	Supervision; review and editing
Paul Jennings	Supervision; review and editing
Jeroen Kool	Conceptualisation; investigation; resources; project administration; supervision; review and editing
Freek J. Vonk	Conceptualisation; investigation; resources; project administration; supervision; review and editing

Chapter 4 – Monitoring snake venom-induced extracellular matrix degradation and identifying proteolytically active venom toxins using fluorescently labelled substrates

Mátyás A. Bittenbinder	Conceptualisation; methodology; investigation; software; data curation; formal analysis; validation; visualisation; writing of the original draft; review and editing
Nick D. Bergkamp	Conceptualisation; methodology; investigation; software; data curation; formal analysis; validation; visualisation; writing of the original draft; review and editing
Julien Slagboom	Methodology; software; data curation; formal analysis; review and editing
Jan Paul M. Bebelman	Conceptualisation; methodology; software; review and editing
Nicholas R. Casewell	Conceptualisation; investigation; review and editing
Marco H. Siderius	Conceptualisation; resources; project administration; supervision; review and editing
Martine J. Smit	Conceptualisation; resources; project administration; supervision; review and editing
Jeroen Kool	Conceptualisation; resources; investigation; project administration; supervision; review and editing
Freek J. Vonk	Conceptualisation; resources; investigation; project administration supervision; review and editing

Chapter 5 – Application of an extracellular matrix-mimicking fluorescent polymer for the detection of proteolytic venom toxins

Mátyás A. Bittenbinder	Conceptualisation; methodology; investigation; formal analysis; data curation; visualisation; project administration; writing of the original draft; review and editing
Eric Wachtel	Conceptualisation; methodology; investigation; formal analysis; data curation; visualisation; project administration; writing of the original draft; review and editing
Bas van de Velde	Methodology; investigation
Julien Slagboom	Methodology; investigation; formal analysis; data curation;
Axel de Monts de Savasse	Investigation
Luis L. Alonso	formal analysis
Nicholas R. Casewell	Review and editing; funding acquisition
Freek J. Vonk	Resources; project administration; funding acquisition
Jeroen Kool	Conceptualisation; resources; data curation; project administration; funding acquisition; review and editing

Chapter 6 – Development of a membrane-disruption assay using phospholipid vesicles as a proxy for the detection of cellular membrane degradation

Mátyás A. Bittenbinder	Conceptualisation; methodology; investigation; software; formal analysis; data curation; visualisation; writing of the original draft; review and editing
Eric Wachtel	Methodology; formal analysis; data curation
Daniel Da Costa Pereira	Methodology; formal analysis; data curation
Julien Slagboom	Formal analysis; data curation
Nicholas R. Casewell	Supervision
Paul Jennings	Supervision; resources
Jeroen Kool	Conceptualisation; data curation; supervision, resources, project administration; review and editing
Freek J. Vonk	Conceptualisation; data curation; supervision, resources, project administration; review and editing

Chapter 7 – Bloody insights: using organ-on-a-chip technology to study haemorrhagic activities of snake venoms on endothelial tubules

Mátyás A. Bittenbinder	Conceptualisation; methodology; investigation; software; project administration; formal analysis; validation; data curation; visualisation; writing of the original draft; review and editing
Flavio Bonanini	Conceptualisation; methodology; investigation; software; project administration; formal analysis; validation; data curation; visualisation; writing of the original draft; review and editing
Dorota Kurek	Conceptualisation; methodology; data curation; supervision; review and editing
Paul Vulto	Methodology; data curation; supervision; review and editing
Jeroen Kool	Conceptualisation; data curation; supervision; review and editing
Freek J. Vonk	Conceptualisation; data curation; supervision; review and editing

Chapter 8 – Discussion, future perspectives & concluding remarks

Mátyás A. Bittenbinder	Wrote the chapter
Jeroen Kool	Reviewed, edited and provided feedback for improvements
Freek J. Vonk	Reviewed, edited and provided feedback for improvements

11.3 List of abbreviations

Abbreviation	Meaning
3D	3-Dimensional
3FTx	Three-finger toxin
ACN	Acetonitrile
ATP	Adenosine triphosphate
BM	Basement membrane
CID	Collision-induced dissociation
CLP	C-type lectin-related protein
CRC	Concentration-response curve
CRiSP	Cysteine-rich secretory protein
CT-3FTx	Cytotoxic three-finger toxin
CTL	C-type lectin
DFA	Difluoroacetic acid
Dis	Disintegrin
DMPS	2,3-Dimercapto-1-propanesulfonic acid
DNA	Deoxyribonucleic acid
DPC	Digital phase contrast
DQ	Dye-quenched
DTT	Dithiothreitol
ECM	Extracellular matrix
EDTA	Ethylenediaminetetraacetic acid
ELISA	Enzyme-linked immunosorbent assay
Em.	Emission wavelength
Ex.	Excitation wavelength
FA	Formic acid
FC	Fluorescent collagen
FG	Fluorescent gelatin
FITC	Collagen–fluorescein
H342	Hoechst 33342
HA	Hyaluronic acid
HIC	Hydrophobic interaction chromatography
HPLC	High-performance liquid chromatography
HT venomics	High-throughput venomics
Hyal	Hyaluronidase
IC_{50}	Half-maximal inhibitory concentration

Abbreviation	Meaning
IEX	Ion exchange chromatography
kDa	Kilodalton
Kun	Kunitz-type peptide
LAAO	L-amino acid oxidase
LC	Liquid chromatography
LDH	L-lactate dehydrogenase
LSTM	Liverpool School of Tropical Medicine
MS	Mass spectrometry
MS/MS	Tandem mass spectrometry
mQ	Ultrapure Milli-Q water
N-3FTx	Neurotoxic three-finger toxin
NUS	National University of Singapore
PBS	Phosphate-buffered saline
PI	Propidium iodide
PLA_2	Phospholipase A_2
PSC	Protein score chromatogram
QTOF	Quadrupole time-of-flight
RFU	Relative fluorescence units
RNA	Ribonucleic acid
ROS	Reactive Oxygen Species
RP-LC	Reversed-phase chromatography
RPTEC/TERT1	Human renal proximal tubular cell line
SD	Standard deviation
SDS-PAGE	Sodium dodecyl sulfate-polyacrylamide gel electrophoresis
SEC	Size-exclusion chromatography
Spp.	Species (plural)
SVMP	Snake venom metalloproteinase
SVSP	Snake venom serine proteinase
TFA	Trifluoroacetic acid
U	Units (chemical)
UV	Ultraviolet
VD assay	Vesicle degradation assay
VU	Vrije Universiteit Amsterdam
WHO	World Health Organization

11.4 Research activities

During my PhD, I had the opportunity to perform lab work in several foreign labs, including Erasmus Medical Center (2019), Hubrecht Institute (2020-2021), Liverpool School of Tropical Medicine (2023), Vrije Universiteit (present) and Naturalis Biodiversity Center (present).

In these four years, I had the lucky opportunity to give over 50 (conference) talks and seminars to broad audiences worldwide. These include University talks, for example, at the University of Queensland (Australia), Denmark Technical University, Liverpool School of Tropical Medicine, Utrecht University and Leiden University, as well as conference talks in Tucson (Arizona, US), Singapore, Paris (France) and Oxford (UK).

I reviewed scientific papers for the following journals: *Toxins*, *Toxicon*, *Toxicon: X* and *Frontiers*. I was also asked to collaborate on and contribute to writing multiple scientific grant proposals. Lastly, I am a proud member of the International Society for Toxinology (IST).

11.5 Science communication

Sharing my fascination for nature with a broad audience is my greatest passion and something that I hold very dear. Fortunately, I regularly got the chance to share (random) animal facts with broad audiences on television, radio, and in newspapers. These media expressions included appearances in talk shows (e.g., Humberto, Op1), on the news (e.g., NOS Jeugdjournaal and RTL Nieuws), in children's programs (e.g., Klokhuis) and on radio broadcasts (e.g., Vroege Vogels on NPO Radio1). Every week, I wrote a column for the regional newspapers of Mediahuis (e.g., Leidsch Dagblad and Haarlems Dagblad) and together with good friend Barend Last, I wrote two children's books: Gif in het Dierenrijk (2022) and Gevaar in het Plantenrijk (2023).

11.6 Words of gratitude | Dankwoord

Thank you for getting this far through my thesis, or for those of you who just arrived at this specific part: welcome! In this section, I would like to express my gratitude to all the people who have either directly contributed to this work or made it possible for me to get through this journey. The work presented in this thesis wouldn't have been possible without the help from all the people who surrounded me these past four years. At this point, it is the moment that you receive the credits that you deserve. A significant part of this is going to be in Dutch.

Allereerst zou ik graag mijn promotoren **Jeroen** en **Freek** willen bedanken voor de begeleiding en alle mooie momenten die we samen hebben beleefd in de afgelopen jaren. Ook wil ik jullie bedanken voor het feit dat jullie deze PhD mogelijk hebben gemaakt. Ik weet nog goed dat Freek me belde met het nieuws dat ik mocht beginnen met een PhD en ik was door het dolle heen. Sterker nog: ik herinner me zelfs de datum waarop ik dit verlossende telefoontje kreeg. Dit was in de zomer van 2019, op 27 juli om precies te zijn. De reden dat deze datum in mijn heugen gegrift staat is dat het ook de verjaardag van mijn moeder is, die er helaas niet meer bij was om het te vieren. Toch denk ik dat ze er op één of andere manier toch weet van heeft gehad, al is het maar omdat haar verjaardag en dit telefoontje zo toevallig samenvielen. Freek, dit moment ga ik nooit meer vergeten, nogmaals bedankt hiervoor! Dit was de start van dit avontuur, waarbij ik door beide heren door dik en dun ben gesteund. **Jeroen**, zonder jouw vaardigheden als *micromanager* hadden mijn dagen op het lab er heel anders uitgezien. Jouw inzichten en ideeën hebben mij geholpen om mijn projecten tot een goed einde te brengen. Als ik soms door de bomen het bos niet meer zag kwam jij altijd met een slimme oplossingen of een verlossend woord, waardoor ik verder kon. Wat ik daarnaast geweldig aan jou vind is dat je me altijd de ruimte geeft om 'mijn eigen ding te doen', zowel op het lab als daarbuiten. Slechts heel af en toe kreeg ik van jou de vraag waarom ik de halve week niet op kantoor was geweest. Deze vrijheid heeft mij absoluut geholpen om mezelf ook buiten de wetenschappelijke kaders te ontwikkelen. Daarnaast heb ik onwijs genoten van onze (avontuurlijke) reizen samen met Julien naar de VS, Singapore en Australië. Van *late-night herping* in Arizona tot zeekrokodillen voeren in Australië, we hebben

het allemaal meegemaakt. Laten we hopen dat we in de toekomst nog regelmatig dit soort te gekke reizen kunnen maken.

Freek, jou wil ik graag bedanken voor de steun gedurende de afgelopen jaren, zowel op wetenschappelijk vlak als op het gebied van de media. Ik vond het prachtig dat ik je altijd kon bellen – ongeacht waar jij je op dat moment dan ook ter wereld bevond – en dat jij altijd met jouw kenmerkende enthousiasme de telefoon opnam. Daarnaast heb ook genoten van onze meetings, zowel online als bij jou thuis waar we onze wetenschappelijke plannen gingen uitwerken. Ik hoop dat we dit in de toekomst kunnen blijven doen en dat we het 'Deep Thoughts' *dream team* kunnen blijven voeden met nieuwe, baanbrekende ideeën.

Dan over naar de mensen bij Naturalis die dit proefschrift mede mogelijk hebben gemaakt. Zonder hen had ik nooit deze droombaan kunnen hebben. Want zeg nou eerlijk: wat is er nou mooier dan onderzoek te doen naar het gif van de giftigste slangen ter wereld? **Maaike**, onwijs bedankt voor alle vertrouwen en steun die je me hebt gegeven. In de eerste plaats door mij de mogelijkheid te geven om dit onderzoek te kunnen doen. Hetzelfde geld natuurlijk voor **Edwin**, die al jaren de verantwoordelijkheid heeft voor het prachtige onderzoeksinstituut en natuurhistorisch museum dat Naturalis Biodiversity Center is. Daarnaast kijk ik erg uit naar onze toekomstige samenwerking, en natuurlijk het organiseren van de aankomende editie van het 'Snakebite' congres. **Johan**, bedankt dat je mij hebt geholpen bij de start van mijn proefschrift en bij het schrijven van enkele subsidievoorstellen. Ik heb altijd erg genoten van onze (online) gesprekken. **Martin**, I am really grateful for you as the head of the VEDE (Vertebrate Evolution, Development and Ecology) group. Not many people are as thoughtful and helpful as you. Although we didn't have many meetings in person as I would have liked – my bad, I should be visiting Naturalis more often – I really enjoyed our short talks over coffee.

During my years as a PhD-candidate, I had the pleasure of working with some fantastic and inspiring people, both inside and outside of the VU and Naturalis. First, I would like to thank the senior staff within the Division of BioAnalytical Chemistry (BAC) at the VU, **Anouk**, **Govert, Isabelle**, **Jeroen**, **Kevin** and **Melissa**, for making our lab such a great place to work. Thanks to your support and guidance, we have the collaborative spirit and the wealth of knowledge that is present within our group. **Anouk**, jou zou ik graag in het bijzonder bedanken

voor het feit dat je bereid was om voorzitter van de promotiecommissie te zijn en voor de tijd die je hebt gestoken in het doorlezen van mijn proefschrift.

Then I would like to thank the fellow members of The Venoms & Drugs (V&D) group – **Julien**, **Haifeng**, **Luis** and **Xiaoyi**. It has been a great pleasure working together with you. **Julien**, wat een avonturen hebben wij beleefd samen met Jeroen. Van jagen op ratelslangen vanuit een golfkarretje in Arizona tot zeekrokodillen voeren in Australië, niks was ons te gek. Maar door al deze te gekke avonturen zou ik bijna vergeten wat we allemaal bínnen Nederland hebben meegemaakt. Op het lab ben je een onmisbare kracht en altijd behulpzaam. Je hebt me meermaals uit de penarie geholpen en was nergens te beroerd voor. En na je inmiddels vijf jaar te kennen kan ik zeggen dat je echt een goede vriend van me bent geworden. **Haifeng**, I am really happy to have you on our V&D team. We have shared many mornings on the 3rd floor, feeding our cells and doing experiments. I really enjoyed our conversations, listening to Mariah Carrey and it is always good fun to go on a trip with you, either to Paris, Singapore or Oxford. **Luis**, como te aprecio muchísimo como persona, voy a intentar escribir mi agradecimiento en mi mejor español. Aquí va: ¡Qué placer ha sido tenerte en nuestro equipo! He disfrutado mucho contigo, hemos reído tanto, hemos podido charlar de todo y nunca me he aburrido contigo. Siempre eres muy servicial, leal y nunca te niegas a ofrecer un oído atento. Eres una persona maravillosa y espero que nos encontremos de nuevo en el futuro. ¡Hasta pronto! **Xiaoyi**, I really appreciate your positive attitude and your bright mind. I enjoyed being part of your project on muscarinic receptor binding.

Then, a well-deserved shoutout to the other PhD students and colleagues from the BAC Department. **Raya**, I always had so much fun with you – whether it was over morning coffee in the pantry, during afternoon chats when we were utterly bored with our work and at borrels. In the last year, we even became gym buddies, along with Amalia, Iuliia, and Julien. Although you sometimes had to push me to go to the gym – and I still hate 'leg-and-bum-day' – I was always satisfied when leaving the gym again. You're a fantastic person, and I am happy to have you as a colleague and friend.

Bas, als ik jou in één woord zou moeten omschrijven zou ik het woord 'topgozer' kiezen. Ik heb genoten van elke minuut die jij bij ons op het lab rondliep. Altijd in voor een praatje – lees: ouwehoeren – en nooit te beroerd om

alles uit je handen te laten vallen om me met mijn technische vragen helpen. Samen hebben we zelfs nog meerdere weekenden in het lab doorgebracht, waar uiteindelijk een pracht van een artikel is uitgekomen – vraag Eric anders even of hij je die kan opsturen ☺. **Hany**, ik heb genoten van onze regelmatige koffietjes in de 'Coffee Corner', waar we van alles bespraken, van podcastplannen, tot de huizenmarkt, alles kwam aan bod. Het was ook erg gezellig met jou die ochtend op de heide waar jij al volleerde cameraman aan de slag ging. Dit heeft de ANWB ongetwijfeld prachtige beelden opgeleverd, dank daarvoor! Oh en die podcast, die gaat er nog een keer komen! Natuurlijk mag ik **Dave** ook niet vergeten. Kerel, wat heb ik een lol gehad met jou! Samen hebben we zowel mooie – en minder vrolijke – tijden beleefd, maar dat hoort erbij. Je was een echte gangmaker en als DJ Dave was je een onmisbare factor tijdens de borrels. Ik hoop je snel weer te spreken, en die wrakduik in de Waddenzee gaan we écht nog een keer maken samen. **Iris**, jij schreef zelf een heel leuk stukje over mij in jouw PhD boekje, en ik kan eigenlijk hetzelfde doen voor jou. Ik heb enorm genoten van jouw enthousiasme en gezelligheid op de VU. We hebben het vaak over onze passies gehad en ik vind het tof om te zien dat jij nu een baan hebt waar je energie van krijgt. En **Kristina**, met jou heb ik altijd geweldig kunnen ouwehoeren over van alles en nog wat. Je was altijd een mooie toevoeging tijdens de borrels maar ook onder werktijd kon ik altijd bij je terecht met een vraag, voor een praatje of een kop koffie. Je wordt gemist! **Amalia** and **Iuliia**, I already mentioned above the fact that we have been gym buddies for the past year, so it is partially thanks to you that I am (finally) doing some exercising! You both are amazing people with whom I very much enjoy spending time, both inside and outside of the lab. Met jou **Chuck**, heb ik altijd erg kunnen lachen om van alles en nog wat. Jouw aanstekelijke lach – die soms vanaf de andere kant van de gang te horen was – maakte mij altijd aan het lachen. Daarnaast ben je een super behulpzame kerel en een mooie toevoeging aan de groep. En oh ja, bedankt nog voor die keer dat je me hebt geholpen met het uitspoelen van m'n ogen nadat ik er per ongelijk slangengif in had gewreven. Ik kan nog zien, dus niks aan 't handje! **Sjors**, bij jou moet ik vooral denken aan de leuke gesprekken over gekke dieren en de cryptische foto's en zoekplaatjes die je me hebt laten zien. Van cobra's en parelhalstortels tot nachtboomslangen, jij houdt me altijd scherp. Ook vind ik het tof dat we voor dezelfde voetbalclub zijn – hup, Ajax,

hup! **Joshka**, ik moet jou natuurlijk bedanken voor jouw trouwe support toen mijn kinderboeken uitkwamen. Als een ware boekenverkoper heb jij deze weten te slijten aan een groot deel van jouw sociale kring. Daarnaast vind ik je gewoon een hele gezellige collega waarmee ik altijd kan lachen. **Jordy**, als ik aan jou denk krijg ik gelijk een lach op m'n gezicht. Niet alleen vanwege je aanstekelijke lach, maar ook omdat ik gelijk moet denken aan al die keren dat je 'even komt hangen' en we dan zo een kwartier aan het kletsen waren, zelfs als we allebei 'druk' waren. Misschien niet altijd even handig, wel gezellig! **Agathe**, it was a pleasure having you around. How cool was it that we even worked together on one of your projects?! **Ariadni**, it was always good fun having you around during working hours and borrels. **Lastly, I would like to** thank all other PhD students and colleagues of the BAC department that I've met over the years – **Andrea, Annika**, **Arif**, **Behrad**, **Carlos**, **Chunfang**, **Guusje**, **Henrik**, **Jesper**, **Julia**, **Jiaxing**, **Jonathan**, **Kevin**; **Luca**, **Ludovica**, **May**, **Robert**, **Ruben**, **Tijmen** and **Wietse** – it was a pleasure to have met you.

Then, I'd like to thank the people at the Division of Molecular and Computational Toxicology (Moltox) for all their help with my cell-based assays. **Lily**, I really enjoyed our time in the lab during COVID-19, when the lab was more or less empty and we were one of the lucky few who were allowed to travel to the lab – most of my colleagues from upstairs were jealous. We had so much fun together and I really miss you in the lab! Hope to see you again soon! **Daniel**, jij zit altijd vol goede ideeën en bent de beste 'sparringpartner' die ik me kan wensen. We hadden regelmatig discussies die meer dan een uur duurden, waar ik altijd erg veel lol in heb gehad. Ik weet trouwens niet of jij je dit realiseert, maar één van jouw ideeën tijdens een van onze discussies is uiteindelijk een op zichzelf staande test geworden voor membraandegradatie (zie Hoofdstuk 6). Lekker gewerkt! Obviously, I couldn't leave out some of the other amazing people at Moltox, namely **Elisabeth**, **Emma**, **Giada**, **Paul**, **Sofia** and **Victoria** – who were always helpful and made the lab a great place to work.

On the other side of the 3rd floor there is another group that deserves a special thank you, namely the Division of Medicinal Chemistry (MedChem). En in de eerste plaats is dat natuurlijk **Nick**, my man! Wat heb ik GENOTEN van onze projecten samen. Ik denk dat we kunnen stellen dat wij een absoluut *dream team* waren. Hadden we weer een extreem lange dag op 't lab – dan heb ik het over

een uur of 14 – voor de boeg? Geen probleem! Jij kwam dan vrolijk om half acht 's ochtends binnen om de boel te starten en ik ging – bijna net zo vrolijk - om half 10 's avonds weer de deur uit. Onze trip naar Liverpool om daar op het lab te werken was prachtig en ik hoop in de toekomst nog mooie projecten met je op te zetten. Daarnaast zou ik graag **Jan Paul**, **Marco** en **Martine** willen bedanken voor hun bijdrage aan het 'SDS-page gelletjes'-project, dat een stuk mooier uitpakte dan we hadden voorzien.

Obviously, I couldn't leave out the collaborators at Mimetas. I still remember vividly when I met with **Dorota** and **Paul** in early 2020, when we attended 'De Wereld Draait Door' in the Westergasfabriek. This is where the first plans were made to see if we could use your organ-on-a-chip system to study snake venom-induced tissue damage. With the amazing help of **Flavio**, we were able to really get this collaboration to a whole new level. Flavio, working with you is just so much fun. Just think of those moments at Mimetas, while writing the paper at the VU or over beers at Mezrab. I'm thrilled with our first joint paper, and I hope this is the first of many more to come!

Even though I didn't spend much time in the labs at Naturalis, I would like to thank all the fellow PhDs at Naturalis that I've met there over the years. Although I am totally aware of the fact that I missed a lot of 'koffietjes en borrels', I really enjoyed the moments that we were together and I felt really welcome, even though I was there only a handful of times.

In the following section, I'd like to thank the people that I haven't mentioned before but whom I collaborated with scientifically in one way or another during these four years. **Prof. José-Maria Gutierrez** ('**Chema**') has been a massive support. We had so many great conversations and fruitful discussions, and I really appreciate the fact that you were always so patient and helpful when I was sometimes stuck writing the review. In addition to this, your absolute expertise in the field of cytotoxicity – over 40 years, if I'm not mistaken – greatly advanced the review as a whole. I sincerely hope that we keep in contact and that we can collaborate on future projects. Then we have **Rachel** and **Nicholas**, our dear collaborators on the other side of the Channel, in Liverpool. **Rachel**, I'm impressed by your positivity and work ethic, and I think you're an incredibly sweet and sincere person. I really enjoy working on our current spin filter study, which is going to be great; I'm confident about that. **Nicholas**, I consider it a great

honour that we have been publishing quite a number of papers together in the past years. From the start of my career in this field, I was impressed by your work, but I'm happy that I now also know you as the wonderful person that you are. **Michael** (**'Mike'**), jou wil ik graag bedanken voor het vertrouwen en de steun die jij me al tijdens mijn Master hebt gegeven waardoor ik van de wetenschap ben gaan houden. Ongetwijfeld hebben de mooie tijden op het Sylvius samen met **Merijn** en **Lianne** bijgedragen aan mijn keuze om het wetenschappelijke carrièrepad te gaan bewandelen. **Fernanda**, we shared many great moments at different places, from driving the famous Apache Trail in Arizona to having late-night dinner at a Hawker Center in Singapore. We had so much fun with Ben, Julien and Jeroen, and I hope we will keep doing this for many years to come. In addition to that, I would like to thank you for the fact that you are willing to be part of the committee and for the time you spent assessing my thesis. **Andreas** and **Timothy**, I would like to thank you for our collaboration on our MENA review and the fact that you hosted me so kindly at DTU.

Although brief, I would like to thank **Prof. Grosveld** and **Dubi** for having me at their lab at the Erasmus MC for the first two months of my PhD. Dubi, you have a heart of gold, and I hope to speak to you again soon.

In addition to all the people mentioned above, I am extremely grateful to the students who have helped me throughout the course of my thesis. **Eric,** thank you for your hard work on Chapter 5 of this thesis, you did an amazing job and I'm sure that one day you will become a colleague in the snake venom field too! **Eric**, **Floor**, **Axel**, **Munevver** and **Huda**, thank you so much for your work on Chapter 6. **Sedef**, I'm really happy with the efforts to making SEC part of our analytical platform. Sakina, thank you for your work on the spin filter assays (to be published). **Mabel** en **Lea**, jullie waren de eerste studenten die ik heb mogen begeleiden, en dat heb ik met veel plezier gedaan! Ondanks het feit dat jullie stage maar kort was, hebben jullie geweldig werk verricht aan de optimalisaties van de LC-scheidingen. **Jorg**, jij bedankt voor al het bloedstollende werk aan de Australian elapids. Tot slot moet ik ook de studenten bedanken die met hun literatuurstudies een mooie basis hebben gevormd voor een aantal nieuwe studies, waaronder de review in Hoofdstuk 2 in dit proefschrift. **Glenn**, **Oran**, **Robert**, **Thomas** en **Ingrida**, bedankt hiervoor!

Lastly, I would like to thank the photographers who were so kind to allow me to use their beautiful pictures in Figure 1 in the first chapter of this thesis. Thank you, **Tyrone Ping** (photos of *A. bibronii* and *D. typus*), **David Jahn** (photos of *M. euryxanthus*) and **Frank Deschandol** (photos of *D. russelii*). In addition to this, I would also like to thank my friend **Wolfgang Wüster** for the great pictures of *N. naja* and *D. russelii* in Figure 3 of the same chapter. I am also very grateful for the fact that you were willing to be our partner in crime when looking for snakes in both the US and Singapore. I'm looking forward to our next adventure!

Naast mijn werk als onderzoeker heb ik een behoorlijk deel van mijn (vrije) tijd gestoken in het delen van mijn fascinatie voor natuur met anderen. Dit had ik niet kunnen doen zonder de mensen bij Naturalis en de VU. In de eerste plaats zou ik de mensen van communicatie bij Naturalis – en in het bijzonder **Amy** en **Bart** – willen bedanken voor hun enthousiasme en behulpzaamheid. Zonder hen hadden we ons werk nooit op zo veel mooie plekken terug gezien. Van 'Op1' tot 'NPO Radio1' en van 'National Geographic' tot de 'BBC', ik heb op zo veel toffe plekken mogen vertellen over ons bijzondere onderzoek. En dat was voor een groot deel te danken aan jullie ijzersterke persberichten. Bedankt daarvoor! Deze dank gaat uiteraard ook uit naar **Corine**, **Francine**, **Gerry** en **Hilmar**.

Buiten de communicatiemensen om zou ik al mijn Naturaliscollega's willen bedanken die mij de afgelopen jaren hebben geholpen met de meest bizarre mediaverzoekjes. Zo gingen we op zoek naar de Surinaamse pad in de collectie van **Esther** en **Pepijn**, en filmden we de grootste dagvlinder ter wereld met **Rob** en **Hannco**. Ik ben jullie onwijs dankbaar, want zonder jullie hulp had ik deze bijzondere dieren nooit kunnen laten zien aan het grote publiek. Mijn dank gaat hierbij uiteraard ook uit naar de mensen bij de VU – **Jacky** en **Marijke** – die me altijd hebben geholpen met het coördineren van – vaak *last minute* – persaanvragen.

Natuurlijk kan ik ook **Selena** in deze niet vergeten. In de tweeënhalf jaar waarin we hebben samengewerkt heb ik je leren kennen als een geweldig persoon en hebben we mooie momenten beleefd. We gaan elkaar hoe dan ook tegenkomen in de toekomst, het ga je goed!

Dan is het nu tijd om de mensen te bedanken die me buiten mijn werk door dik en dun hebben gesteund: mijn vrienden en familie. **Jannik**, ik begin met jou omdat ik jou van mijn vrienden het langste ken. We kennen elkaar sinds

groep drie, en zijn 'vogelmaten' van het eerste uur. Wat onze vriendschap in mijn ogen heel bijzonder maakt, is dat wij samen al heel veel mooie, maar helaas ook verdrietige moment hebben meegemaakt. Ik beschouw je als een van mijn allerbeste vrienden en ik hoop nog jarenlang met je op vogelreizen te kunnen gaan. Daarna volgen natuurlijk mijn maatjes van de middelbare, **Daan**, **Ties**, **Yaro**, **Sybren** en **Simon** – ook al zat Simon op een andere school. We zijn in onze jonge jaren samen half Europa door gereisd, naar 'Sziget' geweest en hebben ik weet niet hoe veel avondjes samen muziek gemaakt. We zien elkaar misschien maar een paar keer per jaar – maar dat maakt niet uit, want onze vriendschap blijft hoe dan ook overeind. Natuurlijk mag ik ook de boy's uit m'n jaarclub niet vergeten. **Bart**, **Ewoud**, **Iskander**, **Jesse**, **Joost**, **Martijn**, **Mathijs**, **Ogier**, **Quint-Hein**, **Robin**, **Stijn** en **Tim** – ook wij gaan inmiddels al heel wat jaren terug, gasten! Clubvakanties, feestjes en ontelbaar veel andere mooie momenten hebben wij beleefd. Maar ook op persoonlijk vlak zijn jullie altijd belangrijk voor me geweest. Zo werd er regelmatig bij me 'ingecheckt' om te kijken of ik niet iets te véél hooi op m'n vork had genomen. Achteraf gezien was soms misschien ook wel zo, maar jullie hebben me altijd in mijn keuzes gesteund en dat waardeer ik echt aan jullie. Dan wil ik m'n maatje **Ogier** in het bijzonder bedanken voor jouw steun de afgelopen jaren. We hebben veel meegemaakt in de 2,5 jaar dat we samen hebben gewoond – mooie en verdrietige momenten – maar we konden altijd bij elkaar terecht en dat vind ik heel waardevol.

Uiteraard mogen ook de mannen van biologie – en dan vooral **Joep**, **Joshua**, **Laurens**, **Maarten**, **Martijn**, **Sjoerd** en **Stijn** – in deze grote lijst van bedankjes niet worden vergeten. Inmiddels gaan we al jaren op mannenweekend naar alle uithoeken van Nederland (en daarbuiten), zitten we samen in een van de beste *pubquiz*-teams van Nederland en zijn we inmiddels al toe aan 'Odessa 9.0' – of is het inmiddels 10.0? Jullie zijn een heerlijk stel gasten en ik hoop dat we elkaar nog lang blijven zien.

Dan nog een paar mensen die om wat voor reden dan ook hierboven nog niet zijn langsgekomen maar die absoluut niet onbenoemd mogen blijven. In de eerste plaats natuurlijk **Caroline**, die tot tweemaal toe mijn huisgenoot is geweest. Onze vriendschap staat al twaalf jaar als een huis – snap je 'm? – en is zelfs zo sterk dat mijn pa je zo'n beetje als bonusdochter beschouwt. Dan een aantal mensen die ik de afgelopen jaren ook als hele goede vrienden ben gaan zien en

waarmee ik langdurig in quarantaine heb mogen doorbrengen. **Boudewijn**, **Geertje** en **Hugo**, wat heb ik genoten van onze tijd als huisgenoten. Ik heb zelden zo veel gelachen als in de jaren dat wij elkaar op de huid zaten tijdens deze gekke periode. Al ben ik wel blij dat we sindsdien veelvuldig Cafés als 'Bedier', 'Kuijper' en 'Hans' hebben kunnen bezoeken. Daarnaast wil ik **Wouter** bedanken voor zijn grenzeloze enthousiasme en rol als aanjager voor allerhande (huis)feestjes, pubquizzen en andere borrelavonden die voor een welkome afleiding hebben gezorgd in de afgelopen jaren.

Jory, **Roel**, **Sterrin**, **Peter** en **Yvette**, ondanks het feit dat onze levens inmiddels over de wereld verspreid zijn – de VS, Tsjechië, Spanje en Nederland – zullen we altijd *close* blijven via onze gezamenlijke Whatsappgroep. **Jory** en **Roel**, wat heb ik genoten van onze whisky-avondjes, waarin we (soms online) tot grote wetenschappelijke inzichten kwamen. **Jory**, jou wil ik graag nog even in het bijzonder bedanken voor jouw bijdrage aan de *cytotox review*. Wat een ongelofelijke topkerel ben jij, altijd positief, eerlijk en oprecht geïnteresseerd in de ander, zelfs op momenten dat de zon voor jou misschien even niet schijnt. En **Sterrin**, ook wij de nodige avonturen meegemaakt de afgelopen jaren! Samen overleven in de Noorse wildernis, waarin we het maar liefst tweeënhalve (!) dag hebben volgehouden. Het was voor ons beiden een groot avontuur en ik zou het zo weer doen – maar dan met een nóg betere voorbereiding. Dan tot slot **Yvette** en **Peter**, zonder jullie zou menig Klokhuisuitzending een stuk minder spannend zijn geweest. En Peet, jou wil ik nog in het bijzonder bedanken voor het doorlezen en corrigeren van 'Gif in het Dierenrijk', waarmee ik het boek met éxtra veel vertrouwen heb kunnen uitgeven.

Dan de lieve **familie Oosterhuis** en in het bijzonder **Brigitte**, die mij soms tijdens drukke periodes hebben meegemaakt, maar waar ik me altijd thuis heb gevoeld. Heel erg bedankt voor al jullie liefde en steun die jullie mij in onze tijd samen hebben gegeven.

Dan uiteraard de familie Heijnen – wat een heerlijke club mensen is. Ondanks het feit dat we elkaar minder vaak zien dan we misschien zouden willen, zijn jullie heel belangrijk voor me. Met Harry heb ik nog zelfs wetenschappelijk overleg gehad over één van onze slangengifstudies, al is dat artikel helaas geen onderdeel van dit boekje geworden.

Szeretnék köszönetet mondani magyar rokonaimnak is, akik lehet, hogy fizikailag nem tudnak ott lenni, de távolról ott vannak - és főleg a szívemben.

En ben nu aangekomen aan de mensen die ik zou willen bedanken voor het feit dat ze me al op jonge leeftijd hebben geïnspireerd. Hierbij mogen **Cora** en **Jan** natuurlijk niet ontbreken. Alle wandelingen door de tuin en bij jullie in de buurt zijn voor mij dé reden geweest om ook van de natuur te gaan houden. Het feit dat ik uiteindelijk bioloog ben geworden is ongetwijfeld voor een groot deel aan jullie te danken! En **Jorke**, het enthousiasme waarmee jij jouw liefde voor de vogels op mij hebt weten over te brengen zal ik nooit vergeten. Deze vonk is al op jonge leeftijd overgesprongen en laat me nooit meer los. Nu dit proefschrift ein-de-lijk is afgerond, heb ik weer de tijd om op pad te gaan, dus dat gaan we dit najaar écht weer eens doen.

Lieve **Karen**, wat ben ik blij met jouw aanwezigheid in mijn leven en die van papa. De afgelopen jaren zijn niet makkelijk geweest en ik ben nog elke dag dankbaar voor het feit dat we mede door jouw wilskracht zo veel 'geluk' hebben gehad. Ik ben blij met jou voor pap en andersom en hoop dat jullie nog lang en in goede gezondheid samen gelukkig kunnen zijn. Misschien dat we volgend jaar dan eindelijk een keer met z'n drieën *Down Under* kunnen gaan – moeten we alléen pap nog even zien te overtuigen. Natuurlijk mag ik ook jouw dochters en kleindochters niet vergeten, **Cathelijne**, **Bella**, **Emma** en **Ruben** en natuurlijk **Jasmijn** en **Esmee**, jullie zijn stuk voor toppers en ik heb jullie in m'n hart gesloten.

Dan, als aller-allerlaatste wil ik mijn allergrootste supporters bedanken. Lieve **papa** en **mama**, zonder jullie had dit proefschrift er nooit gelegen. In de eerste plaats vanwege van het feit dat jij, **papa** de mooist denkbare tekeningen hebt gemaakt. Hiermee heb jij dit proefschrift óók voor mensen buiten de slangengifhoek aantrekkelijk gemaakt – al wil je dit volgens mij nog steeds niet van me aannemen. Ik vind het prachtig dat we hiermee opnieuw een project hebben gehad waarin we konden samenwerken. Eerst twee kinderboeken en nu dit proefschrift waar ik – mede door jouw tekeningen – zo onwijs trots op ben. We hebben inmiddels ontelbaar veel dingen meegemaakt samen en zijn zo ongelofelijk hecht geworden dat ik je naast mijn papa ook als allerbeste kameraad beschouw. Ik hoop dat we snel een van onze andere plannen samen kunnen gaan

uitvoeren nu ik (eindelijk) wat meer ruimte heb na de afronding van dit grote avontuur.

Tot slot wil ik de laatste zinnen van dit proefschrift wijden aan mijn heldin en allergrootste voorbeeld. **Mama**, wat een ongelofelijk gemis dat jij deze bijzondere gebeurtenis niet kunt meemaken. De afgelopen jaren zijn er zo veel momenten geweest waarvan ik weet dat jij het fantastisch had gevonden om deze óók mee te maken. Helaas mag dit niet zo zijn en daarom zullen geluksmomentjes als deze altijd een dubbele lading hebben. Desondanks wil ik positief naar de dingen blijven kijken – zoals ik van jou heb geleerd – en dat ga ik dan ook doen. Daarom draag ik dit proefschrift – mijn 'boekje' – aan jou op, als eerbetoon aan de liefste en meest fantastische vrouw die ik ooit heb gekend.

11